

ISOTOPES OF URANIUM AND RADIUM IN INDIAN RIVERS

BY SUMAN G. BHAT AND S. KRISHNASWAMY

(Tata Institute of Fundamental Research, Homi Bhabha Road, Colaba, Bombay-5)

Received March 24, 1969

(Communicated by Prof. D. Lal, F.A.S.C.)

ABSTRACT

The concentrations of dissolved uranium and radium isotopes have been determined in the waters of several Indian rivers. The concentration of uranium (U-238) is found to vary between 0.01-7.0 micrograms/litre, depending primarily on the terrain through which the river flows. From the available data on the activity ratios, U-234/U-238, concentration of U-238 in rivers and the amount of uranium depositing on the ocean floor, a material balance calculation has been attempted. This shows that the supply of uranium to sea by rivers based on above measurements, is inadequate to explain the observed concentrations of U-238 and U-234 in the oceans.

The Ra-226 concentration of river waters is found to be of the order of 0×1 dpm/litre (varying between 0.05-0.2 dpm/litre). The activity ratios, Ra-228/Ra-226, range between 1 and 4. This large variation is clearly related to the fact that the concentrations of the parent nuclides of Ra-226 and Ra-228 are different. The observed ratios are consistent with those expected from leaching of clays/soils; however, analogous to the situation in the case of uranium, the observed concentrations of radium isotopes in the oceans are too large to be explained by their influx by rivers.

1. INTRODUCTION

It is well known that the significant radioactive disequilibria between the members of the three naturally occurring radioactive series, U-238, U-235 and Th-232 in the hydrosphere are related to their grossly different geochemical behaviours. The first noteworthy observation on disequilibrium between two isotopes in the same series was reported by Russian workers¹ who found that the concentration of U-234 in ground waters was in excess compared to that of its parent, U-238. Similar disequi-

torium between U-234 and U-238 has been reported in sea and river waters by several workers.^{2,7}

During the last few years, more examples of disequilibria have been observed in natural waters.^{8,1*} Moore and Sackett⁸ have shown that the Th-228/Th-232 activity ratios in sea-water are an order of magnitude higher than the expected secular equilibrium value. This result was later corroborated by the studies of Somayajulu *et al.*⁹ Measurements of the two radium isotopes Ra-226 and Ra-228^{12,14} in sea and river waters also show that they are not in equilibrium with their parents, Th-230 and Th-232 respectively.

The above studies are largely confined to the marine environment and data on the concentrations of uranium and radium isotopes in rivers are scanty.^{4,* 1B»¹⁶} Rivers are the primary agency for the introduction of a host of elements, into the sea; eolian transportation of dust and subsequent leaching of trace elements from the dust during its transit through sea-water probably plays an important role in the input of certain elements.¹⁷

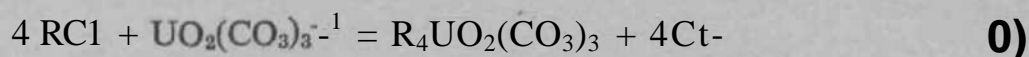
In this paper we report our measurements of the concentrations of U-238, U-234, Ra-228 and Ra-226 in some major Indian river waters. Seasonal variations in the concentrations of uranium have also been studied. A few ground water samples have been analysed for uranium in order to explore the possibilities of determining the extent of effluent seepage into the river waters.

2. EXPERIMENTAL METHODS

Uranium, which exists mainly as an anion complex in natural waters,¹⁸ is usually pre-concentrated from large volumes of water by various methods, the most common being the ferric-hydroxide scavenging. To get a quantitative yield of uranium from water samples by the scavenging method, it is necessary to destroy the anion complex before scavenging and hence the use of an *in situ* scavenging method is limited. If, however, one uses an anion exchange resin to pick up the uranium complex directly, it can serve as a better *in situ* extraction method. Based on studies of the uptake of sulphate, phosphate, and carbonate complexes of uranium on anion exchange resins, some methods have been developed to extract uranium from leachates of ores and natural waters of high uranium content.^{1^}

In this work pre-concentration of uranium from large volumes of water at the sampling site was done using an anion exchange resin, after converting the uranium to a stable UO_2CO_3 complex by addition of suitable

amounts of ammonium carbonate to the water. The uptake mechanism probably is:



Water samples of 400-600 litres were collected in polyethylene drums from the mid-stream regions of the rivers. (For locations of samples, see Fig. 1.) The suspended matter was first removed by allowing it to settle for a period of about 10-12 hours (this step removes all particles of greater than about five micron size). To the clear decanted water, analar grade ammonium carbonate was added to make a concentration of about 0.08 M of the reagent. U-232 was added as a spike and the water was passed through an anion exchange resin (Dowex-1; 50-100 mesh; column volume, ca. 500 ex.), in carbonate medium at a rate of about 20-30 column volumes per hour. The resin was later brought to the laboratory and the mud (if any) was separated by suspending the resin in distilled water. Uranium was eluted from the resin with 4-5 column volumes of 3N ammonium chloride, followed by 2-3 column volumes of hydrochloric acid at pH \approx 4. The ammonium salts were decomposed and the uranium was purified by the procedure of Bhat *et al.*¹¹

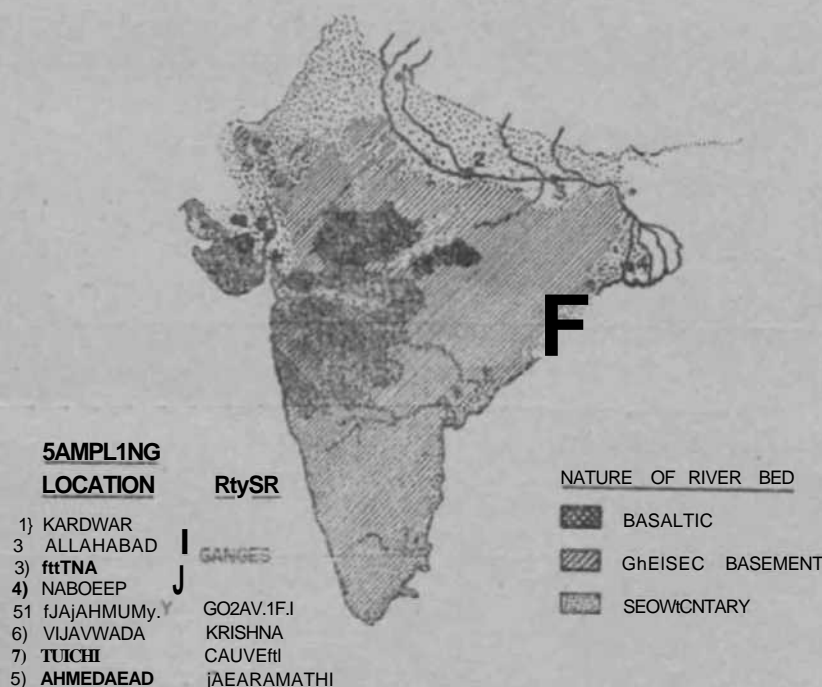


FIG. 1. Map of India showing the major petrological divisions and locations from where the river water samples were collected.

For studying the seasonal variations of uranium content and U-234/U-238 activity ratios, 20-50 litre samples were processed, using smaller amounts of resin.

After purification, an aliquot (less than 1%) of the sample was directly deposited on a platinum planchet, and the total alpha activity was measured using a zinc sulphide detector system.²² Depending on the total alpha activity a suitable fraction of the sample was electroplated on a one inch diameter, 1 mil. thick, platinum disc.

The alpha activities of uranium isotopes were measured on a 128 channel alpha spectrometer employing a one inch diameter Nuclear Diode surface barrier detector.

The efficiency of pick-up of uranium, as determined by laboratory experiments using U-232 tracer was about 70-80%.

The column method used by us has the advantage that it provides a fast and efficient *in situ* pre-concentration step for uranium from large volumes of water. However this procedure has two limitations:

(1) It is applicable only if the uranium isotopes in the waters are present in the + 6 valency state, only when the carbonate complex is formed. To check on this point, we evaporated three 5 liters mud free water samples to dryness, and processed them for uranium. The results are shown in Table 1. The results are in good agreement, within statistical errors which are about 10 per cent.

»

TABLE I

Concentrations of U-238 and U-234/U-238 activity ratios as determined by the column and evaporation methods

Sample	Column method		Evaporation method	
	U-238 concentration (ppb)	U-234/U-238 (activity ratio)	U-238 concentration (ppb)	U-234/U-238 (activity ratio)
Ganges (Haridwar)	1.9±0.2	1.03±0.03	1.8±0.1	1.08±0.06
Ganges (Allahabad)	6.6±0.8	1.04±0.02	6.9±0.4	1.09±0.04
Sabaihati (Ahmedabad)	4.2±0.2	1.57±0.04	3.6±0.1	1.51±0.04

(2) The suspended matter should be separated from the water as efficiently as possible. As the gravitational settling of the particulate matter did not give a complete separation, the possibility of leaching uranium from mud by ammonium carbonate can arise. An estimate of the amount of leachable uranium was obtained by shaking about fifty grams of one of the river sediments with 0.1 M ammonium carbonate for about fifteen hours. It was found that the amount of uranium leached was 0.3 micrograms U-238/gm. of mud; the U-234/U-238 activity ratio was 1.4 ± 0.1 . An upper limit on the contribution of uranium due to leaching of mud present in samples was estimated from the known particulate matter content of these river waters,²² assuming a complete leaching of the normal uranium concentration—3 ppm. By this approach we estimate that not more than ten per cent of the total observed activity in the water can be due to leaching of uranium from the mud.

Thus we conclude that the measured uranium concentrations as well as U-234/U-238 activity ratios represent closely the actual values for dissolved uranium present in the waters.

Ra-226 was determined by measuring its daughter nuclide, Rn-222, essentially by the procedure described by Broecker,²³ from five litre water samples. We replaced the single U-tube used by Broecker by a coiled one, which traps the radon more efficiently. The trapped radon is released directly into the counter, which consists of a two-inch diameter stainless steel chamber coated inside with activated zinc sulphide. The method will be described in detail elsewhere.²² The two short-lived daughter products of radon, v/z , Po-218 and Po-214 grow in the chamber and attain saturation value within about two hours. The scintillations produced by the alpha particles emitted by the three nuclides are recorded by photomultiplier assembly. The alpha counting yield for the above system, using a N.B.S. Ra-226 standard, was measured to be 1.5 ± 0.1 . The background rates were about 3-4 counts per hour.

Blank runs with distilled water did not give any measurable activity above the background. The usual activity signals due to Ra-226 were in the region of 0.5-5 counts per minute.

The activity ratios, Ra-228/Ra-226, were determined from about 200-400 litres of water after the removal of suspended matter by gravitational settling. A preliminary concentration of radium isotopes was carried out at the sampling site by precipitating CaCO_3 , which scavenges most of the radium. CaCO_3 was dissolved in HCl, and Ra-226 concentration was first

determined by radon emanation method. The concentration of Ra-228 was obtained by milking its short-lived daughter Ac-228 (half-life = 6.1 hrs.) by Fe (OH)₃ scavenging. The beta activity of Ac-228 was assayed on a flat rectangular gas flow counter.²⁴ The activity levels of Ac-228 were about 5-10 counts per minute compared to background of 0.1-0.15 counts per minute of the counter.

The samples were remilked; duplicate analyses were in good agreement.

3. RESULTS

The uranium concentrations in micrograms/litre (ppb) and the U-234/U-238 activity ratios are given in Table II, along with the salinity (sum of the major dissolved constituents) data. Table III lists the variation in the uranium concentrations and U-234/U-238 activity ratios during different seasons for the three rivers Ganges, Cauvery and Sabarmati. The radium content (in dpm/litre) and the Ra-228/Ra-226 ratios are given in Table IV (Since the activity levels of Ra-226 in five litre samples were low, the results are reliable only within $\pm 15\%$.)

TABLE II

Concentrations of ²³⁸U and activity ratios, ²³⁴U/²³⁸U, in Indian Rivers

River	Sample location	Date of collection	Nature of river bed	Total dissolved solids (ppm)	Uranium (ppb)	²³⁴ U/ ²³⁸ U (activity ratio)
Ganges	Hardwar	Jan. 1968	Sedimentary	186	1.9210*2	1*0310*03
w	Allahabad	"	"	338	6*5510*80	1*0410*02
it	Patna	"	"	372	4*1210*50	1-12x0*03
ti	Nabdeep	"	"	373	1*5510-16	1*0710*03
Sabarmati	Ahmedabad	Feb. 1968	"	470	3*5010-40	1*3010*03
Godavari	Rajahmundry	at 1967	Basalts and gneissic basement	213	0.18 \pm 0*04	1*3510*03
Krishni	Vijayawada	"	"	205	1*0810*12	1*58 \pm 0*04
Cauvery	Trichi	"	Gneissic basement	310	0*5810*04	1*2810*03
Mutha	Khadakwasla	Sept. 1967	Basaltic	96	0*0110 001	1M410-05
Ulhas	Ulhas nagar	"	"	66	0*0110 < C01	1*3110*12

4. DISCUSSIONS

(a) *Uranium*.—The uranium concentrations observed by us are in good agreement with the values reported earlier for Chambal river,^{2B} but are higher compared to many world rivers.^{4,1fi}

The river Ganges has been sampled at four stations along its course. This river originates in the Southern Himalayas and flows mainly through sedimentary rocks. Uranium concentration values are highest at Allahabad, 6-5 micrograms/litre, decreasing along its course to a value of about 1-5 micrograms/litre near the mouth of the river. This decrease in the concentrations could either be due to the dilution by the tributaries of Yamuna which meets Ganges at Allahabad. These tributaries (not shown in Fig. 1) flow mainly through basement complex. (Basement complex or gneissic basement consists of a mixture of igneous and sedimentary rocks.¹⁵) Another possible explanation involves the precipitation of uranium due to the presence of a reducing environment along its course. The available data are inadequate to choose between these alternatives. The low value at Nabdeep, near the mouth, cannot be explained in part as due to dilution by sea-water because of the observed low chloride content (8 ppm) of the water.

The three South Indian rivers, Cauvery, Godavari and Krishna which mainly flow through basement complex have nearly similar uranium concentrations, 0-6-1 -Oppb, considerably lower than northern rivers (Ganges and Sabarmati). The U-234/U-238 activity ratios of these rivers are however significantly higher compared to Ganges.

The two small rivers Ulhas and Mutha which flow through basaltic terrain (Deccan trap series), have the lowest uranium concentration. The U-234/U-238 activity ratios are higher compared to that of Ganges, but are similar to the ratios observed for the three South Indian rivers.

The river Sabarmati flows mainly through sedimentary deposits similar to that of Ganges. During summer, the water is fed mainly by effluent seepage from ground.²⁷ Both the uranium concentration and U-234/U-238 activity ratio are high (Table II). One ground water sample analysed from an area adjacent to the river was found to have a concentration of 10 micrograms U/litre with U-234/U-238 activity ratio of 1.45 ± 0.05 . Therefore, it seems possible to delineate the extent of effluent seepage (dry discharge) from a study of U-238 concentration and U-234/U-238 activity ratios in ground waters and in river during different seasons, particularly in areas where these parameters are very different in the two cases,

From the data presented in Table II (*see* also Fig. 2), it is clear that rivers draining through sedimentary rocks are generally rich in uranium compared to the rivers flowing through igneous rocks, an observation similar to that reported earlier by Koczy,¹⁸ Also, U-234/U-238 activity ratios in rivers flowing through igneous rocks are higher compared to those flowing through sedimentary rocks⁵—*i.e.*, an anti-correlation between uranium concentration and the activity ratios, U-234/U-238,

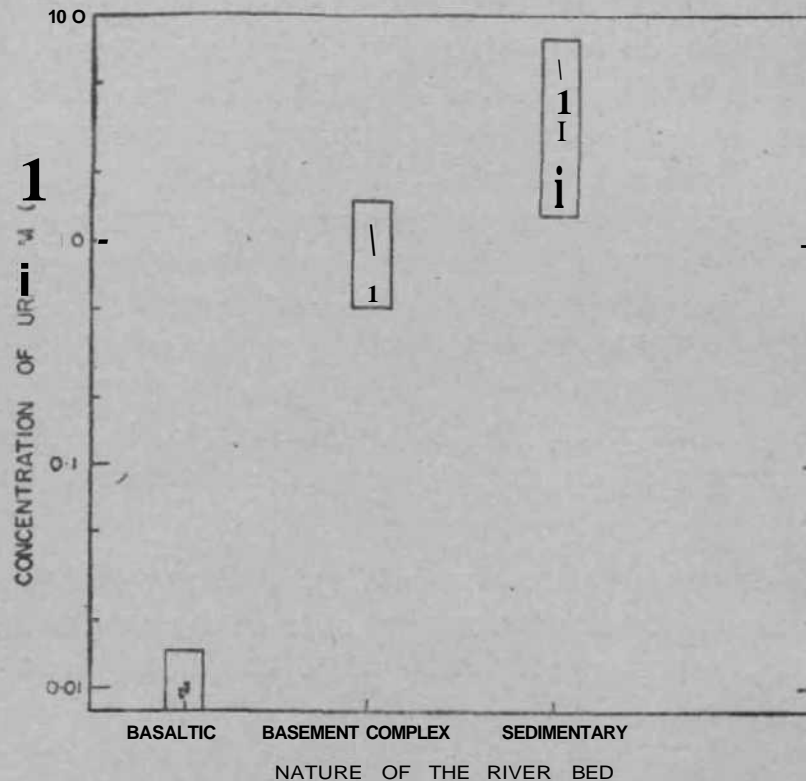


FIG. 2. Observed ranges in concentration of uranium in rivers and the nature of river bed.

In Fig. 3, we have plotted the uranium concentration values against the salinity (total dissolved salts) values from all the world rivers for which the data are available. A general positive correlation seems to be there which is not surprising since salinity values are an approximate measure of the weathering of the terrain through which the river flows.

Table III gives the measured concentrations of U-238 and activity ratios U-234/U-238, for three rivers during different seasons. There does not seem to be any marked variation in the U-234/U-238 activity ratios. The U-238 concentration however decreases significantly during the monsoon period.

From the available data on river discharge to sea,⁸⁸ we obtain a mean activity ratio U-234/U-238 = 1.2 for the Indian rivers. This value is

TABLE III

*Seasonal variation in the concentration of uranium and activity ratios
CA234/C/-238*

River (location)	Date of collection	Uranium (ppb)	U-234/U-238 (activity ratio)
Sabarmati (Ahmedabad)	.. May 1967	2-5±0-40	1-45±0-07
	February 1968	3-5±0-40	1-49±0-03
	April 1968	4-2±0-20	1-57±0-04
	September 1968	2-4±0-12	1-58±0-04
	October 1968	3-0±0-11	1-51±0-02
	December 1968	3-8±0-11	1-47±0-04
Ganges (Allahabad)	.. May 1967	7-0±1-00	1-00±0-04
	January 1968	6-6±0-80	1-04±0-02
	July 1968	0-9±0-03	1-03±0-03
	October 1968	5-7±0-40	1-04±0-02
	November 1968	6-1±0-60	1-08±0-03
	January 1969	5-1±0-30	1-01±0-02
Cauvery (Trichi)	.. February 1967	0-7±0-09	1-30±0-03
	October 1967	0-6±0-04	1-28±0-03
	June 1968	0-3±0-01	1-31±0-04
	October 1968	0-2±0-01	1-29±0-09

close to the published values for principal world rivers, 1-2 for the Russian rivers,⁵ 1-1 for Amazon, and 1-3 for Mississippi.⁴ These rivers comprise about 25% of the world annual river discharge. We therefore estimate that the weighted mean activity ratio, U-234/U-235 for world rivers is about 1-2, with an upper limit of 1*3. As discussed below this result is not consistent with the observed activity ratio of U-234/U-238 in sea-water if one considers rivers to be the dominant source of uranium in ocean. In this case it can be shown that if steady state conditions exist in oceans for uranium:

$$T = \frac{A_r - A_o}{A_4(A_o - 1) - A_r A_8} \tag{2}$$

T is the residence time of uranium in sea-water, A₈ and A₄ are the disintegration constants of U-238 and U-234 respectively, A is the activity ratio of U-234/U-238 and subscripts r and o refer to river and ocean water

respectively. Two additional conditions imposed by the material balance of U-238 are

$$T = K_1 \left(\frac{C_o}{C_r} \right) \quad (3)$$

$$C_s = K_2 C_r \quad (4)$$

where C_r is the weighted average concentration U-238 per litre in river waters, C_o is the U-238 concentration in oceans, C_s is the concentration of authigenic U-238 in pelagic sediments (weight parts), S is the average

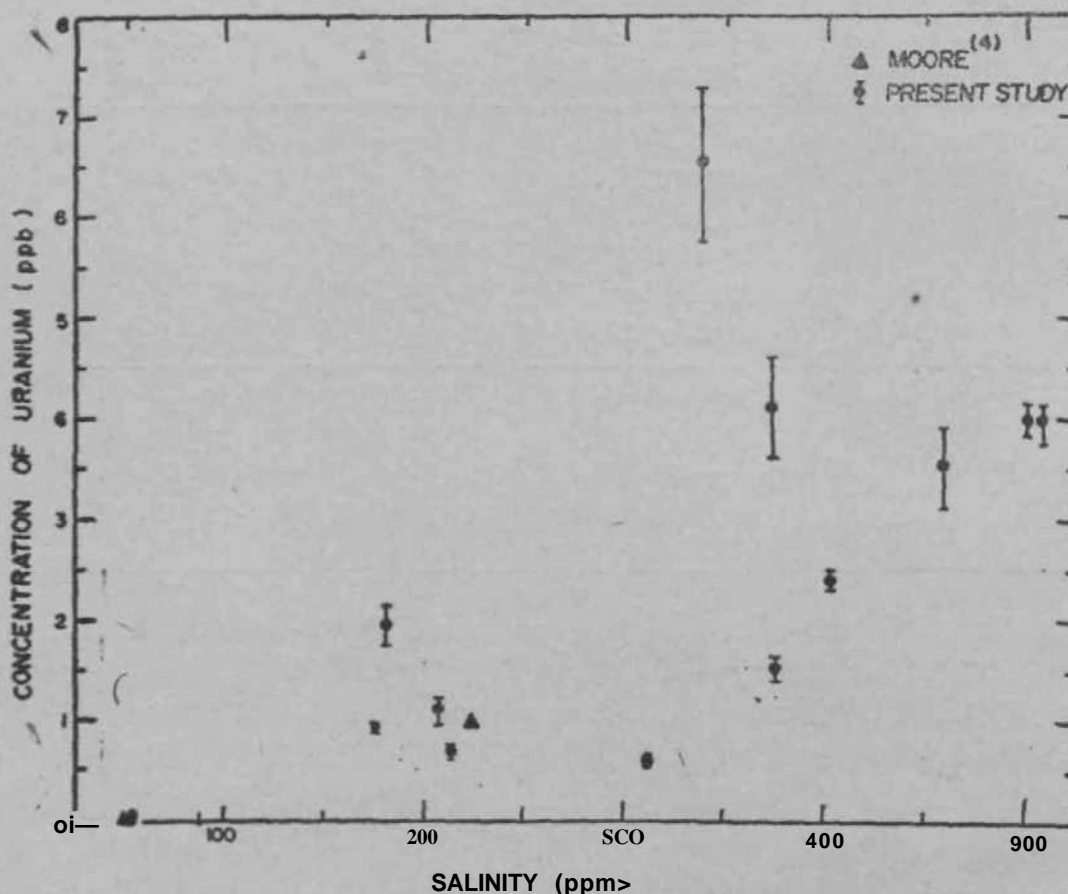


FIG. 3. Measured concentrations of uranium are plotted vs. salinity ("total dissolved salt content"). The salinity data for Amazon and Mississippi are taken from Livingstone,²⁰ those for Indian rivers are from present study.

sedimentation rate ($\text{gm}/\text{cm}^2\text{-yr.}$). The value of the proportionality constant, K_1 has been taken to be $= 3.75 \times 10^6$ yrs, assuming the commonly adopted values of 1.35×10^{21} litres for the oceanic volume and 3.6×10^{17} litres for the volume of global annual river run off.³⁰ The constant K_1 is

calculated to be 10, assuming a mean oceanic depth of 3750 metres and world average sedimentation rate of $1 \text{ gm/cm}^2 \cdot 10^3 \text{ yrs}$.

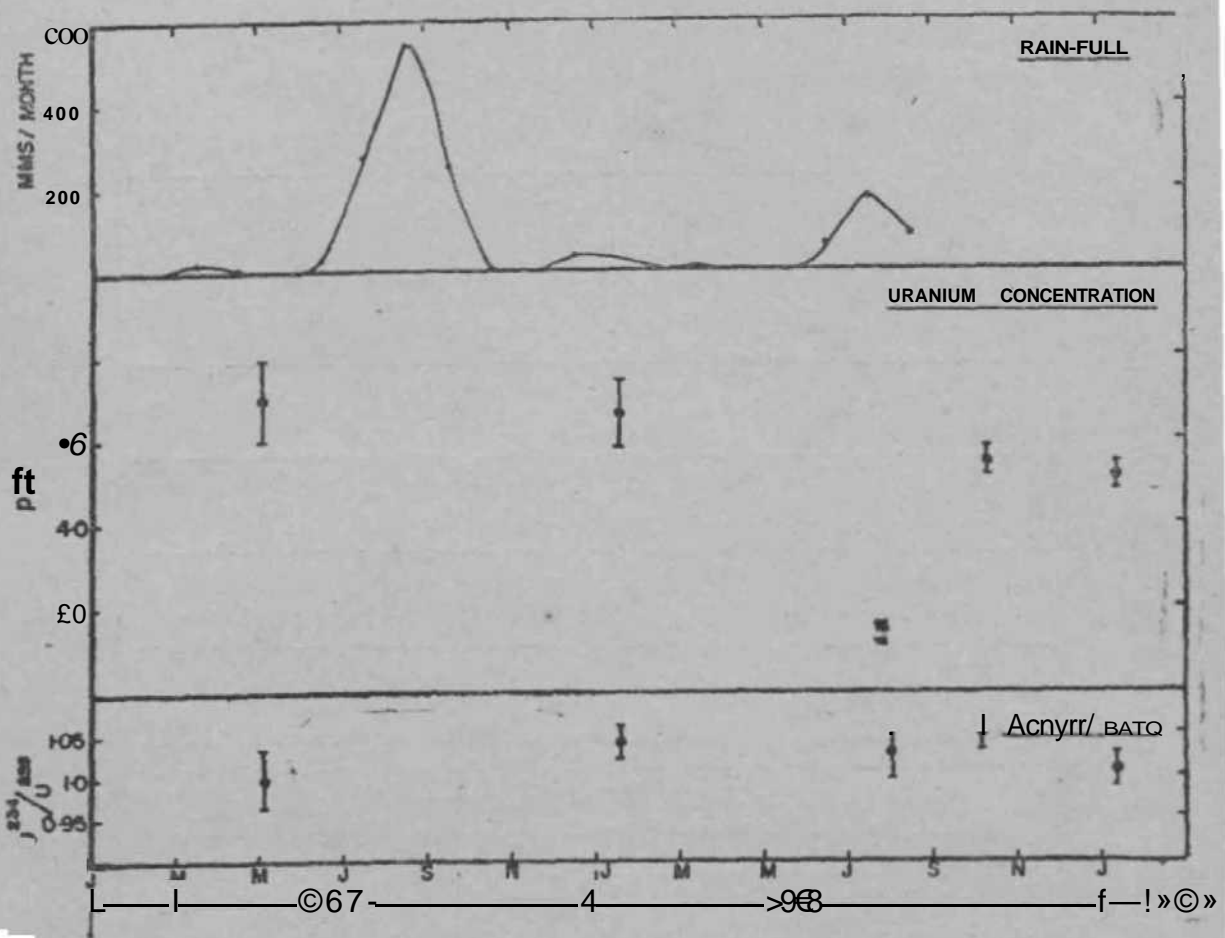


FIG. 4. Measured values of uranium concentration and activity ratios U-234/U-238, in Ganges river sample at Allahabad. The concentration of uranium is observed to decrease during the monsoon period of 1966. No samples were collected during 1967 monsoon.

Figure 5 shows the relation between equations (2), (3) and (4). The shaded bands on the axes give the ranges in the weighted mean of U-234/U-238 activity ratios for the world rivers, concentration of authigenic uranium present in deep sea sediments (based on the results of Ku³¹) and the weighted mean of U-238 concentration in rivers. From this figure it is clear that the amount of uranium depositing on the ocean floor could be explained by input from rivers, i.e., conditions given by equations (3) and (4) are not necessarily violated. However, in order to explain the uranium concentrations observed in the sea by a model in which the input is only by rivers, it becomes necessary to have U-234/U-238 activity ratios at input to exceed 1.3 (considering the upper limit of average U-238 concentration

in rivers) and to exceed 1-6 (to explain the observed concentration of authigenic uranium in deep sea sediments).

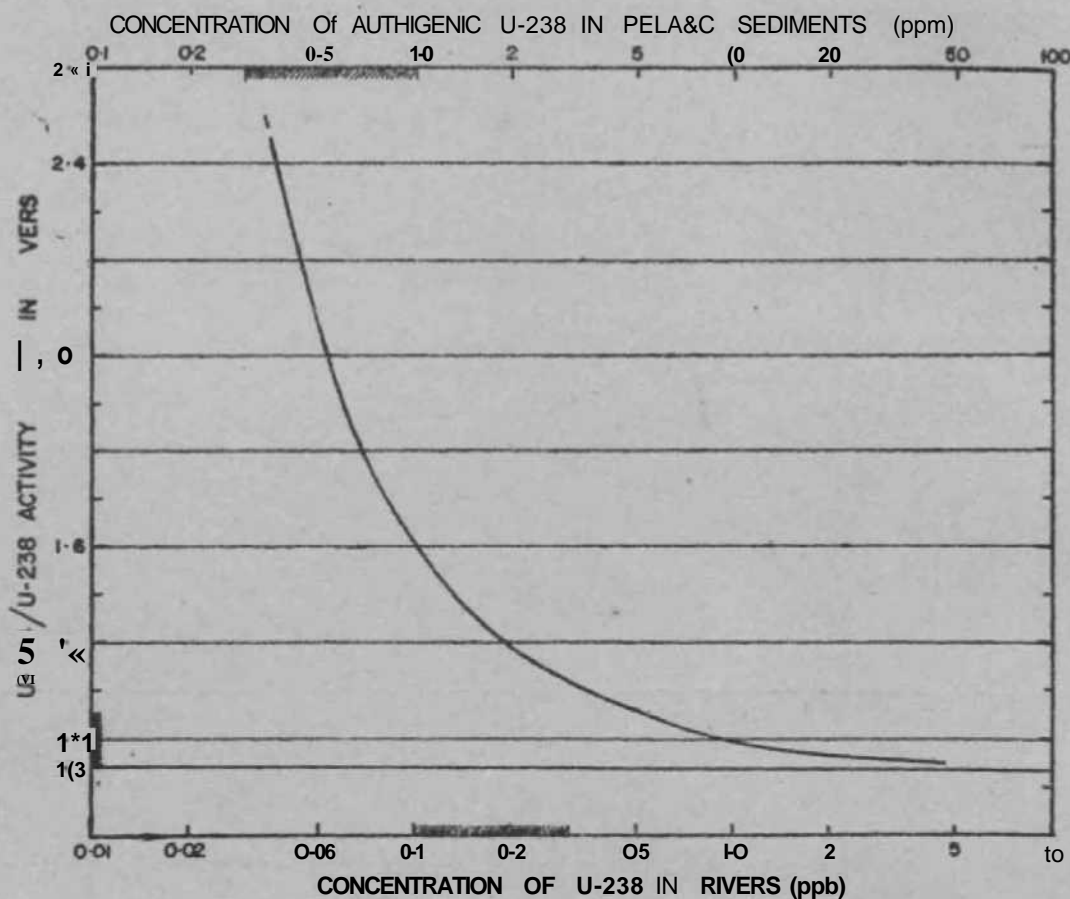


FIG. 5. Theoretically estimated correspondence between average weighted U-234/U-238 activity ratios and U-238 concentration in rivers, based on a steady state river-influx model (see equations 2 and 3). The corresponding expected authigenic U-238 concentrations in pelagic sediments are also given (cf. equation 4).

Hence there must be some other agency/mechanism which constitutes an important source of uranium in the oceans. Further in this source the U-234/U-238 activity ratio should be high (~ 2). One of the possible sources could be the migration of uranium from deep sea sediments as was suggested by Ku³¹ which is supported by the observed deficiency of U-234 in the upper layers of the sediments.³¹ ** This may be due to the fact that there has been a preferential leaching of U-234 in sediments possibly due to the difference in the chemical nature of the two isotopes.

Another possible source is the *in situ* leaching of eolian dust and river suspended load in sea-water. The quantitative aspects of both these alternatives will be discussed in detail elsewhere.¹⁷

TABLE IV

Concentrations of Ra-226 and Ra-228/Ra-226 activity ratios in Indian Rivers*

River	Location	Ra-226 (dpm/litre)	Ra-228/Ra-226 (activity ratio)
Ganges	.. Hardwar	0-20	0-78
do.	.. Nabdeep	..	1-95
Godavari	.. Rajahmundry	0-05	..
Krishna	.. Vijayawada	005	..
Sabarmati	.. Ahmedabad	009	3-40

* The statistical errors in the determination of Ra-226 are $\pm 15\%$ only 5 litre samples were analysed. The activity ratios, Ra-228/Ra-226 are reliable to $\pm 5\%$ samples of 200-400 litres were analysed.

TABLE V

Available data on the concentrations of Uranium and U-234/U-238 activity ratios for world rivers

	Uranium (ppb)	Average U-234/U-238 activity ratio	Mean discharge ⁴¹ (cu.ft./sec.) $\times 10^8$	Reference
Indian rivers	.. 001-70	1-2 (1.00-1.58)	600f	Present study
Russian rivers	1-2 (1.12-1.29)	4000	5
Amazon	.. 0-04	1.1	6000	4
Mississippi	.. 1-0	1-3	620	4

Figures in parentheses give the range.

• Livingstone.⁸⁰

t Private communication from the Officers-in-Charge, Central Water and Power Commission, New Delhi.

It may be added here that it is quite likely that a major portion of the uranium brought to the sea by rivers appears to be deposited in the shelf regions due to reducing conditions prevalent in the coastal regions.³³ If most of the riverborne uranium is deposited on the shelf, then it is required that the ratio in the additional source discussed above should have a value close to 1.5. However, if river influx effectively constitutes greater than 50% of the uranium input to open oceans, then it is necessary that the additional source should have a ratio exceeding a value of 2 or thereabouts.

(b) *Radium*.—The concentrations of Ra-226 in Indian rivers are similar to the published values for other world rivers⁴⁻¹⁵ while those of Ra-228 are at least an order of magnitude higher than the only reported value for Amazon,¹³

In Fig. 6, the Ra-226 concentrations are plotted against the $(Ca+Mg)^{3n}$ concentrations. There seems to be a linear correlation between the

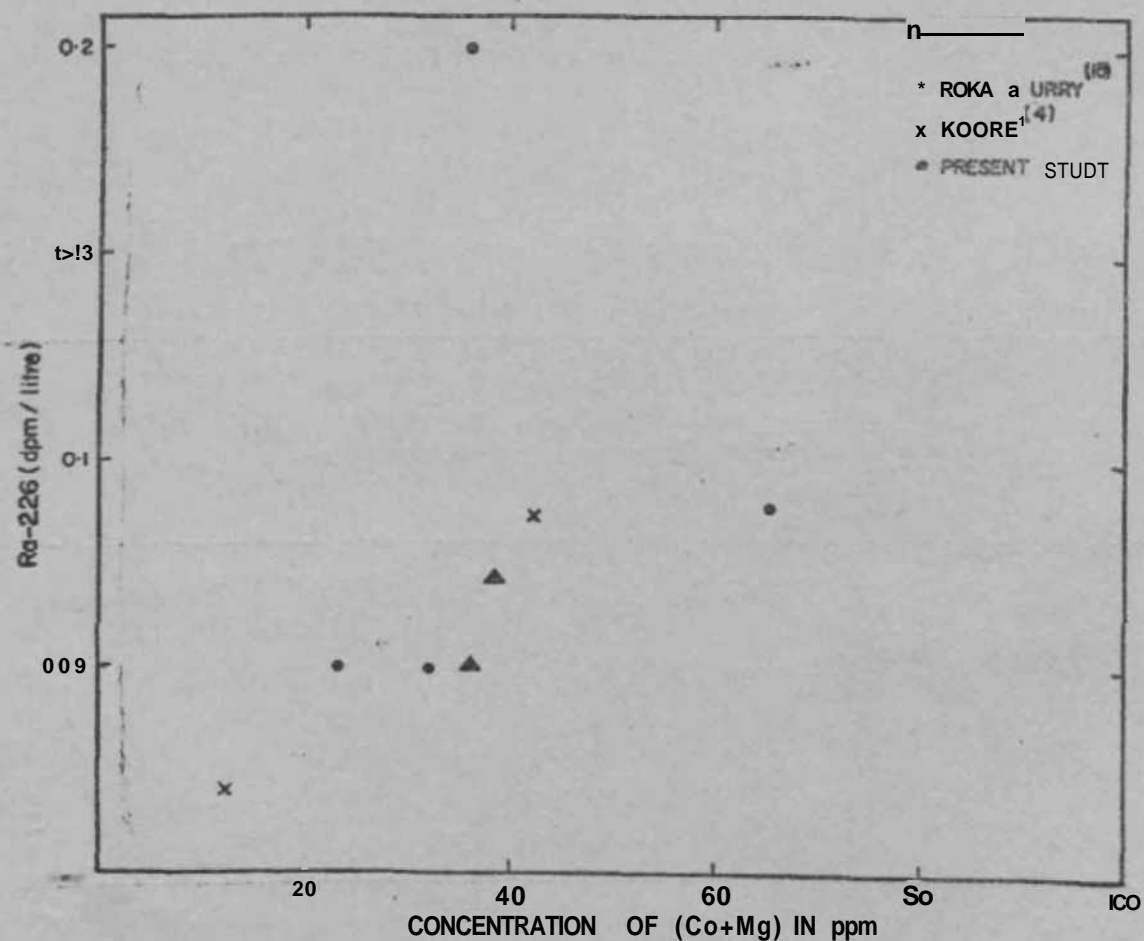


FIG. 6. Measured Ra-226 activity is plotted *versus* $(Ca + Mg)$ concentration of river. The $(Ca + Mg)$ data for Indian rivers are from present study, and for other world rivers, the data are from Livingstone.*

(Ca + Mg) and Ra concentrations which is not unexpected because of the similar behaviour of the alkaline earth elements.

Proceeding in a manner similar to that adopted for uranium and taking the respective mean lives of the radionuclides, Ra-226 and Ra-228 as the upper limits for their residence times in the oceans, it is seen that the observed concentration of these isotopes in rivers fall short by factors of 30 and 10 respectively to explain their observed sea-water concentrations. Once again we note that one cannot satisfactorily make a material balance in these cases. For the long-lived Ra-226, the observed concentrations in sea-water could be explained away in terms of diffusion from deep sea sediments, a mechanism proposed by Koczy.³⁴ However, in the case of Ra-228 which has a short half-life, the observed concentrations in the upper layers of the oceans¹³ cannot be due to diffusion from deep sea sediments.

ACKNOWLEDGEMENTS

We wish to express our gratitude to Professor D. Lai, for the guidance and encouragement throughout the study. We are indebted to Profs. E. D. Goldberg and Rama for critical discussions and suggestions. We are grateful to Dr. V. T. Athavale of B.A.R.C, Trombay, for carrying out the determination of the major cations and anions in river water samples.

We thank the officers-in-charge of Meteorological Department at Allahabad and Trichinapalli for providing us with water samples during different seasons.

We acknowledge the skilful assistance of **Mr. P. K. Talekar** during some phases of the work; and thank **Mr. P. B. Badle** for his **help in one** of the field trips.

REFERENCES

1. Cherdyntsev, V. V., Orlov, D. P., Isabaev, E. A. and Ivanov, V. I. *Geokhimiya*, 1961, 10, 840.
2. Thurber, D. L. .. *J. Geophys. Res.*, 1962, 67, 4518.
3. Koide, M. and Goldberg, E. D. In "*Progress in Oceanography*" editor M. Sears, Pergamon Press, Oxford and New York, 1965, 3, 173.
4. Moore, W. S. .. *Earth Planet, Sci. Let.*, 1967, 2, 231.
5. Kazachevskii, I. V., Cherdyntsev, V. V., Kau'mina, E. A., Sulerzhitskii, L. D., Mochalova, V. F. and Kyuregyan, T. N. *Geokhimiya*, 1964, 11, 1116.

6. Sarma, T. P. and Krishna- moorthy, T. M. *Curr. ScL*, 1968, 37, 422.
7. Veeh, H. H. .. *Geochim. Cosmochim. Acta*, 1968, 32, 117.
8. Moore, W. S. and Sackett, W. M. *J. Geophys. Res.*, 1964, 69, 5401.
9. Somayajulu, B. L. K. and Goldberg, E. D. *Earth Planet Set. Let*, 1966, 1, 102.
10. Sackett, W. M. .. *Science*, 1960, 132, 1761.
11. Bhat, S. G., Krishnaswamy, S., Lai, D, Rama and Moore, W S. *Earth Planet ScL Let.*, 1969, 5, 483.
12. Broecker, W. S. .. *Science*, 1967,158, 1307.
13. Moore, W. S. .. *J. Geophys. Res.*, 1969. 74, 694.
14. Drozhzhin, V. M., Lazarev, K. F. and Nikolaev, D. S. *Radiokhimiya*, 1965, 7, 374.
15. Rona, E. and Urry, W. D. *Am. J. ScL*, 1952, 250, 242.
16. Koczy, F. F., Tomic, E. and Hecht, F. *Geochim. Cosmochim. Acta*, 1957, 11, 86.
17. Bhat, S. G., Krishnaswamy, S. and Lai, D. In preparation.
18. Serebryakova, M. B. .. *Geokhimiya*, 1964, 9, 926.
19. Grindler, J. E. .. *The Radiochemistry of Uranium*, NAS-NS-3050, 1962.
20. Dement'ev, V. S. .. *Radiokhimiya*, 1957, 9, 156.
21. Urgell, M., Bustamente, J. A. P., Rodriguez, T. B., de la Cruz, F. and Cellini, R.F. *Proc. 2nd Intl. Conf. Peaceful Uses of Atomic Energy*, held in Vienna, 1958, 3, 444.
22. Bhat, S. G. .. *M.Sc. Thesis*, Bombay University (1969), in preparation.
23. Broecker, W. S. .. *Proc. "Symposium on Diffusion in Oceans and Freshwaters"* held in Palisades, New York, 1964, p. 116.
24. Lai, D. and Schink, D. R. *Rev. ScL lustrum.*, 1960, 31, 395.
25. Pillai, K. C, Ganapathy, S., Desai, M. V. M. and Ganguly, A. K. *Atomic Energy Establishment Trombay Report*, AEET/H.P./R-13, 1966.,
26. Krishnan, M. S. .. *Introduction to the Geology of India*, Higginbothams (Private) Ltd., Madras, 1958.
27. Shah, R. K., Trivedi, A. M. and Vora, J. C. *Journal of Gujarat University (Vidya)*, 1962. 5, 1963.
28. Officers-in-Charge, Central Water and Power Commission, New Delhi Personal Communication.

29. Menard, H. W. and Smith, S. M. *J. Geophys. Res.*, 1966, 71, 4305.
30. Livingstone, D. A. .. *Data of Geochem., Geol Survey*, Prof. Paper 440, Chapter G, 1963.
31. Ku, T.L. .. *J. Geophys. Res.*, 1965, 70, 3457.
32. Somayajulu, B. L. K. .. Unpublished results.
33. Veeh, H.H. .. *Earth Planet Sci. Let.*, 1967, 3, 145.
34. Koczy, F.F. .. *Proc. 2nd Intl. Conf Peaceful Uses of Atomic Energy*, held in Vienna, 1958, 18, 351.

SORPTION-DESORPTION HYSTERESIS IN FIBROUS SILICA GEL (SANTOCEL C) WITH ISOMERIC MONOHYDRIC ALIPHATIC ALCOHOLS

BY K. SUBBA RAO AND BHAGWAN DAS

[Chemistry Department, Birla Institute of Technology and Science, Pilani (Rajasthan)]

Received September 30, 1968

(Communicated by Dr. B. Sanjiva Rao, F.A.S.C.)

ABSTRACT

By employing the quartz fibre spring technique, sorption-desorption hysteresis at 35° has been studied of Iso-propyl, Iso-Butyl, Sec-Butyl, Tert-Butyl, Active Amyl and Iso-Amyl alcohols on fibrous silica gel (Santocel C) activated at 250°. The isotherms of all the alcohols have clearly defined "knees". By the application of BET theory, the monolayer capacities are determined. Knowing the specific surface area of fibrous silica gel, assuming oriented sorption of the isomeric alcohols with the OH group attached to surface; the cross-sections of the alcohol molecules are calculated. Excepting Iso-Propyl and Sec-Butyl alcohols, all others have cross-sections greater than that of normal aliphatic alcohols. These higher values are to be expected in view of the side CH₃ groups. The exceptional behaviour of Iso-Propyl and Sec-Butyl alcohols is not clear.

Permanent and reproducible hysteresis loops have been obtained in all the cases. Cohan's theory of hysteresis cannot explain the observations satisfactorily. Cavity theory however explains all the cases of hysteresis. The shapes of the isotherms of the different alcohols in the high relative vapour pressure region indicate a variation in contact angles of the alcohols.

INTRODUCTION

FIBROUS Silica Gel of trade name Santocel C has been used in earlier studies¹ on the sorption and desorption hysteresis of normal aliphatic alcohols. -In all the systems studied permanent and reproducible hysteresis loops are obtained. The surface area calculated from monolayer capacity for each alcohol reveals oriented type of sorption in the monolayer.

The present studies have been made with isomeric monohydric aliphatic alcohols with fibrous silica gel. The specific surface of fibrous silica, gel

activated at 250° for 2 hr. has been determined in the earlier investigation¹ by measuring monolayer capacity for the normal aliphatic alcohols and assuming oriented sorption of alcohol molecules perpendicular to surface. Assuming this value of specific surface and oriented sorption of isomeric alcohols on the surface of fibrous silica gel, the cross-sections of the alcohol molecules are calculated and are presented in this paper.

EXPERIMENTAL

The Santocel C obtained from the Monsanto Company, U.S.A., was heated to 250° for 2 hr. in order to remove any organic vapours and the activated gel was used in sorption and desorption studies.

The following sorbates were employed:

Iso-propyl alcohol, B.D.H. (British Drug House), A.R., redistilled, B.P. 82·0°.

Iso-butyl alcohol, B.D.H., A.R., redistilled, B.P. 107·0°.

Sec-butyl alcohol, Basic and Synthetic Chemicals (India), A.R. grade, redistilled, B.P. 97·0°.

Tert-butyl alcohol, B.D.H., L.R., redistilled, B.P. 82·5°.

Active amyl alcohol, E.Merck, E.P., redistilled, B.P. 129·0°.

Iso-amyl alcohol, B.D.H., L.R., redistilled; B.P. 131·0°.

Quartz Fibre Spring Technique

The quartz fibre spring technique employed in the present work has been described in the earlier investigations of the authors.^{2*3}

RESULTS AND DISCUSSIONS

A series of sorptions and desorptions were carried out with Iso-Propyl, Iso-Butyl, Sec-Butyl, Tert-Butyl, Active Amyl and Iso-Amyl alcohols on fibrous silica gel. The experiments were done at 35°. Duplicate experiments were done but the results of one experiment have been given. In all the cases, permanent and reproducible hysteresis loops have been obtained and the loops have been reproduced upto 3rd or 4th cycle of sorption and desorption. The results are shown in Figs. 1-6. The permanent and reproducible hysteresis loops of the different alcohols obtained in the 3rd or 4th cycle have been shown together in Fig. 7 for purpose of comparison by plotting the sorption values against the relative vapour pressure.

In all the systems, except for a small initial sorption due to monolayer formation, the isotherms are practically horizontal and show no appreciable increase in sorption upto relative vapour pressure of about 0.75. In the light of capillary condensation theory of sorption, this indicates the absence of micropores and even the transitional pores as per Dubinin's classification.⁴

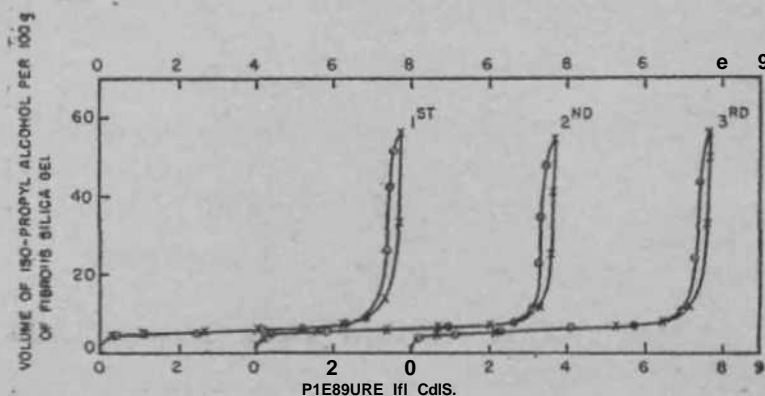


FIG. 1. Sorption and desorption of Iso-Propyl alcohol on fibrous silica gel in 1st, 2nd and 3rd cycles.

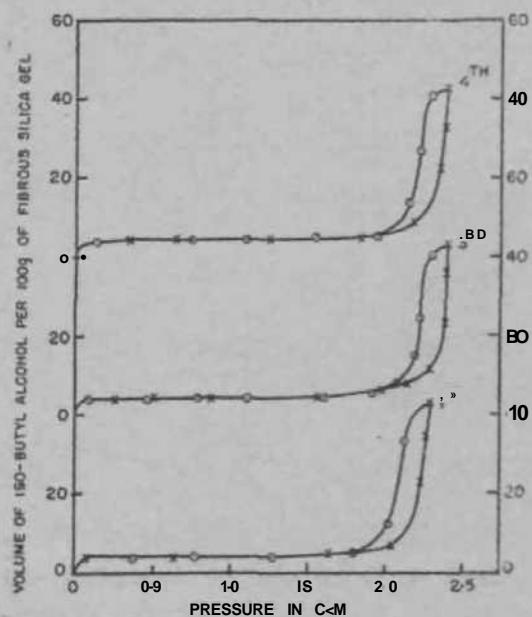


FIG. 2

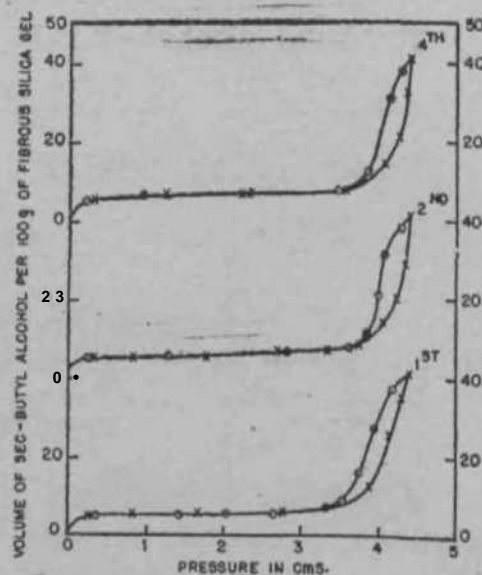


FIG. 3

FIG. 2. Sorption and desorption of Iso-Butyl alcohol on fibrous silica gel in 1st, 3rd and 4th cycles.

FIG. 3. Sorption and desorption of Sec-Butyl alcohol on fibrous silica gel in 1st, 2nd and 4th cycles.

The sorption isotherms have clearly defined "knees" followed by linear sorption. According to BET⁵ theory the "knee" signifies the transition

from monomolecular to multimolecular sorption. Therefore the BET equation has been applied to obtain the monolayer capacity x_m in each case. The BET plots were straight lines.

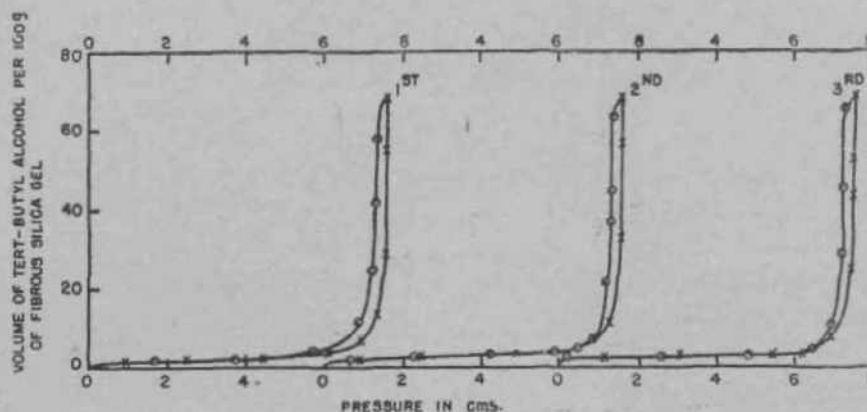


FIG. 4. Sorption and desorption of Tert-Butyl alcohol on fibrous silica gel in 1st, 2nd and 3rd cycles.

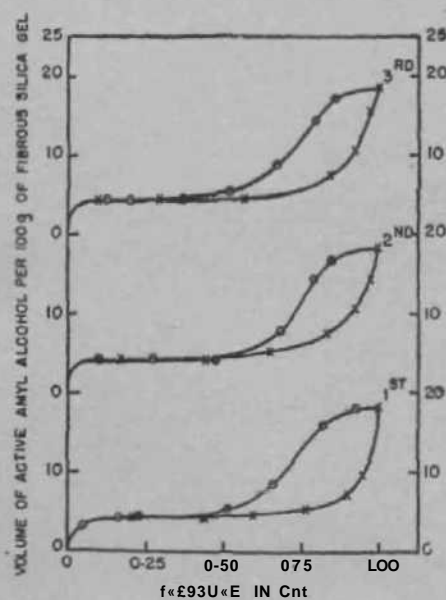


FIG. 5

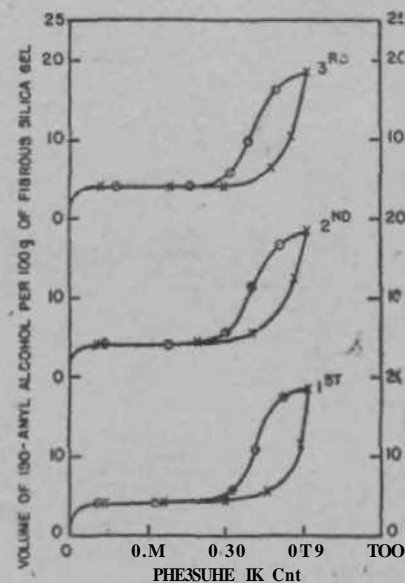


FIG. 6

FIG. 5. Sorption and desorption of Active Amyl alcohol on fibrous silica gel in 1st, 2nd and 3rd cycles.

FIG. 6. Sorption and desorption of Iso-Amyl alcohol on fibrous silica gel in 1st, 2nd and 3rd cycles.

Alternatively, the value of monolayer capacity can also be read out directly from the isotherms with reasonable accuracy.^{6,7} The isotherms of pll alcohols display long straight portion after the "knee". The point at

which the linear portion begins is termed point B and indicates the completion of the monolayer'. The sorption at point B is the monolayer capacity x_B . The value of x_B for each system has been taken directly from the isotherm.

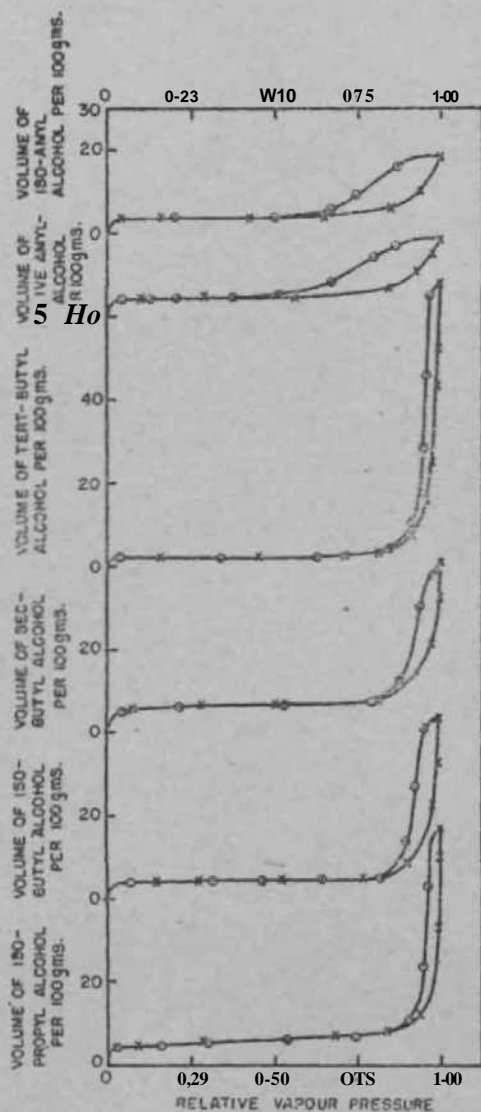


FIG. 7. Sorption and desorption of fibrous silica gel of Iso-Propyl, Iso-Butyl, Sec-butyl, Tert-butyl, Active Amyl and Iso-Amyl alcohols.

The value of monolayer capacities x_m and x_B for the isomeric alcohols and the relative vapour pressures at which the monolayers are fully formed have been given in Table I.

The values of x_m and x_B for each alcohol are almost same. However, there is variation in relative vapour pressures of the different alcohols at which the monolayer is complete,

TABLE I

Monolayer capacities x_m and x_B^ in g. per g. of sorption and the corresponding relative vapour pressure*

	x_m	x_B^*	PIP_0
Iso-Propyl alcohol ..	0.040	0.039	0.10
Iso-Butyl alcohol ..	0.029	0.031	0.13
Sec-Butyl alcohol ..	0.041	0.040	0.09
Tert-Butyl alcohol ..	0.013	0.015	0.05
Active Amyl alcohol..	0.039	0.037	0.20
Iso-Amyl alcohol ..	0.029	0.032	0.15

Monolayer Capacity and Specific Surface

From the monolayer capacity, the specific area of the surface of the sorbent is calculated by the equation⁸:

$$S = \frac{x_m \cdot N \cdot A_m}{M} \times 10^{-20}$$

where

S = Specific surface in $m^2/g.$ of sorbent,

x_m = Monolayer capacity in g. of sorbate per g. of sorbent,

M = Molecular weight of sorbate,

N = Avogadro's constant,

A_m = Molecular cross-section of sorbate in Å^2 .

In the earlier work¹ on the sorption and desorption of normal pionic aliphatic alcohols on fibrous silica gel the specific surface area of the gel has been calculated by assuming oriented sorption of the linear alcohol molecules perpendicular to surface in the monolayer and is found to be $58 m^2/g.$ Assuming this value of the specific surface and also oriented sorption of the isomeric aliphatic alcohol molecules with OH group on the surface of fibrous silica gel, the molecular cross-sections of the isomeric aliphatic alcohols have been calculated and are shown in Table II,

The cross-section of the normal aliphatic alcohol molecules is also given in the table to facilitate comparison.

TABLE II

Molecular cross-sections in A^2 of isomeric alcohol molecules taking the specific surface area of fibrous silica gel as $58 m.^2lg.$

Alcohol	Molecular cross-section in A^2
Iso-Propyl alcohol	.. 14-5
Iso-Butyl alcohol	.. 25-0
Sec-Butyl alcohol	.. 17-4
Tert-Butyl alcohol	.. 55-5
Active Amyl alcohol	.. 22-0
Iso-Amyl alcohol	.. 28-8
Normal aliphatic alcohols (Taken from earlier work ¹)	.. 20-7

The cross-section of the hydrocarbon chain in normal aliphatic alcohols is $20-7 A^2$. Excepting Iso-Propyl and Sec-Butyl alcohols the molecular cross-sections of the isomeric alcohols are higher than $20-7 A^2$. This is to be expected in view of the presence of side CH_3 groups and that isomeric alcohols are not linear in structure unlike normal aliphatic alcohols. That Tertiary Butyl alcohol has the biggest cross-section, i.e., $55-5 A^2$ is a significant finding. This is to be expected as its molecule has 3 side CH_3 groups and is non-linear in structure. The cause of the low values of molecular cross-sections of Iso-Propyl and Sec-Butyl alcohols is not clear.

A search of the literature was made for data on molecular cross-sections of the isomeric alcohols and these could not be obtained.

Sorption-Desorption Hysteresis

All the isomeric alcohols have given permanent and reproducible hysteresis loops. Equilibrium was established within an hour but actually 2 hours were allowed to ensure complete equilibrium. The amounts taken at saturation pressure of Isp-Propyl, Iso-Butyl, Sec-Butyl, Tert-Butyl, Active Amyl

and Iso-amyl alcohols are 56.5, 42.8, 41.5, 68.1, 18.8 and 18.5 cm.³ per 100 g. of fibrous silica gel respectively. The amounts taken of H-Propyl, w-Butyl and n-Amyl alcohols are 38.7, 19.0 and 21.0 cm.³ per 100 g. of gel reported in the previous paper.¹ Excepting the isomers of Amyl alcohol, the sorption values of which at saturation pressure are slightly less than that of H-Amyl alcohol, the saturation values of Propyl and Butyl isomers are 1.5 to 3 times higher than the normal alcohols.

Two theories—Cohan's theory and Cavity theory—have been advanced so far to explain sorption-desorption hysteresis.

Cohan's Theory

Cohan has⁹ explained sorption-desorption hysteresis in terms of the difference in shapes of the meniscus during sorption and desorption—hemispherical in desorption and cylindrical in the initial stages of sorption. In desorption, Kelvin theory of evaporation of liquid from the capillary is assumed but in sorption a cylindrical film of liquid is first formed and next the capillary is filled with liquid as the pressure increases. Assuming this mechanism, he has shown that for a capillary of particular radius, capillary condensation along the sorption branch occurs at a higher relative vapour pressure than capillary evaporation along the desorption branch, thus accounting for hysteresis. He has also shown that pressure p_h at which hysteresis loop begins corresponds to the equilibrium pressure for $r_c = 2D$ where r_c is the radius of the capillary and D is the diameter of sorbate molecule. On the basis of Cohan's theory the value of D is given by the equation

$$D = \frac{-\sigma M}{dRT \ln \frac{p_h}{p_0}}$$

where

M = Molecular weight of sorbate,

d = Density of sorbate,

σ = Surface tension of sorbate.

By applying Cohan's theory to our results, the values of D obtained are shown in Table III. The values of D_{cubic} and $D_{\text{spherical}}$ are also shown to facilitate comparison. $D_{\text{spherical}}$ is calculated from the equation,¹⁰

$$P = 1.33 \times 10^{-8} \times V_m^*$$

where V_m = molecular volume and D_{cubic} from molecular weight and density.

Table III reveals that the molecular diameters D calculated from Cohan's theory are very much higher and vary from 3 to 10 times the values of $D_{\text{apherical}}$. These indicate the limitations of Cohan's theory of hysteresis.

TABLE III

Molecular diameters Z_{cubic} Apherical and D from Cohan's theory in A

	D_{cubic}	$D_{\text{apherical}}$	$D_{\text{cohan's theory}}$
Iso-Propyl alcohol ..	4-3	5-7	60-4
Iso-Butyl alcohol ..	4-5	6-0	38-6
Sec-Butyl alcohol ..	4-5	6-0	40-6
Tert-Butyl alcohol ..	4-6	6-1	50-5
Iso-Amyl alcohol ..	4-8	6-4	5-1

Cavity Theory

According to cavity theory,^{2,3, n} a cavity is a capillary with a constricted neck and may have two or more necks. Filling of these cavities during sorption is progressive whereas emptying during the desorption is sudden and abrupt. The two processes are not coincident. Certain amount of sorbate is entrapped in the cavity during desorption, thus accounting for hysteresis.

The cavity theory alone has been successful in explaining the hysteresis effect and all its allied phenomena such as Drift,^{2,12} Disappearance of the hysteresis loop with solvating liquids,^{2,3,13,16} permanence and reproducibility of the hysteresis loop^{2,17} and Scanning of the loop.^{2,17-19} The approach so far has been qualitative and no quantitative formulation of the theory has been made.

Possible Effect of Contact Angle on the Shape of Sorption and Desorption Isotherms

As in the case of normal aliphatic alcohols,¹ there is marked variation in the size and shape of the isotherms and the hysteresis loops of the iso-

meric alcohols. The isotherms of Tert-Butyl, Iso-Propyl and Iso-Butyl alcohols rise practically asymptotic to the saturation pressure ordinate whereas Sec-Butyl, Iso-amyl and Active Amyl alcohols cut the saturation pressure ordinate at an angle.

Gregg²⁰ has discussed the effect of contact angle of the sorbate on the shape of the isotherm. Ordinarily, in the application of Kelvin equation to the study of the isotherm, the contact angle is assumed to be zero when the surface is pure and free from impurities. This is true of liquids like water which wet the surface, but with liquids which have definite contact angles, the isotherms intersect the ordinate at an angle.

A search of the literature on contact angle was made but the values could not be obtained for isomeric monohydric alcohols. Fox and Zisman²¹ have shown that for many of liquids on solids, the contact angle decreases with decreasing surface tension of the liquid. The values of surface tension^{22*23} of the Tert-Butyl, Iso-Propyl, Iso-Butyl, Sec-Butyl and Iso-Amyl alcohols are 18-8, 20-5, 21-8, 22-2 and 22-7 dynes per cm. at 35° respectively. In the light of Fox and Zisman's conclusion, the contact angles of these alcohols should be in the order Tert-Butyl < Iso-Propyl < Iso-Butyl < Sec-Butyl and < Iso-Amyl alcohol. It is interesting to note that the sorption values at saturation pressure of these alcohols vary in the reverse order Tert-Butyl 68-1% > Iso-Propyl 56-5% > Iso-Butyl 42-8% > Sec-Butyl 41-5% > Iso-Amyl 18-5%. In other words sorbates of low contact angles have the isotherms, rising asymptotically to the saturation pressure ordinate, and high sorption values at saturation pressure, Whereas sorbates of high contact angles have isotherms cutting the saturation pressure at an angle, and low sorption values.

The value of the surface tension of Active Amyl alcohol was not available. But from the shape of the isotherm it follows that the contact angle of Active Amyl alcohol is nearly equal to that of Iso-Amyl alcohol.

ACKNOWLEDGEMENTS

The authors are grateful to Prof. V. Lakshminarayanan, Director, for kind encouragement and facilities in the work, the Ministry of Education, Government of India, for financial help of a Research Training Scholarship to one of the authors (BD) and Monsanto Company, Missouri, U.S.A., for supplying a gift sample of Saptocel C.

REFERENCES

1. Subba Rao, K. and Das, B. *Curr. Sci.*, 1968, 37, 274.
2. Subba Rao, K. .. *Phys. Chem.*, 1941, 45, 500-39.
3. _____ and Das, B. .. *Ibid.*, 1968, 72, 1223.
4. Dubinin, M. M. .. *Quart. Rev. Chem. Soc.*, 1959, 9, 101; *Chem. Rev.*, 1960, 60, 235.
5. Brunauer, S., Emmett, P. H. *J. Am. Chem. Soc.*, 1938, 60, 309.
and Teller, E.
6. Emmett, P. H. and Brunauer, S. *Ibid.*, 1937, 59, 1553.
7. Gregg, S. J. and Sing, K. S. W. *Adsorption, Surface Area and Porosity*, Academic Press, London and New York, 1967, p. 54.
8. _____.. *Ibid.*, 1967, p. 65.
9. Cohan, L. H. .. *J. Am. Chem. Soc.*, 1938, 60, 433.
10. Moelwyn-Hughes, E. A. .. *Kinetics of Reactions in Solutions*, Clarendon Press, Oxford, 1947, p. 7.
11. McBain, J. W. .. *J. Am. Chem. Soc.*, 1935, 57, 699.
12. Subba Rao, K. .. *Curr. Sci.*, 1939, 8, 546.
13. _____.. *Ibid.*, 1940, 9, 19.
14. Subba Rao, G. N., Subba Rao, K. and Sanjiva Rao, B. *Proc. Ind. Acad. Sci.*, 1947, 25, 221.
15. Subba Rao, K., Bhimasena Rao, M. and Sanjiva Rao, B. *Proc. Nat. Inst. Sci. (India)*, 1949, 15, 41.
16. _____, Vasudeva Murthy, A. R. and Sanjiva Rao, B. *Ibid.*, 1950, 16, 1.
17. Subba Rao, K. .. *Proc. Ind. Acad. Sci.*, 1942, 16, 301.
18. _____.. *Curr. Sci.*, 1939, 8, 468.
19. _____.. *Proc. Ind. Acad. Sci.*, 1942, 16, 298.
20. Gregg, S. J. and Sing, K. S. W. *Adsorption Surface Area and Porosity*, Academic Press, London and New York, 1967, pp. 153-54.
21. Fox, H. W. and Zisman, W.A. *J. Colloid. Sci.*, 1950, 5, 514; 1952, 7, 109.
22. Timmermans, J. .. *Physico-chemical Constants of Pure Organic Compounds*, Elsevier Publishing Co., Inc., 1950,
23. *International Critical Tables*, 1928, 4, 453.

ELECTRON SPIN RESONANCE OF Cr^{5+} IN CaWO_4 *

BY K. V. LINGAM, P. G. NAIR AND B. VENKATARAMAN

(Tata Institute of Fundamental Research, Homi Bhabha Road, Bombay-5)

Received April 15, 1969

(Communicated by Prof. B. V. Thosar, F.A.S.C.) .

ABSTRACT

Electron Spin Resonance of CaWO_4 with 0-1% of Cr has been investigated at liquid nitrogen and liquid helium temperatures. The observed ESR spectrum is attributed to Cr^{5+} ion in the substitutional site of W which has a compressed tetrahedral surroundings. A simple point charge calculation based on this geometry explains the observed g anisotropy and hyperfine anisotropy and places the magnetic electron in a predominantly $3d_{3/2}$ orbital. A comparison of these results with those obtained on other isoelectronic systems in similar and different co-ordinations justifies our assignment.

INTRODUCTION

ELECTRON Spin Resonance (ESR) studies on ions with d^1 configuration have been less extensive compared to other configurations with f -electrons. Azarbayejani and Merlo¹ have studied Mo^{5+} in CaWO_4 and found that $S_n > 8JL$ and $A_n < A_j$, a result that is inconsistent with observations on Mo^{5+} in glass and in TiO_2 .^{2,3} It has been suggested by them that other isoelectronic systems like Cr^{6+} and W^{5+} should also be investigated. ESR of Cr in CaWO_4 has been reported earlier by Kedzie *et al.*⁴ who first interpreted the resonance to be from an excited state. A later paper by the same authors⁵ proposes that the ESR spectrum arises from the ground state of Cr^{5+} in the W^{6+} site of CaWO_4 . To our knowledge no detailed analysis of the spectra has appeared. Our preliminary results on Cr^{6+} in CaWO_4 ,⁶ at liquid nitrogen and helium temperatures indicated that the ESR spectrum arises from the ground state of d^1 configuration; also our line widths are larger than those observed by Kedzie *et al.*⁵ Recently, Banks, Greenblatt and McGarvey⁷ have investigated the ESR spectrum of CrO_4^{3-} in single crystals of $\text{Ca}_2\text{PO}_4\text{Cl}$ and have demonstrated the ground state of Cr^{5+} at the centre of a distorted tetrahedron to be one in which the unpaired electron is in a $3d_{z^2}$ orbital which is largely concentrated on the chromium ion.

In this paper we have confirmed our preliminary results,⁶ and have put forward detailed arguments to show that the observed ESR spectrum arises from Cr^{5*} substituted in the distorted tetrahedral site of W^{6+} in CaWO_4 . In the preliminary report⁶ W-site for Cr^{5*} was favoured only on the basis of greater ease of charge compensation as compared with Ca-site and additional reasons are given in this paper to support this assignment. The ground state of Cr^{5+} is argued on the basis of analysis of ξ -values, g_n and g_{X9} and hyperfine constants, A_M and A_j , to be one in which the unpaired electron is in a d_z^* orbital in agreement with the results on Cr^{5*} in $\text{Ca}_3\text{PO}_4\text{Cl}$.⁷

EXPERIMENTAL RESULTS

The CaWO_4 crystal doped with a nominal concentration of 0-1% Cr were obtained from Semi Elements.⁸ The crystal was dark green in colour in contrast to the yellow colour observed for Cr^{64+} in CaWO_4 .⁹ The measurements were made using an X-band superheterodyne spectrometer built in our laboratory.¹⁰ A cylindrical cavity operating in TEM mode was used for measurements at liquid nitrogen and liquid helium temperatures. A rotating Varian 12" magnet (VA 3606) with a Fieldial power supply (VFR 2501) provided the magnetic field. A transistorised proton probe placed near the cavity was used to measure the magnetic field. The microwave frequency and proton resonance frequencies were measured using a Hewlett Packard counter-converter combination.

At room temperature the crystal showed an ESR spectrum which could be attributed to Mn^{24+} impurity. The Mn^{2+} spectrum in CaWO_4 has been examined by Hempstead and Bowers¹¹ and by Kedzie and co-workers.¹² The latter authors have pointed out that the linewidths of the Mn^{2+} spectrum are strongly anisotropic and have also analysed the forbidden transitions. These forbidden transitions were also observed by us and were used to align the crystal. When the magnetic field is along the principal axes the forbidden transition lines should not be seen. Figure 1 is the derivative of the ESR spectrum obtained from our sample at 77° K when the magnetic field is along the tetragonal axis; a broad anisotropic line is observed along with the Mn^{th} lines. At 4-2° K the broad line narrowed and four weak satellites of equal intensity appeared with their centre falling on the centre of the main line. The separation between the satellites is maximum when the magnetic field is in a plane perpendicular to the tetragonal axis of the crystal. When the magnetic field is along the tetragonal axis the satellites could not be resolved as they merge with the main line. The satellites are identified as arising from the hyperfine interaction with the odd isotope

Cr^{5+} ($I = 3/2$) occurring with a natural abundance of 9-54%. Figure 2 shows the derivative of the ESR spectrum at 4.2°K with the magnetic field perpendicular to the tetragonal axis. Many other resonances were observed at 4.2°K and these are presumably from rare-earth impurities present in the crystal.

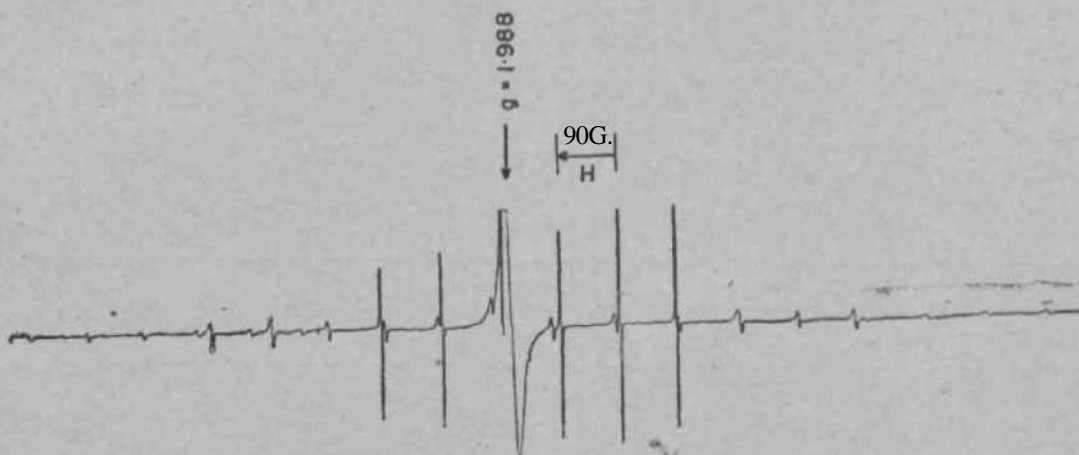


FIG. 1. Derivative of the ESR spectrum of $\text{CaWO}_4\text{:Cr}^{5+}$ at 17 K ; H parallel to c -axis. The intense broad line at the centre is due to Cr^{5+} , the others are from Mn^{2+} .

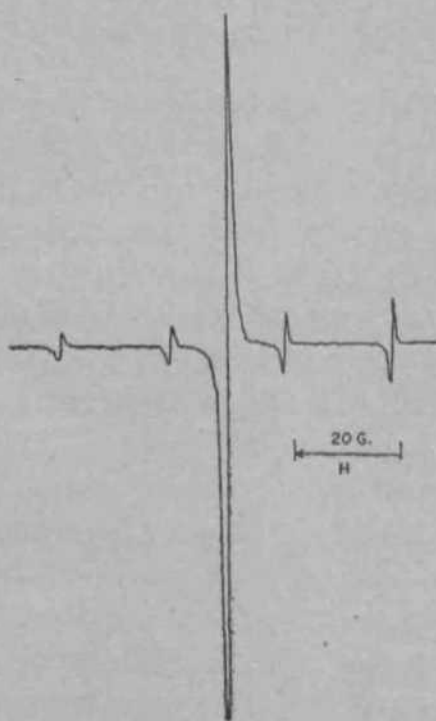


FIG. 2. Derivative of the ESR spectrum of $\text{CaWO}_4\text{:Cr}^{5+}$ at 4.2°K ; H perpendicular to c axis.

The observed resonance could be described with a spin Hamiltonian with axial symmetry and effective spin 1/2. The explicit form is

$$\mathcal{H} = S' n \bar{P} \bar{H} \bar{g} \bar{S} \bar{g} + S x P' (\bar{H} \bar{x} \bar{S} \bar{x} - r' \bar{H} \bar{y} \bar{S} \bar{y}) - p' \bar{H} \bar{z} \bar{S} \bar{z} + r' A J, \bar{V} \bar{S} \bar{I} \bar{x} + \bar{g} \bar{y} \bar{I} \bar{y} \quad (i)$$

Table I compares our values for the parameters in Eq. (1) with those of Kedzie and co-workers.⁵ We could observe a broad resonance at 77° K while they could not observe any resonance attributable to Cr⁵⁺ above 50° K,

TABLE I

Spin-Hamiltonian parameters for Cr⁵⁺ in CaWO₄

g _u	g _l	A _n	A [^]	Temp.	Reference
1-988	1-943	4	23	4-2° K	This paper
±0-004	±0-004	±1-0	±1-0
1-989	1-945	3-5	23	23° K	4
±0-004	±0-004	±0-9	±0-9

THEORY

CaWO₄ has a Scheelite structure¹³ and the light atom positions have been determined by neutron diffraction.¹⁴ The Ca site has eight oxygen neighbours and has the site symmetry of S₄. There are four oxygens at a distance of 2-44 Å and another set of four oxygens at a distance of 2-48 Å. The WO₄ group is mainly tetrahedral with a distortion which can be visualized as a slight compression along the c-axis of the tetrahedron. The measured O-W-O angles are 107-5° (four times) and 113-4° (twice) with W-O bond distance as 1-789 Å. The W site also has a site symmetry of S₄. The structure of Scheelite may be considered as CaO₈ groups and WO₄ tetrahedron alternating according to the space group (*HJa*). A simple calculation shows¹⁵ that the height of the cube, in which WO₄ is inscribed, along the c-axis is 1-96 Å as compared with 2-11 to 2-14 Å for a regular tetrahedron. There are four molecules in the unit cell and the ESR spectra of an anion substituted in any one of the Ca or W sites are indistinguishable since they show identical local S₄ symmetry with a common c-axis. In such cases we have to depend on the characteristics of spin Hamiltonian constants in deciding the substitutional site. We shall proceed with the

assumption that Cr⁶⁺ is likely to be in the substitutional site of W. The question of Cr⁶⁺ substituting for calcium will be discussed later and shown not to conform to our experimental results.

Since WO₄ group in this crystal has a slightly flattened tetrahedral structure, we shall approximate this to D_{4h} for our calculation and this is also borne out by the fact that the observed spectrum fits an axial spin Hamiltonian. The ground state and the magnetic properties of a d¹ system in such a symmetry can be calculated with the assumption that the crystal field has a dominant cubic component together with a small axial field superimposed on it. Such a calculation shows that a cubic field (Td) splits the fivefold orbitally degenerate states into a triplet (t_{2g}) and a doublet (e_g) and for negatively charged ligands, the doublet (e_g) is lower in energy. Addition of a compression along the [001] reduces the symmetry to D_{4h} and the e-orbitals are split further and the lowest of the two Kramer's doublets will be the state of our interest. The two states of the e-orbitals can be labelled as d_{x²-y²} and d_{z²} in the familiar way and one will have to determine which of these is the lower state in our system. Taking into account spin-orbit coupling effects, we can show that for the two states⁷:

for d_{z²}

$$f_t = 2.0023 \quad (2)$$

$$f_c = 2.0023(1-g) \quad (3)$$

$$A_{||} = P \left(-K + \frac{4}{7} + \frac{6}{7} \frac{\lambda}{\Delta} \right) \quad (4)$$

and

$$A_{\perp} = P \left(-K - \frac{4}{7} + \frac{6}{7} \frac{\lambda}{\Delta} \right) \quad (5)$$

and for d_{x²-y²}

$$f_t = 2.0023(1-g) \quad (6)$$

$$f_c = 2.0023(1-g) \quad (7)$$

$$A_{||} = P \left(-K - \frac{4}{7} - \frac{6}{7} \frac{\lambda}{\Delta} \right) \quad (8)$$

and

$$A_{\perp} = P \left(-K + \frac{2}{7} - \frac{11}{7} \frac{\lambda}{\Delta} \right) \quad (9)$$

where g_n and g_{\pm} are the g -values when the magnetic field H is parallel and perpendicular to the tetragonal axis and A_H and A_x are similar hyperfine parameters; A is the spin-orbit coupling constant; $P = 2.0023 g_N \int \delta(r) dv$ and PK is the isotropic hyperfine contact term arising from the v polarization of the inner λ -electrons by the unpaired spin in the rf -orbital; if we ignore to an approximation the further splitting of the t_2 triplet, A is the energy difference between the d_z^* orbital and the triplet and A' is the energy difference between $d_x^*-y^*$ orbital and the triplet. With the assumption that K is positive^{16,17} this simple theory predicts for Cr^{5+} whose A is positive, for d_z^* orbital as the ground state $g_n = 2.0023$ and $g_{\pm} > g_n$ and $|A_n| < |A_{\perp}|$ and for $d_x^*-y^*$ orbital as the ground state $g_{\pm} > g_n$ and $|A_n| > |A_{\perp}|$. Our results in Table I conform to the d_z^* orbital being the ground state for Cr^{6+} in $CaWO_4$.

The value of A/A' can be found from Eq. (3) using the experimentally determined g_{\pm} . To determine K and P from Eqs. (4) and (5) one needs to know the relative signs of A_n and A_{\pm} . Since the relative signs are not known by experiment, we have two possible values for K and P :

$P = -2.05 \times 10^{-3}$ and $K = 0.774$ if A_H and A_{\perp} have the same sign, and $P = -2.91 \times 10^{-3}$ and $K = 0.442$ if A_n and A_{\pm} have the opposite signs. For Cr^{5+} with a nuclear magnetic moment of $-0.4735 g_N$, P is expected to be negative and since K is positive A_{\pm} should be positive. However A_n can be of either sign. In Iron group K is found to lie between $+0.3$ and $+0.9$ ¹⁷ which is found to be consistent with our two estimates for K . From the value of P the estimates for $\int \delta(r) dv$ are **2.027 a.u.** and **2.577 a.u.** for the two possible relative signs.

The quantity x defined by Abragam, Horowitz and Pryce^{18,19} as

$$x = \frac{\langle \sum_i \delta(r_i) S_{zi} \rangle}{\langle S_z \rangle} = -\frac{3}{2} \left(\frac{hca_0^3}{2.0023 g_N \beta \beta_N} \right) PK \quad (10)$$

is a measure of the polarization of the inner filled j -orbitals by the unpaired electrons. This quantity has the possible two values for Cr^{5+} in $CaWO_4$: -2.37 a.u. for the same sign and -1.92 a.u. for opposite signs of A_H and A_{\pm} .

It is thus seen that our crystal field model explains the observed Λ -values and hyperfine parameters for Cr^{5*} in W site with d_z^* as the ground state except for the following discrepancies: (i) The reduction in $(r^{*})_{av}$ from the extrapolated free ion value of 5 a.u. by a factor of about 2 and a similar decrease in the magnitude of x from -2.5 to -2.7 observed in other systems containing Cr^{5*} ;¹⁹ (ii) the observed g_n is less than the free electron value. The first deviation can be understood in terms of the orbital reduction factor of Owen and Stevens,²⁰ which leads to a decrease in $(r^{*3})_{fi}$; when covalency effects in terms of ligand field theory are considered. The decrease in x^c & n be due to a small admixing of 4s-orbitals into the $3d_z^*$ orbital²¹ in addition to the covalency effects. We have not attempted to make any calculations on the basis of the ligand field theory. The deviation of g_n from 2.0023 can be accounted for by taking into account a small rhombic distortion and this point will be considered later.

DISCUSSION

1. Comparison with Other Ions in $CaWO_4$

We shall compare our results on Cr^{5+} in $CaWO_4$ with those obtained on other ions in this crystal. A number of trivalent rare-earth ions²² and S-state ions, like $Mn^{23,4}$, $Eu^{2+,23}$ and Gd^{3+4} have been investigated and in all these cases the substitutional site was found to be Ca only, except for Nd^{3+} which appears to be in both Ca and W sites.^{24*} ²⁵ Fe^{3+} is found only in the W site.²⁶ Apparently, the mechanism of charge compensation for Fe^{3+} in this crystal seems to be rather unusual and there is also a small rhombic component observed in Fe^{3+} spectrum and this results in the non-equivalence of W sites. Similar rhombic distortion has been observed for $W^{5+,27}$ which has Sd^1 configuration. This behaviour does not however appear to be general.²⁴ The paramagnetic resonance of Mo^{5+} with Ad^1 configuration has been observed in this crystal¹ and the spin-Hamiltonian parameters of Mo^{5+} bear a close resemblance to our results. Presumably Mo^{5+} also enters W site and no rhombic distortion has been reported in this case also. In $CaWO_4$, Cr^{5+} , Mo^{5*} , W^{5+} , which have $3d^1$, Ad^1 and $5d^1$ configurations respectively/ resemble one another in their behaviour: $g_n > g_x$ and $A_y < A_x$. They all fall in the same class and the theory developed earlier for Cr^{5*} must be applicable to these systems and the difference found in the spin-Hamiltonian parameters by Azarbajani and Merlo¹ for Mo^{5+} in $CaWO_4$ when compared to Mo^{5+} in other systems can be understood in terms of our model. Table II compares our spin-Hamiltonian parameters with those for Mo^{5+} and W^{6+} in $CaWO_4$.

TABLE II

Spin-Hamiltonian parameters of Cr⁵⁺, Mo⁵⁺ and W⁵⁺ in CaWO₄

Ion	g_a	g_{\parallel}	A_n (KHcmr ¹)	A_a, A_{\parallel} (KHcmr ¹)	Temp.	Reference
53 _{Cr} ⁵⁺	1.988	1.943	4	23	4.2° K	This paper
95 _{Mo} ⁵⁺	1.987	1.887	8.39	41- 18	4.2° K	1
97 _W ⁵⁺	1.987	1.887	8.64	42- 52	4.2° K	1
183 _W ⁵⁺	1.850	1.587 1.60	19.05	53 66	4.2 ⁵ K	27

The isotropic hyperfine contact term, PK, arising from the polarization of the inner d -electrons by the unpaired spin in the d -orbital is listed along with P, K and $\langle r^{-3} \rangle_{av}$ for Cr⁵⁺, Mo⁵⁺, W⁵⁺ in CaWO₄ in Table III and the free ion value for $\langle r^{-3} \rangle_{av}$ is also listed. The isotropic contact term is known to decrease in magnitude with increase in covalency. The expected isotropic hyperfine contact term, PK, for Cr⁵⁺ in solution, $(A_H + 2A_J)/3$, is found to be $16.7 \times 10^{14} \text{cm.}^{-1}$, if we assume A_{\parallel} and A_x have

TABLE III

Values of PK, P, K, $\langle r^{-3} \rangle_{av}$ and $\langle r^{-3} \rangle_{av}^{\text{free ion}}$ for Cr⁵⁺, Mo⁵⁺ and W⁵⁺ in CaWO₄

Ion	$PK \times 10^8$ (cm. ⁻¹)	$P \times 10^8$ (cm. ⁻¹)	K	$\langle r^{-3} \rangle_{av}^{\text{exp.}}$ (a.u.)	$\langle r^{-3} \rangle_{av}^{\text{free ion}}$ (a.u.)	Reference
Cr ⁵⁺	15.9 12.9	2.1 2.9	0.77 0.44	2.0 2.9	5	This paper
Mo ⁵⁺	27.6 25.1	3.3 4.0	0.84 0.63	2.8 3.3	5.8 ..	1
W ⁵⁺	29.5 * 19.9	2.1 3.4	1.42 0.58	27

Note.—The two values, wherever given, are for the same and opposite signs of A_{\parallel} and A_x respectively.

the same sign and is reduced further for opposite signs. This indicates a considerable reduction from the isotropic solution value of $18.5 \times 10^{14} \text{ cm.}^{-1}$ in octahedral surroundings;^{28*} ²⁹ such reduction has been noted for other ions in tetrahedral surroundings, *e.g.*, (MnF_4 in $CaWO_4$ shows a considerable reduction when compared with octahedral surroundings.¹⁶ This seems to indicate larger covalency effects in tetrahedral co-ordination. In Table III, $(r^*)_{av}$ also shows considerable reduction from free ion values.

For Cr^{6*} one can estimate the covalency effects by defining parameters l and m which are the coefficients of the metal d -orbital in the ground (e) and excited state (t_2) respectively in the molecular orbital description. From the reduction of $\langle r^{-8} \rangle_{flt}$, from the free ion value of 3.51 a.u.^{29, 30} and from the λ -shift one estimates: For the same sign of A_{\pm} and A_n , $l^2 = 0.58$; $m^2 = 0.85$ and for the opposite signs of A_{\pm} and A_n , $l^2 = 0.82$; $TW^2 = 0.6$ with A in $CrO_4 \ll 11000 \text{ cmr}^{131}$ and the spin-orbit coupling constant for $Cr^{1+} \wedge 222 \text{ cmr}^1$.^{30, 32} However the argument that the e -orbitals are more localized than the t_2 orbitals in these systems³³ favours the opposite signs for A_n and A_{\pm} for Cr^{5+} in $CaWO_4$. The estimates for l^2 and m^2 should be taken as indicative of a trend rather than as absolute determinations, in view of the nature of approximations.

2. Comparison with Cr^{5*} and Isoelectronic Systems in Different Co-ordinations

Cr^{5*} has been extensively studied in various co-ordinations and a comparison of our results with these confirms further the model we have chosen for Cr^{5*} in $CaWO_4$. These will be discussed under the following three categories: (a) Eightfold co-ordination, (b) Octahedral and (c) Tetrahedral.

(a) *Eightfold co-ordination.*—The only case of eightfold co-ordination with Cr^{6*} studied by ESR is $KaCrO_8$ ³⁴ where Cr^{6+} is in a dodecahedral site and is surrounded by eight oxygens of four peroxide groups. Here ESR of Cr^{6*} can be seen at room temperature in contrast with a tetrahedral arrangement where one has to lower the temperature for observing resonance. The point symmetry at Cr^{6*} site is D_{2d} and the ground state is known from ESR studies to be $B_1 (d_{xy})$ in agreement with that predicted by Randic³⁵ using a point charge model. In the isoelectronic $Mo(CN)_8^{3-}$ and $W(CN)_8^{3-}$ where the geometry of the ligands is that of an Archimidean antiprism, $A_1 (d_z^2)$ is expected to be the ground state;³⁶ the observed g -anisotropy and the hyperfine anisotropy in ESR are similar to what is observed by us for Cr^{5+} in $CaWO_4$. Pappalardo and Wood³⁷ have theoretically predicted that for an ion with fP configuration at the Ca site in $CaWO_4$, where w ?

have an eightfold co-ordination with S_4 symmetry the ground state is a d_z^* orbital and it is unlikely that a similar situation will obtain for a d^1 configuration; this is in agreement with our consideration that Ca^{2+} is not a probable substitutional site for Cr^{5f} .

(b) *Octahedral.*—The isoelectronic vanadyl,^{30, 38} chromyl²⁹ and molybdenyl^{38, 39} complexes have been extensively studied and these have distorted octahedral surroundings. Hare, Bernal and Gray⁴⁰ have examined the case of d^1 in these surroundings and predicted that B_2 is the ground state $^{anc*} g_n < g_{\pm}$ and $A_n > A_{\pm}$, a behaviour that is followed invariably by vanadyl complexes. Certain molybdenyl and chromyl complexes, however, have $ft < Si^{anc*} A_n > A_L$.^{29, 38} The discrepancy in the case of Mo^{5+} systems from the prediction of Hare, Bernal and Gray⁴⁰ has been attributed to a larger spin-orbit coupling and covalency effects.³⁸ Kon and Sharpless²⁹ and Foglio⁴¹ have explained the reversal of g-anisotropy in Cr^{5*} and Mo^{5+} in certain systems by considering contributions from excited states where the excitation corresponds to an electron from one of the occupied bonding orbitals being promoted to the B_2 molecular orbital that is occupied by the magnetic electron. These results on tetragonally distorted octahedral systems show the importance of considering the hyperfine anisotropies in arriving at the plausible ground state. In all these cases $A_u > A_x$ in contrast with what is observed for Cr^{5*} in $CaWO_4$.

(c) *Tetrahedral co-ordination.*—There is a paucity of experimental data for d^1 in tetrahedral co-ordination. Carrington and co-workers³¹ have investigated $(MnO^*)^2-$ in K_2CrO_4 and recently Greenblatt and McGarvey⁷ have studied CrO_4^{3-} in chlorospodiosite, Ca_2PO_4Cl . The ESR of manganate ion³³ in K_2CrO_4 crystal confirmed the arguments of Ballhausen and Liehr⁴² that the unpaired electron should have the e-orbital as the ground state and the analysis of the spin-Hamiltonian parameters assigns the ground state to be mostly a $d_{x^*-y^*}$ orbital. Our results on Cr^{5+} in $CaWO_4$ and that of Greenblatt and McGarvey for CrO_4^{3-} in Ca_2PO_4Cl ⁷ are consistent with the level scheme of Ballhausen and Liehr⁴² and the distortion of the tetrahedron is such as to make the d_z^* orbital the ground state. However in both these cases g_n is less than the predicted value of 2.0023 for such an orbital; this deviation can be accounted for in terms of a rhombic distortion which leads to an admixture between the $d_{x^*-y^*}$ and d_z^* states. Such an admixture can be shown to lead to a g_n less than 2.0023 and also a difference between g_x and g_y . However, the deviation between g_x and g_y is expected to be small and it is believed that this deviation is within our experimental errors. It is likely that the observed variation in line-widths

on rotation about the c-axis may be partly due to a rhombic distortion. These variations in line-widths could not be studied because of interference from other resonances due to unwanted impurities in this crystal. It must be noted that W^{5+} and Fe^{3+} show rhombic symmetry at W site of $CaWO_4$. The larger the spin-orbit coupling the greater will be the* deviation of g_n from 2.0023 and this can be seen from Table II if we compare g_n of Cr^{5+} and W^{5+} in $CaWO_4$.

3. Temperature Effects

As pointed out earlier the ESR spectrum of Cr^{5+} in $CaWO_4$ could be observed only when the temperature was near that of liquid nitrogen. This is true for other d^1 systems in distorted tetrahedral co-ordination.^{1* 7 33 43} Even though d^1 system in distorted tetrahedral co-ordination should be similar to d^* system in distorted octahedral co-ordination (e.g., Cu^{2+}) where resonances are observed at room temperature, the inability to observe resonances for d^1 in tetrahedral co-ordination at room temperature is not understood. However, this supports the assignment of our spectrum to $Cr^{6* \wedge 1}$ in a tetrahedral site (W site) in $CaWO_4$.

CONCLUSIONS

The observed ESR spectrum in chromium doped $CaWO_4$ crystals is attributed to Cr^{5*} ion in the substitutional site of W on the basis of collective evidence. A simple point charge model calculation for a compressed tetrahedron was used to explain the general features of g-anisotropy and hyperfine anisotropy. It was pointed out that the discrepancies noticed by Azarbayejani and Merlo¹ in the g and hyperfine anisotropies for $CaWO_4 : Mo^{5+}$ as compared with other surroundings can be understood in terms of the above model.

The results also showed, without doubt, that in $CaWO_4$, Cr^{5+} the unpaired electron is on the e-orbital and is largely concentrated in $3d_{z^2}$ orbital on the central metal atom, in agreement with the theoretical predictions of Ballhausen and Gray⁴⁴ that the compressed tetrahedron is the stable configuration when covalency is present. A similar situation is obtained in Ca_2PO_4Cl .⁷ However, in the only other d^1 system in tetrahedral surroundings, MnO_4^{a-} in K_2CrO_4 , the ground state is found to be predominantly $d_x^*-y^*$ type of orbital corresponding to an elongated tetrahedron. $CaWO_4$ crystal is of particular interest because in the isoelectronic series $3d \mid 4d \mid 5d^1$ systems all these ions prefer to enter the compressed tetrahedral site of W in accordance with theory.

REFERENCES

1. Azarbajejani, G. H. and Merlo, A. L. *Phys. Rev.*, 1965, 137 A, 489.
2. Garif' Yanov, N. S. and Fedotov, V. N. *Soviet Phys. JETP*, 1963, 16, 269.
3. Kyi, R. T. .. *Phys. Rev.*, 1962, **128**, 151.
4. Kedzie, R. W., Shane, J. R. and Kestigian, M. *Bull. Am. Phys. Soc.*, 1964, 9, 243 (A).
5. ————— .. *Phys. Lett.*, 1964, **11**, 286.
6. **Lingam, K. V., Nair, P. G.** and Venkataraman, B. *Proc. Int. Conference on Spectroscopy, Department of Atomic Energy, Bombay*, 1967, 2, 408.
7. Banks, E., Greenblatt, M. and McGarvey, B. R. *J. Chem. Phys.*, 1967, 47, 3772.
8. Semi-elements, Inc., Saxonburg Boulevard, Saxonburg, PA., U.S.A.
9. Nassau, K. and Broyer, A. M. *Journal of Applied Physics*, 1962, 33, 3064.
10. Nair, P. G. .. *Ph.D. Thesis*, Bombay University, 1968.
11. Hempstead, C. F. and Bowers, K. D. *Phys. Rev.*, 1960, **118**, 131.
12. Lyons, D. H. and Kedzie, R. W. .. *Ibid.*, 1966, **145**, 148.
13. Zalkin, A. and Templeton, D. H. .. *J. Chem. Phys.*, 1964, **40**, 501.
14. Kay, M. L., Frazer, B. C. and Almodovar, I. *Ibid.*, 1964, **40**, 504.
15. Bershov, L. V., Marfunin, A. S. and Mineeva, R. M. *Soviet Phys. JETP*, 1966, **22**, 515.
16. Freeman, A. J. and Watson, R. E. *Magnetism*, Edited by G. T. Rado and H. Shul, Academic Press, Inc., New York, 1965, 2 A, 167.
17. Geschwind, S. .. *Hyperfine Interactions*, Edited by A. J. Freeman and R. B. Frankel, Academic Press, Inc., New York, London, 1967, p. 225.
18. Abragam, A., Horowitz, J. and Pryce, M. H. L. *Proc. Roy. Soc. (London)*, 1955, **230** A, 169.
19. McGarvey, B. R. .. *J. Phys. Chem.*, 1967, 71, 51.
20. Stevens, K. W. H. .. *Proc. Roy. Soc.*, 1953, **219** A, 542;
Owen, J. .. *Disc. Fard. Soc.*, **1955**, **19**, **127**; *Proc. Roy. Soc.*, **1955**, **227** A, 183.
21. Griffith, J. S._m .. *The Theory of Transition Metal Ions*, Cambridge University Press, 1964, p. 328.
22. Kirton>J. .. *Phys. Rev.*, 1965, **139** A, 1930.
23. Bronstein, J. and Volterra, V. *Ibid.*, 1965, 137, 1201.

24. Kedzie, R. W. and Kestigian, M. *Applied Phys. Lett.*, 1963, 3, 86; 1964, 4, 124.
25. Carrett, C. G. B. and Merritt, F. R. *Ibid.*, 1964, 4, 31.
26. Kedzie, R. W., Lyons, D. H. and Kestigian, M. *Phys. Rev.*, 1965, **138**, 918.
27. Azarbayejani, Y. G. H., Chu, K. C. and Kikuchi, C. *Bull. Am. Phys. Soc.*, 1965, 10, 1131; *Ibid.*, 1965, 10, 614.
28. Kon, H. *Inorg. Nucl. Chem.*, 1963, **25**, 933.
29. ——— and Sharpless, N. E. *Chem. Phys.*, 1965, 42, 906.
30. Kivelson, D. and Lee, S. K. *Ibid.*, 1964, **41**, 1896.
31. Banks, E., Greenblatt, M. and Holt, S. *Ibid.*, 1968, 49, 1431.
32. Griffith, J. S. *The Theory of Transition Metal Ions*, Cambridge University Press, 1964, p. 437.
33. Carrington, A., Ingram, D. J. E., Lott, K. A. K., Schonland, D. S. and Symons, M. C. R. *Proc. Roy. Soc. (Lond.)*, 1960, **254 A**, 101; *Ibid.*, 1960, **254 A**, 111.
34. McGarvey, B. R., Swalen, J. D. and Ibers, J. A. *Chem. Phys.*, 1962, 37, 2001; *Ibid.*, 1962, 37, 17.
35. Randić, M. *Chem. Phys.*, 1962, 36, 2094.
36. Hayes, R. G. *Nucl. Phys.*, 1966, **44**, 2211.
37. Pappalardo, R. and Wood, D. L. *Mol. Spec.*, 1963, 10, 81.
38. DeArmond, K., Garrett, B. B. and Gutowsky, H. S. *Chem. Phys.*, 1965, **42**, 1019.
39. Kon, H. and Sharpless, N. E. *Ibid.*, 1966, 70, 105.
40. Hare, C. R., Bernal, I. and Gray, H. B. *Inorganic Chemistry*, 1962, 1, 831.
41. Foglio, M. E. *Proc. Phys. Soc.*, 1967, 91, 620.
42. Ballhausen, C. J. and Liehr, A. D. *Mol. Spec.*, 1958, 2, 342.
43. van Reijen, L. L., Cossee, P. and van Haren, H. J. *Chem. Phys.*, 1963, **38**, 572.
44. Ballhausen, C. J. and Gray, H. B. Private communication.

INFLUENCE OF TEMPERATURE ON THE PHOTOMETRIC DETERMINATION OF SILICON IN FERROUS MATERIALS

BY K. S. R. KRISHNAIAH AND M. S. RAJU

(Research and Control Laboratories, Tata Iron and Steel Company Ltd, Jamshedpur-1)

Received May 17, 1968

(Communicated by Dr. G. V. L. N. Murty, F.A.S.C.)

ABSTRACT

A distinct influence of temperature has been indicated on the colour intensities of the reduced silicomolybdate solution confronted in the estimation of silicon in ferrous materials by the BISRA Methods of Analysis Committee procedure. This influence has been successfully overcome by employing ascorbic acid as a reducing agent in place of stannous chloride and hence the former reagent commends itself for adoption in the above procedure.

INTRODUCTION

IT is fairly well known that temperature has a significant influence on the colour intensities confronted in the photometric determination of silicon. The earlier investigations on the influence of temperature by Thompson and Houlton,¹ Stumm² and Hill³ on the measurement of yellow silicomolybdate and Straub and Grabowski⁴ and BISRA Methods of Analysis Committee⁵ on the measurement of the molybdenum blue complex are upto 30° C. and practically no influence has been indicated. Milton,⁶ Greenfield⁷ and Murty and Sen^{8,9} noted a gradual decrease in the intensity of the molybdenum blue colour at higher temperature, when stannous chloride has been used as a reducing agent. It has been established by the investigations^{10,11} from our laboratories that the colour intensities involved with pure silicate solutions in different procedures are very much governed by temperature. The extent of the influence depends largely on the nature of the acid medium and the reducing agent employed. Ascorbic acid has been successfully employed in all the procedures to overcome the influence of temperature. Studies¹² on the influence of temperature on the colorimetric determination of silicon in cast iron¹³ indicated that the colour intensities decreased when stannous chloride is used and increased when

Photometric Determination of Silicon in Ferrous Materials 43

ascorbic acid is used, the former being more pronounced. However, a 3% ascorbic acid solution containing 0-1% stannous chloride takes care of the influence of temperature to a significant extent.

In the present investigation, the feasibility of adopting the procedure of BISRA Methods of Analysis Committee (*he. cit.*) in tropical countries has been examined.

EXPERIMENTAL

Spekker photoelectric absorptiometer of Messrs. Hilger and Watts using tungsten lamp as light source, Kodak Filter No. 8 (680 *mp*) 1/2 cm. cells and a water setting of 1-30 had been employed for measuring the colour intensities. Gallenkamp thermostatic water-bath has been used for properly controlling the temperature of the solutions.

Solutions with various silicon contents (600 μ g., 400 *pg.*, 300 *ng.*, 200 *pg.*, 100/*xg.*, and 40/*xg.*) were taken, the colour and blank solutions developed at various temperatures (20° G, 25° C, 30° C, 35° C, 40° C. and 45° C.) and the colour intensities measured at respective temperatures at different time intervals after the addition of the reducing agent. The results are presented in Table I.

An examination of the results indicates that there is a marked influence of temperature on the colour intensities involved, the effect being more pronounced at higher temperatures. The influence is not significant right from the beginning at all concentrations of silicon at different temperatures but only after a certain time interval. This time interval is progressively shortened with increase of temperature and the silicon content.

It may, therefore, be concluded that the procedure cannot be adopted at all the prevailing room temperatures in the tropics, unless the laboratories are maintained at low temperature by air-conditioning them. Hence, it is considered desirable to explore the possibilities of appropriate modifications in the procedure to overcome the influence of temperature.

Ascorbic acid, which is a comparatively new reducing agent in the determination of silicon^{14,17} in ferrous and non-ferrous materials has shown considerable promise in our laboratories (*Joe. cit.*) in enabling the colour intensities independent of temperature. So 10 ml. of 5% ascorbic acid solution has been used in place of 1-2% stannous chloride and similar experiments to those using the latter were conducted. The results are presented in Table II.

TABLE I

Influence of temperature on the photometric determination of silicon {Reducing agent: Stannous chlon'de}.

Silicon content (%)	Temp. (°C)	Drum difference																	
		15 minutes						20 minutes						M minutes					
		20	20	30	35	40	45	20	25	30	35	40	45	20	26	30	35	40	46
600	1.190 1.168 1.185 1.175 1.162 1.150	1.188 1.188 1.175 1.168 1.143 1.120	1.186 1.180 1.160 1.128 1.098 1.070																
400	0.800 0.800 0.795 0.700 0.778 0.765	0.788 0.798 0.787 0.785 0.763 0.745	0.798 0.792 0.772 0.758 0.725 0.698																
300	0.680 0.688 0.688 0.685 0.575 0.562	0.583 0.588 0.680 0.578 0.558 0.510	0.588 0.583 0.568 0.555 0.530 0.502																
200	0.398 0.388 0.398 0.395 0.388 0.378	0.398 0.398 0.382 0.390 0.375 0.360	0.308 0.393 0.382 0.375 0.358 0.338																
100	0.198 0.198 0.198 0.195 0.190 0.187	0.198 0.198 0.195 0.192 0.185 0.180	0.198 0.100 0.190 0.188 0.178 0.168																
40	0.080 0.080 0.080 0.080 0.078 0.078	0.080 0.080 0.080 0.080 0.078 0.075	0.080 0.080 0.078 0.078 0.072 0.070																

Silicon content (in. %)	Temp. (°C)	Drum difference											
		ii ! minutes						60 minutes					
		20	25	30	35	40	45	20	25	30	35	40	45
600	1.186 1.168 1.122 1.092 1.052 1.010	1.185 1.180 1.080 1.050 1.014 0.975											
400	0.796 0.782 0.745 0.730 0.688 0.650	0.795 0.772 0.720 0.700 0.660 0.622											
300	0.580 0.575 0.548 0.535 0.505 0.470	0.585 0.568 0.520 0.512 0.480 0.444											
200	0.396 0.388 0.370 0.362 0.338 0.318	0.395 0.382 0.358 0.348 0.320 0.300											
100	0.196 0.192 0.182 0.178 0.168 0.157	0.196 0.188 0.175 0.168 0.158 0.148											
40	0.080 0.078 0.078 0.075 0.070 0.065	0.080 0.077 0.075 0.072 0.067 0.062											

All the above temperatures are within $\pm 1^\circ\text{C}$.

TABLE II

*Influence of temperature on the photometric determination of silicon
{Reducing agent : Ascorbic acid}*

Silicon content (fig.)	Drum difference			
	15 minutes		60 minutes	
	20±1°C.	45±1°C.	20±1°C.	45±1°C.
600	0-890	0-892	0-890	0-894
400	0-593	0-593	0-593	0-594
300	0-443	0-442	0-443	0-443
200	0-298	0-298	0-298	0-298
100	0-153	0-154	0-153	0-154
40	0-063	0-065	0-063	0-065

An examination of the results shows that the colour intensities involved are uninfluenced by temperature and time interval and hence ascorbic acid commends itself for adoption in tropical countries in the procedure under consideration. However, the above reagent suffers from the disadvantage of only 0.75 times as sensitive as stannous chloride. Work has, therefore, been taken in hand to overcome the above drawback.

ACKNOWLEDGEMENTS

The authors' sincere thanks are due to Dr. G. V. L. N. Murty, Chief Chemist, for his keen interest and valuable guidance and Management of the Tata Iron and Steel Co., Ltd., for permission to publish this paper.

REFERENCES

1. Thompson, T. G. and Houlton, H. G. *Ind. Eng. Chem., Anal. Ed.*, 1933, 5, 417.
2. Stumm, J. T. *Proc. A.S.T.M.*, 1944, 44, 749.
3. Hill, U. T. *Anal. Chem.*, 1949, 21, 589.
4. Straub, F. G. and Grabowski, H. A. *Ind. Eng. Chem., Anal. Ed.*, 1944, 16, 574.

5. BISRA Methods of Analysis *J.I.S.I.*, 1950* **165**, 430.
Committee
6. Milton, R. F. .. *Analyst*, 1951, 76, 431.
7. Greenfield, S. .. *Ibid.*, 1959, 84, 380.
8. Murty, G. V. L. N. and *Curr. ScL*, 1948, 17, 363.
Sen, N. C.
9. —————.. *Metallurgia*, 1952, 45, 53.
10. ———, Krishnaiah, K. S. R. *Curr. ScL*, 1965, 34, 561.
and Raju, M. S.
11. —————.. *Proc. Ind. Acad. Sci.*, **1966, 64, 84.**
12. Krishnaiah, K. S. R. and *Tisco.*, 1966, 1?, 111.
Murty, G. V. L. N.
13. Murty, G. V. L. N. .. *Metallurgia*, 1958, 58, 52.
14. Gibson, M. .. *U.K. (Harwell) Atomic Energy Establishment Report, C/R*
521, 1950.
15. **Boutin, R.** *.. *Compt. rend. Congr. Inter. Chim. Ind.*, **1959, 1, 142.**
16. Baczyk, S. .. *Chem. Anal. (Warsaw)*, 1960, 5, 3.
17. Delille, J. .. *Draht*, 1965, **16**, 8.

A KINETIC STUDY OF THE REACTION OF DIOLS WITH HYDROGEN HALIDES

BY P. S. RADHAKRISHNAMURTI AND T. P. VISVANATHAN

{Department of Chemistry, Khallikote College, Berhampur-Ganjam, Orissa, India}

Received August 12, 1968

(Communicated by Prof. S. V. Anantakrishnan, F.A.S.C., F.N.I.)

ABSTRACT

The kinetics of the reaction of diols with various hydrogen halides is discussed. The reaction involves neighbouring group participation as postulated earlier, the rate of substitution being faster for a heavier nucleophile. The reactions are inert in aqueous systems as the X'' nucleophilicity becomes negligible as compared to the nucleophilicity of water. At and above 7.5 per cent, water these reactions do not occur. Variation of dielectric constant also notably affects the process.

INTRODUCTION

IN our previous communication¹ we reported the kinetics of this reaction with HBr and postulated that this reaction involves anchimeric assistance by the hydroxyl group. It was found worthwhile to study the action of other hydrogen halides on diols. We report here certain interesting features of this reaction.

EXPERIMENTAL

Materials.—All the substrates used were obtained from Fluka and checked for purity by the usual procedure. The hydrogen halides used were freshly distilled azeotropic mixtures. The solvent, glacial acetic acid, was purified by the usual procedure and redistilled before use.

Kinetic method.—The kinetics were followed by the procedure described earlier.¹

RESULTS AND DISCUSSION

The second order rate constants are summarized in Tables I and II. As shown in these tables it is clear that the reaction is fastest with hydriodic

acid and slowest with hydrochloric acid. The rate constants of first displacement only are computed for ethylene glycol, propylene glycol and 1:3 butane diol, as the reaction is very sluggish after first substitution. Frost-Schwemer treatment² could not be applied as the timfratios were very high. With 1:4 butane diol the rate constants of both the steps have been computed using Frost-Schwemer method, in the case of HCl and HBr only. In the case of HI the reaction virtually stopped after the first displacement and hence the rate constant of the first displacement alone is reported.

TABLE I

Second order rate constants (l. moles⁻¹ min⁻¹) of first displacement in diols in glacial acetic acid at 80° C.

		HCl		
		Concentration of		K
		diol	HCl*	
Ethylene glycol	••	0-0525 M	0-0518 M	106
Propylene glycol	..	0-04986 M	0-0558 M	0-912
1:3 Butane diol	..	0-04991 M	0-0499 M	0-0238
		HBr		
		Concentration of		K
		diol	HBr	
Ethylene glycol	..	0-04718 M	0-05845 M	5-93
Propylene glycol	..	0-05645 M	0-05770 M	2-35
1:3 Butane diol	..	0-03265 M	0-06465 M	0-2101
		HI		
		Concentration of		k ₂
		diol	HI	
Ethylene glycol	..	0-02634 M	0-05460 M	12-18
Propylene glycol	..	002556 M	0-05415 M	4-24
1:3 Butane diol	..	002588 M	0-05370 M	0-678

TABLE II

Second order rate constants ($10^3 \times k_1 / \text{moles}^{-1} \text{min}^{-1}$) of both the steps in 1:4 butane diol in glacial acetic acid at 80° C.

	Concentration of		k_x	k_2
	diol	Hydrogen halide		
HCl	0.02529 M	0.05050 M	4.95	1.3
HBr	0.02996 M	0.05955 M	10.6	1.97
HI	0.02646 M	0.05320 M	42.1	Very slow

The question of reversible hydrolysis does not arise as halide solvolysis is very slow in a low dielectric medium like glacial acetic acid. The Grunwald-Winstein Y-value for acetic acid is — 1.64 and the relative rate of hydrolysis in glacial acetic acid is only 0.023 as compared to the Y-value for water, +3.56 and the relative rate, 3,650.

The results can be rationalised thus: As these are bimolecular substitutions the rate process is dependent upon the nature of the nucleophile. It is suggested that the heavier members are more nucleophilic largely because their atoms are more polarizable. It looks as if the polarizability phenomenon is only one of the factors for the higher reactivity of the heavier nucleophiles. During the activation process the solvation cage of the attacking nucleophile must be disrupted and a new 'cage' be formed around the activated complex. As the solvation energies of ions increase as their charge to size ratios increase, it requires more energy to desolvate a smaller ion than a larger one having the same charge. Hence small attacking groups exhibit lower nucleophilicity as there is difficulty in removing the molecules of the solvent from the attacking site. The ionisation potential and its solvation energy are the most important factors which are responsible for the relative order observed in the reaction, $I > Br > Cl$.³

There is no complication of esterification in these reactions as hydrogen halides seem to function better as nucleophilic agents than as mere catalysts for esterification. This is quite evident from the rate constants for the respective processes with respect to methanol,

				k 1.moles ⁻¹ seer ¹
Esterification ⁴	..	6	• 6	x 10 ⁻⁶
Substitution			..	<i>I-SSxlOr*</i>

Under our experimental conditions even this remote possibility is ruled out as the concentration of alcohols is very low unlike the larger quantities used in synthetic processes.

Another important feature that requires explanation is the relative slowness of the second step with HI in the case of 1:4 butane diol. Table III shows that the size of the halogen atom that is present in the molecule after the first displacement seems to be important. The steric repulsion seems to be the highest with I~ and least with Cl~, quite in consonance with their sizes.

TABLE III

kjk_t ratios of 1:4 butane diol with hydrogen halides

	HCl	HBr	HI	
<i>kjk₂</i>	3-8	5-4	..	

Effect of Addition of Water

It is very interesting that HBr reaction does not take place beyond 7.5 per cent, water. As the system is becoming aqueous the Br⁻ does not function as an effective nucleophile and there seems to be a competition between H₂O and Br~ and hence there is no reaction as shown in Table IV. The same effect of water has been reported by us earlier in the reaction of HBr with esters.⁵ A plot of log *k* vs. mole fraction of water shows that the reaction stops at mole fraction of water 0.206 (7.55 per cent, water).

Variation of Dielectric Constant

Addition of benzene.—It is interesting to observe that increase in content of hydrocarbon solvent like benzene is accelerating the rate with all the diols (Table V). A plot of log *k* vs. 1/D in all the cases shows fair linearity. Decrease of dielectric constant favouring the reaction is also similar to **what we observed with ester cleavages with HBr.**⁵

TABLE IV

Second order rate constants (k_t l. moles⁻¹ min⁻¹) for ethylene glycol with HBr at 80° C. in acetic acid-water mixtures

Solvent	Mole fraction of water	k_x
100% acetic acid	0	5.93
97.5% acetic acid-2.5% water (v/v)	0.0753	1.0
95% acetic acid-5% water (v/v)	0.1432	0.06
92.5% acetic acid-7.5% water (v/v)	0.205	No reaction

TABLE V

Second order rate constants (l. moles⁻¹ min⁻¹) for diols with HBr at 80° C in acetic acid-benzene mixtures (v/v)

	k_t		
	100%AcOH	10%benzene 90%AcOH	20% benzene 80%AcOH
Ethylene glycol ..	5.93	8.27	10.91
Propylene glycol ..	2.35	5.33	8.05
1:3 Butane diol ..	0.2101	1.00	1.47
1:4 Butane diol*..	0.0106	0.138	0.0184

•First displacement.

Addition of formamide.—The reaction does not take place even at 2.5% of formamide and 97.5% of acetic acid (v/v). This observation along with the observation that the reaction does not take place with 7.5% water and 92.5% acetic acid (v/v) deserves comment. It appears that even small percentages of liquids of high dielectric constant are totally suppressing the nucleophilicity of X- thus stopping the reaction.

Mechanism

We postulated that in these reactions there is neighbouring participation by the hydroxyl group leading to acceleration as evident from the rates of the first displacement. Progressively there is a decrease in the rate of first displacement as the position of OH's is varied. It was postulated that the reaction is composed of two factors: (1) the OH displacing the OH_2^+ forming the epoxide and (2) a relative fast cleavage of the epoxide by the nudeophile. It is evident from the activity of the nucleophiles—I, Br and Cl—that the second factor also is important in addition to the first one. It is not incompatible with the mechanism postulated that both the factors are important as similar observations have been made in elimination reactions, especially Ex. It is seen E_{\pm} is composed of two steps.⁶



Apparently though the rate-determining step is the first one the second factor is also taken into consideration for determining the overall rate of production of olefin. Similar reasoning is enough to explain the relative activity of the nudeophile though they are participating in a relatively fast step as compared to the step of epoxide formation.

ACKNOWLEDGMENTS

The authors wish to thank the Principal and the Management, Khallikote College, Berhampur-Ganjam, Orissa, India, for providing necessary facilities for the work.

REFERENCES

1. Radhakrishnamurti, P. S. and Visvanathan, T. P. *J. Ind. Chem. Soc.*, 1968, 45, 155.
2. Frost, A. A. and Schwemer, W.C. *Ibid.*, 1952, 74, 1268.
3. Gould, E. C. *Inorganic Reactions and Structure*, Henry Hoi and Co., NY, 1955, p. 207.
4. Locning, K. L., Garrett, A. B. and Newman, M. S. *J. Am. Chem. Soc.*, 1952, 74, 3929.
5. Radhakrishnamurti, P. S. and Visvanathan, T. P. *Tetrahedron*, 1968, 24, 5645.
6. Ingold, C. K. *Structure and Mechanism in Organic Chemistry*, G. Bell and Sons, London, 1955, p. 440.

ESR OF CaS : Mn²⁺: A CASE WITH ZERO CUBIC FIELD SPLITTING

BY P. G. NAIR, K. V. LINGAM AND V. G. MACHWE*

(Tata Institute of Fundamental Research, Bombay-5)

Received April 17, 1969

(Communicated by Prof. B. V. Thosar, F.A.S.C.)

ABSTRACT

Electron spin resonance studies on powdered samples of CaS: Mn²⁺ and SrS: Mn²⁺ at 300° and 77° K reveal the usual six-line hyperfine structure due to Mn⁵⁵. CaS: Mn²⁺ exhibits additional fine structure satellites which have been analysed on the basis of a near zero cubic field splitting.

INTRODUCTION

IN the course of luminescence studies by one of the authors (V. G. M.) of CaS and SrS phosphors activated with Bi, Th, etc., the optical spectra recorded on Steinheil (model GH Universal) Raman Spectrograph, showed the presence of an unaccounted band at 581 m μ . apart from the bands attributed to the activators. It was suggested¹ that the unaccounted band may be due to Mn present in the samples as unwanted impurity. To verify the presence of Mn if present in the divalent state, electron spin resonance of the samples in powder form were examined. All the samples showed the presence of Mn²⁺ impurity. However, the CaS : Mn²⁺ samples showed a well-resolved satellite structure. Even though the ESR of CaS : Mn²⁺ has been known² the observation of these satellites has not been reported. Similar satellites have been observed in SrS : Mn²⁺ by Manenkov and Prokhorov³ but our sample of SrS : Mn²⁺ did not reveal such a structure.

In order that the resonance may be seen directly in powder samples it is essential that the spectrum should be nearly isotropic. In cubic symmetry one expects for Mn²⁺, both g-tensor and A-tensor to be isotropic to a high degree. The fine structure being anisotropic gets broadened out and one usually sees only the nearly isotropic 1/2 \rightarrow -1/2 transitions in powder. Both CaS and SrS have simple (NaCl type) cubic structure and

* Solid State Physics Laboratory, Saugar University, Saugar.

Mn^{2+} at the substitutional sites of Ca or Sr experiences an octahedral cubic field. Our analysis shows that CaS : Mn^{2+} represents an interesting system where the cubic field splitting of Mn^{2+} is zero or negligibly small. The effects of other impurities like Bi and Th on the ESR spectra of CaS : Mn^{2+} have also been examined.

EXPERIMENTAL

Preparation of the samples.—The method followed for the preparation of CaS and SrS phosphors is due to Bhawalkar.⁴ To prepare CaS a purified form of $CaSO_4 \cdot 2H_2O$ obtained from gypsum ore was mixed with carbon and fired in a pair of graphite crucibles for two hours at $900^\circ \pm 10^\circ$ C. in a Herau Muffle furnace. For phosphors, required amounts of flux (hypo) and activator were added to the charge before firing. SrS samples were made by exactly similar method from purified $SrSO_4$ obtained from celestite ore.

ESR measurements.—The ESR spectra were recorded at 300° K and 77° K on an X-band superheterodyne spectrometer using 80 cps. field modulation.⁵ The magnetic field was measured on the Varian Fieldial magnet power supply. The readings are accurate to within one gauss when checked against proton measurements. DPPH was used as g^y value marker.

ESR data.—CaS: Mn^{2+} gave the expected hyperfine structure due to Mn^{55} with $I = 5/2$. However, each hyperfine component except the fourth in order of increasing field exhibits satellite structure whose general features can be seen from Fig. 1 which shows the spectrum recorded at room temperature. The maximum width of the satellites (separation between points of extreme slope) is around 2-3 G while the central line is about 1G wide.

When impurities mentioned earlier were present in CaS : Mn^{2+} , it was found that the lines get narrowed, 0.6 G being a typical value for CaS : Mn^{2+} with Bi. As the temperature is lowered the width further decreases. For example, at 77° K. the measured width for the central line of each group in samples containing Bi is less than 0.5 G.

This spectrum could arise if the cubic field splitting parameter ' a ' is zero or negligibly small compared to other terms in the spin Hamiltonian. The Hamiltonian can then be written as :

$$\mathcal{H} = g\beta H.S. + A.I.S \quad (1)$$

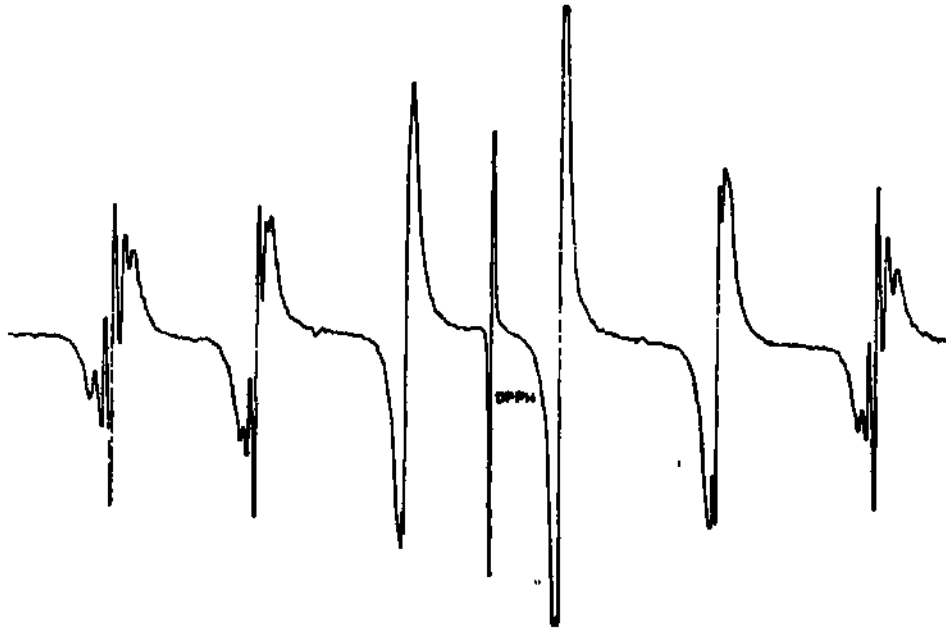


FIG. 1. Derivative of the ESR spectrum of CaS : Mn²⁺ at room temperature. with $S = 5/2$ and $I = 5/2$. From perturbation theory carried upto third order, taking $gB H.S.$ as the largest term the energy levels are given by⁸

$$\begin{aligned}
 E_{Mm} = & g\mu_B H M + A M m + \frac{1}{2} P d + 1) M - S(S + 1)m \\
 & + M m (M - m)] + \frac{A^3}{2g^2\beta^2 H^2} [S(S + 1) m(2m - M) \\
 & + I(I + 1) M (2M - m) + M m (M + m - 3Mm + 1) \\
 & - S(S + 1)I(I + 1)] \quad (2)
 \end{aligned}$$

From B_{mM} the resonance fields for the allowed transitions $M, m \rightarrow M-1, m$ at fixed frequency ν are given by:

$$\begin{aligned}
 H = & H_0 - A m - 4 \frac{A^3}{H_0^3} [1(1 + 1) + m(2M - m - 1)] \\
 & - \frac{A^3}{2H_0^3} [(4M - 2) \{I(I + 1) - m\} - m \{S(S + 1) \\
 & - 3M(M - 1) - 2\}] \quad (3)
 \end{aligned}$$

where $H_0 = h\nu/g\mu_B$ and A is now expressed in gauss. The nuclear quantum number m takes $2I + 1$ values from $+I$ to $-I$, Similarly, M ranges from

+ S to — S. Thus the spectrum consists of 21 + 1 hyperfine components each of which is split into 2S fine structure components by the terms in A^2 and A^8 . In Table I the measured and calculated line positions are compared. A. A. Manenkov and A. M. Prokhorov,³ who have observed similar satellite structure in their samples of SrS : Mn²⁺, have analysed the spectrum similarly and estimated an upper limit of $1.4 \times 10^4 \text{ cm}^{-1}$ for V from the anisotropic line width of the satellites. Our samples of SrS : Mn²⁺ gave a simple 6-line spectrum with no satellite structure. The width of the lines is about 2-6G. Table II gives the 'g' and 'A' values for the two cases.

DISCUSSION

From the comparison given in Table I it can be seen that the agreement between the observed and calculated field positions is very good. The calculated splittings for the fourth line ($m = 1/2$ assuming $A < 0$) is within one gauss and as expected only one line without structure is observed. The intensity ratio among the satellites seems to follow the theoretical ratio of 5:8:9:8:5.

When V is negligibly small the second order contribution to the line widths of the $1/2 \rightarrow -1/2$ transition is correspondingly small and one expects narrow lines. This is in fact verified from the experimental observations. However, the line widths of the satellites are found to be larger than the central lines. In the case of SrS : Mn²⁺ studied by Manenkov and Prokhorov⁸ the broadening of the satellites was assumed to be due to the finite value of the cubic field splitting parameter. This gives rise to broadening of the fine structure satellites in a powder because of the anisotropy. Under such circumstances one expects the line width of the satellites to be temperature independent provided the cubic field splitting is also temperature-independent. But our experiments show that the line widths of the satellites are smaller at lower temperature. In this context it is interesting to notice that even in the single crystals the line widths of the satellites are broader than the central lines for MgO : V²⁺.⁶ This was attributed to the impurities far from the ion which produce crystalline fields of lower symmetry. It appears that the satellite line widths could come from all the factors mentioned above and hence we feel that we cannot estimate an upper value for V just from consideration of satellite line widths.

The decrease in line widths in the case of samples doped with the mentioned impurities is not understood*

It is interesting to note that the SrS : Mn²⁺ samples we studied, did not show any satellite structure and previous workers² do not report such structure in their samples of CaS : Mn²⁺. So, it appears that in both these lattices the value of V can be very small and under suitable conditions particularly depending on the manner in which they are prepared, they show the satellite structure.

TABLE I

Observed and calculated transitions (M, m->M - 1, m) of CaS : Mn²⁺ (Gauss)

V	-5/2		-8/2		-1/2		+1/2		+3/2		+5/2	
	Obs.	Calc.										
-3/2	3178*1	3176*1	3255*1	3256*0	..	3338*2	..	3421*9	..	3500*3	3580-5	3580*2
-1/2	3181-5	3181-6	3259-1	3259-8	3339*9	3340-5	..	3422*0	3502*7	3502*3	3584*6	3584*3
1/2	3186*5	3186-8	3263-0	3263*4	3341-7	3341-8	3422*2	3422-2	3504*9	3504*4	3588-9	3588*6
3/2	3191-5	3191*7	3266*7	3266-7	3342-7	3343*5	..	3422*4	3507*3	3506*8	3593*9	3593*4
5/2	3196*5	319G-2	3270-0	3269*0	..	3345*1	..	3422*7	..*	3509*4	3599*4	3598*4

TABLE II

g and A values of Mn²⁺

	Host		Reference
	CaS	SrS	
g	2-0014	2-0008	This work
	2-0018	2-0015	(2)
	..	2-0009	(3)
A x 10 ⁴ cm. ⁻¹	75-3	74-8	This work
	76-8	76-8	(2)
	..	75-4	(3)

ACKNOWLEDGEMENT

We thank Professor B. Venkataraman and Dr. D. R. Bhawalkar for their interest and for the fruitful discussions during the course of this work.

REFERENCES

1. Tunitskaya, V. F. .. *Dokl. Akad. Nauk., SSSR*, 1953, 91(3), 507.
2. Auzins, P., Orton, J. W. and Wertz, J. E. "Paramagnetic resonance" *Proc. of the First International Conference*, Edited by W. Low, 1962, 1, 90.
3. Manenkov, A. A. and Prokhorov, A. M. *Sov. Phys. JETP*, 1961, 13, 1129.
4. Bhawalkar, D. R. .. *Saugar University Journal, India*, 1951-52, p. 209.
5. Lingam, K. V., Nair, P. G. and Venkataraman, B. *Proc. Nuclear Physics and Solid State Physics Symposium*, 1965, p. 15.
6. van Wieringen, J. S. and Rensen, J. C. "Paramagnetic resonance," *Proc. of the First International Conference.*, Edited by W. Low, 1962, 1, 107.

BOUNDARY LAYER ALONG THE INITIAL LENGTH OF A FLAT PLATE AT ZERO INCIDENCE WITH HOMOGENEOUS SUCTION

BY S. S. SINGH

[Department of Mathematics T. N. B. College, Bhagalpur (Bihar)]*

AND

R. C. CHOUDHARY

(Reader in Mathematics, Ranchi University, Ranchi)

Received September 2, 1968

(Communicated by Dr. B. R. Seth, F.A.Sc.)

ABSTRACT

An investigation has been made into the two-dimensional laminar incompressible boundary layer along the initial length of a semi-infinite flat plate at zero incidence with homogeneous suction. The momentum and the kinetic energy integral equations have been numerically integrated * with the aid of a singly infinite system of boundary layer velocity profiles.

The results obtained are well in agreement with the known exact solution and the process of integration is simpler to be carried out by the use of a monoparametric family of velocity profiles. The method can be used to investigate the boundary layer along a flat plate with arbitrary suction starting either at the leading edge or at some point downstream.

I. INTRODUCTION

FOR calculating two-dimensional laminar boundary layer with suction H. Schlichting¹ evolved a method based on the application of the momentum integral equation. The method can be used only for the cases in which the momentum thickness always increases and by the aid of this the position of the separation point cannot be reliably calculated. The method is not suitable for dealing with a case in which

$$\frac{v_s \theta}{\nu} < -0.5$$

Such a case is possible if suction does not begin at the leading edge but a definite place downstream to such an extent that the initial value of

$$\frac{v_s \theta}{\nu} < -0.5$$

T. P. Torda² developed K. Pohlhausen's approximation method to suit to the problems with suction. In the special case of a problem without suction and without pressure gradient Torda's velocity formulation cannot be used in a certain domain where

$$v \, dx$$

K. Wieghardt³ used the momentum theorem and the energy principle with the velocity formulation of Schlichting to calculate the variation of the parameter $H = \delta^*/\theta$ and determined the optimal suction required to keep the boundary layer laminar at greater Reynolds numbers. E. Truckenbodt⁴ made a numerical estimate of the function in the momentum integral equation and obtained a simplified momentum equation for the calculation of two-dimensional and rotationally symmetric boundary layers with suction. The numerical coefficients were specially chosen to represent the exact value of δ^* at the leading edge and the exact asymptotic value for a flat plate with homogeneous suction. The approximation may not prove very satisfactory in the general case of boundary layers with pressure gradient and suction. Moreover, in such general cases the simplified momentum equation of E. Truckenbodt would be solved by a finite difference method and the labour involved will not be much less than that required for solving the full momentum equation with the satisfaction of the wall compatibility condition.

A. Walz⁵ used a method based on the satisfaction of the momentum and energy theorems for solid boundary problems and suggested that it should be more important to satisfy the energy equation than the wall compatibility equation.

M. R. Head⁶ made a joint use of the momentum and the energy equations along with a doubly infinite family of boundary layer velocity profiles and evolved a method of solution with the aid of charts showing the courses of boundary layer characteristics.

In this paper a numerical step-by-step solution of the momentum integral equation and the kinetic energy integral equation has been obtained for the boundary layer along a flat plate with uniform suction using the singly infinite system of boundary layer velocity profiles given by H. Schlichting.¹ Because of the singularity of the energy equation at the leading edge the momentum equation only has been solved over a short distance with the satisfaction of the wall compatibility condition. The results have been compared with the exact solution of R. Iglisch⁷ and the approximate

solution of E. Truckenbodt.⁴ The results are in close agreement with the exact solution of R. Iglisch and the process of numerical integration becomes simpler than that evolved by M. R. Head⁶ with the use of a mono-parametric velocity formulation.

2. SYMBOLS

The symbols are conventional and most of them are those used by M. R. Head.⁶

x	Distance along the plate.
y	Distance normal to the plate.
U_0	Free stream velocity.
U	Velocity at the edge of boundary layer.
u	Velocity in the boundary layer in x direction.
v	Velocity in the boundary layer in y direction.
v_8	Velocity at the surface of the plate in y direction.
ν^*	Viscosity.
ρ	Density.

$$\nu = \frac{\nu^*}{\rho} \text{ Kinematic viscosity.}$$

$$c = \text{Representative length.}$$

$$\bar{x} = \frac{x}{c}$$

$$\bar{U} = \frac{U}{U_0}$$

$$\delta = \text{Boundary layer thickness.}$$

$$S^* = \int_0^{\infty} (1 - \frac{u}{U}) dy > \text{Displacement thickness.}$$

$$\theta = \int_0^{\infty} \frac{u}{U} (1 - \frac{u}{U}) dy > \text{Momentum thickness.}$$

$$e \quad \int_0^{\infty} \frac{u}{D} L^1 \sim (u)^* dy, \text{ Ener } \delta y \text{ thickness.}$$

$$H = \frac{\delta^*}{\theta}$$

$$H_c = \frac{c}{\theta}$$

$$D = \int (\dot{u})'' (\wedge)^{><f} (?) \text{ Dissipation integral.}$$

$$A = \frac{\theta^2 dU}{v dx}$$

$$l = U \left(\frac{\partial u}{\partial y} \right)_{y=0}$$

$$m = \bar{U} \left(\frac{\partial^2 u}{\partial y^2} \right)_{y=0}$$

$$\frac{c}{v}$$

$$\bar{v}_s = \frac{c}{U_0 V}$$

$$\eta = \frac{y}{\delta}$$

$$\xi = \left(\frac{v_s}{U_0} \right)^2 \frac{U_0 x}{v} = \bar{v}_s^2 \bar{x}$$

T_0 (JC) $\wedge = \tau^*$ ($\wedge J$) local shearing stress at the wall

K =s profile parameter.

f, g = functions as in equations.

\wedge and \tilde{f}

3. EQUATIONS⁶

For two-dimensional steady laminar incompressible boundary layers with suction the momentum integral equation is

$$\frac{dt^*}{d\bar{x}} = \frac{2}{U} [l - (2 + H) A + \lambda] \quad (1)$$

The energy integral equation in a form giving directly the variation of H, is

$$\frac{dH_e}{d\bar{x}} = \frac{1}{U t^*} [2D - H_e \{l - (H - 1) A + A\} + A] \quad (2)$$

and the wall compatibility condition is

$$m = -A + l \quad (3)$$

4. FAMILY OF VELOCITY PROFILES

The one parameter family of velocity profiles given by H. Schlichting¹ for the approximate calculation of boundary layers with suction is

$$g = F_1(\eta) + K F_2(\eta), \quad \eta = \zeta \wedge \quad (4)$$

where

$$F_1(\eta) = 1 - e^{-\eta},$$

$$F_2(\eta) = F_1 - \sin \frac{\eta\pi}{6}, \quad 0 \leq \eta \leq 3$$

$$F_2(\eta) = F_1 - 1, \quad \eta \geq 3$$

and δ^* is a measure of the local boundary layer thickness. For this system of velocity profiles

$$\delta^* = 1 - 0.901 K$$

$$| = 5 + 0.666 K - 0.236 K^*$$

$$\delta^* = -8.333 + 1.575 K - 0.417 K^2 - 0.0075 K^3$$

$$H = \frac{S^*}{6} = \frac{1 - 0.0901 K}{-5 + 0.0666 K - 0.0236 K^2}$$

$$\eta = \frac{8333 + 1575 K - 0.4171 K^2 + 0.0025 K^3}{-5 + 0.0666 K - 0.0236 K^2}$$

$$\lambda = (-5 + 0.0666 K - 0.0236 K^2)(1 + 0.4764 K)$$

$$D = (-5 + 0.0666 K - 0.0236 K^2)(-5 + 0.1567 K + 0.0679 K^2)$$

The variations of η , H , H_e , λ , and D against K are shown in Table I.

The compatibility condition (3) takes the form

$$K = \frac{\frac{8''}{\theta^2} A - \frac{8}{\theta} A - 1}{1 + \frac{\delta}{\theta} \lambda \left(1 - \frac{\pi}{6}\right)} \quad (5)$$

TABLE I

Boundary layer characteristics for various values of the parameter K of Schlichting's profiles (Eqn. 4)

K	η	H_e	H	λ	D
+0-0	•500	1-667	2-000	•500	•250
-0-1	•493	1-657	2-046	•470	•239
-0-2	•486	1-647	2-096	•440	•229
-0-3	•478	1-637	2-149	•410	•219
-0-4	•470	1-627	2-206	•380	•210
-0-5	•461	1-616	2-268	•351	•202
-0-6	•451	1-604	2-335	•322	•194
-0-7	•442	1-592	2-406	•294	•187
-0-8	•432	1-580	2-484	•267	•180
-0-9	•421	1-567	2-568	•241	•174
-1-0	•410	1-553	2-660	•215	•168
-1-1	•398	1-539	2-761	•189	•163
-1-2	•386	1-524	2-870	•165	•153
-1-3	•373	1-509	2-991	•142	•153
-1-4	•360	1-493	3-124	•120	•149
-1-5	•347	1-475	3-271	•099	•145
-1-6	•333	1-456	3-436	•079	•141
-1-7	•319	1-436	3-619	•061	•137
-1-8	•304	1-414	3-828	•043	•133
-1-9	•288	1-390	4-063	•027	•129
-2-0	•272	1-364	4-333	•013	•125
-2-099	•256	1-336	4-642	•000	•120

(Separation)

5. SEMI-INFINITE FLAT PLATE WITH HOMOGENEOUS SUCTION

For laminar boundary layer over the initial length of a flat plate with uniform suction we have

$$U(x) = U_0, \text{ free stream velocity}$$

i.e.,

$$\bar{U} = 1$$

$$A = t^* \frac{d\bar{U}}{d\bar{x}} = 0$$

$$A = \bar{v}_t / **$$

The momentum and energy equations (1) and (2) and the compatibility condition (5) become,

$$\frac{dt^*}{d\bar{x}} = f(K, t^*, \bar{v}_s)$$

where

$$f(K, t^*, \bar{v}_s) = 2 (l + A) = 2 (l + \bar{v}_s t^{**}) \tag{6}$$

$$\frac{dH_t}{d\bar{x}} = g(K, t^*, \bar{v}_s)$$

where

$$g(K, t^*, \bar{v}_s) = \frac{1}{2} [2D - H. \{l + A\} + A] \\ = \frac{1}{2} [2D - H. \{l + \bar{v}_s t^{**}\} + \bar{v}_s t^{**}] \tag{7}$$

and

$$(k + 1)! + [1 + .4764 K] \bar{v}_s t^{**} = 0 \tag{8}$$

6. SIMPLE APPROXIMATION METHOD OF E. TRUCKENBODT

With the aid of the curves (Ref. 1) E. Truckenbodt⁴ has made an approximation and suggested a simplified momentum equation, for two-dimensional boundary layers with suction as

$$\frac{dt^*}{d\bar{x}} = \frac{-441 - 6/l + -882A}{U} \tag{9}$$

For flow along a porous flat plate this reduces to

$$\frac{dt^*}{d\bar{x}} = -4.41 + .882 \frac{v_s}{U} t^* \quad (10)$$

It appears the numerical coefficients have been chosen to reproduce exactly the two cases of $A = 0$ (no suction) and $A = -0.5$ (asymptotic suction profile). Equation (10) has been directly integrated to give

$$.882 \bar{x} \frac{v_s}{U} t^* = 2 \bar{v}_s t^{**} - \log(1 + 2 \bar{v}_s t^{**}) \quad (11)$$

The variation of t^* against \bar{x} for $\frac{v_s}{U} = -1.0$ (Eqn. 11) has been shown as curve (c) in Fig. 1. The approximation to the exact solution is not seen to be very satisfactory.

7. TWO PARAMETER METHOD OF M. R. HEAD

M. R. Head⁶ constructed a doubly infinite family of velocity profiles and evolved a method of calculation based on the satisfaction of momentum and energy equations with the aid of graphs and charts drawn for the characteristic quantities. Exact Blasius values of $f = 0.221$, $\theta = 0$ were borrowed as the initial values at the leading edge of the plate for step-by-step calculation of the boundary layer with suction. The asymptotic values were found to be $f = 0.512$, $\theta = 0.263$ instead of the exact asymptotic values 0.50 and 0.25 respectively. While comparing his results for a flat plate with uniform suction with the exact solution of R. Iglisch he observed discrepancies in the exact and the approximate values of $v_s \delta / \nu$ and $\nu \delta / U$ which were attributed to the moderate degree of accuracy with which T^* / U and H^* had been determined.

8. PRESENT ONE PARAMETER METHOD

8.1. Solution of Momentum and Energy Equations

At the leading edge of the plate ($\bar{x} = 0$) the momentum thickness is zero and the form parameter K is obtained from the compatibility condition (8). For aU values of the suction velocity the initial values are

$$A = 0$$

$$K = -1, \text{ from equation (8)}$$

$$\left. \begin{array}{l} / = -215 \\ H_e = 1.553 \\ D = -168 \end{array} \right\} \text{ from Table I}$$

The step-by-step numerical calculation by Runge-Kutta⁸ method is started at the leading edge of the plate.

The energy Equation (7) exhibits singularity at the leading edge. For a short distance from the leading edge the momentum Equation (6) only is solved with the satisfaction of the compatibility condition (8) for any fixed value of \bar{v}_s . A^* is computed and then $/^*$ is known at the end of the step. Solution of Equation (8) gives K and the values of $/$, H_e , D , and H are read against K from Table I.

Over the next steps now the momentum and the energy equations are solved by Runge-Kutta method for the integration of two simultaneous differential equations. Because of the smallness of t^* occurring in the denominator of the energy equation the step lengths are taken very small at the start.

As Runge-Kutta method is too laborious the momentum and the energy equations are integrated further downstream by Adam's⁹ method. Having obtained the values at five initial points by Runge-Kutta method repeated ascending differences up to the fourth are computed for the functions $/$ and g and the increments in t^* and H_e over the next step length $A \bar{x}$ are calculated by a quadrature formula.

At the next station t^* and H_e become known, \bar{v}_s is kept constant, $/$, H , D are read against H_e from Table I and the functions $/$, g are calculated. The differences at the next point are computed and the calculation proceeds step-by-step.

When $A t^*$ and $A H_e$ become very small for any step-length the step-length $A \bar{x}$ is doubled. A fresh difference Table is constructed with the values at five preceding points at an interval of doubled step-length and the calculation is carried on.

The asymptotic state for homogeneous suction is reached when

$$\frac{dt^*}{d\bar{x}} = 0 \text{ and } dx^* = 0$$

The functions f and g both vanish when $A = -0.50$ and $K = 0$. Hence the asymptotic state values are

$$t^* = \frac{.50}{-\bar{v}_s}, \quad \bar{v}_s < 0$$

and

$$K = 0,$$

i.e.,

$$\left. \begin{array}{l} H_e = 1.667 \\ H = 2 \\ f = -50 \\ D = -25 \end{array} \right\} \text{Table I.}$$

the values are in agreement with those for the known asymptotic suction profile.

8.2. Comparison with the Exact Solution of R. Iglisch

R. Iglisch⁷ carried out a detailed investigation into the flow in the initial length and found that the asymptotic state is reached after a length of about

$$\bar{v}_s^2 \bar{x} = 4 \tag{12}$$

For the known asymptotic suction profile

$$t^* \bar{v}_s = \frac{.50}{\bar{v}_s} \tag{13}$$

Therefore, for $\bar{v}_s = -1, -1.5, -2$ the initial lengths would be about $\bar{x} = 4, 1.78, 1$ (Eqn. 12) and the asymptotic values of t^* are $0.25, 0.111, 0.0625$ (Eqn. 13) respectively.

The momentum and the energy equations have been solved for $\bar{v}_s = -1, -1.5, -2$ and the values of t^* have been found to be $t^* = -228, -102, -58$ at $\bar{x} = 4, 1.80, 1$ respectively.

The curves of t^* , f and H , against \bar{x} have been plotted in Figs. 3 to 5.

A comparison of the values of t^* and H for $\bar{v}_s = -1.0$ obtained by various methods has been made in Figs. 1 and 2. The course of t^* for $\bar{v}_s = -1$ obtained by the present method is represented as curve (a) in Fig. 1 and is found to be very close to the curve (b) representing the exact solution of Iglisch.

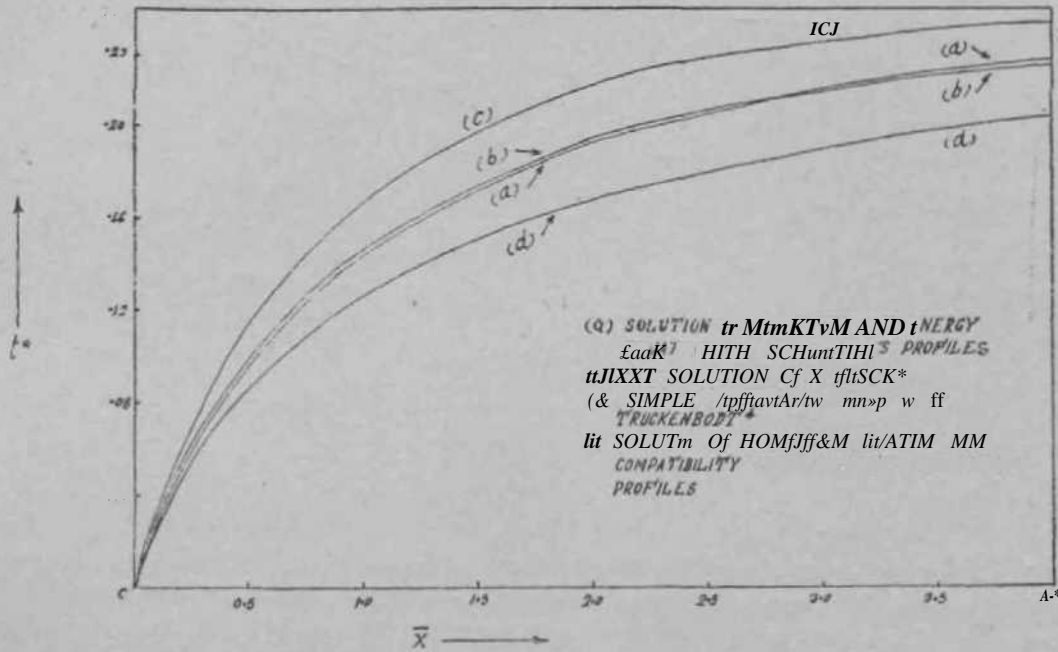


FIG. 1. Boundary layer along the initial length of a flat plate at zero incidence with homogeneous suction. Curves of t^* against \bar{x} for $\bar{v}_s = -1.0$.

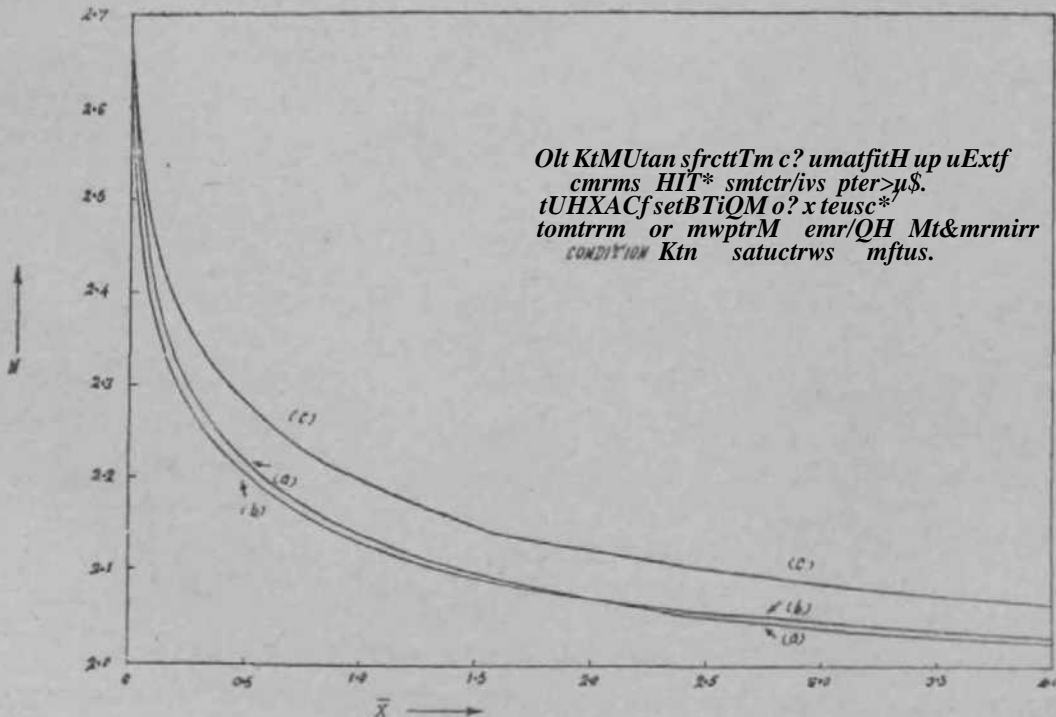


FIG. 2. Boundary layer along the initial length of a flat plate at zero incidence with homogeneous suction. Curves of H against \bar{x} for $\bar{v}_s = -1.0$.

8.3. Solution of Momentum Equation with the Satisfaction of Compatibility Condition

A comparison of Equations (6) and (10) suggests that more accurate results might be achieved by solving the momentum Equation (6) with the

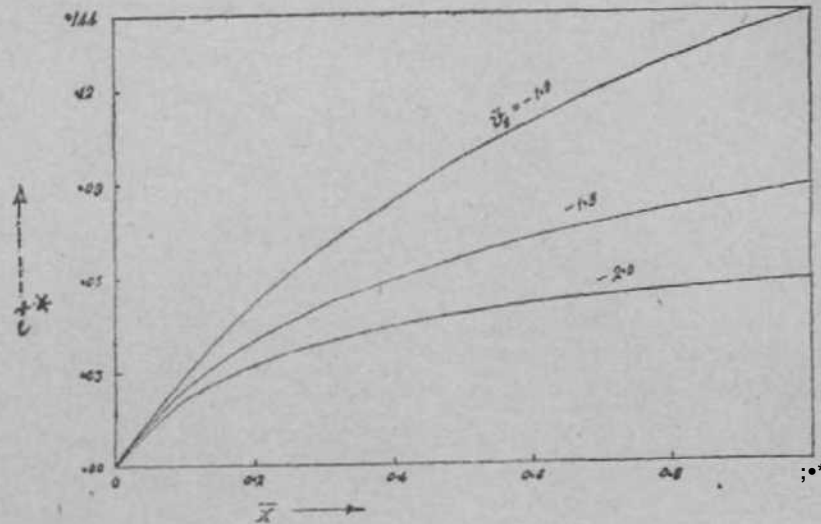


FIG. 3. Boundary layer along the initial length of a flat plate at zero incidence with homogeneous suction. Momentum thickness parameter δ^*/x plotted against \bar{x} for different values of v , [solution of momentum and energy equations with Schlichting's profiles].

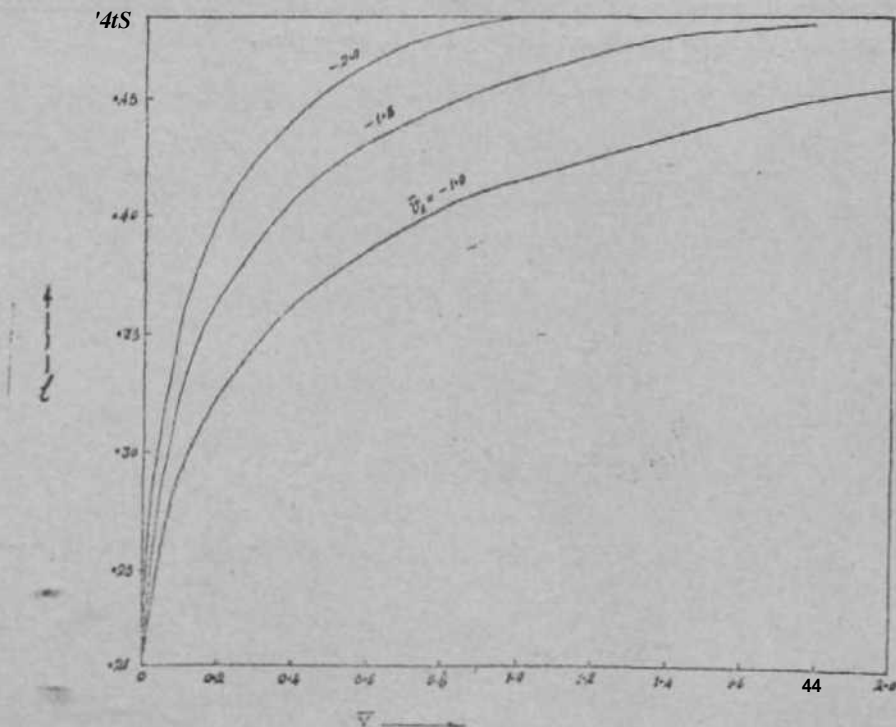


FIG. 4. Boundary layer along the initial length of a flat plate at zero incidence with homogeneous suction. H_e plotted against \bar{x} for different values of v [numerical solution of momentum and energy equations with Schlichting's profiles].

satisfaction of the compatibility condition (8) than by solving the simplified momentum Equation (10).

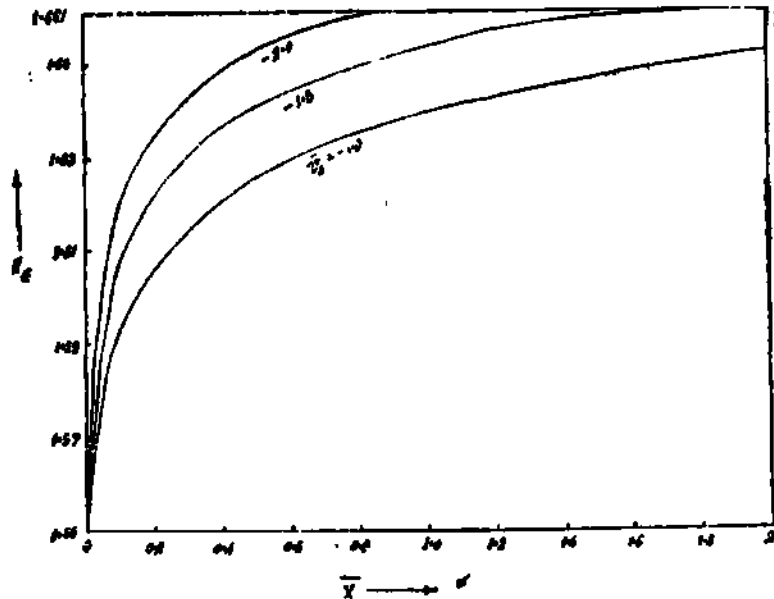


FIG. 5. Boundary layer along the initial length of a flat plate at zero incidence with homogeneous suction. Curves of t^* against \bar{x} for different values of v_s , [solution of momentum and energy equations with Schlichting's profiles].

With the values at the leading edge the momentum equation has been solved for $v_s = -1$ by Runge-Kutta⁸ method for five initial steps and then by Adam's⁹ method using a quadrature formula.

The asymptotic state is seen to have been reached later. For $v_s = -1$, the value at $x = 4$ of t^* is -204 which is much less than the corresponding exact value of Iglisch $t^* \wedge -226$ and the value of E. Truckenbott $t^* = -244$. The corresponding value obtained by the joint use of the momentum and the energy equations is $t^* = -228$.

The course of t^* obtained by the solution of the momentum equation with the compatibility condition is given by curve (d) in Fig. 1 and that obtained by the simplified approximation method of Truckentodt (Eqn. 11) is represented by curve (c). The curve (a) representing the solution of the momentum and the energy equations is seen to be the most satisfactory.

9. DISCUSSION

With increasing rate of suction the momentum thickness parameter t^* decreases and the asymptotic suction profile is reached earlier. Because of the use of a singly infinite system of velocity profiles the process of computation has become much easier whereas the results obtained by the joint

use of the momentum and the energy equations are quite well in agreement with the exact solution.

The method can be reliably used to find the boundary layer over a flat plate with solid entry length. If suction is started at a point where the boundary layer has so much developed that $v_s B/\nu < -0.5$, then at the starting point the solution of Equation (8) will give a positive value of K . $dt^* J d\bar{x}$ and dH/dx will be negative so that t^* and H_ϵ will both begin to decrease to their asymptotic values of $A = -0.5$ and $H_\infty = 1.667$.

REFERENCES

1. Schlichting, H. .. ^MAn approximate method for the calculation of laminar boundary layer with suction for bodies of arbitrary shape," *N.A.C.A. Tech. Memo.*, 1949, 1216.
2. Torda, T. P. .. "Boundary layer control by continuous surface suction or injection," *J. Maths. Phys.*, 1952, 31, S. 206-13.
3. Wiegardt, K. .. "On the calculation of plane and axisymmetric boundary layers with continuous suction," *Ing. Arch.*, 1954, 22, 368-77.
4. Tmckenbodt, E. .. "A simple approximation method for calculating the laminar friction layer with suction," *Forehg. Geb. Ing. Wes.*, 1956, 22, 147-57.
5. Walz, A. .. "Application of the energy equation by K. Wiegardt to one parameter velocity profiles in laminar boundary layers," *Ing. Arch.*, 1948, 10, 243-48.
6. Head, M. R. .. "An approximate method of calculating the laminar boundary layer in two-dimensional incompressible flow," *A. R. C. Tech. Report R. and M. No. 3132*, 1959.
7. Iglisch, R. .. "Exact calculation of the laminar boundary layer in longitudinal flow over a flat plate with homogeneous suction," *N.A.C.A. Tech. Memo.*, 1949, 1205.
8. Scarborough, J. B. .. *Numerical Mathematical Analysis*, Johns Hopkins Press, Baltimore, 1958, 317.
9. Bennett, A., Milne, W. E. and Batemaa, H. .. *Numerical Integration of Differential Equations*, Dover Publications, Inc., New York, 10, N.Y., 1956, pp. 73.

LAMINAR JET OF A COMPRESSIBLE PSEUDO-PLASTIC FLUID

BY N. L. KALATHIA AND R. K. JAIN

(Department of Mathematics, I.I. T., Kanpur, India)

Received April 6, 1967

(Communicated by Prof. J. N. Kapur, F.A.S.C.)

ABSTRACT

Similarity solutions of the boundary layer equations for compressible pseudo-plastic fluids for plane symmetrical jet are obtained in a closed form. Behaviour of velocity component perpendicular to the axis of the jet is discussed in detail.

INTRODUCTION

TOOSE (1952) obtained solution in closed form for a plane symmetrical jet of a compressible fluid. Toose's assertion about the behaviour of transverse velocity component was corrected later by Kapur (1958). Kapur (1962, 1963) discussed incompressible two-dimensional jet for pseudo-plastic power law fluids. Here we attempt to extend Kapur's analysis to include compressibility effects. We obtain similarity solutions in a closed form and discuss the behaviour of transverse component of velocity in detail.

BASIC EQUATIONS

We use cartesian co-ordinates taking axis of the jet as x-axis and y-axis perpendicular to it. Origin is some fixed point on jet axis. Suffixes a , j and a will denote values in the undisturbed stream, at the orifice and on the axis of the jet respectively.

Two-dimensional boundary layer equations in the absence of pressure gradient for compressible pseudo-plastic power law fluid are easily obtained (Kapur, 1963) as the following:

$$\rho u \frac{\partial u}{\partial x} + \rho v \frac{\partial u}{\partial y} = \frac{\partial}{\partial y} \left[\mu \left| \frac{\partial u}{\partial y} \right|^{n-1} \frac{\partial u}{\partial y} \right] \quad (1)$$

$$\rho u \frac{\partial}{\partial x} (c_p t) + \rho v \frac{\partial}{\partial y} (c_p t) = \frac{\partial}{\partial y} \left(k \frac{\partial t}{\partial y} \right) + \mu \left| \frac{\partial u}{\partial y} \right|^{n-1} \left(\frac{\partial u}{\partial y} \right)^2 \quad (2)$$

$$\rho (P \ll) + \rho (P \gg) = 0 \quad (3)$$

$$-p_t = pJa = Pjtj'' \quad (4)$$

where ρ denotes density; T absolute temperature; μ the coefficient of viscosity; C_p specific heat at constant pressure; k the coefficient of thermal conductivity; and $(u, v, 0)$ the velocity field. Further we have made use of stress and rate of strain relationship given by

$$h_{ij} = \mu \left| \sum_{m=1}^3 \sum_{n=1}^3 \epsilon_{nm} \epsilon_{mn} \right|^{(n-1)/2} e_{ij}$$

which defines power law fluids, n being the characteristic of the fluid. μ is in general dependent on temperature. This dependence is taken to be the same as by Toose (1952) so that

$$\frac{\mu}{\mu_j} = \left(\frac{T}{T_j} \right)^m, \quad \frac{1}{2} < m < \frac{1}{L} \quad (5)$$

Since the jet is symmetrical and the transverse component of velocity is to vanish on the jet axis, therefore,

$$v = \frac{\partial \psi}{\partial y} = 0 \quad \text{at } y = 0. \quad (6)$$

Further axial component of velocity vanishes at an infinite distance from the jet axis, therefore,

$$u \rightarrow 0 \quad \text{as } y \rightarrow \infty \quad (7)$$

(6) and (7) constitute the boundary conditions of the present problem. We make a change of independent variables from JC and y to x and ψ where ψ is a stream function defined as

$$y = \frac{\partial \psi}{\partial x}$$

It reduces equation (1) to

$$\rho_j \frac{\partial u}{\partial x} = \frac{\partial}{\partial \psi} \left[\mu \left| u \frac{\rho}{\rho_j} \frac{\partial u}{\partial \psi} \right|^{n-1} u \frac{\rho}{\rho_j} \frac{\partial \psi}{\partial \psi} \right]. \quad (8)$$

Further if we denote

$$U = \frac{u}{u_j}, \quad T = \frac{T}{T_j}, \quad X = \frac{x}{L}, \quad \Psi = \frac{\psi}{\sqrt{u_j v_j L}}$$

$$\lambda = \frac{\mu}{\mu_j} = \left(\frac{T}{T_j} \right)^m = T^m, \quad \Omega = \frac{\rho}{\rho_j}$$

Equation of state and momentum equation reduce to

$$\Omega T = 1$$

and

$$\frac{5)U}{d?k} = A \frac{\partial}{\partial \Psi} \left[T^{m-n} U^n \left| \frac{\partial U}{\partial \psi} \right|^{n-1} \frac{\partial}{\partial \Psi} \right] H1 \tag{9}$$

where

$$A = \frac{w_j^{3T1-S}}{p \cdot (T1-1)/2 \ L(W-D/2)}$$

and

$$vk = \dots$$

At this stage we make the following assumption:

(i) $m = n$, so that for the fluid under consideration $\backslash < n < 1$. Thus the fluid is a Pseudo-Plastic one.

(ii) Velocity profiles in the jet exhibit similarity at all the points downstream of the orifice. This is reasonable if boundary layer and mixing region in the jet both vanish at the orifice.

In fact we are interested in the similarity solutions of the equation $\sqrt{9}$. For this we assume

$$U = XPF(f) \quad \text{where} \quad f = \Psi^{q} * X^r \tag{10}$$

p, q and r are constants and are to be determined. From (9) and (10) one obtains that the similarity solutions are possible provided.

$$9 = 1 \quad \text{and} \quad (1 - 2n)p = 1 + (n + 1) r. \tag{11}$$

Further in the absence of pressure gradient, the rate of flow of momentum across any section of the jet is constant, say M_0 . So that

$$\begin{aligned} M_0 &= 2 \int_{y=0}^{or.} \rho u^2 dy = 2 \int_t^{\infty} \rho_j u \frac{\partial \psi}{\partial y} dy \\ &= 2\rho_j u_j \sqrt{u_j v_j} L \int_0^{\infty} X^{p-r} F(\xi) d\xi \end{aligned}$$

In order that M_0 is a constant* $p = r$, which gives

$$1 \tag{12}$$

Making use of (10), (11) and (12), equation (9) reduces to

$$\frac{1}{3nA} \frac{d}{d\xi} F(\xi) = \frac{d}{d\xi} [(-FF')^n]$$

where we have made use the fact that aw/ty , *i.e.*, F' is negative.

Integration of the above equation gives -

$$- \pi - i/n \quad p' \quad \rightarrow jff \quad i/\gg$$

where

$$B = \left(\frac{1}{3} \right)^{i/n}$$

and the constant of integration vanishes because

$$F' = 0 \quad \text{for} \quad \xi = 0.$$

Integrating once again, it gives

$$\frac{p(2n-i)/n}{anrr-} - \frac{lj\xi < i+Ti)/n}{TTiT} + \text{const}^*$$

But for

$$g = 0, \quad F = 1,$$

so that

$$\text{const.} = \frac{1}{2} \frac{i}{-1}$$

Hence

$$F^{(2n-i)/n} = \left[\frac{1}{2} \frac{1}{-1} - \frac{B}{1+n} \xi^{(1+n)/n} \right] (2n-1)$$

or

$$F = \left[1 - \frac{2n-1}{1+n} B \xi^{(1+n)/n} \right]^{n/(2n-1)} \tag{13}$$

Thus the problem is completely solved. Now we shall attempt to give an interpretation to this solution.

Solution in terms of physical co-ordinates.—As θ can be treated a function of x and y as well as of x and ξ , therefore

$$d\psi = \left(\frac{\partial\psi}{\partial x}\right)_{\xi} dx + \left(\frac{\partial\psi}{\partial\xi}\right)_{x} d\xi = \left(\frac{\partial\psi}{\partial y}\right)_{x} dy + \left(\frac{\partial\psi}{\partial x}\right)_{y} dx.$$

Explicitly it gives

$$\frac{1}{Tn} \xi \sqrt{\frac{u_j v_j}{L}} X^{1/3n-1} dx + X^{1/3n} \sqrt{u_j v_j L} \left(\frac{\partial\xi}{\partial x}\right)_{y} dx \\ + X v \sqrt{v L} \xi (\wedge) \gg * = \frac{\rho}{\rho_j} u dy - \frac{\rho}{\rho_j} v dx.$$

Alternatively we obtain

$$\Omega u = X^{1/3n} \sqrt{u_j v_j L} \left(\frac{\partial\xi}{\partial y}\right)_{x} \\ - \Omega v = -\frac{1}{5} \xi \sqrt{\frac{u_j v_j}{L}} X^{1/3n-1} + X^{1/3n} \sqrt{v L} \xi (\wedge) \gg * = \frac{\rho}{\rho_j} u dy - \frac{\rho}{\rho_j} v dx$$

If the value of $Q > (il? > x)y$ is substituted in the second equation, it reduces to an identity. Therefore, v is to be determined through some other means. The first of the above relations can also be written as

$$\left(\frac{\partial y}{\partial\xi}\right)_{x} = X^{2/3n} \sqrt{\frac{v_j L}{u_j}} \frac{T}{F(\xi)}$$

On integration from a to f , it yields

$$y = X^{2/3n} \sqrt{\frac{v_j L}{u_j}} \int_a^f \frac{T}{F(\xi)} d\xi + \phi(X)$$

where a and $\phi(X)$ are arbitrary. For $y = 0$, one can take $\wedge = 0$, which implies

T

For complete determination of velocity field, validity of Crocco's relation

$$t = A + Bw - \frac{u^2}{2C_p}$$

is assumed which is true irrespective of the form of w and A and B are constants to be determined from the conditions

$$t = t_j \quad \text{when} \quad u = u_j$$

$$t = t_a \quad \text{when} \quad u = 0.$$

If t_0 is the stagnation temperature of the undisturbed jet, it can easily be shown that

$$T = T_a + (1 - T_0) u^2 + u (T_0 - T_a). \quad (15)$$

Further

$$T_0 = 1 + \frac{\gamma - 1}{2} M_j^2.$$

One finds that v/u can be expressed as

$$\frac{v}{u} = - \frac{T_x}{\frac{\partial \psi}{\partial y}} = \sqrt{\frac{v_j}{Lu_j} \frac{dY}{dX}}.$$

Using equations (10), (13), (15) and explicit values for u one gets

$$v = \sqrt{\frac{u_j v_j}{L}} \left[\frac{T_a}{X^{1+1/3n}} \left\{ \frac{2}{3n} \phi(n) \beta_t \left(\frac{n}{n+1}, \frac{1-n}{1-2n} \right) \left(1 - \frac{2n-1}{n+1} B \xi^{(1+n)/n} \right)^{n/(2n-1)} - \frac{1}{3n} \xi \right\} + \frac{\gamma-1}{2} M_j^2 \left\{ 1 - \frac{2n-1}{n+1} B \xi^{(1+n)/n} \right\}^{2n/(2n-1)} \frac{1}{3n} \frac{\xi}{X^{1+1/3n}} \right] \quad (16)$$

where

$$\phi(n) = \left(\frac{n}{2n-1} \right) \left(\frac{2n-1}{n+1} \right)^{1/(n+1)} \left(\frac{1}{B} \right)^{n/(2n+1)} \quad (17)$$

$$\beta_t \left(\frac{n}{n+1}, \frac{1-n}{1-2n} \right)$$

is incomplete Beta function defined as

$$j8j(l,w) = \int_0^{\xi} x^{ul}(l-x)^{m'l} dx.$$

Also

$$u = u_j X^{-1/3} \left(\frac{In - 1}{1 - \wedge_j B^{\wedge' *}} \right)^{n/(fi-i)} \tag{18}$$

We note from (16) that the coefficient of $1/X^{1+1/3n}$ will always be positive while coefficient of $1/X^{1+1/3n}$ will be positive for small values of f and will become negative for other values of ξ . Further v vanishes for $\xi = 0$ and approaches a finite negative value as

$$\xi \rightarrow \left(\frac{n+1}{2a-1} \cdot \frac{1}{B} \right)^{n/(n+1)}$$

Also $(\$/yH)x$ is always positive so that for every fixed X , as y increases ξ increases. Thus, for every X there is a value of y such that upto that value, the transverse velocity is directed away from the jet axis and after that the transverse velocity is directed towards the jet axis.

The equation of the curve which divides the regions in which transverse velocity is directed towards or away from the jet axis is given by

$$y = X \int_0^{\xi} \left[\wedge \wedge \wedge Mj2 X, 28n Fi0 + X \sim im vT_0 \sim T_a \right] d\xi,$$

$$\frac{T_a}{X^{1-1/3n}} \left[-\frac{2}{3n} \phi(n) \beta_{\xi} \left(\frac{n}{n+1}, \frac{1-n}{1-2n} \right) \left(1 - \frac{2n-1}{n+1} B^{\xi(1+n)/n} \right)^{n/(2n-1)} + \frac{1}{3n} \xi \right]$$

$$\frac{1}{3n} \frac{v-i}{2} Mj s X^{1+1/3n} r \frac{2M-1}{n+1} D S \frac{12n/<an-i}{I} \sim \circ.$$

where ξ is the parameter.

Characteristic length.—We note that values of ξ for $y = 0$ and $y \rightarrow \infty$ are respectively $\xi = 0$ and

$$\xi = \left[\frac{1}{(2n-1)Bj} \right]$$

therefore

$$\begin{aligned}
 M_0 &= 2\rho_j u_j^{3/2} \sqrt{v_j L} \int_{y=0}^{cc} X^{p-r} F(\xi) d\xi \\
 &= 2\rho_j u_j^{3/2} \sqrt{v_j L} \int_0^1 (1-Z)^{n/(2n-1)} Z^{-1/(n+1)} + (n) dr \\
 &= 2\rho_j u_j^{3/2} \sqrt{v_j L} \phi(n) \beta\left(\frac{n}{n+1}, \frac{3n-1}{2n-1}\right).
 \end{aligned}$$

This equation determines the value of L for a known M_0 . For $n = 1$, it reduces to the case discussed by Toose (1952).

Degenerate case.—In the degenerate case when $t_j = f_a$, that is, $T_a = 1$ and the orifice velocity UJ is very small then M_j will be very small, the axial and transverse component of velocity in the present situation will be given by

$$\begin{aligned}
 UJ &= X^{-W} \left[1 - \frac{1}{n+1} B_{\xi^{(1+n)/n}}^{n/(2n-1)} \right] \\
 v - V &= \frac{1}{L} \left[\frac{1}{X^{1-1/3n}} \left\{ \frac{2}{3n} \phi(n) \beta\left(\frac{n}{n+1}, \frac{1-n}{1-2n}\right) \left(1 - \frac{2n-1}{B_{\xi^{(1+n)/n}}^{n/(2n-1)}} - \frac{1}{3n} \xi \right) \right\} \right].
 \end{aligned}$$

REFERENCES

- Kapur, J. N. .. *Quart. J. M^A. Appl. Math.*, 1958, 11, 423.
 _____ .. *Phys. Soc. Jap.*, 1962, 17, 1303.
 _____ .. *Ibid.*, 1963, 18, 144.
 Toose, D. G. .. *Quart. J. Meeh. Appl. Math.*, 1952, 5, 155.

ALKYLATION AND ARAALKYLATION OF* N-HETEROCYCLES

Part R* Methylation and Benzylation of 5 (or 6)-Methyl Benzimidazoles

BY K. KONDAL REDDY AND N. V. SUBBA RAO, F.A.S.C.

(Department of Chemistry, Osmania University, Hyderabad-!)

Received August 10, 1968

ABSTRACT

Methylation and benzylation of 5 (or 6)-methyl benzimidazoles has been carried out under uniform conditions. The structures of the products obtained have been established by comparison with authentic samples prepared by unambiguous methods. The results obtained are explained on the basis of inductive effect of the methyl group and the relative basicity of the two nitrogen atoms.

INTRODUCTION

THE tautomeric character of 5 (or 6)-methyl benzimidazoles was first established by Fischer and co-workers.^{1,3} Methylation of 2, 5 (or 6)-dimethyl benzimidazole² (I, R = CH₃) with methyl iodide was reported to give a separable mixture of 1, 2, 5- (II, R=R' = CH₃) and 1, 2, 6- (III, R, R'=CH₃) trimethyl benzimidazoles in almost equal proportion in addition to 1,2, 3, 5-tetramethyl benzimidazolium iodide (IV, R = R' = CH₃). It was also shown that (II) and (III) with excess of methyl iodide gave the same methiodide³ (IV), thus indicating the possibility of formation of isomeric benzimidazoles from tautomeric benzimidazoles by N-substitution and the formation of one and the same benzimidazolium salt on quaternisation of either isomer.

The benzimidazole obtained by Bamberger and Lorenzen⁴ by the action of methyl iodide on the sodium and silver salts of 2, 5 (or 6)-dimethyl benzimidazole was assigned the structure (II, R, R' = CH₃) by Phillips.⁵ The results obtained by Phillips and more recently by others are summarised in Table 1.

*Part I: Rao and Ratnam, *J. Chem. Soc.*, 1959, p. 3087.

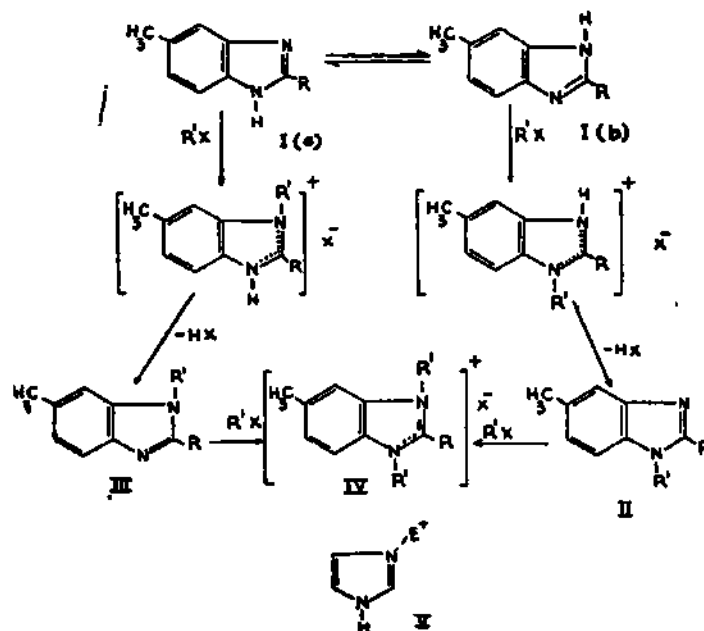


TABLE I

Results of N-substitution in 5 (or 6)-methyl benzimidazoles (I)

S.No.	R(inl)	Reagent	Product	
			Ratio of 1,5- to 1,6-isomer	Reference
1.	H	CH ₃ I in CH ₃ OH	1,6-isomer only	5
2.	H	(CH ₃) ₂ SO ₄	1 : 10	5
3.	H	(CH ₃) ₂ SO ₄ +OH ⁻	1 : 1	5
4.	H	CH ₃ SO ₃ -OK+OH ⁻	9 : 1	6
5.	-CH ₃	CH ₃ I in CH ₃ OH	1,2, S-isomer and its methiodide	5
6.	CH ₃	(CH ₃) ₂ SO ₄	1 : 10	5
7.	CH ₃	(CH ₃) ₂ SO ₄ +OH ⁻	1 : 1	5
8.	C ₆ H ₅	C ₆ H ₅ CH ₂ Cl, CH ₃ COONa+I ₂	1,2, 6-isomer only	7

The results obtained by Fischer do not throw sufficient light on the tautomeric behaviour of 5 (or 6)-methyl benzimidazoles, since in most cases the products of alkylation were quaternary salts. The results obtained by Phillips indicate that the course of N-substitution to a large extent depends

on the experimental conditions of alkylation. The oily product obtained on methylation of 5 (or 6)-methyl benzimidazole⁵ by methyl iodide was presumed to be 1,6-isomer (III, R = H, R' = CH₃), without establishing its identity with an authentic sample. Further, the position of methyl group in "2,2'-dimethyl-3'-benzyl benzimidazole" obtained by Bamberger and Lorenzen⁴ by allowing benzyl chloride to react with 2, 5 (or 6)-dimethyl benzimidazole in ethanolic sodium ethoxide is left undecided.

In view of the varying results obtained under different conditions of alkylation, a study of methylation and benzylation of tautomeric 5 (or 6)-methyl benzimidazoles (I, R = H, CH₃ and C₆H₅) has been undertaken, adopting throughout the same experimental conditions in order to evaluate the possible influence of substituents on the course of N-substitution.

5 (or 6)-Methyl⁵-, 2, 5 (or 6)-dimethyl⁶-, and 2-phenyl-5 (or 6)-methyl⁸ benzimidazoles have been prepared by standard methods. To characterise the products of N-substitution the required N-substituted 5-methyl and 6-methyl benzimidazoles have been obtained by unambiguous methods.⁹ In addition, 1, 5-dimethyl-2-phenyl and 1, 6-dimethyl-2-phenyl benzimidazoles have now been prepared for this purpose. Methylation and benzylation have been carried out using only one mole of the reagent under mild alkaline conditions to minimise the chances of quaternisation. Methylations have been carried out by refluxing the benzimidazole for several hours with methyl iodide in dry acetone in the presence of anhydrous potassium carbonate. The benzimidazoles have been benzylated using freshly distilled benzyl chloride in the presence of fused sodium acetate and a speck of iodine.⁷ The results of methylation and benzylation are included in Table II.

In the methylation of all the three benzimidazoles used, formation of quaternary salt (IV) was noticed. Benzylation of 5 (or 6)-methyl benzimidazole at 100° led to the formation of quaternary salt in considerable quantities. However, on benzylation at 170-80° no quaternary compounds were isolated. In the case of 2, 5 (or 6)-dimethyl benzimidazole benzylation above 100° seems to resinify the product. At 100° a good yield of N-benzyl derivative together with some quaternary salt has been obtained. Quaternary salts could be separated from the free bases taking advantage of the insolubility of the former in dry benzene. The N-methyl isomers obtained on methylation of 5 (or 6)-methyl benzimidazole were separated by chromatography over alumina. The mixture of N-benzyl isomers obtained on benzylation, however, could be satisfactorily separated into its components by fractional crystallisation from aqueous ethanol,

TABLE II

Results of methylation and benzylation of 5 (or G)-methyl benzimidazoles (I)

S.No.	R(inl)	Conditions	Relative percentage yield of Products		
			1,5-isomer	1, 6-isomer	Quater-nary salt
1.	H	CH ₃ I in acetone, potassium carbonate, 40 hrs.	23	47	30
2.	CH ₃	CH ₃ I in acetone, potassium carbonate. 40 hrs.	55	..	45
3.	C«Hj	CH ₃ I in acetone, potassium carbonate, 40 hrs.	50	..	50
4.	H	C«H ₆ CH ₂ Cl, CH ₃ COONa I ₂ , 12 hrs., 170—180°	37	63	..
5.	CH ₃	C ₆ H ₅ CH ₂ Cl, CH ₃ COONa, I ₂ , 12 hrs., 100°	..	64	36
6.	C ₆ H ₅	C ₆ H ₅ CH ₂ Cl, CH ₃ COONa, I ₂ , 10 hrs., 170°	..	100	..

The orientation of N-substitution in imidazole derivatives depends on the mechanism and type of species involved. Under neutral conditions methylation of imidazoles was shown to involve the neutral molecule by S_E2'-mechanism,¹⁰ i.e., attack by the electrophilic reagent (E⁺) at the tertiary nitrogen atom of the ring followed by the proton loss from the imino group (V). The same mechanism can be extended to 5 (or 6)-substituted benzimidazoles. Unlike in imidazole, the problem is not so simple in 5 (or 6)-methyl benzimidazoles, since they can exist as a mixture of two tautomers (I a and I b). The electron release by the methyl group in the benzene ring would be expected to increase the electron density, at the nitrogen para to the methyl group. If tautomer ratio is the measure of relative basicity of two nitrogen atoms, structure (I a) would be more stable and predominant. Methylation of 5 (or 6)-methyl benzimidazole gave a mixture of 1,5- and 1, 6-isomers, the latter being obtained comparatively in larger proportion. The formation of 1, 6-isomer can be expected by the attack of the alkylating agent at the tertiary nitrogen atom in the tautomer

(I *a*) followed by dehydrohalogenation. However, the expected relation between the basicity of nitrogen and its nucleophilic power suggests that the tautomer (I *b*) present in low concentration will have the higher rate coefficient for substitution by S_E2'-mechanism. Thus the tautomer (I' *b*) to the extent it is present is likely to be more reactive and can form 1, 5-isomer. Thus the formation of 1, 5- and 1, 6-isomers can be explained. On methylation of 2, 5 (or 6)-dimethyl benzimidazole and 5 (or 6)-methyl-2-phenyl benzimidazole besides 1, 5-isomer considerable amounts of quaternary salts are formed. During the alkylation if quaternary salt is formed it is difficult to interpret, as it might have been formed from 1, 6-isomer or 1,5-isomer. In the case of 5 (or 6)-methyl benzimidazoles it may be expected that 1, 6-isomer is formed first and that it undergoes quaternisation later. The substituent in 2-position of tautomeric benzimidazole does not seem to have any significant effect in tautomer stabilisation, since it is symmetrically situated with respect to both nitrogens. In this respect benzylation experiments are more helpful as the quaternary salts are not formed in two cases and the formation of 1, 6-isomer in larger amounts on benzylation is in accordance with the mechanism proposed earlier.⁷

EXPERIMENTAL

1, 5-Dimethyl-2-phenyl benzimidazole.—To N¹-methyl-4-methyl-0-phenylene-diamine¹² (1.5 g.) in alcohol (15 ml.) was added benzaldehyde (1.2 g.) and nitrobenzene (15 ml.) and refluxed for two hours. The solution remaining after the evaporation of alcohol was steam-distilled to remove nitrobenzene and unreacted aldehyde. The residue (1.0 g.) after crystallisation from dilute alcohol and finally from petroleum ether gave 1, 5-dimethyl-2-phenyl benzimidazole as colourless needles, m.p. 131° (Found: C : 81.3; H : 6.5; N : 12.3. C₁₆H₁₄N₂ requires C : 81.1; H : 6.3; N : 12.6%).

1, 6-Dimethyl-2-phenyl benzimidazole.—Condensation of N²-methyl-4-methyl-0-phenylene-diamine¹² (1.2 g.) with benzaldehyde in alcoholic nitrobenzene gave crude 1,6-dimethyl-2-phenyl benzimidazole (0.75 g.). On crystallisation first from alcohol and finally from ethyl acetate-petroleum ether mixture the pure benzimidazole was obtained as colourless bushy needles, m.p. 138° (Found: C : 81.3; H : 6.6; N : 12.4. C₁₆H₁₄N₂ requires C : 81.1; H : 6.3; N : 12.6%).

Methylation of 5 (or 6)-methyl benzimidazole.—A mixture of 5 (or 6)-methyl benzimidazole (1.3 g.) and methyl iodide (1.5 g.) in dry acetone (50 ml.) was refluxed over anhydrous potassium carbonate for forty hours. After evaporation of acetone, water (100 ml.) was added to the residue and

extracted with several small portions of chloroform. The chloroform extracts were dried and evaporated. The gummy residue obtained was treated with dry benzene (50 ml.) when the insoluble quaternary salt (0.25 g.) separated out. It crystallised from alcohol in needles, m.p. 227° and analysed for 1,3,5-trimethylbenzimidazolium iodide (Found: C : 41.5; H: 4.8; N : 9.5. $C_{10}H_{13}IN_2$ requires C : 41.7; H : 4.5; N : 9.7%).

The low melting solid obtained on evaporation of filtrate was dissolved in benzene (15 ml.) and chromatographed over alumina. The yellow band separated was eluted with benzene. First elutions gave compound (A), colourless needles from petroleum ether ($40-60^{\circ}$), m.p. 74° . The final elutions with benzene-ethyl acetate mixture (2:1) gave compound (B), colourless needles from benzene-petroleum ether, m.p. 95° . The middle fractions gave an oil, which on resubmitting to chromatography gave further quantities of (A) and (B). The yields of (A) and (B) were 0.4 g. and 0.2 g. respectively. (A) and (B) have been found to be identical in all respects with 1,6-dimethyl¹³ and 1,5-dimethyl¹⁴ benzimidazoles respectively, synthesised by unambiguous methods.

Methylation of 2,5 (or 6)-dimethyl benzimidazole.—Methylation of 2,5 (or 6)-dimethyl benzimidazole (1.6 g.) with methyl iodide (1.6 g.) in acetone over potassium carbonate gave a low melting solid. This was triturated with benzene (75 ml.) and the insoluble quaternary salt was filtered (0.5 g.). It crystallised from alcohol as rectangular rods, m.p. $165-66^{\circ}$, and analysed for 1,2,3,5-tetramethyl benzimidazolium iodide (Found: C : 43.5; H : 5.2; N : 9.1; $C_6H_{15}IN_2$ requires C : 43.7; H : 5.0; N: 9.3%). The residue obtained on evaporation of the filtrate (0.6 g.) was recrystallised from petroleum ether ($40-60^{\circ}$) giving colourless needles, m.p. 140° . This compound was found to be identical in all respects with a synthetic sample of 1,2,5-trimethyl benzimidazole.¹² Its mixed melting point with 1,2,6-trimethyl benzimidazole¹² was depressed ($80-98^{\circ}$).

Methylation of 5 (or 6)-methyl-2-phenyl benzimidazole.—Methylation of 5 (or 6)-methyl-2-phenyl benzimidazole (0.65 g.) with methyl iodide (0.5 g.) in dry acetone over potassium carbonate gave a solid. This was treated with dry benzene (50 ml.). The benzene insoluble compound (0.2 g.), crystallised from acetone petroleum ether in colourless needles, m.p. 215° and analysed for 1,3,5-trimethyl-2-phenyl benzimidazolium iodide (Found: C : 52.4; H : 4.9; N : 7.4. $C_{16}H_{17}IN_2$ requires C : 52.7; H : 4.6; N : 7.7%). The filtrate was passed over a column of alumina. Elution with benzene gave a compound (A; 0.2 g.), colourless plates m.p. 130° , from benzene petroleum ether. Final elutions with ethylacetate-benzene

gave a compound (B; 0.12 g.), m.p. 242°. By comparison with authentic samples A and B were found to be identical with 1, 5-dimethyl-2-phenyl and 5 (or 6)-methyl-2-phenyl benzimidazoles respectively.

Benylation of 5 (or 6)-methyl benzimidazole.—A mixture of 5 (or 6)-methyl benzimidazole (0.95 g.), freshly-distilled benzyl chloride (0.9 g.), fused sodium acetate (1.0 g.) and a speck of iodine was heated on an oil-bath maintained at 170-80° for twelve hours. The reaction mixture while still hot was poured into crushed ice with vigorous stirring and the solid (0.9 g.) separated was filtered and recrystallised from alcohol giving a colourless solid, m.p. 120-30°. Crystallisation of this from dilute alcohol (1 :2) gave a compound m.p. 170° rectangular rods (A; 0.5 g.) and the filtrate on concentration gave a compound, m.p. 140° (B; 0.3 g.), colourless rectangular plates. A and B were identical with 1-benzyl-6-methyl and 5-methyl benzimidazoles respectively by comparison with synthetic samples.⁹

Benylation of 2, 5 (or 6)-dimethyl benzimidazole.—Benzylation of 2, 5 (or 6)-dimethyl benzimidazole (0.6 g.) with benzyl chloride (0.55 g.) in the presence of fused sodium acetate and iodine on water-bath for twelve hours gave a low melting solid. It was washed several times with cold water and then with cold petroleum ether. The residue was treated with dry benzene (50 ml.) and the benzene-insoluble compound (0.2 g.) was filtered and recrystallised from alcohol in hexagonal plates, m.p. 261-62°. This analysed for 1,3-dibenzyl-2,5-dimethyl benzimidazolium chloride (Found: C : 75.9; H : 6.2; N : 7.5. $C_{23}H_{23}ClN_2$ requires C : 76.1; H: 6.2; N : 7.7%). The solid obtained on evaporation of the benzene solution was purified by recrystallisation from aqueous ethanol (1 :2) giving colourless plates (0.35 g.), m.p. 141°. This was found to be 1-benzyl-2, 6-dimethyl benzimidazole by comparison with synthetic samples of 1-benzyl-2, 5- and 2, 6-dimethyl benzimidazoles.⁹

Benylation of 5 (or 6)-methyl-2-phenyl benzimidazole.—5 (or 6)-Methyl-2-phenyl benzimidazole (1.5 g.) was benzylated by heating with benzyl chloride (0.8 g.) in the presence of sodium acetate and iodine, at 170-80° for twelve hours. The reaction mixture was added to excess of crushed ice when a resinous solid separated out which when treated with a little alcohol gave a granular solid (1.39 g.). This was filtered and recrystallised from alcohol and benzene yielding colourless prismatic rods, m.p. 195°. This was found to be identical with an authentic sample of 1-benzyl-2-phenyl-6-methyl benzimidazole.⁷

REFERENCES

1. Fischer and Becker .. *Bar.*, 1902, 35, 1258.
2. ———— and Romer .. *J. Prakt. Chem.*, 1906, 73, 419.
3. Fischer .. *Ibid.*, 1907, 75, 88.
4. Bamberger and Lorenzen .. *Ann.*, 1893, 273, 283.
5. Phillips .. *J. Chem. Soc.*, 1931, p. 1143.
6. Aliprandi *ctal.* .. *Chem. Abstr.*, 1962, 56, 15500.
7. Rao and Ratnam .. *J. Chem. Soc.*, 1959, p. 3087.
8. Porai-Koshits *et al* .. *J. Gen. Ch*m.*, 1947, 17, 1768; 1949, 19, 1945.
9. Reddy, Rao and Ratnam .. *Ind. J. Chem.*, 1963, 1, 96.
10. Ingold .. *Structure and Mechanism in Organic Chemistry*, Bell and Sons Ltd., London, 1953. Chap. 6, pp. 8 and 10.
11. Grimison, Ridd and Smith .. *J. Chem. Soc.*, 1960, p. 1352.
12. Green and Day .. *J. Am. Chem. Soc.*, 1942, 64, 1167.
13. Beaven *et al.* .. *J. Pharm. Pharmacol.*, 1949, 1, 975.
14. Fischer .. *Ber.*, 1889, 22, 195.

ON SOME IDENTITIES OF H-FUNCTION

BY P. ANANDANI

(Department of Mathematics, Holkar Science College, Indore)

Received January 24, 1968

(Communicated by Dr. P. L. Bhatnagar)

ABSTRACT

In this paper we establish some identities of H-functions involving complex arguments.

Fox (2, p. 408), introduced the H-function in the form of Mellin-Barnes type integral, which has been symbolically denoted by Gupta and Jain (3).

$$H_{p,q}^{m,n} \left[x \left| \begin{matrix} \{(a_p, \alpha_p)\} \\ \{(\beta_q, \beta_q)\} \end{matrix} \right. \right] \\
 = \frac{1}{2\pi i} \int_{\tau}^{\tau} \frac{\prod_{j=1}^m \Gamma(b_j - \beta_j s) \prod_{j=1}^n \Gamma(1 - a_j + \alpha_j s)}{\prod_{j=1}^g \Gamma(\lambda_j + \mu_j s) \prod_{j=1}^r \Gamma(\lambda_j - \mu_j s)} x^s ds, \quad (1.1)$$

where $\{(l_r, y_r)\}$ stands for the set of the parameters $(l_i, y_i), \dots, (l_r, Y_r)$ x is not equal to zero and empty product is interpreted as unity; l, q, m and n are integers satisfying $1 < m < q; 0 < n < p; a_j (j = 1, 2, \dots, l), \lambda_j (j = 1, 2, \dots, g)$ are positive numbers and $\alpha_j (j = 1, 2, \dots, l), \beta_j (j = 1, 2, \dots, q)$ are complex numbers such that no pole of $r(bh - (Jhs)$ ($h = 1, 2, \dots, l/w$) coincides with any pole of $F(1 - \lambda + a_j j)$ ($j = 1, 2, \dots, n$), i.e.,

$$\alpha_i (b_h + \nu) \neq \beta_h (a_i - \lambda - 1) \quad (1.2)$$

($\nu, i = 0, 1, \dots; h = 1, 2, \dots, m; i = 1, 2, \dots, n$).

2. We establish the following identities:

$$\begin{aligned} & H_{p,q}^{m,n} \left[x \left| \begin{matrix} \{(a_p, \alpha_p)\} \\ \{(b_q, \beta_q)\} \end{matrix} \right. \right] \\ &= \frac{1}{2\pi i} \left\{ e^{i\pi b_{m+1}} H_{p,q}^{m+1,n} \left[x e^{-i\pi \beta_{m+1}} \left| \begin{matrix} \{(a_p, \alpha_p)\} \\ \{(b_q, \beta_q)\} \end{matrix} \right. \right] \right. \\ &\quad \left. - e^{-i\pi b_{m+1}} H_{p,q}^{m+1,n} \left[x e^{i\pi \beta_{m+1}} \left| \begin{matrix} \{(a_p, \alpha_p)\} \\ \{(b_q, \beta_q)\} \end{matrix} \right. \right] \right\}, \end{aligned} \quad (2.1)$$

provided $l > \sum_{j=1}^m \beta_j - 1$. 4

$$\begin{aligned} & H_{p,q}^{m,n} \left[x \left| \begin{matrix} \{(a_p, \alpha_p)\} \\ \{(b_q, \beta_q)\} \end{matrix} \right. \right] \\ &= \frac{1}{2\pi i} \left\{ e^{i\pi a_{n+1}} H_{p,q}^{m,n} \left[x e^{-i\pi \alpha_{n+1}} \left| \begin{matrix} \{(a_p, \alpha_p)\} \\ \{(b_q, \beta_q)\} \end{matrix} \right. \right] \right. \\ &\quad \left. - e^{-i\pi a_{n+1}} H_{p,q}^{m,n} \left[x e^{i\pi \alpha_{n+1}} \left| \begin{matrix} \{(a_p, \alpha_p)\} \\ \{(b_q, \beta_q)\} \end{matrix} \right. \right] \right\}, \end{aligned} \quad (2.2)$$

where $n < \sum_{j=1}^m \alpha_j - 1$.

Proof.—To prove (2.1), expressing the H-function on the left-hand side as Mellin-Barnes type integral (1.1), we have

$$\frac{1}{2\pi i} \int_{\tau} \frac{\prod_{j=1}^m \Gamma(b_j - \beta_j s) \prod_{j=1}^n \Gamma(1 - a_j + \alpha_j s)}{\prod_{j=m+1}^q \Gamma(1 - b_j + \beta_j s) \prod_{j=n+1}^p \Gamma(a_j - \alpha_j s)} x^s ds,$$

that is

$$\text{if } \frac{1}{2\pi i} \int_{\tau} \frac{\prod_{j=1}^{m+1} \Gamma(b_j - \beta_j s) \prod_{j=1}^n \Gamma(1 - a_j + \alpha_j s)}{\prod_{j=m+2}^q \Gamma(1 - b_j + \beta_j s) \prod_{j=n+1}^p \Gamma(a_j - \alpha_j s) \Gamma(b_{m+1} - \beta_{m+1} s) \Gamma(1 - b_{m+1} + \beta_{m+1} s)} x^s ds, \quad (2.3)$$

now in view of

$$\Gamma(z) \Gamma(1-z) = \frac{\pi}{\sin \pi z} \quad \text{and} \quad \sin z = \frac{e^{iz} - e^{-iz}}{2i}$$

we can write

$$\begin{aligned} & \Gamma(b_{m+1} - \beta_{m+1}s) \Gamma(1 - a_{m+1} + \beta_{m+1}s) \\ &= \frac{\pi}{\sin(b_{m+1} - \beta_{m+1}s)\pi} \\ &= \frac{I\pi}{e^{i\pi(b_{m+1} - \beta_{m+1}s)} - e^{-i\pi(b_{m+1} - \beta_{m+1}s)}} \end{aligned}$$

therefore (2.3), reduces to

$$\begin{aligned} & \frac{1}{2\pi i} \left[\frac{1}{2\pi i} \int_{\gamma} \dots \int_{\gamma} \frac{C}{J} \frac{\Gamma(b_j - \beta_j s) \prod_{j=1}^n \Gamma(1 - a_j + a_j s)}{ni - bj - Pjs} \frac{\Gamma(1 - a_j + a_j s)}{\Gamma(r(a_j - a_j s))} (xe^{-i\pi\beta_{m+1}})^s ds \right. \\ & \left. - \frac{1}{2\pi i} e^{-i\pi b_{m+1}} \int_{\gamma} \frac{\Gamma(b_j - \beta_j s) \prod_{j=1}^n \Gamma(1 - a_j + a_j s)}{\Gamma(1 - b_j + \beta_j s) \prod_{j=1}^n \Gamma(a_j - a_j s)} (xe^{i\pi\beta_{m+1}})^s ds \right] \end{aligned}$$

again, using (1.1), the definition of H-function, we get the result (2.1).

Similarly (2.2), can easily be established.

Particular Cases.—Taking $\alpha_j = 1$ ($j = 1, 2, \dots, n$; $A = 1, 2, \dots, ?$) in (2.1) and (2.2), the H-function reduces to Meijer's G-function and thereby we get known results [1, p. 210 (14)].

ACKNOWLEDGEMENT

The author is thankful to Dr. R. K. Saxena of G.S. Technological Institute, Indore, for his kind help in the preparation of this paper.

REFERENCES

1. Erdelyi, A. *et al.* .. *H.T.F.*, 1953, Vol. I.
2. Fox, C. .. *Trans. Amer. Math. Soc.*, 1961, 98,408.
3. Gupta, K. C. and Jain, U. C. .. To appear in *Proc. Nat. Acad. Sci., India.*

THE KINETICS OF THE DECARBOXYLATION OF MALONIC ACID IN ESTERS

BY R. GOPALAN AND I. M. MATHAI

{Madras Christian College, Tambaram East, Madras-59}

Received November 30, 1968

(Communicated by Prof. S. V. Anantkrishnan, F.A.S.C.)

ABSTRACT

Kinetic data are reported for the decarboxylation of malonic acid in esters at different temperatures. The activation parameters are calculated and shown to favour the polar mechanism for the decarboxylation. Inductive and steric effects of the various solvents on the rate are discussed.

INTRODUCTION

KINETIC studies have been carried out in the past on the decarboxylation of malonic acid in a variety of solvents selected from a wide range of different homologous series. These include aromatic amines, aromatic and aliphatic alcohols, mono-carboxylic acids, aromatic nitro compounds, sulf-#oxides and poly hydroxy compounds.¹¹¹ In all these solvents it has been visualised that the electrophilic carbonyl carbon atom of undissociated malonic acid apparently co-ordinated with an unshared pair of electrons on a nudeophilic atom of a polar molecule. This is then assumed to favour the subsequent cleavage of malonic acid into acetic acid and carbon dioxide.¹⁵

Apparently, no kinetic work has been done with esters as the solvents. If the reaction proceeds by the indicated mechanism, it is reasonable to expect the unshared electrons on the alkyl oxygen atom of ester to co-ordinate with malonic acid, thereby promoting decarboxylation. The present paper describes the results of kinetic studies in four esters, namely, methyl benzoate,[^] ethyl benzoate, benzyl benzoate and ethyl cinnamate.

EXPERIMENTAL

Reagent.—Reagent grade malonic acid (melting point 135-2° C.) 100-0% assay was used in this investigation.

Solvents.—The esters used as solvents in this investigation were highest purity chemicals. They were fractionally distilled at atmospheric pressure just before the start of the kinetic run. The physical constants of the esters are given in Table I.

TABLE I
Physical constants of the esters

Ester	Boiling point observed at 760 mm. pressure °C, Unconnected	Refractive Index measured 30° C.	Dielectric constant (from lit.) ³
Methyl Benzoate ..	199-6	1-511	>6-59
Ethyl Benzoate ..	212-4	1-504	6-02
Benzyl Benzoate ..	323-7	1-566	4-9
<i>trans</i> -Ethyl Cinnamate ..	270-8	1-557	6-1

Apparatus and Technique.—The course of the reaction was followed by measuring the volume of carbon dioxide evolved at definite time intervals. The experimental set up was mainly based on that of Louis Watts Clark.² In these experiments a sample of accurately weighed malonic acid was taken in a fragile glass capsule and held in position on a movable iron support away from the reaction vessel inside the closed system. At the appropriate time the iron support was made to collapse by means of a magnet from outside and the capsule dropped into the vigorously stirred solvent, which had been thermostated using a vapour bath at constant pressure.

RESULTS

Decarboxylation experiments were carried out in each solvent at three or four different temperatures over approximately a 20° C. temperature range. Two or three experiments were performed at each temperature in each solvent. For each experiment exactly 50 ml. of solvent saturated with pure dry carbon dioxide gas was used. However, a wide variation in the ratio of solvent to solute did not show any effect on the rate of reaction. Every sample of malonic acid yielded the stoichiometric volume of carbon dioxide within experimental error. For example, in the case of benzyl benzoate 0*15615 gm. of malonic acid produced 36-9 ml. (V*) of carbon dioxide at 30-0 ± 0-05° C, the stoichiometric volume being 37-1 ml. This

particularly eliminated the possibility of any other interaction (f/my-esterification type) between malonic acid and the ester. This was further confirmed by a study of refractive index. A little malonic acid was dissolved in each ester separately and the solution kept for about a week. Then the acid was removed and the refractive index of the ester determined. In no case any change in refractive index was observed.

Excellent first-order kinetics were observed over the major part of the reaction with agreeable reproducibility. In all the cases the plot of $\log \{a-x\}$ versus the time gave good straight lines. The average values of the apparent first-order rate constants for the reaction in the four esters at the different temperatures studied, obtained from the slopes of the experimental logarithmic plots, are given in Table II. For the purpose of comparison the rate

TABLE II

Apparent first-order rate constants for the decarboxylation of malonic acid in esters

Solvent	Temperature ° C.	$k_{\pm} \times 10^6$ seer ¹
Methyl Benzoate	110-0	4-776±0-02
	125-7	19-380±0-016
	137-0	50-51 ±0-030
Ethyl Benzoate	104-7	2-615±0-012
	107-1	3-088±0-014
	128-1	14-93 ±0-070
	137-0	27-35 ±0-024
Benzyl Benzoate	108-5	2-721±0-03
	123-2	~8-578±0-01
	127-5	11-48 ±0-08
	136-1	22-16 ±0-047
/ra/u-Ethyl Cinnamate	110-0	6-243±0-09
	125-2	16-85 ±0-06
	143-0	52-05 ±0-10

constant at a fixed temperature, 125° C, was evaluated for each solvent making use of the Arrhenius Equation. The activation parameters calculated on the basis of the Eyring Equation^{4*}

$$k = \frac{KT}{h} e^{-\Delta H/RT} e^{\Delta S/R}$$

are shown in Table III. A plot of $\log k$ versus $1/T$ was linear in every case as shown in Fig. 1.

TABLE III

Activation parameters for the decarboxylation of malonic acid in esters

Solvent	$k_{125}^{\circ\text{C}}$ seer ¹	A seer ¹	E • K. cal.	AS.e.u.	A F K. cal.	AH K. cal.
Methyl Benzoate	1.820×10^4	1.31×10^{11}	27.0	- 3.5	30.3	31.7
Ethyl Benzoate	1.202×10^4	1.32×10^8	21.9	- 9.5	30.6	26.8
Benzyl Benzoate	9.605×10^6	$5.2 \times 10^*$	23.2	- 8.3	30.8	27.4
<i>trans</i> -Ethyl Cinnamate	$1.679 \times 10^{-*}$	3.1×10^1	20.5	- 10.7	30.4	26.1

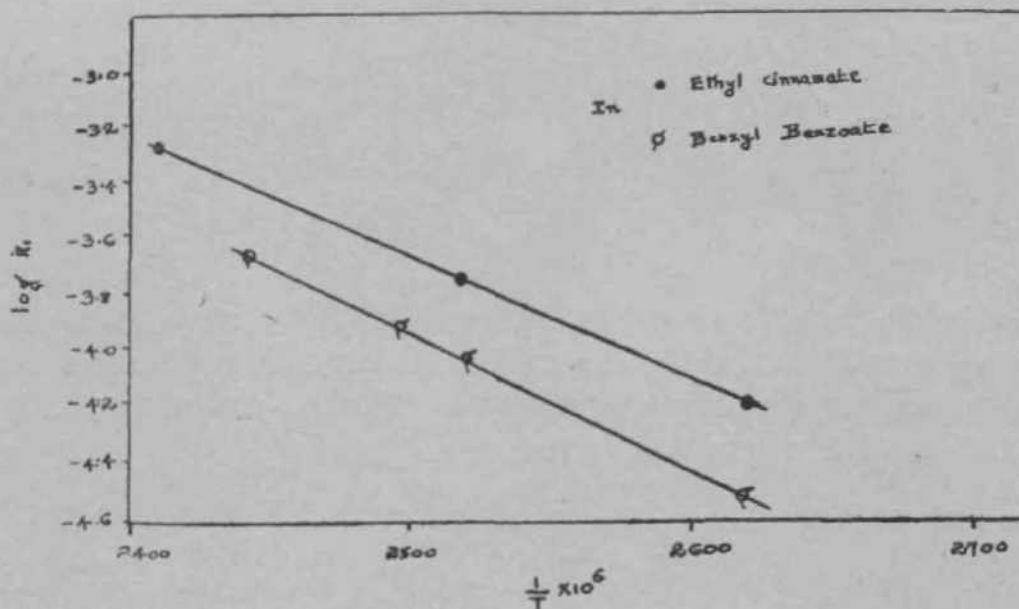


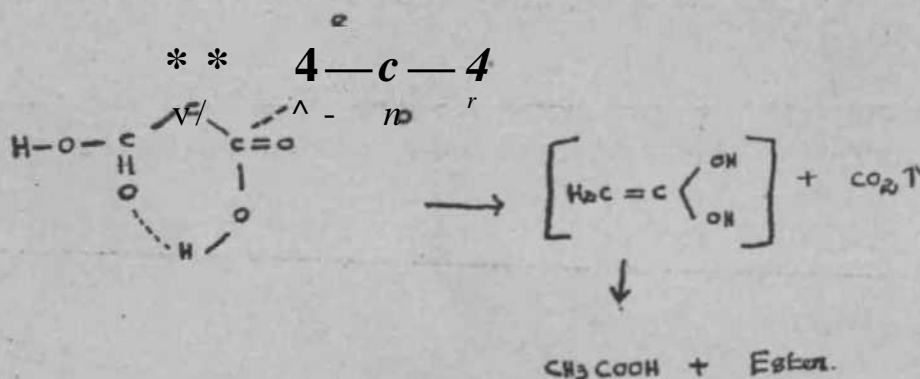
Fig. 1. A plot of $\log k$, versus $1/T$.

DISCUSSION

The data in Table III prove the reasonableness of the proposed mechanism for the decarboxylation of malonic acid. It will be observed from Table III that the energy of activation is least in ethyl cinnamate and maximum in methyl benzoate. The order of E^* in the esters can be given as

Methyl benzoate > Benzyl benzoate > Ethyl benzoate > Ethyl cinnamate.

The A H values also fall in the same order. These can be understood if we consider the proposed mechanism, according to which the transition state consists of a complex formed by mutual attractions between the electrophile-nucleophile pairs. It is well known that the hydroxyl oxygen atom of the carboxylic acids may act as Lewis base, donating an unshared pair of electrons to an electrophilic agent. Based on this we can expect the alkyl oxygen of the ester group to be more nucleophilic in character due to the + I effect of the alkyl group. Accordingly for the decarboxylation of malonic acid in the ester, the transition state can be reasonably pictured thus :



Thus in the transition state the nucleophilic alkyl oxygen of the ester group interacts with one of the electrophilic carbonyl carbon atoms of the acid facilitating the cleavage subsequently. The rate-determining step is the formation of the transition state.

The ease of formation of the transition state will be determined by two factors:

- (i) the effective negative charge on the nucleophilic atom and
- (ii) the accepting ability of the electrophilic atom.

From Table 111 we can observe that the activation energy and the enthalpy decrease as the effective negative charge on the nucleophilic atom increases. Based on the order of inductive effects⁵ the alkyl oxygen atom in ethyl benzoate can be considered more nucleophilic when compared to the oxygen in methyl benzoate and this is reflected in lowering of energy

of activation as well as enthalpy of reaction. The decrease of E^* and AH in benzyl benzoate when compared to methyl benzoate can be due to greater +E effect on the part of the phenyl group.⁶ The minimum values in ethyl cinnamate can be attributed to the added nucleophilicity of the alkyl oxygen atom of the ester due to release by ethyl group on one side and phenyl group with extended conjugation on the other.⁷

The entropy of activation in any reaction generally decreases as the steric hindrance increases.⁴⁶ The entropy values observed here are in clear conformity with this principle. In methyl benzoate which would be expected to cause the least steric hindrance the ΔS value is maximum. Ethyl cinnamate with its maximum volume shows least entropy of activation, whereas the values are intermediate in ethyl benzoate and benzyl benzoate

The free energy values are almost constant in all the esters within experimental error, indicating that the same carbon-carbon bond is broken in all the cases.

Further a plot of AH versus ΔS gives a straight line as shown in Fig. 2 indicating that the mechanism of decarboxylation is same in all the solvents.⁸

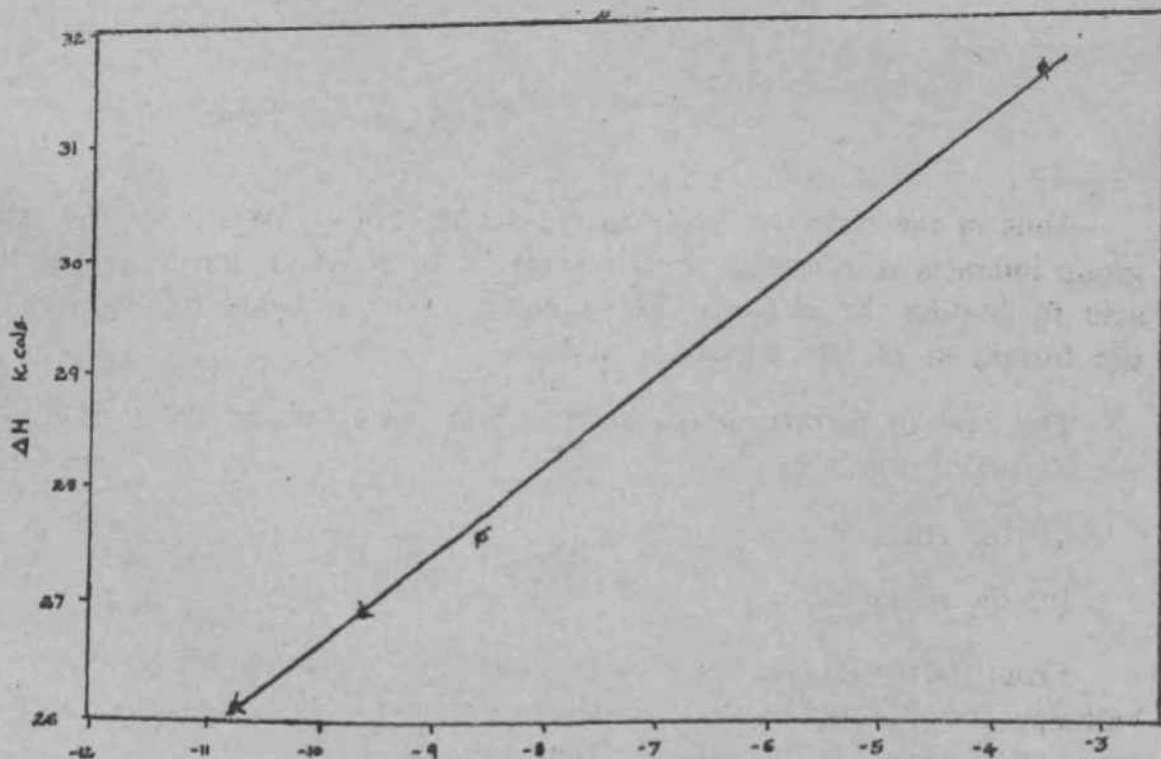


Fig. 2. A plot of Entropy versus Enthalpy

A final evidence for the validity of the polar mechanism for decarboxylation comes when we compare the values of dielectric constants in Table I with the observed rate constants at 125° C. The rate constant increases with increase of dielectric constant of the medium.

ACKNOWLEDGEMENT

The authors wish to express their thankfulness to Dr. S. V. Anantakrishnan, F.N.L, Madras Christian College and Dr. L. W. Clark, Western Carolina College, U.S.A., for their suggestions. R. G. thanks the Government of India for giving a scholarship during the period of this investigation.

REFERENCES

- 1 a. Clark, L. W. .. *J. Phys. Chem.*, 1960, 64, 692.
- b. Fraenkel, G., Belford, R. L. .. *J. Am. Chem. Soc.*, 1954, 76, 15.
 and Yankwich, P. E.
2. Clark, L. W. .. *J. Phys. Chem.*, 1956, 60, 1150.
3. Weissbeiger, .. *Technique of Organic Chemistry*, Interscience Publishers, Inc., New York, 1955, Vol VII.
- 4 a. Glsstone, S., Laidler, K. J. .. *The Theory of Rate Processes*, McGraw-Hill Book Co.,
 and Eyring, H. Inc., New York, N.Y., 1941, p. 14.
- b. ————— .. *Ibid.*, 1941, p. 22.
5. Ingold, C. K. .. *Structure and Mechanism in Organic Chemistry*, G. Bell
 and Sons Ltd., London, 1953, p. 71.
6. ————— .. *Ibid.*, 1953, p. 657.
7. ————— .. *Ibid.*, 1953, p. 740.
8. Leffier, J. E. .. *J. Org. Chem.*, 1955, 20, 1202.

MEIJER'S G-FUNCTION AND THE TEMPERATURE IN A NONHOMOGENEOUS BAR

BY S. D. BAJPAI*

[Department of Applied Mathematics, Shri G.S. Technological Institute, Indore-3 (M.P.)]

Received November 25, 1967

(Communicated by Prof. P. L. Bhatnagar, F.A.S.C.)

ABSTRACT

In this paper we have employed Meijer's G-function to solve a problem of the temperature in a nonhomogeneous bar and shown how Meijer's G-function may be found useful in solving many problems of applied mathematics.

1. INTRODUCTION

As an example of the use of Meijer's G-function in heat conduction we shall consider the problem of determining a function $u(x, t)$, if $u=f(x)$ when $t=0$, where $u(x, t)$ represents the temperature in a nonhomogeneous bar with ends at $x = -1$ and $x = 1$ in which the thermal conductivity is proportional to $1 - x^2$ and if the lateral surface of the bar is insulated, the heat equation has the form [1, p. 197, (8)]

$$\frac{\partial u}{\partial t} = b \frac{\partial}{\partial x} \left[(1 - x^2) \frac{\partial u}{\partial x} \right], \quad (1.1)$$

where b is a constant, provided the thermal coefficient cS is a constant [1, p. 17, Sec. 9]. The ends $x = \pm 1$ are also insulated because the conductivity vanishes there.

In what follows for sake of brevity a_r denotes a_1, \dots, a_r ; A is a positive integer and the symbol $A(K^a)$ represents the set of parameters

$$\frac{0}{\lambda}, \frac{a+1}{\lambda}, \dots, \frac{a+A-1}{\lambda}.$$

In this paper we have considered

$$u = f(x) = (1 - x)^a G_{r+1}^r \left[x(1 - x)^\lambda \mid \lambda \right] \quad (1.2)$$

Present address ; Regional Engineering College, Kumksñetra (Haryana).

The following formula is required in the proof:

$$\int_{-1}^1 (1-x)^\sigma P_m(x) G_{r,s}^{p,q} \left[z(1-x)^\lambda \left| \begin{matrix} a_r \\ b_s \end{matrix} \right. \right] dx$$

$$= \frac{2^{\sigma+1}}{\lambda} G_{r+s\lambda, \sigma+2\lambda}^{p+\lambda, \sigma+\lambda} \left[\begin{matrix} A(A, -a), a_r, A(A, -a) \\ A(A, -\sigma-m), b_s, A(A, -\sigma-m) \end{matrix} \right] \quad (0-3)$$

where

$$r + s < 2(p + q), \quad |\arg z| < (p + q - \frac{1}{2}r - \frac{1}{2}s)\pi,$$

$$\operatorname{Re}(a + \lambda b_j) > -1, \quad j = 1, 2, \dots, p.$$

which follows from [3, p. 198, (3.2)].

2. The solution to be obtained is

$$u(x, t) = \frac{2^\sigma}{\lambda} \sum_{n=0}^{\infty} (2n+1) G_{r+s\lambda, \sigma+2\lambda}^{p+\lambda, \sigma+\lambda}$$

$$\times \left[2^\lambda z \left| \begin{matrix} A(A, -a), \text{ or } A(A, -o) \\ \Delta(\lambda, -a + ri), b_u, A(A, -1 - \sigma - n) \end{matrix} \right. \right]$$

$$\times P_n(x) e^{-bn(n+1)t}, \quad (2.1)$$

where

$$r + s < 2(p + q), \quad |\arg z| < (p + q - \frac{1}{2}r - \frac{1}{2}s)\pi,$$

$$\operatorname{Re}(a + \lambda b_j) > -1, \quad j = 1, 2, \dots, p.$$

Proof.—The solution of the problem as given in [1, p. 197, (8)] is

$$u(x, t) = \sum_{n=0}^{\infty} A_n P_n(x) e^{-bn(n+1)t} \quad (2.2)$$

If $\lambda = 0$, then by virtue of (1.2), we have

$$(1-x)^\sigma G_{r,s}^{p,q} \left[z(1-x)^\lambda \left| \begin{matrix} a_r \\ b_s \end{matrix} \right. \right] = \sum_{n=0}^{\infty} A_n P_n(x) \quad (2.3)$$

Multiplying both sides of (2-3) by $P_m(x)$ and integrating with respect to x from -1 to 1 , we obtain

$$\int_{-1}^1 (1-x)^r P_m(x) G'_{r,s}(z) dx = \int_{-1}^1 A_n P_m(x) P_n(x) dx \tag{2.4}$$

Using (1-3) and the orthogonality property of Legendre polynomials [p. 277, (13) and (14)], we get

$$A_{r,s} = (2m+1) G_{r+s, r+s}^{r+s, r+s}(z) \int_{-1}^1 (1-x)^r P_m(x) P_n(x) dx \tag{2.5}$$

where

$$r + s < 2(p + q), \quad |\arg z| < (p + q - |r - s|)n_0$$

$$\operatorname{Re}(a + Afy) > -1, \quad J = 1, 2, \dots, \infty$$

Now with the help of (2.2) and (2.5) the solution (2.1) follows immediately.

On specializing the parameters, the G-function may be converted into Bessel functions, Legendre functions, and other higher transcendental functions [2, pp. 434-444]. Therefore, the $f(x)$ given in (1.2) is of general character and hence may encompass several cases of interest.

ACKNOWLEDGEMENT

I am thankful to Dr. V. M. Bhise for his keen interest in the preparation of this paper. My thanks are also due to Principal Dr. S. M. Das Gupta for the facilities he gave to me.

REFERENCES

1. Churchill, R. V. .. *Fourier Series and Boundary Value Problems*, McGraw-Hill, New York, 1942.
2. Erdelyi, A. .. *Tables of Integral Transforms*, McGraw-Hill, New York, 1954, 2.
3. Saxena, R. K. .. "On some results involving Jacobi polynomials," *Journal of Indian Math. Soc.*, 1964, 28 (3 and 4,) 197-202,

CERTAIN SERIES INVOLVING PRODUCTS OF LAGUERRE POLYNOMIALS

BY H. M. SRIVASTAVA *

(Department of Mathematics, West Virginia University, Morgantown, West Virginia, U.S.A.)

Received August 17, 1968

(Communicated by Dr. R. S. Varma, F.A.S.C.)

ABSTRACT

The author discusses here certain infinite sums of products of generalized Laguerre polynomials.

IN a recent paper published in these *Proceedings* Rangarajan⁴ obtained the sums of two infinite series involving products of Laguerre polynomials in the formsf

$$\begin{aligned} & \sum_{n=0}^{\infty} \frac{n!}{(\alpha+1)_n} L_n^{(\alpha)}(x) L_n^{(\beta)}(y) z^n \\ &= (1-z)^{-\beta-1} \exp. \left[-\frac{(x+y)z}{1-z} \right] \\ & \quad \times \Phi_3 \left[\alpha - \beta; \alpha + 1; \frac{xz}{1-z}, \frac{xyz}{(1-z)^2} \right] \end{aligned} \quad (1)$$

and

$$\begin{aligned} & \sum_{n=0}^{\infty} \frac{n!}{(\alpha+1)_n} L_n^{(\alpha)}(x) L_n^{(\beta-n)}(y) z^n \\ &= (1+z)^\beta \exp. (-yz) {}_2F_2 \left[-j; \alpha + 1; \frac{xz}{1+z}, xyz \right], \end{aligned} \quad (2)$$

* Present address : Department of Mathematics, University of Victoria, Victoria, British Columbia, Canada.

tNote that the formula (1) appears incorrectly on page 362 of Rangarajan's paper referred to above.

where Φ_3 denotes a Humbert's confluent hypergeometric function in two arguments defined by means of (cf Erd61yi et al.⁹ p. 225)

$$\Phi_3 [a; \beta; x, y] = \sum_{m, n=0}^{\infty} \frac{(a)_{m+n}}{(a)_{m+n}} \frac{x^m y^n}{m! n!} \tag{3}$$

It may be of interest to observe that formula (1) in a more general form was proved many decades earlier by Erdélyi¹ and that both (1) and (2) admit themselves of further elegant generalizations which we have recently derived elsewhere (see Srivastava^{6*7}).

Indeed from the definition (3) it follows that

$$\begin{aligned} \Phi_3 \left[a; \beta; \frac{xz}{1-z}, \frac{xyz}{(1-z)^2} \right] &= \sum_{n=0}^{\infty} \frac{1}{(a+1)_n n!} {}_1F_1 \left[\begin{matrix} a-\beta; \\ a+n+1; \end{matrix} \frac{xz}{1-z} \right] \left[\frac{xyz}{(1-z)^2} \right]^n \\ &= \exp. \left(\frac{xz}{1-z} \right) \sum_{n=0}^{\infty} \frac{1}{(a+1)_n n!} \\ &\quad \times {}_1F_1 \left[\begin{matrix} \beta+n+1; \\ a+n+1; \end{matrix} \frac{-xz}{1-z} \right] \left[\frac{xyz}{(1-z)^2} \right]^n \end{aligned}$$

by Kummer's theorem (cf. Erd61yi et al.,² p. 253)

$${}_1F_1 \left[\begin{matrix} a; \\ c; \end{matrix} z \right] = \exp(z) {}_1F_1 \left[\begin{matrix} c-a; \\ c; \end{matrix} -z \right]$$

and (1) assumes the desired form

$$\sum_{n=0}^{\infty} \frac{n!}{(a)_n} L_n^{(a-1)}(x) L_n^{(\beta-1)}(y) z^n$$

$$\begin{aligned}
&= (1-z)^{-\beta} \exp. \left(\frac{yz}{z-1} \right) \\
&\quad \times \sum_{n=0}^{\infty} \frac{1}{(\alpha)_n n!} {}_1F_1 \left[\begin{matrix} \beta+n; \\ \alpha+n; \end{matrix} \frac{xz}{z-1} \right] \left[\frac{xyz}{(1-z)^2} \right]^n. \quad (4)
\end{aligned}$$

Obviously, this is a special case of Erdélyi's formula* (cf. Erdélyi,¹ p. 344)

$$\begin{aligned}
&\sum_{n=0}^{\infty} \frac{(\gamma)_n n!}{(\alpha)_n (\beta)_n} L_n^{(\alpha-1)}(x) L_n^{(\beta-1)}(y) z^n \\
&= (1-z)^{-\gamma} \sum_{n=0}^{\infty} \frac{(\gamma)_n}{(\alpha)_n (\beta)_n n!} \cdot {}_1F_1 \left[\begin{matrix} \gamma+n; \\ \alpha+n; \end{matrix} \frac{xz}{z-1} \right] \\
&\quad \times {}_1F_1 \left[\begin{matrix} \gamma+n; \\ \beta+n; \end{matrix} \frac{yz}{z-1} \right] \left[\frac{xyz}{(1-z)^2} \right]^n, \quad |z| < 1, \quad (5)
\end{aligned}$$

when $y = j\delta$.

We conclude with the remark that in the course of an attempt to give extensions of the well-known Hille-Hardy formula (c/l., e.g., Erdélyi *et al.*,³ p. 189)

$$\begin{aligned}
&\sum_{n=0}^{\infty} \frac{1}{\Gamma(n+a+1)} L_n^{(a)}(x) L_n^{(a)}(y) z^n \\
&= (1-z)^{-1} \exp. \left[-\frac{(x+y)z}{1-z} \right] \\
&\quad \times (xyz)^{-1/2} I_0 \left[\frac{2\sqrt{xyz}}{1-z} \right], \quad |z| < 1, \quad (6)
\end{aligned}$$

which follows readily from (4) and (5) when $a = j\delta = y$, we have recently invoked the Laplace and the inverse Laplace transform techniques and the method of finite mathematical induction to obtain several new and distinct

* See also the formula (27) on page 288 of Erdélyi *et al.** For an elementary method of derivation of (5) in a slightly different form see formula (2-3) on page 306 of Srivastava.⁵

bilinear generating functions for certain classes of generalized hypergeometric polynomials. For instance, we have (cf. Srivastava⁶)

$$\begin{aligned} & \sum_{n=0}^{\infty} \frac{(\lambda)_n}{n!} {}_{p+1}F_q \left[\begin{matrix} -n, a_1, \dots, a_p \\ b_1, \dots, b_q \end{matrix}; x \right] {}_{r+1}F_s \left[\begin{matrix} -n, a_x, \dots, a_r \\ \dots \end{matrix}; yz \right] \\ &= (1-z)^{-\lambda} \sum_{n=0}^{\infty} \frac{(\lambda)_n (a_1)_n \dots (a_p)_n (\beta_1)_n \dots (\beta_s)_n}{n! (b_1)_n \dots (b_q)_n} \left[\frac{xyz}{(1-z)^2} \right]^n \\ & \quad \times {}_{p+1}F_q \left[\begin{matrix} \lambda + n, a_1 + n, \dots, a_p + n \\ b_1 + n, \dots, b_q + n \end{matrix}; \frac{yz}{z-1} \right] \\ & \quad \times {}_{r+1}F_s \left[\begin{matrix} A + n, a_1 + n, \dots, a_r + n \\ \beta_1 + n, \dots, \beta_s + n \end{matrix}; yz \right] \end{aligned} \tag{7}$$

and

$$\begin{aligned} & \sum_{n=0}^{\infty} \frac{(\lambda)_n}{n!} {}_{p+1}F_q \left[\begin{matrix} -n, a_1, \dots, a_p \\ b_1, \dots, b_q \end{matrix}; x \right] {}_{r+1}F_s \left[\begin{matrix} -n, a_1, \dots, a_r \\ 1 - A - n, \beta_1, \dots, \beta_s \end{matrix}; yz \right] z^n \\ &= (1-z)^{-\lambda} \sum_{n=0}^{\infty} \frac{(a_1)_n \dots (a_p)_n (a_1)_n \dots (a_r)_n (-xyz)^n}{(b_1)_n \dots (b_q)_n n!} \\ & \quad \times {}_{p+1}F_q \left[\begin{matrix} \lambda, a_1 + n, \dots, a_p + n \\ b_1 + n, \dots, b_q + n \end{matrix}; \frac{yz}{z-1} \right] {}_{r+1}F_s \left[\begin{matrix} a_1 + n, \dots, a_r + n \\ \beta_1 + n, \dots, \beta_s + n \end{matrix}; yz \right], \end{aligned} \tag{8}$$

under the conditions of validity discussed in Srivastava.⁵⁻⁶

The formula (7) extends several hitherto scattered results in the theory of generalized hypergeometric polynomials, while in the special case

$$p = r = s = 0, \quad q = U, \quad b_x = l + a_0, \quad A = -l$$

(8) corresponds to the formula (2) which, in turn, reduces to the known generating relation (cf. Erdélyi *et al.*,³ p. 215)

$$\begin{aligned} & \sum_{n=0}^{\infty} \frac{(-1)^n n!}{\Gamma(a+n+1)} L_n^{(a)}(x) L_n^{(\beta-n)}(y) \\ &= x^{-\frac{1}{2}(a-\beta)} y^{-\frac{1}{2}(a+\beta)} \exp(y) J_{a+\beta}(2\sqrt{xy}) \end{aligned}$$

in the limit when $z \rightarrow -1$.

REFERENCES

- | | |
|-----------------------|--|
| 1. Erdélyi, A. | .. <i>Compositio Math.</i> , 1939, 6, 336-47. |
| 2. ————— <i>et al</i> | .. <i>Higher Transcendental Functions</i> , Vol. I, McGraw-Hill, New York, 1953. |
| 3. ————— | .. <i>Ibid.</i> , Vol. II, McGraw-Hill, New York, 1953. |
| 4. Rangarajao. S. K. | .. <i>Proc. Ind. Acad. Set</i> , Sec. A, 1964, 58, 362-67. |
| 5. Srivastava, H. M. | .. <i>Math. Comp.</i> , 1969, 23, 305-11; see also <i>Notices Amer. Math. Soc.</i> , 1968, 15, 634-35. |
| 6. ————— | .. <i>Glasnik Mat., Ser.</i> , III, 1969, 4, 67-73. |
| 7. ————— | .. <i>Notices Amer. Math. Soc.</i> , 1969, 16, 411, 674- |

THE LIFETIMES OF POSITRONS IN OXIDES OF ARSENIC AND ANTIMONY

BY V. G. KULKARNI, R. G. LAGU, GIRISH CHANDRA AND
B. V. THOSAR, F.A.S.C.

(Tata Institute of Fundamental Research, Bombay-5, India)

Received June 4, 1969

ABSTRACT

The lifetimes of positrons in crystalline powders of dimeric oxides of arsenic and antimony, and in trioxymethylene and polyoxymethylene are reported. In As_4O_6 and polyoxymethylene a longer component τ_4 is observed in addition to the usually observed τ_2 component. The variation of τ_4 with temperature and pressure is studied in As_4O_6 . On the basis of these results and the X-ray diffraction pictures, it is suggested that ortho-positronium atoms quenched in intercrystallite regions in As_4O_6 gives rise to τ_4 .

INTRODUCTION

It is well known that the long component τ_2 , observed in the lifetime spectra of positrons annihilating in a condensed medium is due to the quenching of the ortho-positronium atoms by the electrons of the medium.¹ τ_2 is usually in the range of 1 to 5 nanoseconds. Recently, however, another longer component, τ_4 , of the order of a few tens of nanoseconds, has been observed in some ionic oxides like MgO , Al_2O_3 , BeO , etc.²⁻⁴ In most of these cases τ_4 has an intensity (I_4) smaller than the intensity (I_2) of the τ_2 component. The origin of such long components is not clearly understood at present.

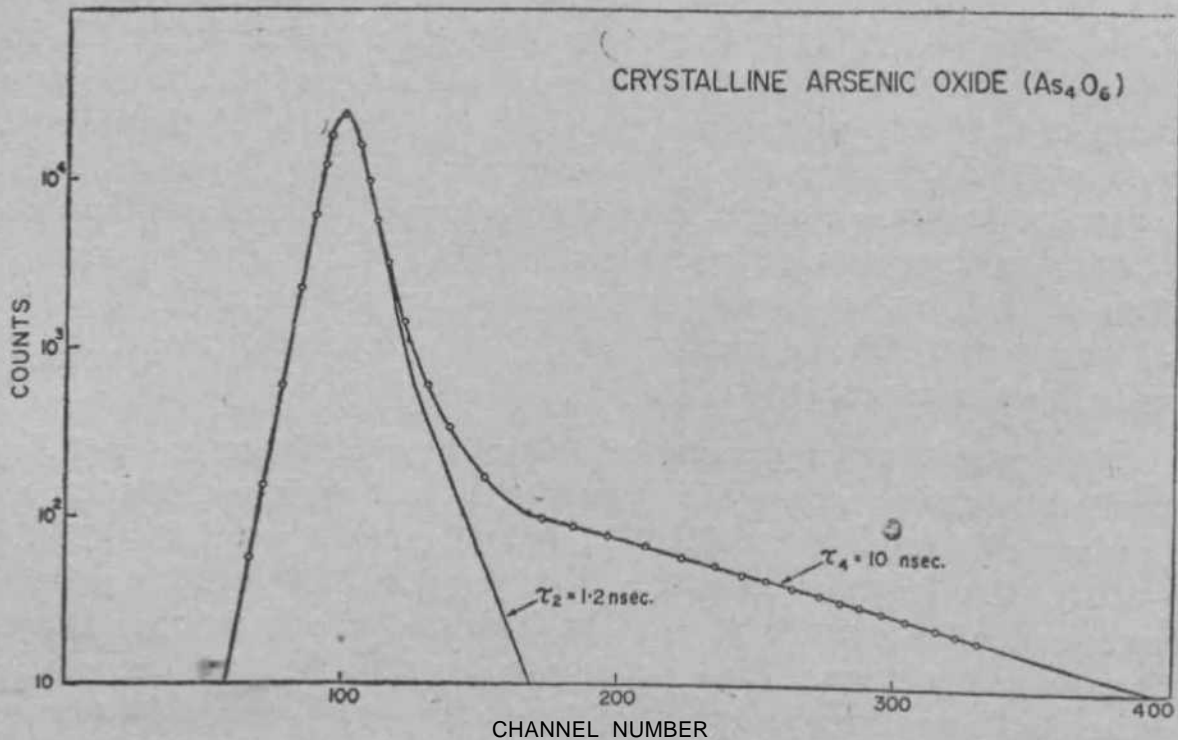
The present paper reports the lifetimes of positrons in crystalline powders of dimeric oxides of arsenic (As_4O_6) and antimony (Sb_4O_6), and in trioxane [trioxymethylene $(\text{CH}_2\text{O})_3$] and polyoxymethylene [$\text{H}-(\text{CH}_2\text{O})_n-\text{OH}$]. The longer component τ_4 is observed in As_4O_6 , and in polyoxymethylene. The variation of τ_4 in As_4O_6 is studied as a function of temperature and pressure. These results together with the Laue transmission patterns and powder photographs obtained for crystalline and heat-treated samples suggest that τ_4 could arise out of ortho-positronium atoms quenched in intercrystallite regions.

EXPERIMENTAL SET-UP

The standard slow-fast coincidence set-up used in this work to measure the lifetimes of positrons, and the procedure to compute the intensity of the delayed component have been reported earlier.¹ The delayed component T_2 and its intensity are obtained by subtracting the T_4 part from the total spectrum, when two delayed components are present.

RESULTS AND DISCUSSION

Text-Figure 1 shows a typical lifetime spectrum obtained for crystalline As_4O_6 at room temperature, showing two delayed components, $T_2 = 1.2$ ns and $T_4 = 10$ ns. The variation in the values and intensities of the delayed components as a function of temperature and pressure is shown in Table I. As the temperature is increased beyond $100^\circ C$, T_4 begins to decrease and at about $135^\circ C$, T_4 disappears irreversibly, *i.e.*, does not reappear on cooling the sample back to room temperature. The experiment was carried out with the sample in vacuum, the tube containing the pellets and the Na^{32} source being evacuated continuously, so as to avoid the effects due to oxygen, and was repeated several times to ensure the irreversible disappearance of r_4 at about $135^\circ C$. When As_4O_6 pellets were



TEXT-FIG. 1. Typical time distribution of positron-annihilation quanta in polycrystalline As_4O_6 , at room temperature (schematic).

subjected to a pressure of 100 tons/sq. inch, the value of T_4 decreases. These pellets also exhibit an irreversible disappearance of r_4 at about 135° C. as seen from Table. I.

TABLE I

Sample	Temperature ° C.	t ns	$h\%$	τ_4 ns	I.%
As ₄ O ₆ pellets prepared under 5—75 tons/sq. inch cooled to	27	1-2±0-1	25±2	10±1	5±1
	100	1*2±0-1	9±2	8±1	16±2
	150	1-8±0-2	13±2	••	..
	200	1-8±0-2	13±2	••	..
	27	1-2±0-1	11±2	••	..
As ₄ O ₆ pellets prepared under 100 tons/sq. inch cooled back to	27	<1	••	6-5±1	5±2
	100	<1	..	5±1	5±2
	130	1-3±0-2	6±2	..	••
	200	1-2±0-2	13±2	..	••
	27	1-2±0-2	13±2	..	•«
Arsenic trioxide glass	27	2.0±0.1	11±1	••	••
Sb ₄ O ₆	27	3-1±0-1	5±1	••	••
Trioxane	27	1-2±0-1	27±2
Polyoxymethylene	27	2.1±0.1	9±2	13±1	~0-4

Sen and Patro⁵ have shown that the longer component T_4 observed in Al₂O₃ arises out of two photon events. They have observed T_4 by two different methods, with the standard slow-fast coincidence set-up and also with the triple slow double fast coincidence set-up designed to detect only two photon events, and have obtained the same value (63 ns) for T_4 in Al₂O₃. From this result they conclude that T_4 is associated with two photon decay and not with three photon decay. Their work suggests that T_2 and T_4 could arise out of ortho-positronium atoms quenched in two different kinds of sites in the medium.

As₄O₆ exists at room temperature in arsenolite phase.⁶ This molecular phase is built up from As₄O₆ molecules arranged in such a way that

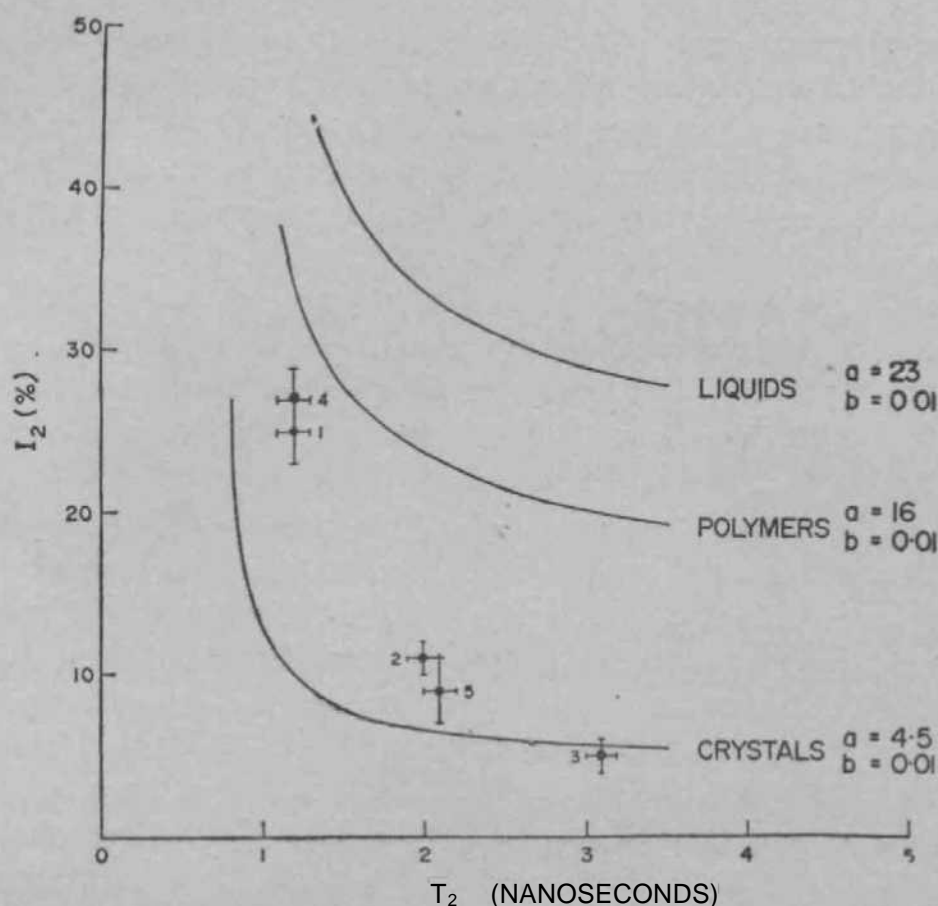
their centroids occupy the lattice points of a diamond structure ($a = 11.06$ Å). The basic unit is a three-sided pyramid with the arsenic atom at its apex and the oxygen atoms at the other three corners. Four such units are bonded together through the oxygen atoms, to form a molecular unit, As_4O_6 . Weak van der Waals forces bind As_4O_6 units into a crystalline molecular lattice.

The data of lifetimes of positrons in arsenic oxide can be interpreted, if we suppose that the usual slow component T_2 arises out of ortho-positronium atoms annihilating within the crystallite by the pick-off process, while T_4 is due to ortho-positronium atoms annihilating in the intercrystallite regions. Above 100°C . As_4O_6 begins to vaporise appreciably, and the size of the crystallite is reduced. The continuous mass thus formed by fusing together of crystallites at about 135°C . has a glassy appearance. It is known that the polished surfaces of arsenolite begin to exhibit roughening⁶ when heated beyond 95°C . Arsenic trioxide glass, known to possess a semi-ordered structure, prepared by heating As_4O_6 in vacuum up to 500°C . does not exhibit T_4 .

A decrease in the volume of the intercrystallite sites can also be achieved by subjecting the material to sufficiently high pressures. As_4O_6 pellets prepared under a high pressure of 100 tons/sq. inch (as compared to 0.5 to 0.75 tons/sq. inch, used normally) show a measurable decrease in T_4 . The irreversible disappearance of T_4 at about 135°C . is reproduced for these samples also.

The Laue transmission patterns obtained with MoK α radiation for crystalline As_4O_6 , As_4O_6 heated up to 200°C , and arsenic trioxide glass are shown in Plate I, Fig. 1. The pattern for crystalline As_4O_6 consists of discrete spots, which merge into continuous rings in the pattern for the arsenic trioxide glass, the sample heated up to 200°C . showing an intermediate pattern.

The powder photographs for these samples obtained with Cu K α radiation are shown in Plate II, Fig. 2. The large angle scattering, seen for crystalline As_4O_6 , shows a decrease in intensity for the sample heated up to 200°C . and is nearly absent for the arsenic trioxide glass. These results show⁷ that the crystallite size of the sample decreases upon heating and that the arsenic trioxide glass is in a semi-ordered crystalline form. These results and the observed variation of T_4 with temperature and pressure are consistent with the suggested origin of r_4 .



TEXT-FIG. 2. Observed values of I_2 and T_2 for (1) Polycrystalline As_4O_6 , (2) Arsenic Trioxide (glass) heated to $500^\circ C$, (3) Polycrystalline Sb_4O_6 , (4) Trioxane, (5) Polyoxymethylene plotted over the $V T_2$ correlation curves.

ANTIMONY OXIDE (Sb_4O_6)

Antimony oxide has a structure similar to that of arsenic oxide,* but the sample is composed of crystallites very much smaller in size, as indicated by the Laue transmission pattern and the powder photograph for Sb_4O_6 shown in Plates 1 and 11 respectively. Sb_4O_6 exhibits only one delayed component $r_2 = 3.1$ ns with an intensity $I_3 = 5\%$. The values of T_1 and I_2 do not change when the sample is heated in vacuum up to $500^\circ C$. The Laue pattern and the powder photograph for Sb_4O_6 heated up to $500^\circ C$ are found to be similar to those obtained for Sb_4O_6 shown in Plates I and II. It is interesting to note that the X-ray patterns and positron lifetime studies are together useful in investigating such structural changes,

TRIOXANE

Crystalline trioxane has the property that it polymerises in the solid state⁸ under irradiation by γ -rays, and retains a highly crystalline character

even in the polymer phase. The crystalline character of these two phases has been studied extensively by Okamura *et al.*⁵ by X-ray diffraction. Trioxane in polymer phase (polyoxymethylene) was obtained by irradiating polycrystalline trioxane monomer with γ -rays from a 22-5KC source of Co^{60} . The polymer phase is separated from the monomer phase by dissolving the monomer in methyl alcohol. The results of lifetime measurements of positrons in both these phases of trioxane, given in Table I, show that the monomer phase exhibits only one delayed component $T_2 = 1-2\text{ns}$ with an intensity of 27%. The polymer phase exhibits two delayed components, the longer one $T_4 = 13\text{ ns}$ having a much smaller intensity $I_4 \approx 0.4\%$.

A correlation between the value (r_2) and the intensity (I_2) of the delayed component based on a free volume model for molecular materials has been reported earlier.^{1,9} Here the intensity is plotted against r_2 for molecular materials in different states of aggregation, and three distinct curves are obtained for fully amorphous solids and liquids, semi-crystalline polymers and crystals. The point for Sb_4O_6 lies on the crystal curve. The point, corresponding to crystalline As_4O_6 , lies near the crystal curve, while that corresponding to semi-ordered arsenic trioxide glass lies between the curves for crystals and polymers. The points corresponding to trioxane monomer and trioxane polymer fall very close to the crystal curve.

These results seem to suggest that the second long component (r_j) observed in the lifetime spectrum of positrons in arsenic oxide is probably due to ortho-positronium atoms annihilating by the pick-off process in inter-crystallite sites. This conclusion seems to be justified by the observed changes in T_4 in arsenic oxide as a function of temperature and pressure and by the X-ray diffraction patterns.

REFERENCES

1. Lagu, R. G., Kulkarni, V. G., Thosar, B. V. and Girish Chandra *Proc. Ind. Acad. Sci.* 1969, 69, 48.
2. Paulin, R. and Ambrosino, G. *Positron Annihilation*, Academic Press, 1967, p. 345.
3. _____" .. *C.R. Acad. Sci. Paris*, 1966, 263, 207.
4. _____^ .. *Jour, de Phys.*, 1968, 29, 263.
5. Sen, P. and Patro, A. P. .. *Phys. Letters*, 1968, 28A, 414,

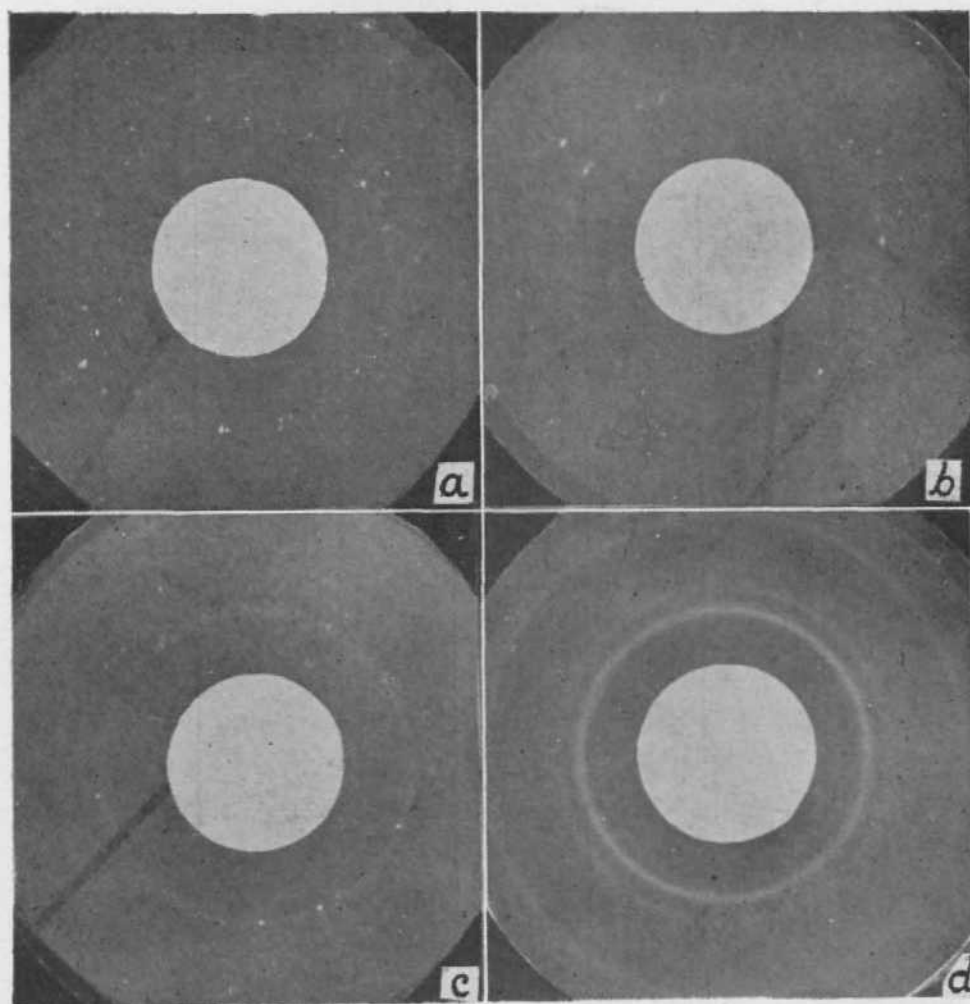


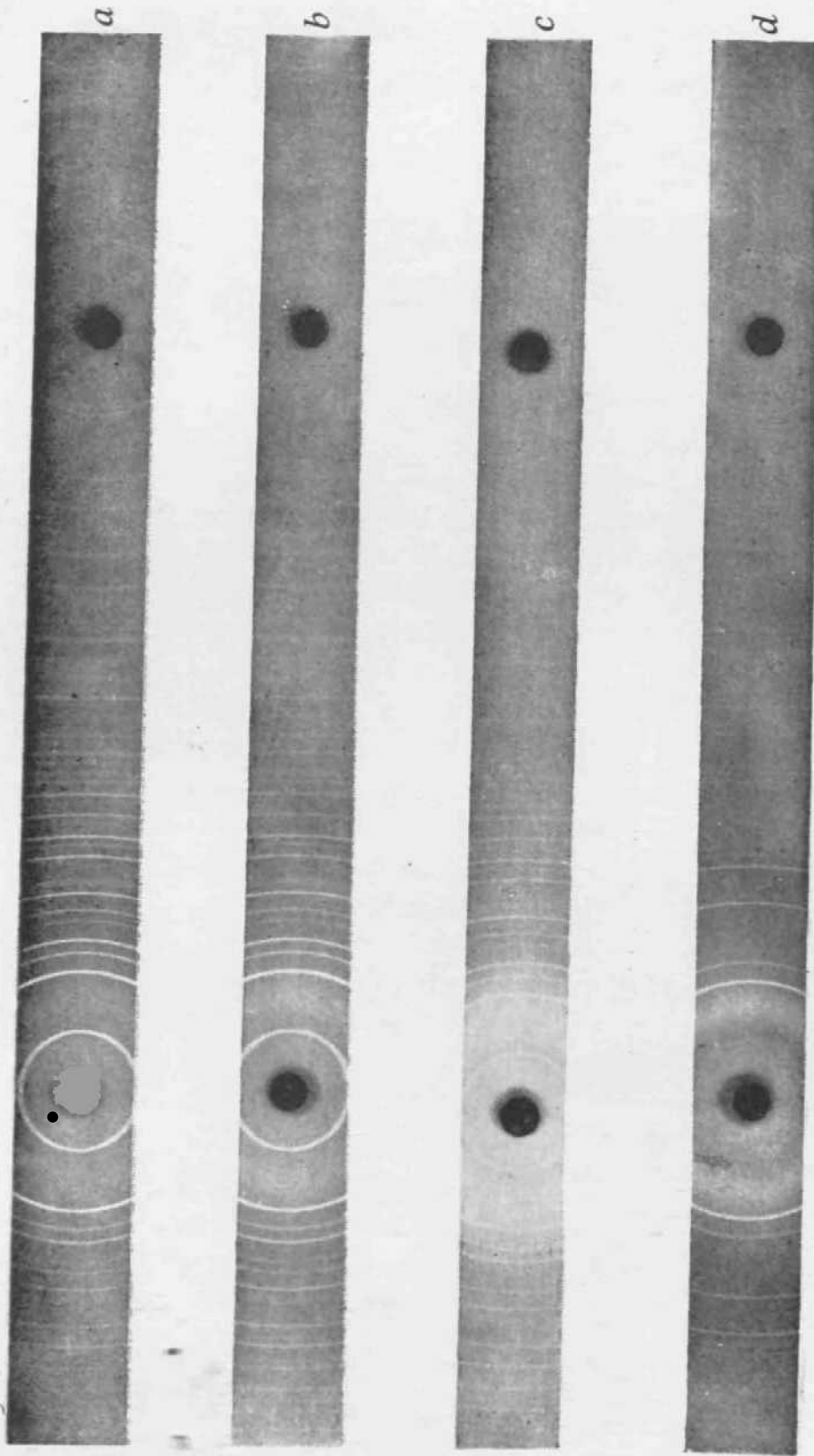
FIG. 1, X-Ray Laue Transmission Patterns

(a) Polycrystalline As_2O_3

(A) As_4O_6 heat-treated up to $200^\circ C$.

(c) Arsenic trioxide Glass

(d) Polycrystalline Sb_2O_3



46
o
de
I II
ic
rys

ft r-v ^s

ay

Fig. U.

(a) Polycrystalline As_4O_6
(b) Amorphous As_4O_6

The Lifetimes of Positrons in Oxides of Arsenic and Antimony 113

6. Becker, K. A., Plieth, K. and Stranski, I. N. *Progr. in Inorganic Chemistry*, Interscience, 1962, 4, I.
7. Cullity, B. D. .. *Elements of X-ray Diffraction*, Addison-Wesley, 1956, p. **261**.
8. Okamura, S., Hayashi, K. and Yasuhisha *J. Poly. Sci.*, 1962, 5*, 925.
9. Thosar, B. V., Kulkarni, V. G., Lagu, R. G. and Girish Chandra *Phys. Letters*, 1969, 28 A, 760,

VALIDITY OF LORENTZ INVARIANCE AT EXTREMELY HIGH ENERGIES

BY A. SUBRAMANIAN AND R. H. VATCHA

(Tata Institute of Fundamental Research, Bombay)

Received June 9, 1969

(Communicated by Prof. B. V. Sieekantan, F.A.S.C.)

ABSTRACT

Experimental data on the distribution of times of arrival of electrons (and muons) in extensive air showers produced by cosmic rays in the energy range 10^{12} - 10^{19} eV have been examined to see if there is any evidence for a departure of the velocity of ultra-high energy particles from that of light as suggested by the model proposed by Pavlopoulos. No evidence for such a departure has been found. An upper limit to the "fundamental length" occurring in the theory is obtained as $\sim 10^{-21}$ cm.

PAVLOPOULOS¹ has suggested the possibility of breakdown of Lorentz invariance if electromagnetic radiation obeys the wave equation

$$(-\nabla^2 + D) \psi = 0 \quad (1)$$

where l_0 is a universal constant of dimensions of length ($\sim 10^{-13}$ cm.). The relation between frequency and wave number for radiation obeying (1) is given by

$$\omega^2 = c^2 k^2 (1 + l_0^2 k^2) \quad (2)$$

where c is the velocity of light. From (2) we can write the relation between group velocity and wave number as

$$v_g = \frac{1 + 2l_0^2 k^2}{c(1 + l_0^2 k^2)} \quad (3)$$

In Fig. 1 is given a relation between $\beta (= v/c)$ and $l_0 E$, where E is the energy of the photon. Since the change in β is significant at $l_0 E > 10^{-14}$ BeV cm. we can find effects of this in the time structure of extensive air shower particles produced by ultra-high energy cosmic ray particles in the atmosphere, if values of $l_0 < 10^{-16}$ cm. are involved. For the purpose of analysing available data on the time structure of extensive air shower

particles, we have made the plausible assumption that if (1) is valid for photons, for particles with non-zero rest mass the familiar formula

$$E^2 = c^2 p^2 + m_0^2 c^4 \tag{4}$$

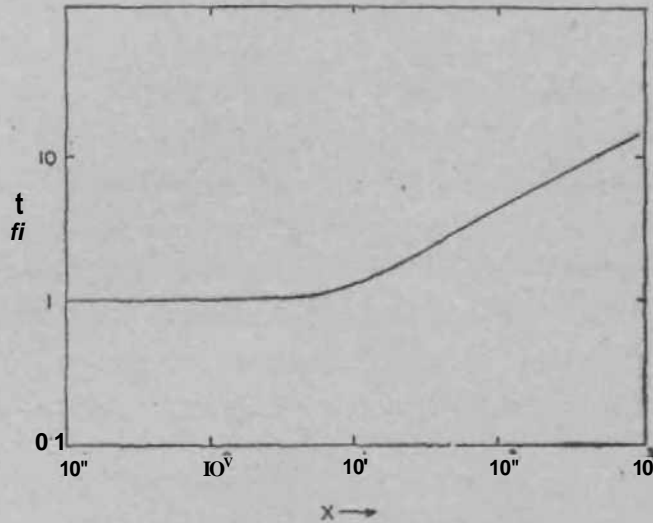


Fig. 1. The relation between velocity ($\beta = u/c$) and $X \cdot 10^{11} / E$ where l_0 is in cm. and E in BeV.

is modified as

$$E^2 = c^2 p^2 \left(1 + \frac{p^2 l_0^2}{\hbar^2} \right) + m_0^2 c^4 \tag{5}$$

such that (4) is valid when $l_0 \rightarrow 0$ and the velocity relation (3) holds good for particles of non-zero rest mass at energies $E \gg m_0 c^2$.

We have made a Monte Carlo calculation of the time spread in the electrons at a given level in γ -ray initiated showers in the atmosphere. In this calculation we have further assumed that cross-sections for pair production and bremsstrahlung for photons and electrons respectively are given by the usual Bethe-Heitler formula at extremely high energies although a finite $l_0 < 10^{-16}$ cm. may be introduced. It may be mentioned here that even at high energies most of the cross-section will be accounted for by low momentum transfer processes and only at high momentum transfers of the order of several GeV/c could there possibly be a change by the introduction of l_0 of the above magnitude. We rule out the possibility of $l_0 \sim 10^{-14}$ cm. from present experiments on the validity of quantum electrodynamics (QED) down to distances of this order.⁸ It is of interest to point

out that the static solution of equation (1) in the presence of a point charge leads to

$$\psi = \frac{e}{r} \left[1 - \exp\left(\frac{-r}{l_0}\right) \right] \quad (6)$$

which form occurs also in Lorentz invariant modifications of the photon propagator in QED.^{3*} Therefore, any modifications of the wave equation as in (1) should be consistent with known limits of l_0 obtained from tests of QED. However, it is important to note that any limit lower than that obtained from QED from tests of the consequences of equation (1) does not necessarily validate QED up to that limit. Further, $l_0 > 10^{-15}$ cm. will be in conflict with numerous measurements on the velocities of high energy particles and the validity of Lorentz transformations at accelerator energies.

In Fig. 2 is given the width of the distribution in the time of arrival of electrons as a function of l_0 for a y-ray initiated shower in the atmo-

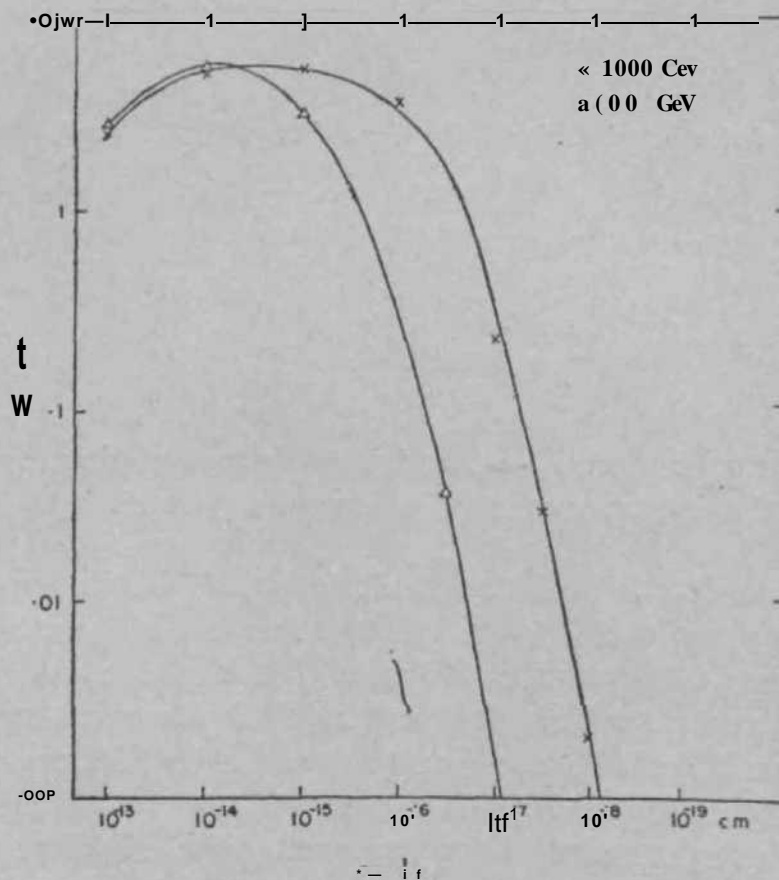
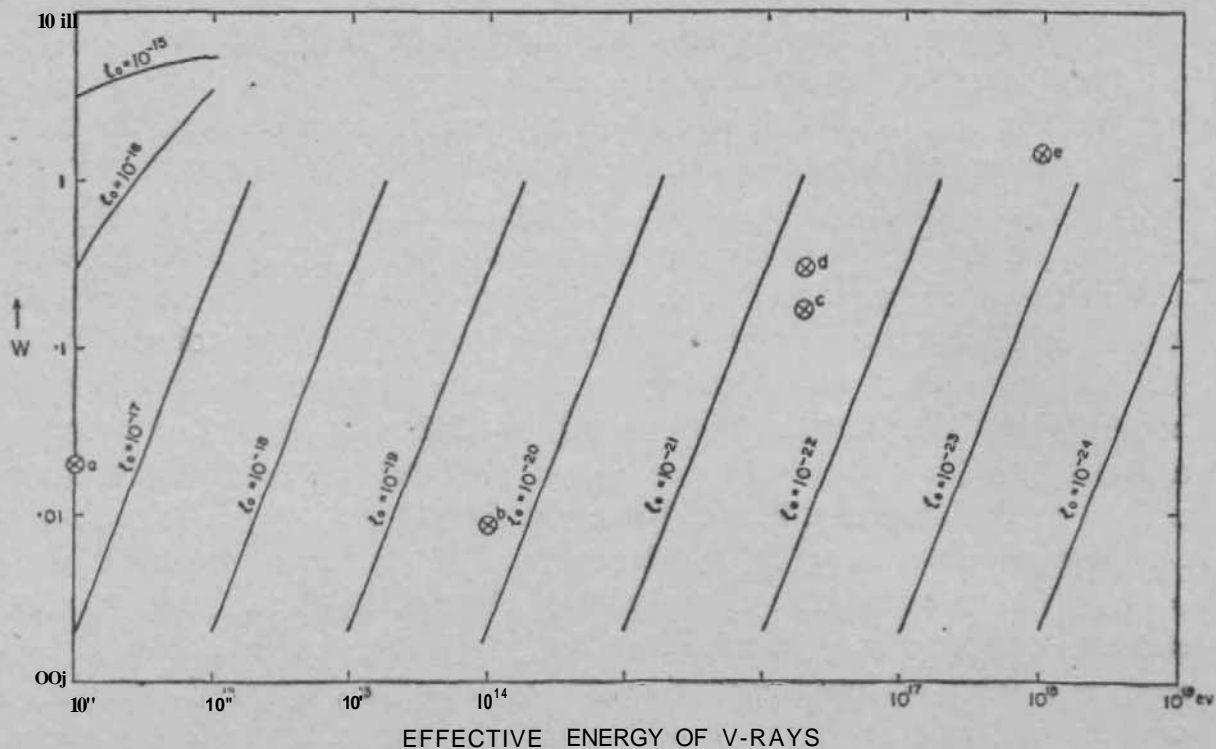


FIG. 2. Calculated width of the distribution of time of arrival of electrons (90% of total number) in y-ray initiated showers plotted as a function of l_0 , for two values of y-ray energies. The simulated showers had an origin at a depth of 400 gm./cm.² in the atmosphere and the widths were calculated at a depth of 800 gm./cm.²

*We are aware of the limitations involved in such simple modifications. See Ref. (4).

sphere. The spread due to multiple Coulomb scattering of electrons has not been taken into account in the calculations. We find that the width is a function mainly of $\lambda_0 E$ and relatively weakly dependent on the depth of the atmosphere at which the shower is initiated (consequently weakly dependent also on the depth of observation) at least for λ_0 values well past the peak on the right in Fig. 2, for a given energy. Thus, in Fig. 3 is made a comparison of experimental data with curves drawn for various λ_0 by scaling up Fig. 2 appropriately for $E > 10^{12}$ eV. The extrapolated widths will be somewhat of an underestimate since the range of the cascades will be larger at higher energies but this will not affect significantly the present analysis. At the highest energies, y-rays produced in the first few interactions in the atmosphere would account for the majority of electrons at the level of observation in the lower part of the atmosphere. At such energies the time structure at the level of observation due to a nuclear cascade can approximately be calculated by treating the shower as if it is initiated by a y-ray of lower energy $\sim 10\%$ of the primary energy. Therefore, we have not calculated the detailed effects of nuclear cascade in the time distributions since experimentally the widths increase if at all only at the highest energies (Fig. 3).

One cannot interpret straightaway that the increase in the time spread of particles observed at energies $\sim 10^{17}$ eV could be due to the existence of an $\lambda_0 \sim 10^{-21}$ cm. The increase can reasonably be attributed to path length differences among muons arriving at large distances from the core of air showers (300-1500 m)⁶ and also to multiple Coulomb scattering of electrons arriving at those distances.⁵⁰ In fact, the observed spread at energies $\leq 10^{15}$ eV is generally attributed to multiple Coulomb scattering of electrons alone since observations are confined to relatively small distances from the core. At large distances, muons make a significant contribution to the particles observed. The notable feature of the existence of an λ_0 is that the width, as shown in Fig. 3, should change rapidly as one varies the energy by an order of magnitude, after due allowance has been made for effects of multiple Coulomb scattering of electrons and muon spread. More measurements and detailed calculations are necessary at energies $\sim 10^{17}$ eV to see if there is an effect due to the existence of an $\lambda_0 \sim 10^{-21}$ cm. However, it would be difficult to detect an $\lambda_0 < 10^{-24}$ cm. with the scarce flux of showers of energy $\sim 10^{20}$ eV. Thus we can conclude that an upper limit of λ_0 is $\sim 10^{-21}$ cm. This limit would be $\sim 10^{-25}$ cm., if the entire observed widths can be accounted for by the normal mechanisms suggested above.



incident γ -ray energy, expected for various l_0 values (in cm.) is given by the curves. The observed widths, indicated by crossed circles, have been taken from reference (5). The effective energy of γ -rays for the observed air showers have been set at $0.1 E_0$ where E_0 is the energy of the showers.

One of us (R. H. Vatcha) would like to thank Professor B. V. Sreekantan, Dr. B. K. Chatterjee and Dr. G. T. Murthy for useful discussions in the early stages of this work.

REFERENCES

1. Pavlopoulos, T. G. .. *Phys. Rev.*, 1967, 1S9, 1106.
2. Panofsky, W. K. H. .. *Proc. Heidelberg International Conf. on Elementary Particles*, 1968, p. 371.
3. Drell, S. .. *Annals of Physics*, 1958, 4, 75.
4. Kroll, N. M. .. *Nuovo Cimento*, 1966, 45A, 65.
5. (o) Jones, L. W., Lyon, D. E. Jr., Ramana Murthy, P. V., DeMcester, G., Hartung, R. W., Mikamo, S., Reeder, D. D., Subramanian, A., Cork, B., ftayton, B., BenvenuUi, A., Marquit, E., Kearney, P. D., Bussian, A. E, Mills, F., Radmer, C. and Winter, W. R,

- (AJBassi, P., Clark, G. and Rossi, B. *Phys. Rev.*, 1953, 92, 441.
- (c) Baxter, A. J., Watson, A. A. and Wilson, J. G. *Proc. Ninth Int. Conf. on Cosmic Rays, London, 1965, 2, 724.*
- W)Linsley, J. and Scarsi, L. .. *Phys. Rev.*, 1962, **128**, 2384.
- (e)——,——and Rossi, B. .. *Phys. Rev. Lett.*, 1961, 6, 485.
6. Hillas, A. M. *Proc. Ninth Int. Conf. on Cosmic Rays, London, 1965, 2, 758.*

INDIRECT POLAROGRAPHIC DETERMINATION OF STABILITY CONSTANTS

IV. Thiosulphate Complexes

BY S. C. SARAIYA AND A. K. SUNDARAM, F.A.S.C.

(Analytical Division, Bhabha Atomic Research Centre, Trombay, Bombay-74)

Received March 10, 1969

ABSTRACT

The stability constants of cadmium thiosulphate complexes have been determined in 25% methanol medium. The stability constants of thiosulphate complexes of zinc and lanthanum have been determined by the indirect method using cadmium as the indicator ion.

INTRODUCTION

IN continuation of our earlier work^{1,2,3} on the determination of the stability constants of complexes which are either irreversibly reduced or even not reducible at the dropping mercury electrode, the thiosulphate complexes of zinc and lanthanum have been studied by the indirect method.

EXPERIMENTAL

The apparatus was the same as that used in our earlier studies. Stock solutions of cadmium sulphate (E. Merck, G.R.), zinc sulphate (E. Merck, G.R.), lanthanum nitrate (E. Merck, G.R.) and sodium thiosulphate (B.D.H., AnalaR) were standardised by conventional methods.⁴

RESULTS AND DISCUSSION

Cadmium was chosen as the indicator ion for the determination of the stability constants of zinc and lanthanum thiosulphate complexes. The half-wave potentials of cadmium were measured at different concentrations of sodium thiosulphate. The plot of E^* vs. pA indicated the presence of the third complex and the logarithm of the stability constant was calculated as 6.3 which was in good agreement with the reported value of 6.33.⁶

Polarograms of cadmium were also taken in 25% methanol in the presence of thiosulphate. The stability constants of the complexes were calculated as $\log \beta_2 = 5.6$ and $\log \beta_3 = 7.6$.

Zinc.—Polarograms of solutions containing 0.4mM cadmium and 0.1 M zinc were taken at different concentrations of thiosulphate. The half-wave potentials are represented in Fig. 1. The nature of the electrode reaction for cadmium was not affected in the presence of zinc. The free ligand concentration (A) was calculated from the shift in the half-wave potential of cadmium (read from the smooth curve) in the presence of zinc.

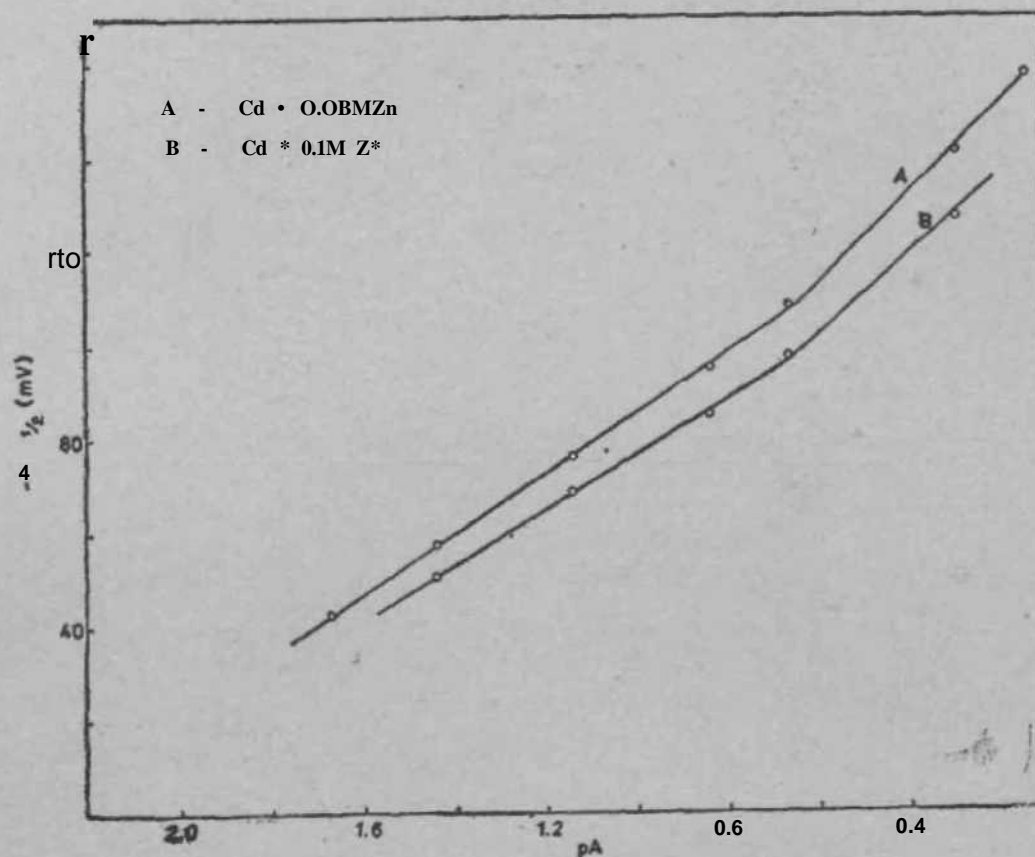


Fig. 1. Plots of $E_{1/2}$ VS. i_{∞} .

The results were also confirmed with 0.05 M zinc. Bjerrum's function, f_1 , calculated from the equation

$$\bar{n} = \frac{C_{WA} - A}{C_{ta}} \quad (1)$$

is given in Fig. 2 B. These values were solved for the stability constants by the method of Rossotti and Rossotti.⁶ The values of β_1 , β_2 and β_4 are 110, 50 and 2150 respectively, β_1 being absent as indicated by the negative intercept, \bar{n} values calculated from these values agreed well with the experimental values (Table I).

TABLE I

Experimental and calculated \bar{n} values

$A = 110, A = 50, \beta_4 = 2150.$

pA	h	
	Experimental	Calculated
1-6	0-14	0-14
1-5	0-215	0-21
1-4	0-33	0-32
1-3	0-49	0-48
1-2	0-71	0-71
1-1	1-00	1-00
1-0	1-40	1-36
0-9	1-82	1-76
0-8	2-21	2-17
0-7	2-57	2-57
0-6	2-92	2-92
0-5	3-24	3-22
0-4	3-53	3-45

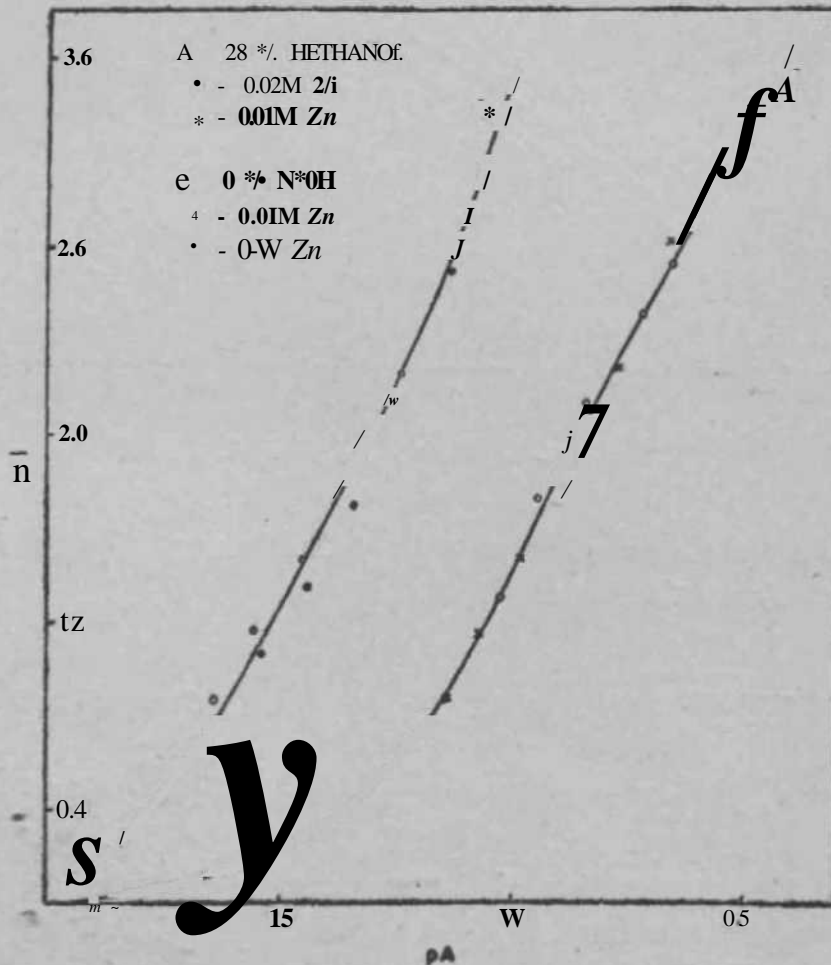


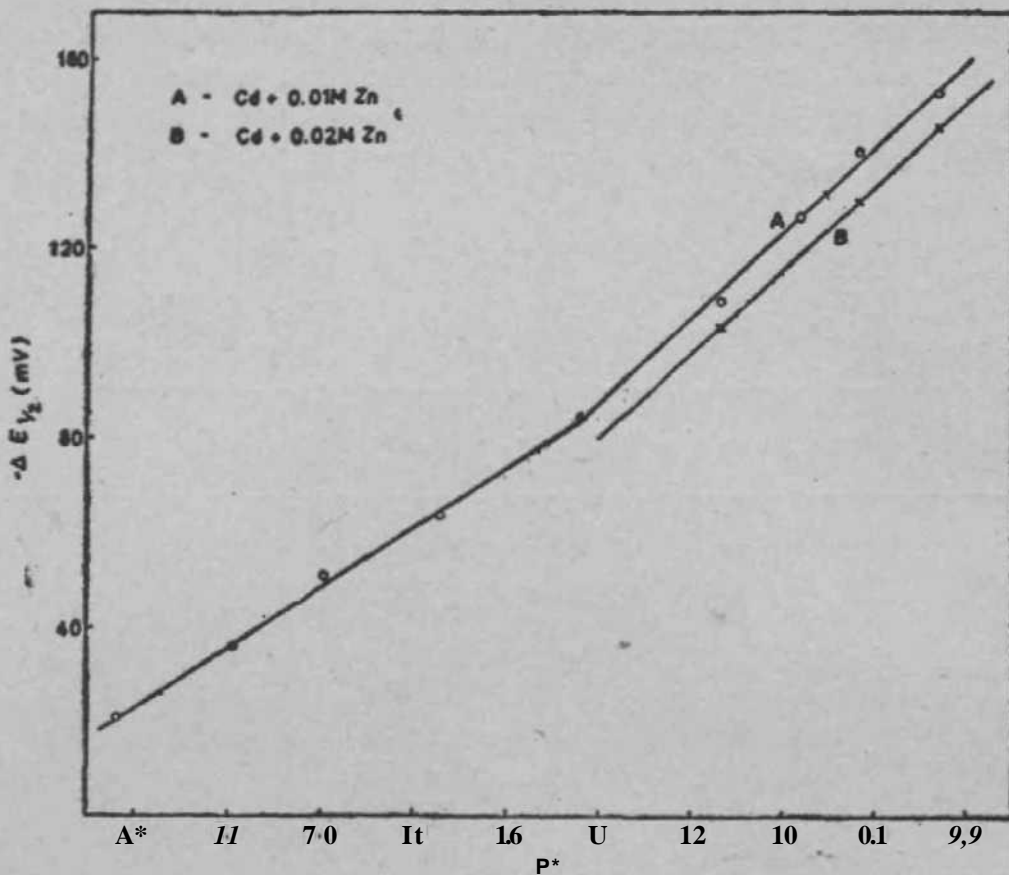
FIG. 2. H vs. pA.

Similar experiments were carried out in 25% methanol for the determination of the stability constants of zinc thiosulphate complexes. The results are given in Figs. 3 and 2 A. The stability constants were, calculated as $\log \beta_3 = 2.79$, $\log ft, \wedge 4 * 0$ and $\log \beta_2 \approx 4.78$ (from slope).

TABLE II
Free ligand and \bar{n} values for La-S₂O₃ system

$-\log C_A$	$-\log A$	$C_A - A$	ft
La = 0.096 M			
1.8	2.065	0.0073	0.076
1.6	1.870	0.0115	0.12
1.4	1.670	0.0184	0.19 [^]
1.2	1.480	0.0300	0.31
1.0	1.275	0.0469	0.49
0.8	1.080	0.0760	0.79
0.6	0.890	0.1220	1.27
La = 0.048 M			
1.6	1.75	0.007	0.14
1.4	1.55	0.012	0.25
1.2	1.35	0.018	0.38
1.0	1.15	0.029	0.60
0.8	1.06	0.039	0.81
0.6	0.96	0.049	1.02
0.5	0.86	0.062	1.50
0.4	0.76	0.077	1.60

Lanthanum.—The stability constants of lanthanum thiosulphate complexes were also determined by this method. The half-wave potentials of cadmium were measured in the presence and absence of lanthanum at different concentrations of thiosulphate (Fig. 4).^N The concentration of the free ligand and h values (Table II) were calculated by the method explained earlier. The stability constants calculated by the method of Rossotti and Rossotti are $\log ft = 0.82$, $\log \beta_2 = 0.6$ and $\log \beta_3 = 2.58$. The reported value for $\log ft$ from spectrophotometric and distribution studies is 0.17⁷ and the existence of the third species has also been indicated[^].



Flo. 3. Plot of ΔE_j vs. pA (25% methanol).

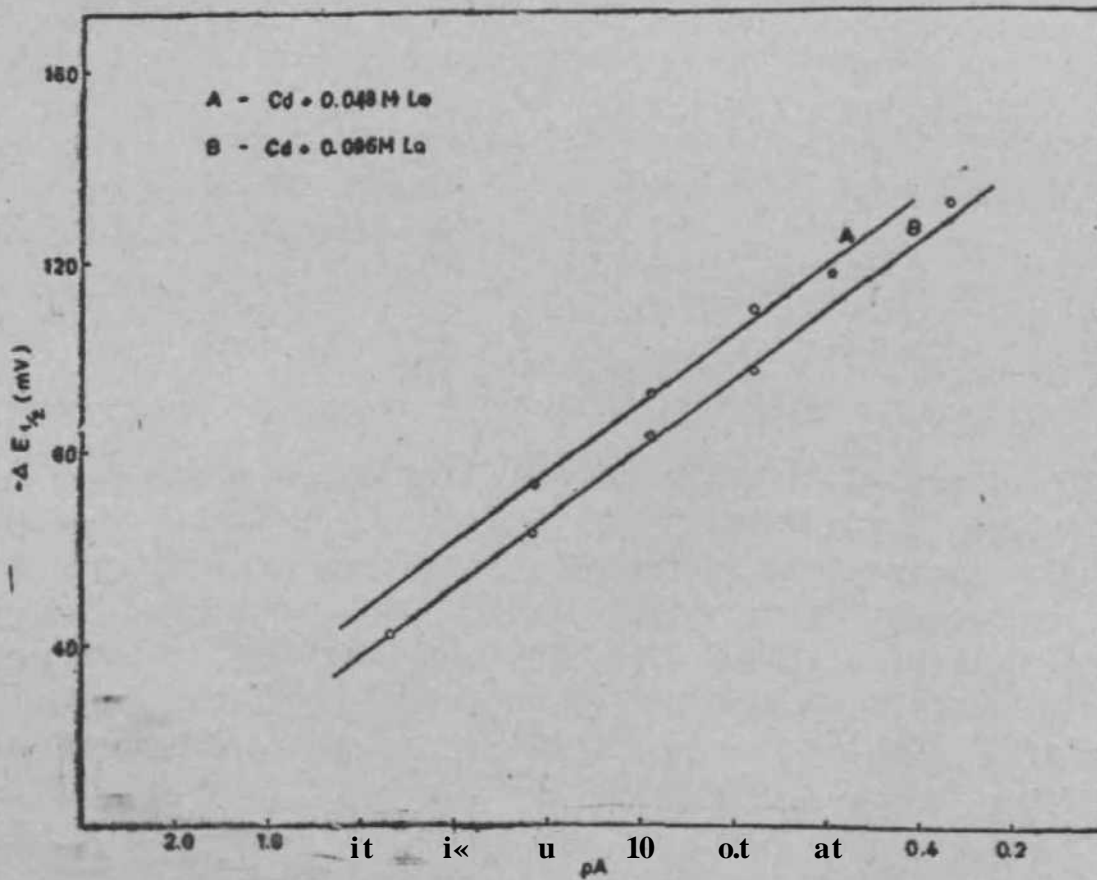


FIG. 4. Plots of ΔE_j w. pA ,

ACKNOWLEDGEMENT

The authors wish to thank Dr. V. T. Athavale, Head, Analytical Division, for his keen interest in this work.

REFERENCES

1. Saraiya, S. C. and Sundaram, A. K. *Proc. Symposium on Electrode Processes*, Jodhpur, 1966, p. 50.
2. Sundaresan, R., Saraiya, S. C. and Sundaram, A. K. *Proc. Ind. Acad. Sci.*, 1967, **56**, 246.
3. ————— .. *Curr. Sci.*, 1967, 36, 255.
4. Vogel, A. I. .. *A Text-book of Quantitative Analysis*, Longmans, Green and Co., Ltd., 1964.
5. Stromberg, A. G. and Bykov, I. E. *Zhur. Obschei. Khim.*, 1949, 19, 245.
6. Rossotti, F. J. C. and Rossotti, H. S. *Acta Chem. Scand.*, 1955, 9, 1166.
7. Mattem, K. L. .. *UCRL-U07*, 1951.
8. Dutt, N. K. and Gupta, A. K. *J. Ind. Chem. Soc.*, 1952, **29**, 105.

FORCE CONSTANTS, GENERALISED MEAN-SQUARE AMPLITUDES OF VIBRATION, SHRINKAGE CONSTANTS AND CORIOLIS COUPLING COEFFICIENTS OF GeH_3CCH AND GeD_3CCH

BY PROF. K. VENKATESWARLU, F.A.S.C., DR. V. MALATHY DEVI

AND

A. NATARAJAN

(Department of Physics, Kerala University Centre, Cochin-22)

Received April 6, 1968

ABSTRACT

General valence force constants have been evaluated for GeH_3CCH and GeD_3CCH . Generalised mean-square amplitudes of vibration have been obtained and the shrinkage constants have been calculated using the perpendicular mean-square amplitudes of vibration. Coriolis coupling constants have also been determined.

1. INTRODUCTION

THOMAS AND LAURIE¹ have made the first precise structural study of the molecule GeH_3CCH from the microwave spectrum and reported the various parameters. Lovejoy and Baker² have obtained the infrared spectra of GeH_3CCH and GeD_3CCH in the gaseous state and assigned all their fundamentals. These molecules belong to the point group C_{2v} consisting of five totally symmetric a_1 modes and five doubly degenerate e modes, all the ten fundamentals being infrared active.

Very recently, Rao and Rai³ have determined the general valence force constants of these molecules but they have transferred many of the bending and interaction force constants from the previous work.^{4,5} Further, they have not made use of the latest parameters available from microwave data¹ but borrowed from the earlier work on similar molecules.^{4,5} Hence, the force constants have been reinvestigated on the basis of general valence force field using the latest parameters pertaining to germylacetylene. The generalised mean-square amplitudes of vibra-

tion, shrinkage constants and the Coriolis coupling coefficients have also been obtained for the first time in this investigation.

2. POTENTIAL CONSTANTS, MEAN-SQUARE AMPLITUDES OF VIBRATION AND SHRINKAGE EFFECT

The symmetry co-ordinates, satisfying the orthogonality and normalization conditions and which transform according to the characters of the point group C_{3V} have been constructed. The kinetic energy matrix G has been obtained using the relation $G = BM^{-1}B'$, where M^{-1} is a diagonal matrix of the reciprocal masses and B is the transformation matrix from Cartesian displacement co-ordinates to internal co-ordinates. The force constant matrix F has been derived assuming a general valence type of potential function. By solving the secular equation⁶ $|FG - EA| = 0$, a reasonable set of force constants has been evaluated.

The elements of the symmetrised mean-square amplitude matrix E have been obtained using the relation,⁷ $E = LAL$ where L and A have their usual significance. The L matrix has been determined from the general valence force constants.

The generalised mean-square amplitudes which include the mean-square parallel amplitudes $\langle(Az)^2\rangle$, the mean-square perpendicular amplitudes, $\langle(A^*)^2\rangle$ and $\langle(A)0^2\rangle$ and the mean cross products $\langle(A^* A^*)\rangle$, $\langle(A^* A_j)\rangle$ and $\langle(A^{\wedge} A^{\wedge})\rangle$ have been obtained by the method of Morino and Hirota.⁸ In order to compute these quantities, the symmetry co-ordinates S are to be expressed in terms of Cartesian displacement co-ordinates X . They are related through the relation, $X = AS$, where A is the transformation matrix given by $A = M^{-1}B'G^{-1}K$. Here G^{-1} is the inverse of the kinetic energy matrix and B is such that $S = BX$. Expressions have been derived for the parallel and perpendicular mean-square amplitudes for the various bonded and non-bonded atom pair. Making use of the elements of E and A matrices in the above expressions, the generalised mean-square amplitudes have been evaluated.

The shortening or shrinkage of the internuclear distances can be calculated from spectroscopic data, using the perpendicular mean-square amplitudes of vibration as has been pointed out by Morino.⁹ For the molecules under study, the following shrinkages are found to exist:

$$\begin{aligned}
 -\delta_{46} &= \frac{\tau_{46}}{R+r_c} - \frac{\tau_{45}}{R} - \frac{\tau_{56}}{r_c} \\
 \text{" } \delta_{47} &= \frac{\tau_{47}}{R+r_c+D} - \frac{\tau_{45}}{R} - \frac{156}{r_c} - \frac{167}{D} \\
 &= \frac{\tau_{57}}{r_c+D} - \frac{\tau_{56}}{r_c} - \frac{\tau_{67}}{D},
 \end{aligned}$$

where

$$\tau_{ij} = \frac{\langle (\Delta x_{ij})^2 \rangle}{2 \langle (A_{ytj})^2 \rangle},$$

$\langle (A^*ij)^2 \rangle$ and $\langle (A.Kij)^2 \rangle$ representing the respective perpendicular mean-square amplitude values.

3. CORIOLIS COUPLING CONSTANTS

Applying Jahn's rule,¹⁰ the non-vanishing zeta values are found to be of the type l^z arising from the coupling $ex e$ and ξ^x and t^y due to the coupling $a_x x e$. These constants have been estimated using the matrix relation, $\xi^a = L^{-1} C^a I^{-1}$, where L is the normal co-ordinate transformation matrix and C^a ($a = x, y, z$) is the skew symmetric matrix obtained by the vector method of Meal and Polo.¹¹ The C^a matrix elements are given below:

$ex e$ Coupling:

$$C^z_{\langle a, eb \rangle} = \frac{4}{3} \mu_{ce}$$

$$C^z_{7a, 7b} = 2 \left[\frac{1}{a} + \frac{a}{3J} \right]^2 \mu_{ce} + \frac{3}{2a^2} \mu_c$$

$$C^z_{9a, 9b} = b^2 \mu_c + \left(b + \frac{1}{b} \right)^2 \mu_c + \frac{1}{b^2} \mu_H$$

$$C^z_{9a, 9b} = 3 \mu_{ce} - \frac{\mu_x}{2}$$

$$C^z_{1-a, 10b} = \frac{1}{c} \mu_{ce} + \frac{1}{cJ} \mu_e + \frac{1}{c^2} \mu_c$$

$$C_{6a,7b}^z = -\sqrt{2}\mu_{Ge} \left(\frac{1}{a} + \frac{a}{3}\right)$$

$$C_{6a,8b}^z = 0$$

$$C_{6a,9b}^z = \sqrt{2}\mu_x + \frac{4}{3}\sqrt{2}\mu_{Ge}$$

$$C_{6a,10b}^z = -\frac{2}{\sqrt{3}}c\mu_{Ge}$$

$$C_{7a,8b}^z = -\sqrt{\frac{3}{2}}\frac{b}{a}\mu_c$$

$$C_{7a,9b}^z = -\frac{a}{2}\mu_x - 2\left(\frac{1}{a} + \frac{a}{3}\right)\mu_{Ge}$$

$$C_{7a,10b}^z = \sqrt{\frac{3}{2}}\left(\frac{1}{a} + \frac{a}{3}\right)c\mu_{Ge} + \sqrt{\frac{3}{2}}\frac{\mu_c}{a}\left(c + \frac{1}{c}\right)$$

$$C_{8a,9b}^z = 0$$

$$C_{8a,10b}^z = -b\left(c + \frac{1}{c}\right)\mu_c - \left(b + \frac{1}{b}\right)\mu_c$$

$$C_{9a,10b}^z = -\sqrt{\frac{8}{3}}c\mu_{Ge};$$

a_1 X c Coupling:

$$C_{1,6a}^v = -C_{1,6b}^x = 0$$

$$C_{1,7a}^v = -C_{1,7b}^x = 0$$

$$C_{1,8(1)}^v = -C_{1,8(2)}^x = -\mu_c\left(b + \frac{1}{b}\right) - \frac{1}{b}\mu_x$$

$$C_{1,9(1)}^v = -C_{1,9(2)}^x = 0$$

$$C_{1,10(1)}^v = -C_{1,10(2)}^x = \frac{1}{g}\mu_c$$

$$C_{2,6a}^v = -c^*,_{6b} = 0$$

$$C^{y_{2,7a}} = -C^{x_{2,7b}} = -\sqrt{\frac{3}{2}} \frac{1}{a}$$

$$C^{y_{2,8a}} = -C^{x_{2,8b}} = b\mu_c + \left(\frac{1}{b} + b\right)\mu_c$$

$$C^{y_{2,9a}} = -C^{x_{2,9b}} = 0$$

$$C^{y_{2,10a}} = -C^{x_{2,10b}} = -\left(c + \frac{1}{c}\right)\mu_c - \frac{1}{c}\mu_c$$

$$C^{y_{3,6a}} = -C^{x_{3,6b}} = \frac{2}{3}\mu_{Ge}$$

$$C^{y_{3,7a}} = -C^{x_{3,7b}} = -\frac{a}{\sqrt{2}}\mu_x - \frac{1}{\sqrt{2}}\left(\frac{1}{a} + \frac{a}{3}\right)\mu_{Ge}$$

$$C^{y_{3,8a}} = -C^{x_{3,8b}} = 0$$

$$C^{y_{3,9a}} = -C^{x_{3,9b}} = \mu_{Ge}$$

$$C^{y_{3,10a}} = -C^{x_{3,10b}} = -\sqrt{3}\mu_{Ge}$$

$$C^{y_{4,1a}} = -C^{x_{4,1b}} = \frac{1}{2}(1+a)\mu_x - \frac{4}{3}(1+a)\mu_{Ge}$$

$$C^{y_{4,7a}} = -C^{x_{4,7b}} = \sqrt{2}(1+a)\left(\frac{1}{a} + \frac{a}{3}\right)\mu_{Ge}$$

$$C^{y_{4,8a}} = -C^{x_{4,8b}} = 0$$

$$C^{y_{4,9a}} = -C^{x_{4,9b}} = -\frac{1}{\sqrt{2}}(1+a)\mu_x - \frac{4}{3}\sqrt{2}(1+a)\mu_{Ge}$$

$$C^{y_{4,10a}} = -C^{x_{4,10b}} = -3(1+a)\mu_{Ge}$$

$$C^{y_{5,6a}} = -C^{x_{5,6b}} = -\frac{2}{\sqrt{3}}\mu_{Ge}$$

$$C^{y_{5,7a}} = -C^{x_{5,7b}} = \sqrt{\frac{3}{2}}\left(\frac{1}{a} + \frac{a}{3}\right)\mu_{Ge} + \sqrt{\frac{3}{2}}\frac{1}{a}\mu_c$$

$$C^y_{5,8a} = -C^x_{5,8b} = -b\mu_c$$

$$C^y_{5,9b} = -C^x_{5,9b} = -\sqrt{\frac{8}{3}}\mu_{\text{Ge}}$$

$$C^y_{5,10a} = -C^x_{5,10b} = c f_{\text{Ge}} + \left(c + \frac{1}{c}\right)\mu_c$$

where jz_x ($X = \text{H}$ or D), $1/x_{\text{Ge}}$, $1/x_c$ and $1/x_{\text{H}}$ represent the reciprocal masses of the respective atoms and

$$a = \sqrt{\frac{R}{r}}, \quad b = \sqrt{\frac{D}{r_c}}, \quad c = \sqrt{\frac{r_c}{R}}.$$

4. RESULTS AND DISCUSSION

The molecular parameters¹ are given in Table I. The angles α and β are taken to be tetrahedral. The internal co-ordinates, numbering of atoms and orientation of the principal axes are shown in Fig. 1.

TABLE I

Molecular parameters (A) of germylacetylene

Distance	GeH_3CCH
r	1.521
R	1.896
r_c	1.208
D	1.056

The angles α and β are tetrahedral

The secular equations have been solved to obtain the F matrix elements. The frequencies have been finally calculated which agreed reasonably well with the observed values. The calculated and the observed fundamental frequencies are given in Table II. The appropriate set of force constants is presented in Table III. The mean amplitudes of vibration are given in Table IV.

It is found that the stretching force constants of Ge—x and C≡Q obtained in the present study, are in good agreement with the values reported

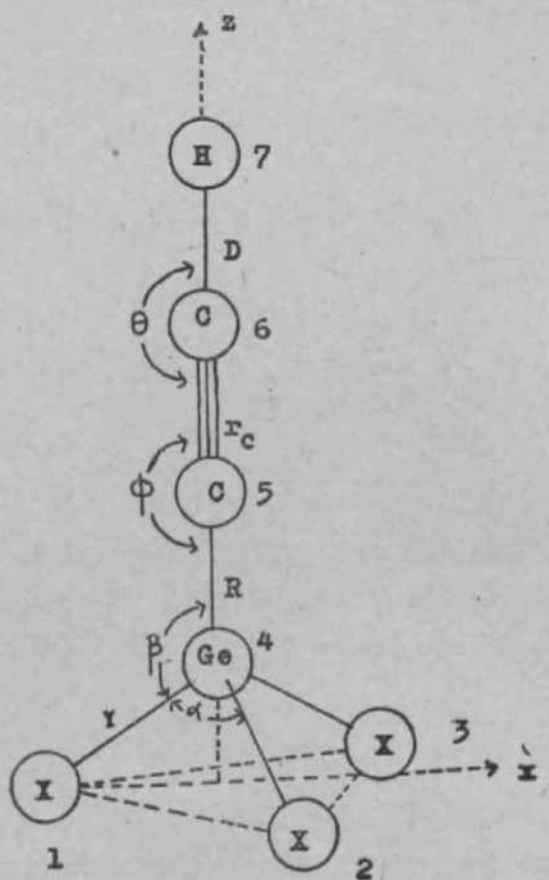


FIG. 1. The internal co-ordinates, numbering of atoms and orientation of the principal axes of gertnylacetylene.

for corresponding bonds in related molecules.¹²⁻¹⁴ The infrared spectra" and electron diffraction¹⁶ studies have shown that single bonds adjacent to triple bonds in the acetylenes and cyanides are significantly shorter than the normal tetrahedral carbon bond. Microwave studies of the linear acetylenes¹⁷⁻¹⁸ and cyanides^{18, 18} also show the same effect. The higher force constants and the smaller mean amplitude values of the Ge—C[^]bond maybe attributed to this shortening. The Ge—C bond is 0.05 Å shorter¹ than the value reported for methyl germane³⁰ and is consistent with a change in carbon hybridization from *sp** to *sp*.

The generalised mean-square amplitudes of vibration are reported in Table V. Substitution of deuterium does not affect the parallel mean amplitudes of the other bonds, but the perpendicular mean amplitudes are

very much altered. The shrinkage constants are presented in Table VI. The shrinkage effect in GeD_3CCH is found to be slightly more than in GeH_3CCH , since the perpendicular mean-square amplitudes are found to be higher in the former case.

TABLE II

Observed and calculated vibrational frequencies (cm^{-1}) of GeH^iCCH and GeD_jCCH

Species	Designation	GeH_iCCH		GeD_jCCH	
		Observed	Calculated	Observed	Calculated
a_1	ν_1	3313-5	3314	3316-5	3316
	ν_2	2160	2065	2052-5	2065
	ν_3	2120	2120	1525	1505
	ν_4	843-8	843	608	607
	ν_5	530	528	518	524
e	ν_6	2117-2	2117	1525	1525
	ν_7	886	885	643-2	643
	ν_8	673	700	673	678
	ν_9	643-8	643	484	485
	ν_{10}	216-4	218	202-8	203

The Coriolis coupling constants are given in Tables VII and VIII. These constants for the degenerated coupling have been obtained from the spectral analysis by Lovejoy and Baker.² They have shown that $\xi_8 + \xi_{10} = 1.975$ and both ξ_8 and ξ_{10} might be positive and approximately equal but slightly less than the unity. The values determined in this investigation for ξ_8 and ξ_{10} are in good agreement with the observation made by them. Further, they have predicted a value of -0.052 for ξ_6 , -0.248 for ξ_7 and 0.364 for ξ_9 . Though the numerical values obtained in the present study are not widely different from those values, the signs of these constants are found to be exactly reverse.

TABLE III
Force constants (md/A) of GeH₃CCH and GeD₃CCH

Force constant	GeH ₃ CCH	GeD ₃ CCH
k_r	2-631	2-663
k_f	3-273	3-273
f_{fl}	15-140	15-140
f_e	5-888	5-888
f_{fb}	0-1291	0-1408
f_t	0-3373	0-3540
f_{fb}	0-1396	0-1228
f_{ft}	0-1461	0-1241
f	0-0160	0-0001
$J_{r,0}$	0-0398	0-0398
$J_{r,0}$	0-0050	0-0050
f_{i^*}	0-0018	0-0018
J_{r^*}	0-0055	0-0117
$f_{a?}$	0-0102	0-0212
$f_{a?}$	0-0616	0-0660
$f_{j < \beta e}$	-0-0722	-0-0595
$(f_{\alpha\alpha} - f_{\alpha\beta})$	-0-0515	-0-0515

TABLE IV
Mean-square amplitudes of vibration (A^2) of GeH₃CCH and GeD₃CCH

Designation	GeH ₃ CCH	GeD ₃ CCH
σ_r	0-008005	0-005645
σ_n	0-002166	0-002210
$\sigma_{r\phi}$	0-001329	0-001330
σ_n	0-005645	0-005514
σ_β	0-070530	0-052749
σ_β	0-030830	0-023912
σ_ϕ	0-046620	0-050676
σ_θ	0-058480	0-061626
σ_{rr}	-0-000040	-0-000052
$\sigma_{r\alpha}$	-0-000285	-0-000269
$\sigma_{\alpha\alpha}$	-0-000515	-0-000503
$\sigma_{\alpha\alpha}$	-0-000037	-0-000051
σ_{fa}	-0-000207	-0-000287
$\sigma_{r\beta}$	-0-000197	-0-000273
$\sigma_{\alpha\beta}$	0-009650	0-007178
$\sigma_{\phi\theta}$	0-015460	0-016810
$(\sigma_{\alpha\alpha} - \sigma_{\alpha\beta})$	0-000567	0-000843

TABLE V

Generalised mean-square amplitudes ($10^{-4} A^3$) of vibration in GeH₉CCH and GeD_zCCH

Atom Pair	Designation	GeH ₉ CCH	GeD ₃ CCH _j
Ge-X	$\langle(Az)^8\rangle$	79-960	56-410
	$\langle(A^*)^2\rangle$	277-524	221-876
	$\langle(A^{\wedge})^2\rangle$	183-775	137-600
	$\langle(Az Ax)\rangle$	0-280	0-230
Ge-C ₆	$\langle(A^*)^2\rangle$	21-660	22-120
	$\langle(A^*)^2\rangle = \langle(A_j)^2\rangle$	78-236	83-701
C _B ≡C.	$\langle(Az)^2\rangle$	13-310	13-360
	$\langle(A^* n = \langle(A>0^2)\rangle$	136-549	159-200
C.-H ₇	$\langle(Az)^2\rangle$	56-450	55-140
	$\langle(A^*)^2\rangle = \langle(Ay)^2\rangle$	726-700	782-029
X,··-X,	$\langle(\Delta z)^2\rangle$	284-470	208-970
	$\langle(Ax)^2\rangle$	191-250	141-400
	$\langle(\Delta y)^2\rangle$	568-184	455-165
	$\langle(Ax Ay)\rangle$	75-919	62-621
X [^] -C.	$\langle(Az)^2\rangle$	155-684	118-670
	$\langle(\Delta x)^2\rangle$	333-705	293-808
	$\langle(A>0^2\rangle$	296-884	248-942
	$\langle(Az Ax)\rangle$	-79-140	-61 -268
Xx·C,	$\langle(Az)^2\rangle$	225-670	188-427
	$\langle(Ax)^2\rangle$	142-976	99-355
	$\langle(Ay)^2\rangle$	171-502	122-856
	$\langle(\Delta z \Delta x)\rangle$	-92-056	-69-525
Xx··-H ₇	$\langle(Az)^2\rangle$	415-539	384-023
	$\langle(AJC)^2\rangle$	663-107	683-834
	$\langle(Ay)^2\rangle$	829-888	873-083
	$\langle(Az Ax)\rangle$	197-658	246-950
Ge··C,	$\langle(Az)^2\rangle$	24-650	25-430
	$\langle(Ax)^2\rangle = \langle(Ay)^2\rangle$	11-987	17-272
Ge··H ₇	$\langle(Az)^2\rangle$	75-400	75-200
	$\langle(A^*)^2\rangle = \langle(Ay)^2\rangle$	765-058	853-468
$\langle V \cdot H_7$	$\langle(Az)^2\rangle$	64040	64-420
	$\langle(A^*)^2\rangle = \langle(Ay)^2\rangle$	1228-190	1360-686

TABLE VI

Shrinkage effect (A) in GeH₃CCH and GeD₃CCH

Designation	GeH ₃ CCH	GeD ₃ CCH
δ_{4-6}	0-015051	0-017039
δ_{4-7}	0-065877	0-070975
σ_{4-7}	0-025900	0-027000

TABLE VII

Zeta values for GeH₃CCH and GeD₃CCH (e x e) coupling

ζ_{ij}^*	GeH ₃ CCH	GeD ₃ CCH
2*66	0-01818	0-03568
Y* b 77	0-45327	0-48789
2*88	0-88880	0-89773
Y* b 99	-0-29980	-0-31169
2*10, 10	0-96134	0-91825
2*6, 7	-0-47820	-0-48395
2*6, 8	-0-30180	0-19220
2*6, 9	0-75010	0-77970
2*6, 10	0-06990	0-09152
2*7, 8	-0-22190	0-22664
£\.	-0-11160	-0-03680
£*7. 10	0-13730	0-17423
£%.»	0-11670	0-05246
$\zeta_{8, 10}^*$	0-04521	-0-08020
$\zeta_{9, 10}^*$	0-10350	0-12844

TABLE VIII

Zeta values for $GeH^{\wedge}CCH$ and GeD_3CCH ($a_x \times e$) coupling

$C:V, -P.$	GeH_8CCH	$GeDsCCH$
Pi..	0 0	0
Pi. 7	0-2638	-0-4704
Pi, 8	-0-8395	-0-7606
rw in	-0-1309	-0-0568
Pi. 10	-0-4529	-0-4450
P& 6	0	0
$P_2. 7$	-0-3218	0
P2.8	0-3677	0-5064
p_2, \bullet	0-0072	-0-0450
P2.10	-0-8450	-0-8370
P_s, \bullet	0-0092	0-0181
$P.. 7$	-0-6362	-0-6102
P8.8	-0-2464	0-2747
$P^*.$	-0-2234	-0-1860
PMO	0-1652	0-2193
$4^*4, 6$	-0-7136	-0-7196
P4.7	0-3274	0-3214
P4.8	0-2086	-0-1269
P4..	-0-5293	-0-5473
$\begin{matrix} \gamma \\ b \end{matrix} 4, 10$	-0-0470	-0-0581
$\begin{matrix} \gamma \\ b \end{matrix} 5, 6$	0-0003	0-0008
P5.7	0-2045	0-2193
P5.8	0-0188	-0-1573
$P_{6>}$	0-0590	0-0780
Ps. 10	0-1785	0-1377

For germylacetylene molecule, the following zeta sum rule is found to be satisfied for the degenerate coupling:

$$\sum_{l=0}^{10} I_A I_B = I_A + I_B = 2022.$$

Here I_A and I_B represent the moments of inertia about the symmetry axis and any other axis respectively.

ACKNOWLEDGEMENT

Two of the authors (V. M. and A. N.) are thankful to the Council of Scientific and Industrial Research and Ministry of Education, Government of India for the award of Senior and Junior Research Fellowships respectively.

REFERENCES

1. Thomas E. C. and Victor W. Laurie *J. Chem. Phys.*, 1966, 44, 2602.
2. Lovejoy, R. W. and Baker, D. R. *Ibid.*, 1967, 46, 658.
3. Rao. D. V. R. A. and Rai, D. K. *Curr. Sci.*, 1968, 37, 41.
4. Meister, A. G. *J. Chem. Phys.*, 1948, 16, 950.
5. Krishna Pillai. M. G. and Peruroal, A. *Bull. Soc. Chim. Beig.*, 19⁴, 73, 29.
6. Wilson, E. B. *J. Chem. Phys.*, 1939, 7, 1047; 1941, 9, 76.
7. Cyvin, S J. *Ada Polytechnica Scandinavica*, 1960, Ph. 6, p. 2⁷9.
8. Morino, Y and Hirota, E. *J. Chem. Phys.*, 1955, 23, 737.
9. _____ *Acta Crvst.*, 1960, 13, 1107.
10. Jahn, H. A. *Phys. Rev.*, 1939, 56, 680.
11. Meal, J. H. and Polo, S. R. *J. Chem. Phys.*, 1956, 24, 1119, 1126.
12. Venkateswarlu, K. and Mariamma, P. Mathew *Ind. Jour. Pure and Appl. Phys.*, 1967, 5, 17.
13. Clark, E. A. and Weber, A. *J. Chem. Phys.*, 1966, 45, 1759.
14. Venkateswarlu, K. and Natarajan, *A. (To be published).
15. Herzberg, G., Patat, F. and Verleger, II. *J. Phys. Chem.*, 1937, 41, 123.

16. Pauling, L., Springal, H. D. and Palmer, K. J. *J. Am. Chem. Soc.*, 1939, 61, 927.
17. Westernberg, A. A. and Wilson, E. B. Jr. *Ibid.*, 1950, 72, 199.
18. ———, Goldstein, J. H. and Wilson E. B. Jr. *J. Chem. Phys.*, 1949, 17, 1319.
19. Kessler, M., Ring, H., Trambarulo, R. and Cordy, W. *Phys. Rev.*, 1950, 79, 54.
20. Laurie, V. W. *J. Chem. Phys.*, 1959, 30, 1210.

ON TWO-BODY CHANNELS IN THE INTERACTIONS OF NEGATIVE PIONS WITH PROTONS IN THE FEW GeV REGION

BY S. K. TULI

(Department of Physics, Banaras Hindu University, Varanasi)

Received August 3, 1968

(Communicated by Dr. Yash Pal, F.A.S.C.)

ABSTRACT

A compilation on the reactions $trp \rightarrow ir-p$, $tcp \rightarrow p^*n$ and $irp \rightarrow p\sim p$ at nine laboratory momenta between 1.59 and 4.16 GeV/c is presented and certain common features of these channels brought out. Relevant basic parameters for production angular distribution are obtained and their values interpreted. It is found that the diffraction peaks do not shrink as the centre of mass energy increases.

THIS note presents a compilation on some aspects of certain two-body channels produced in the interactions of negative pions with hydrogen. Exclusively liquid hydrogen bubble chamber data is used in the interest of uniformity; this insures a meaningful comparison of the relevant parameters at different energies since most bubble chamber experiments use more or less similar criteria in the analysis of events. The present study covers essentially the channels involving elastic scattering and the production of rho meson in the few GeV region. We have attempted a methodical organisation of the data from experiments¹⁻⁹ at laboratory momenta 1.59 GeV/c, 2.0 GeV/c, 2.26 GeV/c, 2.7 GeV/c, 2.75 GeV/c, 3.0 GeV/c, 3.3 GeV/c, 4.0 GeV/c and 4.16 GeV/c and investigated their systematics. The present work aims at making a phenomenological analysis of the experimental data in which model dependent specific assumptions are avoided as far as possible.

The cross-sections due to the elastic scattering and the inelastic scattering involving the production of a single pion constitute a significant proportion of the total cross-section in this energy region. A major fraction of the single pion production events consists of quasi two-body final states. The more common of these final states comprise of a pion resonant state along

with a nucleon, a nucleon isobar along with a pion or a nucleon isobar along with a pion resonant state. The actual reactions we have studied are:

$$(1) \quad \nu T-p \rightarrow ir-p; \quad (2) \quad irp \rightarrow \rho^0 n; \quad (3) \quad \pi^- p \rightarrow \rho^- p.$$

Table I shows the relevant cross-sections from the various experiments. It is seen that towards the end of the energy region considered the cross-section in each one of the channels drops rather slowly. With the limited energy interval that we have at our disposal one is perhaps not justified in asking whether or not the cross-sections tend towards an asymptotic limit.

TABLE I

Partial cross-section for two prong production in rrp interactions
Cross-section, mb

Momentum Gev/C	1.59	2*0	2*26	2*7	2<.75	3*0	3*63	4*0	4*16
Channel									
$n-p \rightarrow \nu P$..	9.65 ±0*30	7*34 ±0-24	9.51 ±0-39	7.7 ±0-3	7.2 ±0*1	6*3 ±0-3	..	6*62 ±0-22	5.77 ±0-13
$\nu p \rightarrow t' Trp \nu P$..	4.48 ±0*15	3*28 ±0-19	<#	2.4 ±0-2	2.8 ±0*1	1.8 ±0-2	2*23 ±0-18	2*22 ±0-10	1.88 ±0<.05
$rTp \rightarrow iTv+n$..	6*45 i0-17	7*08 ±0<.27	..	3.9 ±0-2	3>.9 ±0-1	3*2 ±0-2	3.79 ±0-24	3*16 ±0*13	2.85 ±0-07
$\pi^- p \rightarrow \rho^0 n$ ↳ $\pi^+ \pi^-$	1.8 ±0-1	3*0 ±0-4	..	2.3 ±0<.2	1.1 ±0-1	1.2 ±0-1	1.12 ±0-1	0.8 ±0-1	1.52 ±0-47
$n'p \rightarrow P'p$ ↳ $\pi^- \pi^0$	1.0 ±0<.1	1.2 ±0-2	..	1*3 ±0-2	0*8 ±0-2	0*6 ±0-1	0.35	0.5 ±0-1	0.585 ± -032

A common feature of all these two-body reactions is their strong peripheral nature manifested particularly in the sharp forward peaking of the scattering angular distribution. It is instructive to plot the elastic differential cross-section on a semi-logarithmic scale as a function of $\cos \theta$ where θ is the scattering angle of the pion in the centre of mass system. The elastic scattering differential cross-section exhibits a noticeable second maximum in all the experiments, while some of the experiments also suggest the presence of another maximum in the backward hemisphere. The position of the second maximum is rather poorly defined in most experiments and sometimes seems to be noticed as a mere shoulder of the fast drop in the forward peak (as appears to be the case for the data⁹ at 4.16 GeV/c) thus suggesting an apparent variation in the structure of the scattering angular distribution beyond the first minimum as a function of incident momentum.

The position of secondary maximum in terms of $(-t)$ (the squared four momentum transferred to the nucleon) however seems to be essentially the same at different energies as seen from Table II and Fig. 1.

TABLE II

Position of the secondary maximum in $n\sim p$ elastic scattering angular distribution at different momenta

Laboratory momentum (GeV/c)	Position $\cos \theta$	Position (-t) (GeV/c) ^a
1-59	0-05	1-12
2-0	0-22	1-18
2-7	0-27	1-72
3-0	0-47	1-29

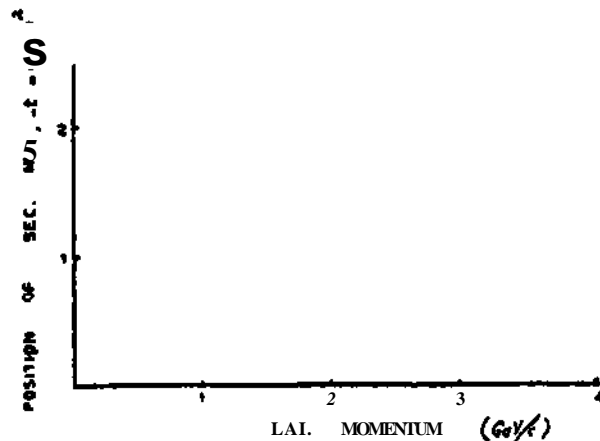


FIG. 1. Position of the secondary maximum in the elastic scattering angular distribution in terms of $(-t)$ in units of (GeV/c)^a versus the laboratory momentum.

Various aspects of this obvious diffraction-like structure have been studied. The most elementary of these is to fit the forward, $|f|_{\theta=0}$ (GeV/c)², angular distribution to a purely exponential diffraction pattern of the type:

$$\frac{da}{dt} = \left(\frac{da}{dt} \right)_{t=0} e^{-At}.$$

Table III lists the values of the best fit slope A at the various energies for the three different channels. In the light of the experimental errors one

TABLE III

Slope A in $(\text{GeV}/c)^{-2}$ for $dajdt = \{dajdt\}_{t=0} \pm A|t|$

Channel	1*59	2-0	2*26	2-7	2-75	3-0	3-3	4*0	4*16
1. $\pi^+ \pi^+ \rightarrow \pi^+ \pi^+$	7.29 ±0.35	7.5 ±0.6	8.7 ±0.2	7.77 ±0.05	..	6.8 ±0.7	..	8.53 ±0.49	7.36 ±0.14
2. $\pi^+ \pi^+ \rightarrow \pi^+ \pi^+$	9.1 ±0.6	7.7 ±0.9	..	10.26 ±0.06	9.8 ±0.6	7.4 ±0.7	9.3 ±0.9	8.7 ±0.7	..
3. $\pi^+ \pi^+ \rightarrow \pi^+ \pi^0$	G-8 ±9.9	5.8 ±0.8	..	9.32 ±0.08	7.6 ±0.5	5.9 ±0.9	9.1 ±1.2	8.8 ±0.7	..

can qualitatively say that the value of A for a particular channel is essentially the same at different laboratory momenta and there is not much difference in the A-values for the three channels thus implying the existence of a more or less definite interaction size. The value of $A = 7.6 \pm 0.5$ $(\text{GeV}/c)^{-2}$ for the elastic scattering channel obtained by the least squares method as the best fit to the data discussed here is in agreement with the value $7.4 \pm 0.2 (\text{GeV}/c)^{-2}$ found by a spark chamber experiment¹⁰ in the interval 2-3-6-0 GeV/c. We would like to observe however that A has certainly not reached the rather constant value of 9 $(\text{GeV}/c)^{-2}$ suggested by high energy experiments.¹¹ Further, the A-value corresponding to channel 2 is consistently higher than that for the other two channels. This might have something to do with the peculiar nature of the exchange trajectories in case of this channel as contrasted with those for the other two channels. The question of exchange trajectories is further discussed in one of the following paragraphs.

One can compute the square of the imaginary part of the forward scattering amplitude from the optical theorem:

$$\text{Im } f(0) = \frac{\lambda}{4\pi} \times (\text{total cross-section}).$$

These optical theorem predictions for the elastic scattering channel are compared with the experimental forward scattering cross-section in Table IV and Fig. 2. They indicate that for most of the data considered in this energy region the contribution to the scattering cross-section from the imaginary part dominates over that from the real part of the amplitude.

experimental value of the forward cross-section is however always appreciably larger than the theoretical one thus being consistent with the presence of some real part. Column 4 of Table IV lists the magnitude of the ratio of the real part of the forward scattering amplitude to the imaginary part of the forward scattering amplitude. These numbers must be interpreted in the light of the errors coming from uncertainties in the total cross-section, limitations in obtaining the experimental forward cross-section by an extrapolation procedure and the fact that the effect of Coulomb scattering has been neglected. Saxer¹² has computed this ratio on the basis of the predictions of dispersion relations. In our energy interval his value ranges from 13 to 21%. A set of counter measurements by Foley *et al*¹³ yield an effective ratio of about 30% in the momentum range of 8 to 10 GeV/c with a fast energy dependence indicated by the near vanishing of this ratio around 12 GeV/c. Optical model with constant opacity, a , gives for the elastic and total cross-section, respectively, the expressions $TTR^2(1-a)^2$ and $2TTR^2(1-a)$. The ratio (elastic cross-section)/(total cross-section) = $(1-a)/2$ is presented in Table V and Fig. 3. Our compilation is consistent with an essentially constant 50% absorption in the region of investigation. Our value of the ratio is considerably larger than the rather constant value¹⁴ of 0.172 ± 0.004 quoted for the energy region 8 to 20 GeV.

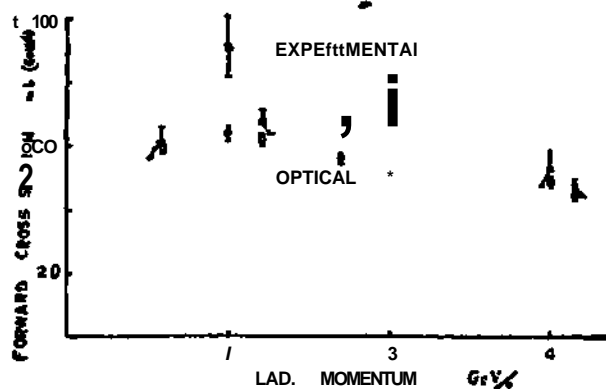


Fig. 2. Forward differential cross-section computed from the optical theorem, and experimental values, as a function of incident momentum.

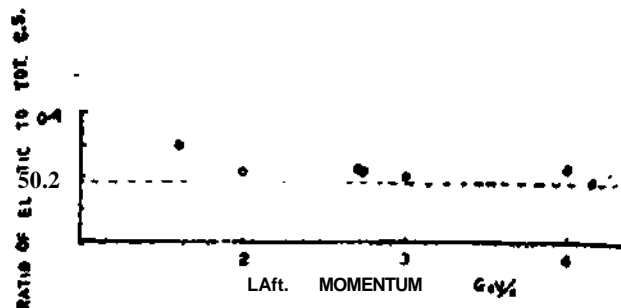


FIG. 3. Momentum dependence of the ratio of the elastic to the total cross-section, the dotted line is the upper limit of the ratio in the Van Hove model.

In the model of Van Hove¹⁵ elastic scattering amplitude asymptotically becomes pure imaginary when a large multiplicity and a weak correlation among secondary particles produced in inelastic collisions is assumed together with a Gaussian form for the inelastic overlap function. Several quantities of interest can then be determined in terms of the exponent of the overlap function and a parameter called ρ_0 (range: 0 to 0.5). The ratio

TABLE IV

Forward cross-section (σ_{fwd}): optical theorem and experimental points. Magnitude of the ratio of the real part of the forward cross-section to the imaginary part of the forward cross-section

Momentum (GeV/c)	Optical	Experimental	$ \text{Re}(\sigma_{\text{fwd}})/\text{Im}(\sigma_{\text{fwd}}) $
1.59	59.1 ± 0.8	60 ± 4	0.1
2.0	64.3 ± 1.1	91 ± 7	0.6
2.26	62.1 ± 1.0	68 ± 3	0.3
2.7	56.1 ± 0.9	73 ± 3	0.5
3.0	52.0 ± 0.8	79 ± 6	0.7
4.0	48.9 ± 0.7	53 ± 5	0.3
4.16	44.5 ± 1.0	47 ± 1	0.2

TABLE V

Ratio of elastic to total cross-section, viz., $(1 - a)/2$

Momentum (GeV/c)	$(1 - a)/2$
1.59	0.30 ± 0.01
2.0	0.22 ± 0.01
2.7	0.23 ± 0.01
2.75	0.22 ± 0.01
3.0	0.20 ± 0.01
4.0	0.23 ± 0.01
4.16	0.19 ± 0.01

of the elastic cross-section to the total cross-section is predicted to increase with f_0 and attains the value 0.185 for the upper limit. Figure 3 shows the experimental values of the ratio along with the upper bound predicted by the model. Though the experimental values have not quite reached this limit, there is not much difference between the two even at a relatively low momentum of about 4 GeV/c.

TABLE VI

Cross-section affixed value of t for different channels at the various laboratory momenta
Cross-section, mb

Channel	Momentum (GeV/c)	vunus of M^2	1-59	2-0	2-7	2-75	3-0	4-0	4-10
$\pi^+ p \rightarrow K^+ p$	2	..	0.99	1.75	1.10	..	1.71	1.20	0.66
	6	..	0.51	0.96	0.63	..	0.99	0.00	0.36
	10	..	0.26	0.44	0.36	..	0.58	0.24	0.20
	14	..	0.14	0.28	0.20	..	0.32	0.20	0.11
$\pi^+ p \rightarrow p^* n$ $* \rightarrow n$ in	2	..	0*26	0.2G	0.19	0.17	0.17	0*21	..
	6	..	0.13	0.13	0.09	0*08	0.12	0.10	..
	10	..	0*06	0.07	0.04	0.04	0.07	0.03	..
	14	..	0.03	0.04	0.02	0.02	0.04	0.02	..
$\pi^+ p \rightarrow p p$	2	..	0.11	0.09	0.12	0*09	0.13	0.14	..
	6	..	0.07	0.06	0.06	0.05	0.08	0.07	..
	10	..	0.03	0.03	0.03	0.03	0.03	0.03	..
	14	..	0.02	0.02	0*02	0.01	0.03	0.02	..

The behaviour of the width of the diffraction pattern is now examined in terms of the gross predictions of Regge Pole Theory.¹⁶ Channel 1 admits the exchange of the following trajectories: P [Vacuum trajectory with $a_p(0) \sim 1$], F (having same quantum numbers as P but with $a_p(0) \sim 0.5$), p [with $a_p(0) \sim 0.3$] and $AIUt$ (which is required to understand the presence of a backward peak). Channels 2 and 3 can both accommodate a n as well as $A_S.A_?$ trajectory is not $Y^{\wedge}ry$ different from $>$ trajectory. At higher

energies the effect of small J trajectories, like w , presumably becomes unimportant. Channel 3 can in addition proceed through the exchange of an ω [$a_w(0) \sim 0.2$] or a $\langle f \rangle$. The two trajectories are so close that they act as only one pole. The two-body channels 2 and 3 have also been examined from another point of view. The experimental decay angular distributions for p have been extensively studied in the light of peripheral model corrected for absorption¹⁷ and suggest that both the reactions are dominated by pion exchange. In case of channel 3, however, the best fit to data requires the inclusion of some contribution from the vector exchange. By analysing p'' data from several experiments in the momentum range of 2 to 8 GeV/c, Yen *et al.*¹⁸ have found that the parameter measuring the relative strength of ρ to $7T$ exchange has a value of $-(0.31 \pm 0.03)$, if negative or $+(0.39 \pm 0.04)$, if positive. Some predictions can be made about the behaviour of the forward cross-section when a single pole has a dominating role to play. In case of process 1, vacuum trajectory would obviously have such a role. This being an essentially flat trajectory implies that the value of A for this process ought to be the smallest. Of course, we have no reason to believe that only one Regge pole contributes to the forward cross-section for channels 2 and 3. For fixed values of t the cross-section is computed at different laboratory momenta for the three channels. This is summarised in Table VI and shows that for a given l the cross-section stays essentially constant with increasing energy for each one of the three channels. The result is consistent with the non-shrinkage of the diffraction peak. This is in contrast with the observations on two-body channels produced in K^+P interactions¹⁹ (3-5 GeV/c) where the distributions shrink as the centre of mass energy increases. A one pole Regge analysis would suggest that the diffraction pattern must shrink logarithmically with energy. In the high energy limit²⁰

$$\frac{d\sigma_{\ell}(\cdot)}{dcr, \wedge} \frac{d}{dt} = \left(\frac{j_1}{s_2} \right)^2 [\alpha_{\ell}(t) - 1]$$

where $\alpha_j(l)$ is the leading Regge trajectory contributing to a particular process l . Our analysis gives essentially constant $d\sigma/dt$ at different values of energy for a fixed momentum transfer and would thus require an unusually large value ~ 1 for $\alpha_x(l)$. For process 1 this is consistent with single Regge pole dominance since vacuum trajectory has a very small slope and as such $\alpha_1(l)$ stays close to 1 for a large range of t . For processes 2 and 3 no single

trajectory can yield such a large value for $a^*(t)$. • One possible simple explanation is that unlike the K^+P interactions case, the processes here cannot be understood in terms of the exchange of a limited number of important trajectories; further unlike the K^+P case the high energy range of applicability of the Regge pole analysis may not have been reached in TTp scattering at laboratory momenta considered in this work.

We conclude that the three reactions examined are all characterised by strong peripheral production. They fail to exhibit, within statistics, any shrinkage of the diffraction peaks and one is thus not able to describe them qualitatively in terms of a simple Regge pole model.

ACKNOWLEDGEMENT

We wish to acknowledge the help of Harnek Singh in compiling a part of the data included in this note.

REFERENCES

1. Saday-Orsay-Bari-Bologna Collaboration *Nuovo Cimento*, 1963, 29, 513, 515.
2. Tuli, S. K. .. *Ph.D. Thesis*, Florida State University, 1964 (Unpublished).
3. Reynolds, B. G. *et al* .. *Phys. Lett.*, 1967, **24B**, 311.
4. Miller, D. H., Gutay, L., Johnson, P. B., Loeffler, F. J., Mellwain, R. L., Sprafka, R. J. and Willmann, R. B. *Purdue University Report*, **COO-1428-19**.
5. Saday-Orsay-Bari-Bologna Collaboration *Nuovo Cimento*, **1965, 35**, 713.
6. Hagopian, V. .. *Ph.D. Thesis*, University of Pennsylvania, 1963.
7. Guirgossian, Z. G. T. .. *UCRL Report*, 10731, 1963.
8. ABBHLM Collaboration .. *Nuovo Cimento*, 1964, 31, 729.
9. Eisner, R. L., Johnson, P. B., Klein, P. R., Peters, R. E., Sahni, R. J., Yen, W. L. and Tautfest, G. W. *Purdue University Report*, 1967.
10. Coffin, C. T. *et al* .. *Phys. Rev.*, 1967, 159, 1169.
11. As quoted, for instance, by L. Van Hove, Lectures given at *CERN Report*, 65-22.
12. Šaxer, H. I.- .. *University of Michigan Technical Report*, 03106-19- T. 1964.

13. Foley, K. J. *et al.* .. *Phys. Rev. Lett.*, 1965, 14, 74.
14. Focacci, M. N. **and** .. *CERN Report*, 66-18.
Giacomelli, G.
15. **Van** Hove, L. .. Reference 11.
16. Omnes, R. L. .. *Ann. Rev. Nuc. Sc.* 1966, 16, 263 and other references
therein.
17. Jackson, J. D. .. *Nuovo Cimento*, 1964, **34**, 1644.
18. Yen, W. L. *et al.* .. *Phys. Rev. Lett.*, 1967, 18, 1091.
19. CERN-Bruxelles Collaboration *CERNI TCI Physics Report*, 66-17, 1967.
20. Philips, R. J. and Rarita, W. .. *Phys. Rev.*, 1965, **139B**, 1336.

EFFECT OF CROSS-VELOCITY ON THE STABILITY OF SUPERPOSED FLUIDS

BY S. C. AGRAWAL AND G. S. AGRAWAL

(Department of Mathematics, Indian Institute of Technology, Kanpur, India)

Received August, 31, 1967

(Communicated by Prof. J. N. Kapur, F.A.S.C.)

ABSTRACT

In the present paper we discuss the stability of the interface between two layers of incompressible and inviscid fluids of different but constant densities, streaming in different directions. The velocities in the different directions of the two fluid layers give rise to the concept of cross-velocity. We show that it destabilizes the interface while if p and U are continuous functions then it has stabilizing effect.

1. INTRODUCTION

THE stability of an interface between two fluids in relative motion was first investigated by Helmholtz (1868) and Kelvin (1910) and it was shown that stable arrangement in the absence of streaming becomes unstable, however small the relative velocity of the fluid layers may be. It corresponds to a physical situation where wind is blowing over stagnant or streaming water. It is also true that the direction of streaming and the direction of wind will not, in general, be the same. Therefore, we may say that upper layer of fluid has two components of velocity in general; one in the direction of streaming of lower layer and another perpendicular to it and in the same plane. We shall call it cross-velocity. So far the effect of cross-velocity has not been discussed at all in the literature. Intuitively one feels that it is bound to make the system more unstable. In the present paper we confirm it analytically and further investigate the extent to which it makes the system unstable.

The immediate question, similar to the question posed after Kelvin and Helmholtz and later answered by Taylor (1931), Goldstien (1931), Drazin (1958), Miles (1961) and Howard (1961), also arises here. "Will cross-velocity have similar effect if density and* velocity are continuously varying?" We make an attempt to answer this question. Unlike the problem of Miles,

Howard and others, velocity at any point in the fluid is allowed to have arbitrary direction in the plane parallel to the plates and vary continuously as a function of transverse co-ordinate. We shall note that the cross-velocity, under the conditions stated above, has stabilizing character.

2. FORMULATION OF THE PROBLEM

The heterogeneous and non-viscous fluid is confined between two rigid plates at a distance $2a$ apart. Origin of the co-ordinates is taken in the middle of the plates which are parallel to x - y plane, z -axis is taken to be perpendicular to the plates. The initial state of the system is given by

$$U(z) = [U_1(z), U_2(z), 0]$$

$$p = p(z)$$

$$p = p(z)$$

The linearised perturbation equations of momentum, continuity and incompressibility are

$$\left. \begin{aligned} \rho \frac{\partial u'}{\partial t} + \rho U_1 \frac{\partial u'}{\partial x} + \rho U_2 \frac{\partial u'}{\partial y} + \rho w' \frac{dU_1}{dz} &= - \frac{\partial \delta p}{\partial x} \\ \rho \frac{\partial v'}{\partial t} + \rho U_1 \frac{\partial v'}{\partial x} + \rho U_2 \frac{\partial v'}{\partial y} + \rho w' \frac{dU_2}{dz} &= - \frac{\partial \delta p}{\partial y} \\ \rho \frac{\partial w'}{\partial t} + \rho U_1 \frac{\partial w'}{\partial x} + \rho U_2 \frac{\partial w'}{\partial y} &= - \frac{\partial \delta p}{\partial z} - g \delta \rho \end{aligned} \right\} \quad (1)$$

$$\frac{\partial u'}{\partial x} + \frac{\partial v'}{\partial y} + \frac{\partial w'}{\partial z} = 0 \quad (2)$$

$$\frac{\partial \delta \rho'}{\partial t} + U_1 \frac{\partial \delta \rho'}{\partial x} + U_2 \frac{\partial \delta \rho'}{\partial y} = - w' \frac{d\rho}{dz} \quad (3)$$

where $u', v', w', \delta p'$ and $\delta \rho'$ are the disturbances in velocity, density and pressure respectively. We make normal mode analysis so that x, y, z and t dependence of any perturbation quantity $f'(x, y, z, t)$ be given by

$$f'(x, y, z, t) = (q - c)f(z) \exp i(k_x x + k_y y - ct) \quad (4)$$

where

$$q = k_x U_1 + k_y U_2$$

After putting these disturbances in equations (1), (2) and (3) and carrying out elimination of $w, v, \delta \rho$ and δp , we can obtain one equation in w alone,

Assuming the density variation of the type $P = p_0 e^{-Pz}$ where δ is constant, the equation in w is

$$D [pWDw] + \rho k^2 [pg - W^2] w = 0 \quad (5)$$

where

$$W = q - c$$

with the boundary conditions

$$w = 0 \text{ at } z = -a \text{ and } a \quad (6)$$

If we apply the transformation $G = W^* w$ to the equation (5), we obtain

$$(\rho WG')' - [i(\rho q'Y + k^* \rho W + \rho W^{-1} (i q'^* - \delta A^2))] G = 0. \quad (7)$$

Obviously, G has to satisfy the boundary condition

$$G = 0 \text{ at } z = -a \text{ and } a \quad (8)$$

Hereafter the prime will represent the derivative with respect to z .

The non-vanishing of $(q - c)$ is ensured by the assumption that $c \neq 0$. Multiplying the equation (7) by G^* , the complex conjugate of G , and integrating within the limits of z , we get

$$\int_{-a}^a \rho W [|DG|^2 + k^2 |G|^2] dz + 2 \int_{-a}^a (\rho q') |G|^2 dz + \int_{-a}^a \rho W^* \left[\frac{1}{4} q'^2 - g\beta k^2 \right] \left| \frac{G}{W} \right|^2 dz = 0. \quad (9)$$

Equating the imaginary part of (9) to zero, one gets

$$\left. \int_{-a}^a \rho [|G'|^2 + k^2 |G|^2] dz + \int_{-a}^a \rho \left[g\beta k^2 - \frac{1}{4} q'^2 \right] \left| \frac{G}{W} \right|^2 dz \right\} = 0. \quad (10)$$

Since $c \neq 0$, the equation (10) is satisfied if

$$g\beta k^2 > \frac{1}{4} q'^2.$$

If a is the direction of wave vector with the axis of x_0 , then the sufficient condition for stability is

$$J(z) = \frac{g\beta}{U_2^2} > \frac{1}{4} \cos^2(a-\theta) \quad (11)$$

where

$$U_2^2 = VW^2 \sim TW^2.$$

While in the absence of cross-velocity and with $a = 0$, the sufficient condition for stability is

$$J(*) > * \quad (12)$$

Since right-hand side of (12) is greater than the right-hand side of (11), the region of stability is more for $U_2 \neq 0$. It confirms the stabilizing character of cross velocity.

We also conclude from above discussion that in the absence of cross-velocity $U_2 = 0$, the condition for stability for three-dimensional disturbances takes the form

$$J > i \cos^2 a. \quad (13)$$

Again the right-hand side of (13) is smaller than that of (12) confirming that for $U_2 = 0$, three dimensional disturbances are more stabilizing than two-dimensional disturbances. Therefore, for obtaining sufficient condition of stability only two-dimensional disturbances need be considered. This has earlier been proved by Yih (1955) in an alternative way.

But in the presence of cross-velocity U_2 the sufficient condition for stability, for three-dimensional and two-dimensional disturbances are respectively

$$J > i \cos^2 (a - \theta) \quad (14)$$

and

$$J > i \cos^2 \theta. \quad (15)$$

Thus for $U_2 \neq 0$ three dimensional disturbances have more destabilizing effect than two-dimensional ones, hence one has necessarily to consider three-dimensional disturbances.

3. STABILITY OF AN INTERFACE BETWEEN TWO FLUID LAYERS

We now consider the stability of the interface between two fluid layers of different but constant densities ρ_1 and ρ_2 both having the constant streaming at an angle θ to each other. If U and V are the velocities of the upper and lower fluid layers respectively and if x-axis is chosen in the direction of V , the stationary state is given by

$$\mathbf{K} = (V, 0, 0)$$

$$U = (U \cos \theta, U \sin \theta, 0) = (U_1, U_2, 0).$$

The two fluid layers extending from $z = -\infty$ to $z = \infty$ are assumed to be separated by $z = 0$. ρ_1 is the density of the lower fluid. Then the equation (5) reduces to the following for determining w in each of the regions

$$\rho W^2 (D^2 - k^2) w = 0 \quad (16)$$

where

$$W = k_x U_1 + k_y U_2 - c \quad \text{for } z > 0 \quad (17)$$

and

$$W = k_x V - c \quad \text{for } z < 0. \quad (18)$$

The general solution of this equation is the linear combination of

$$e^{kz} \quad \text{and} \quad e^{-kz}.$$

Now since w cannot increase exponentially on either side of the interface at $z = 0$ and since w/W must be continuous on this surface, the appropriate solution of (16) can be written as

$$w_1 = A (k_x V - c) e^{kz} \quad \text{for } z < 0; \quad (19)$$

$$w_2 = A (k_x U_1 + k_y U_2 - c) e^{-kz} \quad \text{for } z > 0. \quad (20)$$

Now we need only one condition to determine A . We neglect the surface tension. Moreover, since we are dealing with the superposed fluids, the continuity of stress normal to interface yields the required condition. It is obtained by integrating the following equation in from $-\epsilon$ to ϵ and then taking the limit when $\epsilon \rightarrow 0$

$$W D (p D w) - p k^2 W w - g \rho_1^2 (D p) \epsilon \rightarrow 0.$$

Integration of the 2nd term yields zero as it is finitely discontinuous function across the interface. Hence, one gets

$$A_0 WPDW) - gk^2 A_0 GO (\wedge) o = 0. \tag{21}$$

where

$$\Delta_0 f = f_{0+} - f_{0-}$$

and $(v/W)_0$ is the velocity at the interface $z = 0$ using (17)-(20), equation (21) gives the characteristic equation as follows:

$$c^2 - 2 \{a_2 (k_x V_i + k_y J J_2) + c L \pm V k_x\} c + a_2 (k_x U_1 - k_y J J_2)^* + a k_x^* V^2 + gk (a_2 - a_x) = 0$$

where

$$a_2 = \frac{P_i}{P_i + p_2} \quad a_1 = \frac{P_i}{P_i + P_2}$$

Thus we obtain

$$C = \{a_2 Q k_x U_1 + k_y U_2\} + a_1 V k_x \pm \sqrt{gk (a_1 - a_2) - a_1 a_2 \{k_x (U_1 - V) + k_y U_2\}^2}$$

If a is the direction of wave vector to the axis of x then

$$C = k \{ (a_2 U_1 + a_1 V) \cos a + a_2 U_2 \sin a \} \pm VA: \{ (a_1 - a_2) \cos^2 a - a_1 a_2 \{ (U_1 - V) \cos a + U_2 \sin a \}^2 \}$$

Thus, for the stable arrangement $\{p_1 > p_2\}$ in the absence of streaming, the sufficient condition for stability is that

$$k < \frac{g (a_1 - a_2)}{a_1 a_2 \{ (U_1 - V) \cos a + U_2 \sin a \}^2} \tag{22}$$

The condition (22) will still hold if we replace the right-hand side by a lesser quantity or in other words instead of $\{(U_x - V) \cos a + U_2 \sin a\}^2$ we put its maximum $\{(U_x - V)^2 + U_2^2\}$. Thus, the sufficient condition for stability is that

$$k < \frac{g (a_1 - a_2)}{a_1 a_2 \{ (U_1 - V)^2 + U_2^2 \}} \tag{23}$$

But if the layers have the streaming in the same direction (23) will reduce to

$$k < \frac{g(C_1 - a_2)}{a_1 a_2 (U_1 - V)^2} \quad (24)$$

Since the right-hand side of (23) is less than the right hand side of (24), the cross velocity reduces the region of stability and hence on Kelvin-Helmholtz-instability it has destabilizing effect.

ACKNOWLEDGEMENT

We thank Dr. R. K. Jain for his help in preparing this paper.

REFERENCES

- | | |
|---------------|---|
| Helmholtz, H. | .. <i>Wissenschaftliche Abhandlungen</i> , 1882. |
| Kelvin | .. <i>Mathematical and Physical Papers IV</i> , 1910, pp. 76-85. |
| Taylor, G. I. | .. <i>Proc. Roy. Soc. (London)</i> , A, 1931, 132 , 499-523. |
| Goldstien, S. | .. <i>Ibid.</i> , 1931, pp. 524-48. |
| Drazin, P. G. | .. <i>J. Fluid Mech.</i> , 1958, 4 , 214-24. |
| Miles, J. W. | .. <i>Ibid.</i> , 1961, 10 , 496. |
| Howard, L. N. | .. <i>Ibid.</i> , 1961, 10 , 509. |
| Yib, C. S. | .. <i>Quart. Appl. Math.</i> , 1955, 12 , 434-35. |

OXIDATION OF α -HYDROXY ACIDS AND DERIVATIVES BY Cr (VI) OXIDE*

BY S. SUNDARAM AND N. VENKATASUBRAMANIAN

(Department of Chemistry* Vivekananda College, Madras-A)

Received March 24, 1969

(Communicated by Prof. S. V. Anantkrishnan, F.A.S.C.)

ABSTRACT

The kinetics of the chromic acid oxidation of α -hydroxy acids, their salts and esters has been investigated in binary solvent mixtures of acetic acid and water. The results indicate that the Westheimer hypothesis of a rate-determining proton-abstraction from a preformed chromate ester is unlikely. Substituent and salt effects indicate the likelihood of a mechanism involving a rate-determining hydride ion abstraction assisted by a proximate substituent.

INTRODUCTION

THE chromic acid oxidation of lactic, malic and mandelic acids was studied by Dhar and co-workers¹ and recently by Bakore and Narain.² The latter investigators have explained their rate data in terms of the Westheimer mechanism,^{3,4} namely, the rate-determining loss of a proton from a preformed chromate ester. A study of the oxidation of α -deuterio mandelic acid⁶ has revealed that the -C-H bond on the α -carbon atom is broken in the rate-determining step. We have now investigated the chromic acid oxidation of a representative selection of α -hydroxy acids and their derivatives and a few other related compounds in binary solvent mixtures of acetic acid and water under conditions of constant ionic strength and pH.

EXPERIMENTAL

All the organic compounds used were of the extra pure variety (Fluka AG/Koch-Light) and were used without further purification. The experimental procedure was the same as in our earlier publications, the rate of disappearance of chromic acid being followed iodometrically.⁶ The specific rate constants were calculated from the integrated rate equation for a second-order reaction and graphically. All second-order rate constants

* From the *Ph.D. Thesis* of S. Sundaram approved by the University of Madras, 1968.

are expressed as litre-mole⁻¹ seer¹. Experiments were carried out in duplicate and the velocity constants are reproducible within 3%. The stoichiometry, hydroxy acid : chromic acid ³:2 was obtained in the oxidation of mandelic acid and benzaldehyde was obtained as major oxidation product in over 80% yield.

RESULTS AND DISCUSSION

The kinetics of the oxidation of mandelic, malic and lactic acids conform to a total order of two—first with respect to the gross concentration of Cr (VI) and also first with respect to the substrate. The individual orders with respect to the hydroxy acid and Cr (VI) oxide were also confirmed by conventional methods. The same kinetic picture was also obtained in the oxidation of ethyl and benzyl mandelates, ethyl and benzyl lactates and also the salts of lactic and mandelic acids. The second-order rate constants obtained in different solvent systems of acetic acid and water are presented in Table I. We have included the rate constants for the oxidation of isopropyl alcohol and *a*-phenyl ethyl alcohol from an earlier investigation^{7*8} for purposes of comparison. The Arrhenius parameters calculated from the temperature dependence of the rate are presented in Table II.

TABLE I

Compound	Solvent composition (HOAc)			
	40%	50%	60%	70%
Lactic acid	53-1	65-5	73-2	..
Malic acid	63-3	82-4	105	..
Mandelic acid	341	456	591	..
Isopropyl alcohol*	2-33	5-67	11-6	..
<i>a</i> -Phenyl ethanol*	..	32-9	63-8	..
Ethyl mandelate	..	13-5	15-2	..
Benzyl mandelate	..	616	7-44	10-1
Ethyl lactate	4-33	6-41	8-57	..
Benzyl lactate	..	3-06	410	7-01
Sodium lactate	..	65-6	75-2	..
Potassium mandelate	355	422

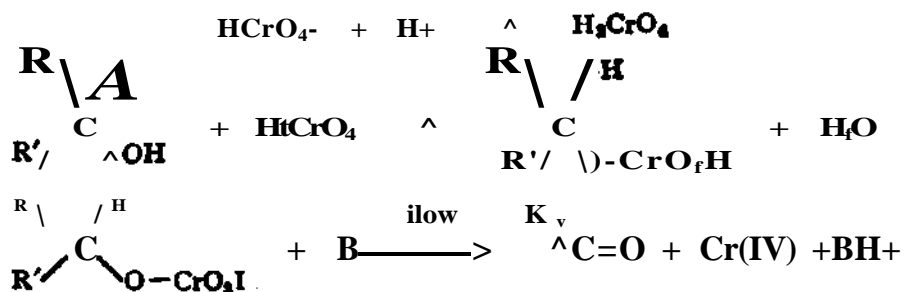
* From Venkatasubramanian and Anantakrishnan (1960).

TABLE II

Solvent composition - 50% HOAc — 50% H₂O

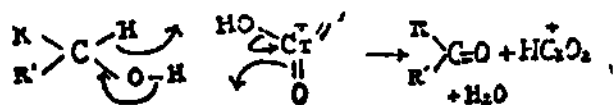
Compound	A E k.cal./mole	A S e.u.
Lactic acid	9.79	-4.2
Malic acid	12.0	-3.5
Mandelic acid	14.8	-2.3
Ethyl lactate	13.1	-3.7
Benzyl lactate	10.6	-4.6
Ethyl mandelate	10.5	-4.3
Benzyl mandelate	13.1	-3.7

The Westheimer mechanism for the oxidation of an α -hydroxy acid (following that of a secondary alcohol) is as follows:



(B = base; R = -CH₂- or -C₆H₅; R' = -COOH, -COOEt or -COOCH₂C₆H₅).

An alternative mechanism proposed by Roček⁹ and later by Ananta-krishnan and Venkatasubramanian⁷ involves a cyclic hydride ion abstraction.



A unimolecular decomposition of the ester by an internal proton transfer has been suggested by Kwart and Francis¹⁰ and has been modified by Lee and Stewart.¹¹

The present work shows that the chromic acid oxidation of lactic, malic and mandelic acids follows the mechanism

lactic acid < malic acid < mandelic acid.

Independently looked at, this sequence conforms to the Westheimer mechanism. This is also the order observed by Bakore and Narain.² But using results of the oxidations of other derivatives of α -hydroxy acids in our present investigations, certain anomalies become apparent. The order with reference to the hydroxy acids and esters in the case of both lactic acid and mandelic acid is

lactic acid > ethyl lactate > benzyl lactate

mandelic acid > ethyl mandelate > benzyl mandelate.

Further sodium lactate and potassium mandelate are oxidised at the same rate as the parent acids themselves. This suggests that the oxidation involves the same entity. It is likely that under the conditions of the experiment, at pH 3-5, the hydroxy acids react essentially as the corresponding ions (pK_{tt} for lactic and mandelic acids are 3.87 and 3.38 respectively). The anion has also been postulated as the reactive intermediate in the acid permanganate oxidation of mandelic acid.¹² That the anion is the reactive entity could be proved in an indirect way. For, if this be the case, the reaction between this anion and $H\overset{+}{C}rO_3$ would show a dependence on ionic strength. This has been experimentally observed in a series of experiments where the ionic strength has been varied (Table III).

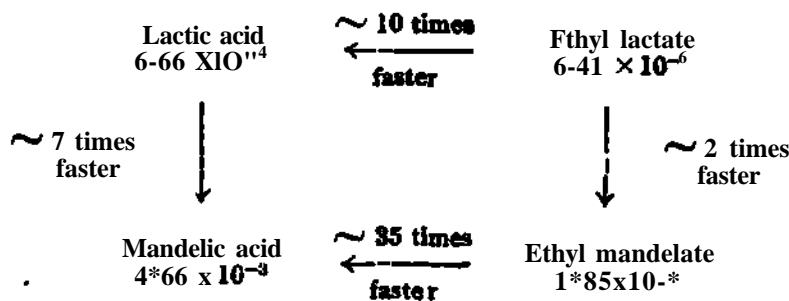
TABLE III

Compound : Mandelic acid

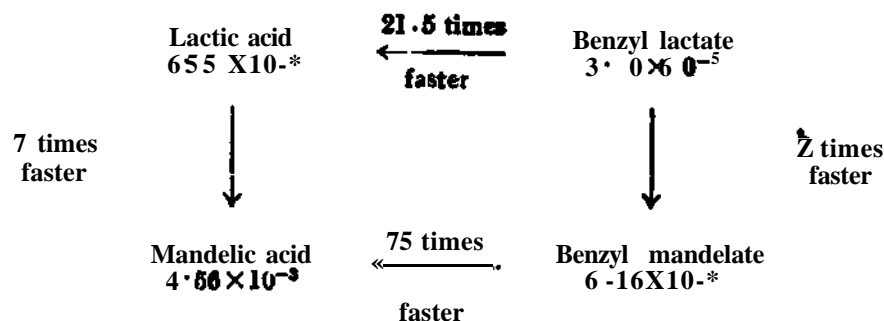
Temp. 45° c.

Solvent composition (% v/v) (\overline{HOAc} - H_2O)	μ $(\overline{KOAc}$ - KCl)	$\sqrt{\mu}$	$k_2 \times 10^3$ (litre-mole ⁻¹ seer ¹)
60-40	0.40	0.633	4.61
60-40	0.35	0.592	5.07
60-40	0.30	0.548	5.12
60-40	0.20	0.447	5.74

We also observe an interesting correlation in the oxidation rates of the acids and the esters.



SCHEME 1

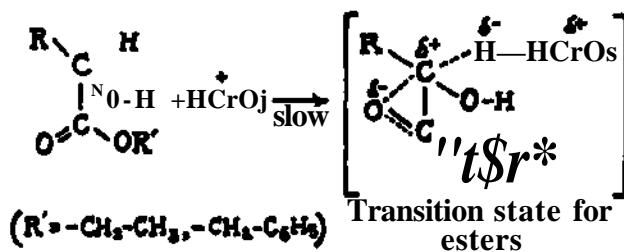
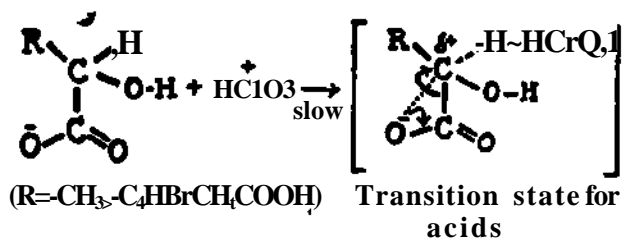


SCHEME 2

(Schemes 1 and 2 are the correlation diagrams for the oxidation of α -hydroxy acids and their derivatives in 50% acetic acid at 45° C. The numerical values are the second-order constants in litre-mole⁻¹ sec⁻¹).

In both the schemes it is noticed that while the replacement of a -CH₃ group, by a phenyl group in the esters, gives a rate enhancement by a factor of 2, a similar replacement in the parent acids gives a seven-fold increase in rate. Similarly, while the replacement of a -COOEt by a -COOH group (ethyl lactate to lactic acid) gives a rate enhancement only by ten times, a similar replacement in ethyl mandelate gives a thirty-five-fold increase in rate. In the benzyl esters likewise an approximately twenty-fold increase in the lactic acid series corresponds with a seventy-five-fold increase between benzyl mandelate and mandelic acid. This correlation, we must point out, underscores a combination effect that arises when the -COOH and phenyl groups are present in one and the same compound (*viz.*, mandelic acid) and not when either the phenyl group alone is present (as in the mandelates) or when the -COOH only is present (as in lactic acid). Any mechanism that is proposed for the oxidation of α -hydroxy acids must, therefore, be capable of explaining this enhanced reactivity of mandelic acid,

The partial negative charge on the carbonyl oxygen of the carboxylate would be largest (equivalent to $1/2 e$) in the case of the carboxylate ion, much less in the case of the carboethoxy group and least in the case of the $-\text{COOCH}_2\text{C}_6\text{H}_5$ group. Further, the electrostatic stabilisation of the



electron-deficient transition state (which may be regarded as possessing a zwitter ionic type of structure due to carbonyl polarization) will be maximum in the case of the mandelic acid anion in two ways—for the partial positive charge on the secondary carbon atom is now stabilized both by the proximate negatively charged oxygen and also by the π -electron cloud of the attached benzene ring. This would then readily account for the extra rate benefit observed in the case of mandelic acid alone and also for the ready decarboxylation to yield benzaldehyde. The +1 effect of the $-\text{COO}^-$ group will also aid a hydride removal. The slower reactivity of the esters get explained as consequent to a lower stabilisation of the transition state. That the decarboxylation provides a driving force for the oxidation, is also seen to be in conformity with the very slow oxidation of β -hydroxy butyric acid (sodium salt) and cyclohexanol-2-carboxylic acid (Table IV)—compounds in which the $-\text{COOH}$ group is insulated from the carbonium centre by an intervening carbon atom. It is also pertinent to point out that γ -lactones do not undergo oxidation by chromic acid. For example, γ -valero lactone did not undergo any oxidation in 50% acetic acid at 45°C . even after three days.

TABLE IV

Solvent composition : 60% HOAc— 40% H₂O

Temp. 45° C.

Compound	$f_c \times 10^B$ (Utre-mole ¹¹ seer ¹)
Lactic acid	.. 65-5
β -Hydroxy butyric acid sodium salt monohydrate	.. 1-37
Cyclohexanol-2-carboxylic acid	.. 2-50

ACKNOWLEDGEMENT

We thank the C.S.I.R. (India) for the maintenance grant for a research scheme and for the award of a Junior Research Fellowship to one of us (S. S.).

REFERENCES

- Bhattacharya, A. K. and Dhar, N. R. *Z. Anorg. Chem.*, 1928, **169**, 381.
- Bakore, G. V. and Shyam Narain *J. Chem. Soc.*, 1963, **3419** (634).
- Westheimer, F. H. and Nicolaidis, N. *J. Amer. Chem. Soc.*, 1949, 71, 25.
- Wenheimer, F. H. .. *Chem. Revs.*, 1949, 45, 419.
- Kemp, T. J. and Waters, W. A. *J. Chem. Soc.*, 1964, p. **1192**.
- Venkatasubramanian, N. .. *Proc. Ind. Acad. Sci.*, 1959, 50, 156.
- and Anantkrishnan, S.V. *Ibid.** 1960, 51, 310.
- .. *Ibid.*, 1961, 53, 80.
- Roček, J. .. *Collection Czech. Chem. Commun.*, **1958**, 23, 833.
- Kwait, H. and Francis, P. S. .. *J. Amer. Chem. Soc.*, 1955, 77, 4907.
- Stewart, R. and Lee, D. G. .. *Can. J. Chem.*, 1964, **42**, 439.
- Bakore, G. V., Rama Shanker and Urmila, G. *Ind. J. Chem.*, 1963. 1, 331.
- Jayaraman, fl. -. *Ibid.*, 1964, 2, 94.
- Westheimer, F. H. and Chang, Y. W. *J. Amer. Chem. Soc.*, 1960, 82, 1401.

HEAT TRANSFER IN CHANNEL FLOW OF A MICROPOLAR FLUID

BY MISS RENUKA RAJAGOPALAN AND K. S. BHATNAGAR

{Department of Applied Mathematics, Indian Institute of Science, Bangalore-2}

Received October 9, 1967

(Communicated by Prof. P. L. Bhatnagar. F.A.S.C.)

ABSTRACT

The study of heat transfer in channel flow has been done by previous authors for Newtonian and elastico-viscous fluids, it is the aim of the present paper to study the temperature profile for flow of a micropolar fluid in a channel induced by a constant axial pressure gradient, when the walls are maintained at constant temperatures. We have examined the effects of microrotation on the temperature profile and on the kinetic energy of the fluid. Three cases have been chosen by us for detailed study: (i) both the walls are maintained at different constant temperatures, (ii) both the walls are maintained at the same constant temperature, (iii) one wall is kept at a constant temperature and there is no heat flux at the other wall.

1. INTRODUCTION

THE equations determining the velocity field and temperature field within a fluid in motion are, in general, interrelated. However, when buoyancy forces are disregarded and when the properties of the fluid may be assumed to be independent of the temperature, the velocity field does not depend on the temperature field, while the temperature field does depend on the velocity field. One of us² (R. R.) has recently studied the problem of velocity distribution in steady pressure gradient flow in a channel of a micropolar fluid. The aim of the present paper is to study the process of heat transfer in the above flow when the walls are maintained at constant temperature. We have examined the effects of microrotation on the temperature profile and have compared the results with those of forced convection in Newtonian fluids.³ Previous authors^{4,5,6} have investigated the nature of the temperature distribution in the above type of flow of several elastico-viscous non-Newtonian fluids and have studied in particular the effects of elasticity on the flow.

We use the energy equation of micropolar fluids given by Eringen¹ in which the presence of coefficients of viscosity and gyroviscosity account for the heat generated by frictional and microrotational effects. Moreover, the presence of microrotation modifies the kinetic energy of the fluid.

In the numerical work, we have taken a number of values of the product of the Prandtl and Eckert number corresponding to both moderate and high velocity distributions in the following cases:

- (i) both the plates are kept at different constant temperatures,
- (ii) both the plates are kept at same constant temperature,
- (iii) one plate is at a constant temperature and the heat flux from the other plate into the fluid is prescribed.

2. FORMULATION OF THE PROBLEM

We choose a rectangular Cartesian system with the axis of x in the direction of the flow and the two plates are given by $\bar{y} = h$ and $\bar{y} = -h$. In the case of incompressible flow, the equations determining the velocity and temperature of the fluid are:

$$v_{k,k} = 0, \quad (2.1)$$

$$\begin{aligned} -P_{,k} + (*v + Pv)_{,k} + (H>V + K_v) v_{kt} u + K_{,,} \epsilon_{lm} v_m j \\ + />(A-fyc) = 0, \end{aligned} \quad (2.2)$$

$$\begin{aligned} (<*v + Pv) ^l, kl + Y_v V k M + K_{ff} C_{fc} i f o V r o j i - 2K_{,,} v_{fc} \\ + p(lk - Pk) = 0, \end{aligned} \quad (2.3)$$

and

$$\begin{aligned} \rho \dot{\epsilon} = -p d_{kk} + \lambda_v d_{ll} d_{kk} + (2\mu_v + K_v) d_{kl} d_{lk} \\ + 2K_v (\omega_k - v_k) (\omega_k - v_k) + a_v v_{k,k} v_{l,l} \\ + \beta_v v_{k,l} v_{l,k} + \gamma_v v_{i,k} v_{i,k} - q_{k,k} + ph, \end{aligned} \quad (2.4)$$

where $A_{,,}$, $/^*$, $J\mathfrak{E}$, are coefficients of viscosity, $a_{,,}$, 0_F , $y_{\mathfrak{F}}$ are coefficients of gyroviscosity, p is the density and $/$ is a constant on the assumption of microisotropy of the fluid, (v_k) (v_k) are the velocity and the microrotation vectors respectively, c is the internal energy density per unit mass, (q_k) is the heat

flux vector and h is the heat source per unit mass, (rfd) is the deformation rate tensor and (ω_m) is the vorticity vector given by

$$\begin{aligned}\omega_{kl} &= -\epsilon_{klm}\omega_m, \\ &= \frac{1}{2}(v_{k,l} - v_{l,k}),\end{aligned}\quad (2.5)$$

a suffix following a comma denoting covariant differentiation.

The components of velocity and microrotation in the case of channel flow induced by a constant pressure gradient dp/dx have been determined earlier.² Choosing

$$\begin{aligned}v_1 &= \bar{u}(\bar{y}), & v_2 &= 0, & v_3 &= 0, \\ v_1 &= 0, & v_2 &= 0, & v_3 &= \bar{v}(\bar{y}),\end{aligned}\quad (2.6)$$

and non-dimensionalising according to the following scheme:

$$\begin{aligned}\bar{u} &= u_0 u, & \bar{y} &= hy, & \bar{v} &= h v, & \frac{\mu_0 h^2}{\gamma_0} &= n_2, \\ \frac{K_0 h^2}{2\mu_0 + K_0} &= n_2, & u_0 &= -\frac{h^2 \bar{c}_p}{2\mu_0 + K_0},\end{aligned}\quad (2.7)$$

we obtain

$$u = \frac{1}{2} \left[1 - v^8 \frac{n^*}{\langle 2 + W_3 \rangle} \frac{1}{a} \frac{\cosh a - \cosh ay}{\sinh a} \right],$$

$$v = \frac{\sinh ay}{\sinh a}.$$

where

$$a = i_M \frac{*_{3}(2K_0 + jia)}{W_2 + \langle 3 \rangle}, \quad (2.8)$$

u and v satisfy the boundary conditions of "No slip" and "No micro-slip" at the channel wall, namely

$$u = 0 \text{ on } y = \pm J, \quad v = 0 \text{ on } y = \pm J_f \quad (2.9)$$

In the presence of this velocity field, the equation determining the temperature is given by

$$\frac{d^2 T}{dy^2} + \frac{E\sigma}{2} \left(\frac{du}{dy}\right)^2 + \frac{2n_2}{n_2 + n_3} E\sigma \left(\frac{1}{2} \frac{du}{dy} + v\right)^2 + \frac{E\sigma}{2n_2 + n_3} \left(\frac{dv}{dy}\right)^2 = 0, \quad (2.10)$$

where T is the non-dimensional temperature, E the Eckert number and σ the Prandtl number suitably defined.

Case 1

Both the walls are maintained at different constant temperatures (the upper wall at higher temperature). The boundary conditions in this case are :

$$f = \bar{T}_L \text{ on } \bar{y} = -h, \quad \bar{T} = \bar{T}_u \text{ on } \bar{y} = h. \quad (2.11)$$

Non-dimensionalising the temperature by the following relation:

$$\bar{T} = T u - \bar{T}_L,$$

and defining the Prandtl and Eckert numbers by

$$E = \frac{u_0^2}{C_p (\bar{T}_u - \bar{T}_L)}, \quad \sigma = \frac{C_p}{K} (2\mu_v + K_v),$$

we now have to solve the equation (2.10) subject to boundary conditions

$$T = 0 \text{ on } y = -1, \quad T = 1 \text{ on } y = 1. \quad (2.12)$$

This gives us the temperature distribution

$$T = \frac{1}{2}(y+1) + \frac{E\sigma}{6}(1-y^2) + \frac{E\sigma}{2n_2+n_3} F(y), \quad (2.13)$$

where

$$F(y) = -\left(\frac{1}{4} - \frac{1}{2}y\right) + \frac{1}{4} \frac{\cosh^2 a - \cosh^2 ay}{\sinh^2 a} + \frac{1}{4} \frac{\cosh^2 a - \cosh^2 2ay}{\sinh^2 a}, \quad (2.14)$$

The first two terms give the temperature distribution same as the Newtonian fluid with viscosity $(2/\lambda + K_w)$, while $F(y)$ takes account of the microrotation of the fluid.

From (2.13), we have

$$\left. \frac{dT}{dy} \right|_{y=1} = \frac{1}{2} - E\sigma \left\{ \frac{2}{3} - \frac{a \coth a - 1}{2n_2 + n_3} \right\},$$

and

$$\left. \frac{dT}{dy} \right|_{y=1} = \frac{1}{2} + E\sigma \left\{ \frac{2}{3} - \frac{a \coth a - 1}{2/l_2 + \ll \eta} \right\}, \quad (2.15)$$

from which we deduce for a viscous fluid without microrotation, the following expressions for the temperature gradients at the walls :

$$\left. \frac{dT}{dy} \right|_{y=1} = \frac{2/3}{3\sqrt{4}} - E\sigma \left(\frac{2/3}{3\sqrt{4}} + E\sigma \right), \quad \left. \frac{dT}{dy} \right|_{y=1} = \frac{2/3}{3\sqrt{4}} + E\sigma.$$

From the first relation (2.15'), it is clear that heat flows into or from the upper plate into the fluid according as

$$Ea > \text{ or } < J.$$

Hence if we fix \bar{T}_U and \bar{T}_L , there exists a critical value

$$u_{oc} = \left[\frac{3}{4} \frac{\bar{J}_v}{(2\mu_v + K_v)} (\bar{T}_U - \bar{T}_L) \right]^{\frac{1}{2}}$$

of u_0 such that when $u_0 < u_{oc}$, the heat will flow from the upper plate to the fluid, while the reverse happens when $u_0 > u_{oc}$. From the second relation in (2.15'), we find that the fluid always imparts heat to the lower plate to maintain it at a constant temperature \bar{T}_L .

The total heat flux from the fluid to the walls

$$\begin{aligned} &= K \frac{(\bar{T}_U - \bar{T}_L)}{h} \left[\left. \frac{dT}{dy} \right|_{y=1} - \left. \frac{dT}{dy} \right|_{y=1} \right], \\ &= \frac{4}{3} E\sigma \cdot \frac{K (\bar{T}_U - \bar{T}_L)}{h}, \end{aligned} \quad (2.16)$$

This quantity is always positive and though, when $E < 3/4$, heat flows from the wall to the fluid, the total heat flux is always from the fluid to the wall. The heat generated by friction is given out to the walls.

For micropolar fluids, when $dT/dy < 0$ at the upper wall heat flows from the fluid to the wall. This occurs when

$$E\sigma \left[\frac{T_2}{3} - \frac{a \coth a - 1}{2n_2 + n_3} \right] > \frac{1}{2} \tag{2.17}$$

Since $(a \coth a - 1)$ is always greater than zero, the effect of microrotation is to raise the critical value of $E\sigma$ below which heat flows from the warmer wall to the fluid. That is, the critical value of u_0 is raised above which the heat begins to flow from the fluid to the warmer wall. The total heat flux from the fluid to the walls

$$= \frac{K(\bar{T}_u - \bar{T}_L)}{h} - \frac{2E\sigma \left[\frac{a \coth a - 1}{2n_2 + n_3} \right]}{V} \tag{2.18}$$

Since $(a \coth a - 1)/(2n_2 + n_3)$ is always less than $2/3$ for all n_2 and n_3 the heat flux will be from the fluid to the wall, the cooler wall will always take heat from the fluid, while the warmer wall takes heat from the fluid when $E\sigma$ exceeds a critical value. The total heat flux for a micropolar fluid is less than that for the corresponding Newtonian fluid with a coefficient of viscosity $(2/\mu_w + K_v)$. This suggests that there is less dissipation of kinetic energy within a micropolar fluid and this results in the temperature at each point of a micropolar fluid being less than that for a Newtonian fluid.

We study next the kinetic energy (K.E.) of simple microfluid, which includes in it the contribution due to microrotation also. If V be a material volume of the fluid, the kinetic energy in V is given by

$$K.E. = \int_V \rho v'_k v'_k dv' \tag{2.19}$$

Since

$$K.E. = \int_V \rho v_k^2 dv + \int_V \rho v_k v_{sk}^{st} dv, \tag{2.20}$$

where

$$\int_V p' dv' = p dv, \quad \int_V p' f^l dv' = 0,$$

and

$$\int_{\Omega} \rho' \xi'^i \xi'^j dv' = \rho i^{ij} dv;$$

i^{sl} is a constant for the deformed body called the 'micro-inertia moments'. In the case of a micropolar fluid

$$p_i = f i^{sl} = J \int_{\Omega} \delta^{sl}, \quad \nu_{lk} = \epsilon_{mlk} \nu_m, \quad \nu_{sk} = \epsilon_{nsk} \nu_n,$$

$$\therefore \text{K.E.} = \int_{\Omega} \rho v k^{2dv} + \int_{\Omega} \rho \mu e^{2dv} \quad (2.21)$$

In the present case, we have

$$\begin{aligned} \text{K.E.} = & \int_{\Omega} \rho u^* h \left[\frac{1}{2} \frac{r}{L} \coth a \left(\frac{1}{3} + \frac{1}{4} \right) \right. \\ & \left. + \frac{1}{2} \frac{r^2}{(n_2 + n_3) a^2} (3 \coth^2 a - 1 - 3 \coth a) \right] \\ & + 2j_0 \left\{ \frac{5}{6} + \frac{2}{3} \coth a - \coth^2 a \right\} \int_{\Omega} \rho \end{aligned} \quad (2.22)$$

Numerical computations, performed for micropolar fluids with $(n_2+n_3)j_0 = 4n_3/a^2$, show that the kinetic energy for this class of micropolar fluids is less than that for the Newtonian fluids. Moreover, from the first equation in (2.8), we conclude that at each location the fluid velocity for these micropolar fluids is less than that for the Newtonian fluids.

Case 2

Both the walls are maintained at the same temperature \bar{T}_c . Non-dimensionalising the temperature f by

$$T = \frac{T - \bar{T}_e}{\bar{T}_c},$$

and defining

$$\frac{\mu_0}{\mu} = \frac{j_0^2}{C_p \bar{T}_c}, \quad \mu = \frac{\mu_0}{C_p \bar{T}_c} \left[1 - \frac{\mu_0}{C_p \bar{T}_c} \left(\frac{1}{2} + \frac{\mu_0}{C_p \bar{T}_c} \right) \right]$$

ill

Miss RENUKA RAJAGOPALAN AND k. S. BHATNAGAA

we solve equation (2.10) subject to boundary conditions

$$T = 0 \quad \text{on } \hat{n} = \pm 1. \quad (2.24)$$

This gives

$$T = \frac{E\sigma}{6} (1 - y^4) + \frac{E\sigma}{2n_2 + n_3} F(y), \quad (2.25)$$

where $F(y)$ is given by (2.10).

The first term gives the contribution of a Newtonian viscosity ($2\mu_v + K_v$). The second term being always negative (as noted by numerical computation). We notice here also that the temperature at each point of the fluid is less than that of the corresponding Newtonian fluid. Computing dT/dy at the two walls, we find that the fluid gives less heat to the walls than the Newtonian fluid. The total heat flux from the fluid to the walls in this case

$$[22] \quad \text{acotha} = \frac{1}{2} \ln \frac{1+K}{1-K}$$

Case 3

There is no heat flux from the fluid to the lower wall, that is the lower wall is perfectly insulated against the heat flow. Let us maintain the upper wall at a constant temperature $f u$ and define the dimensionless temperature T by $T = (f - \bar{T}u)/f u$. Using the relations (2.23), and solving the equation (2.10), under the boundary conditions

$$T = 0 \quad \text{at } y = 1_r$$

$$\frac{dT}{dy} = 0 \quad \text{at } y = -1. \quad (2.27)$$

we obtain

$$T = \frac{E\sigma}{6} (5 - 4y - y^4) + \frac{1}{2} \ln \frac{1+K}{1-K} F(y) \quad (2.28)$$

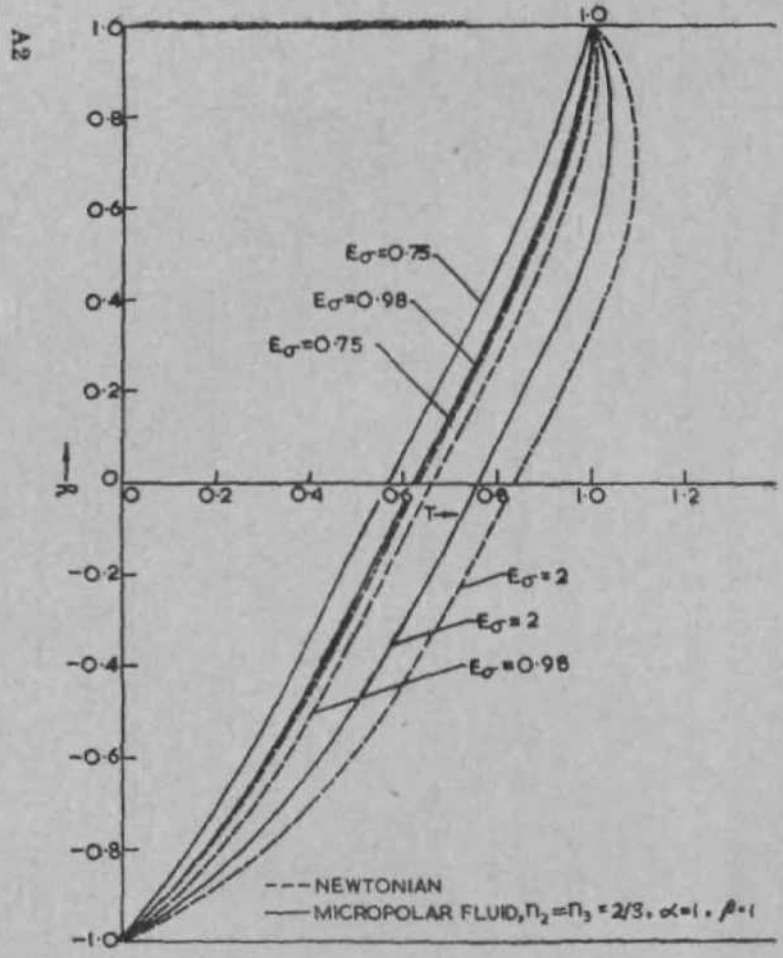


FIG. 1 (a)

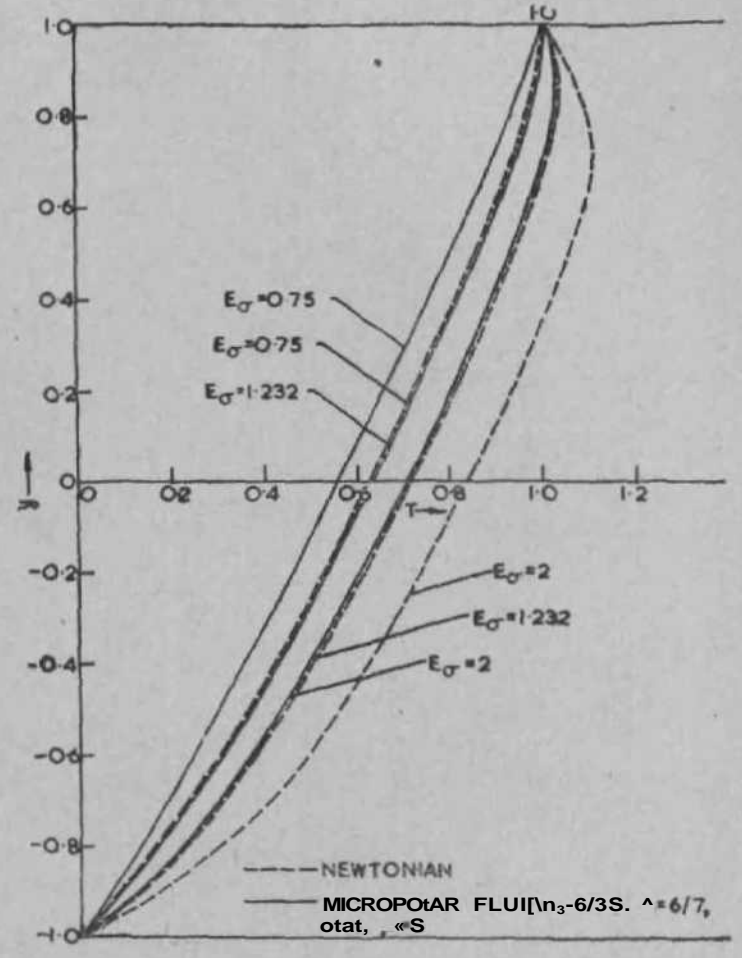


FIG. 1 (b)

Again T is less at each point of a micropolar fluid than for the corresponding Newtonian fluid.

We have at the upper wall

$$\left. \frac{dT}{dy} \right|_{y=1} = \frac{r}{L} \left[\frac{2}{3} - \frac{\text{acotha} - 1}{2n_2 + n_3} \right] \quad (2.29)$$

so that there is heat flux at the upper wall. The heat flows from the fluid to the upper wall, the heat flux being less than that for a Newtonian fluid. The maximum temperature within the fluid occurs at the lower wall, and this adiabatic wall temperature is given by

$$T = \frac{\mu_0 r^2}{2k\sigma} \left[\frac{2}{3} - \frac{\text{acotha} - 1}{2n_2 + n_3} \right] \quad (2.30)$$

3. DISCUSSION OF RESULTS

Case 1.—We have performed numerical calculations for two specific micropolar fluids whose parameters are given by $n_2 = n_3 = 2/3$ and $n_2 = 6/35$, $w_3 = 6/7$. The velocity profiles for these two fluids lie within the Newtonian parabolic profile so that the velocity at each point of these fluids is less than that for the corresponding Newtonian fluid. It is noticed that for given value of Ea , the temperature at each point of these fluids is also less than that for the corresponding Newtonian fluid. Besides, a higher value of Ea is required before the fluid begins to give heat to the warmer wall, the critical value of Ea for the Newtonian fluids is $3/4$, while for the above micropolar fluids it is 0.98 and 1.232 respectively. As the ratio w_3/w_2 increases for micropolar fluids, the temperature profile continuously recedes from the Newtonian profile and there is less dissipation of kinetic energy within the fluid. Figures 1 (a) and 1 (b) show the temperature profile for this case. We note that in the case of Newtonian fluids, there is a greater dissipation of K.E., more heat is generated and the warmer wall gets heat from the fluid for a smaller critical value of w_0 , than for a micropolar fluid. In order to control the large generation of heat within a Newtonian fluid and to increase the critical value of w_0 , additives may be added to the fluid to make it micropolar in nature.

Similar observations are noticed in Cases 2 and 3. Figures 2 and 3 show the temperature profile for these cases.

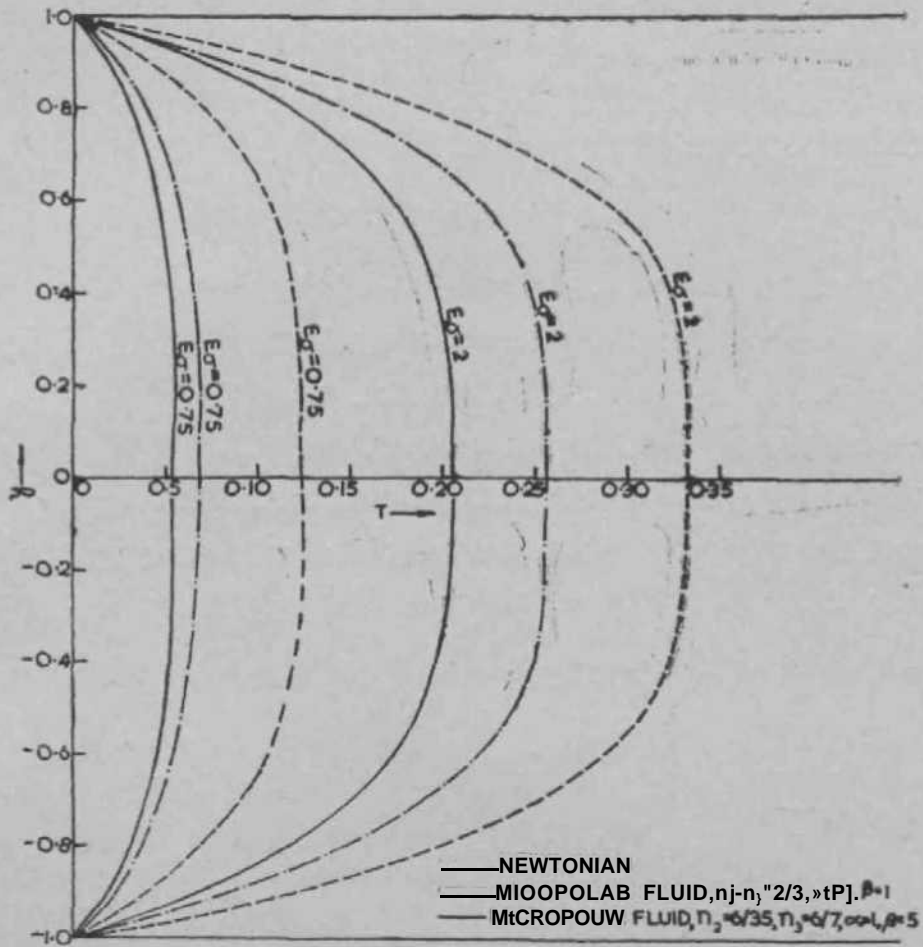


FIG. 2

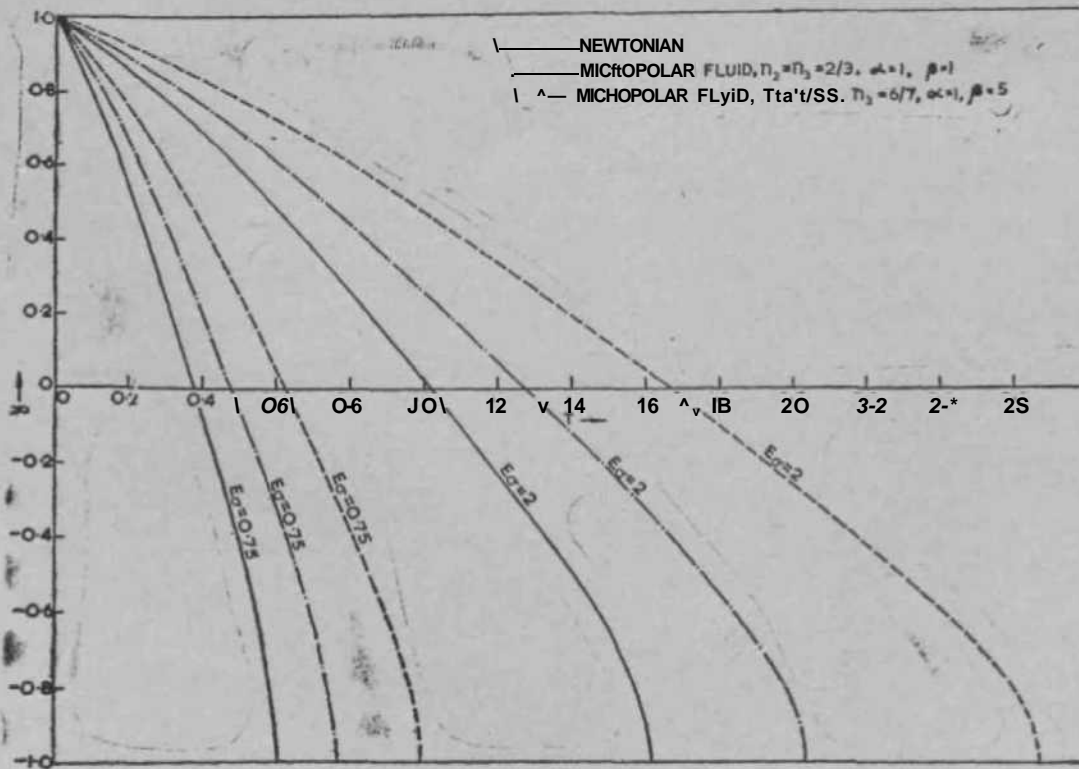


FIG. 3

4. ACKNOWLEDGEMENT

The authors are grateful to Prof. P. L. Bhatnagar for help and guidance during the preparation of the paper.

5. REFERENCES

- 1 Eringen, A. C. .. *Jour. Math. Mech.*, 1966, 16, 1.
2. Renuka Rajagopalan .. *Jour. Ind. Inst. Sd.*, 1968, 50, 57.
3. Schlichting, H. .. *ZAMM*, 1951, 31, 78.
4. Bhatnagar, P. L. .. *ZAMP*, 1966, 17, 646.
5. Jain, M.K. .. *App. Sd. Res.*, 1963, 11 A, 295.
- 6 Mishra, S. P. .. *Proc. Ind. Acad. Sci.*, 1965, 61, 219.
7. Eringen, A. C. .. *Int. Jour. Engg. Set*, 1964, 2, 205.

THE SLOW STATIONARY FLOW OF A VISCOUS LIQUID ABOUT POROUS SPHEROIDS

BY N. V. SAMBASIVA RAO AND S. K. LAKSHMANA RAO

[Department of Mathematics, Regional Engineering College, Warangal (A.P.), India]

Received September 7, 1967

(Communicated by Prof. B. S. Madhava Rao, F.A.S.C.)

ABSTRACT

The slow stationary flow of a viscous liquid about porous spheroids is examined. The solution describing the Stokes stream function is found to be a one-parameter family of surfaces and for special values of the parameter we recover the flow past impermeable spheroids. The ranges of the parameter are determined and the case of the porous sphere as well as that of a porous disc are deduced as limiting case.

1. INTRODUCTION

THE effect of porosity of walls on the velocity and pressure distributions of the flow of a viscous liquid in space bounded by the walls was originally considered by A. S. Berman¹ assuming the velocity of leaving the walls to be independent of position. Adopting the same boundary conditions, J. R. Sellars² and S. W. Yuan³ considered some further problems. In the case of viscous flow through an annulus with porous walls, A. S. Berman⁴ has set the rate of injection at one wall equal to the rate of suction at the other wall. In all these problems the permeability velocity on the boundary is assumed to be given. There are also problems in which the permeability velocity is not known in advance and is to be determined in the process of solution and in such problems the properties of the porous medium of the body, about which the flow takes place, are important.

The slow stationary flow of a viscous liquid about porous shells is a problem of this type. Recently, A. I. Leonov⁵ has examined the flow about a porous spherical shell whose thickness is small compared to the minimum defining dimension of the region of the flow, adopting the conditions on the porous boundary surface that the component of the permeability velocity in the tangent plane is zero and that normal component of the velocity is continuous across the boundary. In this paper we investigate the slow stationary flow of a viscous liquid about porous spheroidal shells,

adopting the boundary conditions mentioned above. Even as in ^m, the solution provides a single parameter family of spheroidal boundaries. The Stokesian flow past spheroids with impermeable boundaries given by L. E. Payne and W. H. Pell⁶ concords with the present solutions for special values of the parameter. The solution in ^{L5} for the case of a permeable spherical boundary as well as that for a porous circular disc are also obtainable from the present solutions by some limiting procedures.

2. FORMULATION OF THE PROBLEM

Let us consider a uniform stream flowing past a porous spheroid placed with its axis of symmetry in the direction of stream as referred to a system of cylindrical polar co-ordinates (r, θ) with the axis of symmetry as x-axis. Let u, v, w be the velocity components in the directions of r, θ respectively. Let us further take that the free-stream velocity U is in the increasing direction of x . In this situation, the flow will be axi-symmetrical and hence $w=0$. The equation of continuity now becomes

$$\frac{\partial u}{\partial r} + \frac{1}{r} \frac{\partial}{\partial \theta} (rv) = 0. \quad (2.1)$$

If ψ is the Stokes stream function defined by

$$u = \frac{1}{r} \frac{d\psi}{d\theta}, \quad v = -\frac{1}{r} \frac{d\psi}{dr}, \quad (2.2)$$

the equation of continuity is satisfied. The equation to be satisfied by ψ in the case of Stokesian flow is

$$\nabla^2 \psi = 0 \quad (2.3a)$$

where

$$\nabla^2 \psi = \frac{1}{r} \frac{\partial}{\partial r} \left(r \frac{\partial \psi}{\partial r} \right) + \frac{1}{r^2} \frac{\partial^2 \psi}{\partial \theta^2} \quad (2.3b)$$

Let R_e and R_i be respectively the regions external and internal to the porous surface. Let ψ_e and ψ_i denote the stream functions regular in R_e and R_i respectively. Let da and dn be respectively the elemental line-segments in the tangential and normal directions to the surface (in the meridional plane). The problem then is to obtain regular solutions of the differential equations

$$\nabla^2 \psi_e = 0 \quad \text{in } R_e \quad (2.4a)$$

$$\nabla^2 \psi_i = 0 \quad \text{in } R_i \quad (2.4b)$$

subject to the following boundary conditions:

$$(i) \quad 0e-\gg \text{£}Ur^2 \text{ at infinity,} \tag{2.5 a}$$

$$(ii) \quad \frac{\partial \text{£}}{\partial n} = 0 \text{ on the porous surface,} \tag{2-5 b}$$

and

$$(iii) \quad \text{£} = -\frac{\partial \text{£}}{\partial \sigma} \text{ at the porous surface.} \tag{2.5 c}$$

3. PROLATE SPHEROID

The transformation

$$z = c \cosh \text{£} \quad (c > \delta) \tag{3.1}$$

where $z = x + ir$, $\text{£} = f + iy$ gives $x = c \cosh \text{£} \cos \eta$ and $r = c \sinh \text{£} \sin \eta$, thus introducing elliptic co-ordinates in the xr plane and therefore the curve $\text{£} = f_0$ is an ellipse in the meridian plane whose semi-axes are $c \cosh \text{£}_0$, $c \sinh \text{£}_0$. Thus $\text{£} = f_0$ defines a prolate spheroid and in the exterior region R_c of this spheroid we have $\text{£} > \text{£}_0$, $0 < \eta < \pi$ while in the interior region R_i , $0 < \text{£} < \text{£}_0$, $0 < \eta < \pi$. Following L. E. Payne and W- H. Pell,⁶ we may take the solution of $\nabla^2 \psi = 0$ in the form

$$\psi = \frac{1}{2} Ur^2 (1 - \psi^1 - \psi^2) \tag{3.2}$$

where $\psi^i(\text{£}, r)$ denote any solution of

$$\mathbf{L}_k(\psi) = \frac{\partial^2 \psi}{\partial x^2} + \frac{\partial^2 \psi}{\partial r^2} + \frac{k}{r} \frac{\partial \psi}{\partial r} = 0 \quad (-\infty < \text{£} < \infty). \tag{3.3}$$

Put $\cosh i = s$, $\cos \eta = r$ and let $\cosh \text{£}_0 = -V$

It is easily seen that (cf. E. W. Hobson⁷)

$$\psi^1 = \frac{f Q_n(s) P_n(t)}{L P_n(s) P_n(t)} \text{ in } R_c$$

$$L P_n(s) P_n(t) \text{ (0 in } R_i)$$

and

$$\psi^2 = \begin{cases} f Q_m(s) C^m P_m(t) \text{ in } R_c \\ P_m^{(1)}(s) P_m^{(1)}(t) \text{ (0 in } R_i) \end{cases} \quad \begin{matrix} m = 1, 2, 3, \dots \\ \sim \quad \quad \quad * \end{matrix} \tag{3.5}$$

where P_n and Q_n denote Legendre functions of the first and second kind respectively and the superscripts in (3.5) indicate differentiation. To accord with the requirements of the regularity, we choose

$$if^i = \begin{cases} *e = \int_{z,} *r^* \ll - \$ A_n Q_n(*) P_n(0 - \sum_{m=1}^{\infty} B_m Q_m^U) \text{ to } P_m^{(1)}(t) \\ * = i \cdot Ur^* f \sum_{m=1}^{\infty} C P, (s) P_n (0 + \sum_{m=1}^{\infty} D_m P_m \langle \rangle (s) P_m^{(1)}(t) \end{cases} \quad (3.6)$$

To match the conditions of the problem, we take $A_x = 0 = C_{if}$ $A_n = 0 = C_n$ ($n > 3, 4, 5, \dots$) and $B_2 = 0 = D_2$, $B_m = 0 = D_m$ ($m \wedge 4, 5, 6, \dots$). After inserting expressions for P_n , Q_n and noting that $r = c \sinh f \sin r \setminus$, we have

$$\psi_e = \frac{1}{2} U c^2 (s^2 - 1) (1 - \wedge^2) [1 - A Q_0 \text{ to } - B (3t^2 - 1) Q_2(s) - C Q_1^{(1)} \text{ to } - D (5f^* - 1) Q_3^{\wedge} \text{ to}] \quad (3.7)$$

$$\psi_i = \frac{1}{2} U c^2 (s^* - 1) (1 - *^2) [E - F (J^a + \langle \bullet \rangle) + G^* V] \quad (3.8)$$

where A, B, C, D, E, F, G are constants.

It can easily be seen that ip^1 and \wedge^3 as taken in (3.4) and (3.5) vanish at infinity, i.e., as $s \rightarrow \infty$. Thus the condition (2.5 c) is satisfied. The other conditions (2.5 b) and (2.5 c) correspond to

$$\frac{\partial \psi_e}{\partial s} = 0, \quad \frac{\partial \psi_i}{\partial s} = 0 \quad \text{at } s = s_0, \quad -1 \leq t \leq 1 \quad (3.9 a)$$

$$\frac{\partial \psi_e}{\partial t} = \frac{\partial \psi_i}{\partial t} \quad \text{at } s = s_0, \quad -1 \leq t \leq 1. \quad (3.9 b)$$

The vanishing of the derivatives in (3.9 a) at $s = s_t$ and for all t in $-1 < t < 1$ is possible only when the coefficients of different powers of t in the derivatives vanish when $s = s_0$ and hence we get

$$B [2s_0 Q (s_0) - Q_t (s_0)] + 10 D Q_8 (s_0) = 0, \quad (3 \cdot 10 a)$$

$$2s_0 - A [2s_0 Q_0 (s_0) - 1] + B [4s_0 Q_a (s_0) - 2Q_x (s_0)J - 2C Q! (s_0) + 12D Q, (J_0) = 0, \quad (3 > 10 A)$$

$$F = G (2s_0^2$$

$$E - F (2s_0^2 - 1) = 0. \quad (3.10 d)$$

The continuity of the derivatives in (3.9 b) at $s = s_0$ for all s_0 in $0 < s_0 < 1$ is achieved by equating the coefficients of like powers of t on both sides when $s = s_0$ and thus we have

$$3BQ_2(s_0) + 5DQ_3(s_0) = G(s_0^2 - 1), \tag{3.11 a}$$

$$-2 + 2AQ_0(s_0) - 8BQ_2(s_0) + 2CQ_1(s_0) - 12DQ_3(s_0) = J_0 \tag{3.11 b}$$

$$-4G(s_0^2 - 1) \tag{3.11 c}$$

From the muster of equations (3.10) and (3-11), we see that

$$A = \frac{10G(s_0^2 - 1)Q_3(s_0)}{\Delta}, \tag{3.12 a}$$

$$B = - \frac{[10G(s_0^2 - 1)Q_3(s_0)]}{A'}, \tag{3.12 b}$$

$$C = \frac{[3 - 3AQ_0(s_0) - 215Q_8(s_0)fa] - 2G(3s_0^2 - 2)(j_0^{s_1} - D)}{3Q_x^w(s_0)} \tag{3.12 c}$$

$$D = \frac{G(s_0^2 - 1)[(25Q_8(s_0) - Q_1fa)J]}{A'}, \tag{3.12 d}$$

$$E = G(2s_0^2 - 1)^2, \tag{3.12 e}$$

$$F = G(25s_0^2 - 1) \tag{3.12 f}$$

where

$$A = 3[s_0 - (J_0^9 + 1)Q_0fa] \tag{3.13 a}$$

and

$$A' = fiQi^{\wedge}(j_0)Qsfa - Qi^{\wedge}(j_0)Qsfa \tag{3.13 ft}$$

The velocity components can be determined by

$$v_i = \frac{1}{c^2} \frac{\partial \hat{u}}{\partial t} \tag{3.14 a}$$

and

$$q_n = \frac{-1}{c^2} \frac{\partial \hat{u}}{\partial s} \tag{3-14 ft}$$

It can be seen from (3.9) and (3.14) that the components of velocity are continuous across the spheroid. The expression for q_{\pm} and q_{\sim} in (3.14 a), (3.14 b) are indeterminate when $s = 1, t = \pm 1$, which give the foci ($x = \pm c, r = 0$). However, the singularities herein are removable and limits at those points exist. From (3.12), we notice that A, B, C, D, E, F are functions of the constant G, which we call the porosity parameter. We have therefore a single parameter family of regular flows with normal permeability at the surface. When $G = 0$, the stream function ϕ identically vanishes throughout R^* and so $G = 0$ corresponds to Stokes flow past an impermeable prolate spheroid. The solutions (3.7), (3.8), (3.12), (3.13) concord with the results in M on putting the parameter $G = 0$.

The normal velocity at the surface is given by

$$W_{s=s_0} = V_0 = 2GU \left(\frac{1}{c} - 1 \right) \frac{1}{2} (V - \dots) i_u \tag{3.15}$$

The pressure is to be determined by the equations

$$\frac{\partial P}{\partial s} = \frac{-ft}{c(\lambda^2 - 1)} \frac{\partial L}{\partial t} - \frac{\partial P}{\partial t} = \frac{ft}{c(1 - f^2)} \frac{\partial L}{\partial s} \tag{3.16a}$$

where

$$\lambda = \frac{1}{c} \sqrt{c^2 - s^2} \quad \lambda^2 = 1 - \frac{s^2}{c^2} \tag{3.16b}$$

We therefore have

$$p_e = \frac{\mu U t}{c} [6BQ_1(s) - f \pm \frac{A}{c}] + \text{const, in } R, \tag{3.17 a}$$

$$p_i = -4G(5J_0 - 3) \frac{U}{c} \pm \text{const, in } R, \tag{3.17 b}$$

Leaving the additive constants in the above, we see that the pressure is discontinuous on the porous surface and this discontinuity is responsible for the flow across the porous surface. The jump p in the pressure at the surface is given by

$$(\Delta p)_{s_0} = (p_e)_{s=s_0} - (p_i)_{s=s_0} = \frac{1}{c} \left(\frac{ft}{1 - f^2} - 6BQ_1 \right) \tag{3.18 a}$$

where

$$a = 6BQ_1 f + 4GJ_0 (5J_0 - 3), \tag{3.18 b}$$

and

$$j\beta = \langle w_c^2 - 2B - A. \tag{3.18 c}$$

For physically possible flows, we must have

$$\text{for } -1 < t < 0, V_0 < 0 \text{ and } Afc, > 0$$

and

$$\text{for } 0 < f < 1, V_0 S^* > 0 \text{ and } \Delta p_s \leq 0.$$

Thus it is essential to have $G > 0$ and $j\beta - at^* < 0$ for all t ($-1 < t^* < 1$). It can be shown that $\alpha > 0$ when $G > 0$. Hence, we must have $\beta < 0$ when $G \geq 0$. This leads to the restriction

$$0 < G < G_0 \tag{3.19 a}$$

where

$$G_0 = \frac{3A'}{[10A(V-1)\{3VQ_x f_0\} - jQ_s \sqrt{s_0} + 2\Delta'(s_0^2 - 1) - 2\Delta\Delta' s_0^2 (5s_0^2 - 3)]} \tag{3.196}$$

which can also be expanded in powers of $1/J_0$ in the form

$$G_0 \sim \frac{1}{f} \left(\frac{1}{J} + \frac{1}{W} + \dots \right) \frac{1}{R^*} \tag{3.19 c}$$

The drag D on the spheroid is obtained on using the formula

$$D = 2\langle e \rangle (s_0^* - 1)^* T [\rangle (V - D^* (Tu \sim T^*_{tt}), \dots, - s_0 (1 - t^2)^{1/2} (T^e_{t\eta} - T^i_{t\eta})_{s=1}] A, \tag{3.20}$$

where $T_{\{t\}}$, $T_{\{n\}}$ are fluid stresses and the superscripts e and i indicate the regions to which they belong. Thus we have

$$D = 4w/tUcA. \tag{3.21}$$

When

$$G = 0, A = \frac{L}{[(s_0^2 + 1)Q_0(s_0) - s_0]}$$

and we have

$$D = 8\pi U c [(V + 1) Q_0 - J_0]^{1/2} \quad (3-21 a)$$

for the impermeable prolate spheroid.

The spherical polar co-ordinate system (p, θ, ϕ) can be regarded as a limiting system of the elliptic polar system (f, ξ, η) by allowing $c \rightarrow \infty$, $a \rightarrow \infty$ but keeping $cs = p$. Then $\xi \rightarrow \theta$. To recover the results of A. I. Leonov⁶ for the Stokes flow past a porous sphere of radius a , we may put $G = (4A - 1) c^2/2a^4$ and allow $c \rightarrow \infty$, $a \rightarrow \infty$ but keeping $cs = p$ and $cs_0 = a$, where A is the porosity parameter. We find that the results are concordant.*

We find that the results are concordant.*

4. OBLATE SPHEROID

The transformation

$$z = c \sinh \zeta \quad (c > 0) \quad (4.1)$$

where $z = x + iy$, $\zeta = \xi + i\eta$ gives $x = c \sinh \xi \cos \eta$, $y = c \cosh \xi \sin \eta$ thus introducing elliptic co-ordinates in xr -plane and therefore the curve $\eta = \eta_0$ is an ellipse in the meridian plane whose semi-axes are $c \cosh \eta_0$, $c \sinh \eta_0$ and $\xi = \xi_0$ gives the oblate spheroid. In the exterior region R_e of the spheroid we have $\xi < \xi_0$; $0 < \eta < \pi$ and in the interior region R_i , $0 < \xi < \xi_0$; $0 < \eta < \pi$. Let $\cosh \xi = T$, $\cos \eta = t$, $\cosh \xi_0 = T_0$, $\cos \eta_0 = t_0$ before we seek solutions ψ_n of the type $\psi_n = J_n U r^a (1 - 0^1 - 0^3)$. It is readily seen that⁷

$$\psi_n = \begin{cases} Q_n^{(1)}(i\tau) P_n^{(1)}(t) & \text{in } R_e \\ P_n^{(1)}(i\tau) P_n^{(1)}(t) & \text{in } R_i \end{cases} \quad n = 0, 1, 2, \dots \quad (4.2)$$

and

$$\psi_n = \begin{cases} Q_n^{(1)}(i\tau) P_n^{(1)}(t) & \text{in } R_e \\ P_n^{(1)}(i\tau) P_n^{(1)}(t) & \text{in } R_i \end{cases} \quad n = 2, 3, \dots \quad (4.3)$$

*The expression $8/3w \eta U a$ (11-35 A) for the drag in the case of a sphere in ψ is slightly defective though it yields the correct value when $A \gg 1/4$ for an impermeable sphere. The actual expression is $8w \eta U (1 - A)$.

Here we choose

$$\hat{\Lambda} = \begin{cases} \text{tfk} = \left| \text{Ur}_L^2 \text{fl} - S A_n \text{Pn} (0 \text{ Qn} (\text{fr}) - \sum_{\ll-i}^{\infty} B_m \text{Pm}^{(1)} (') \text{Qm}^{(1)} (*)) \right] \\ * = \int_{\cdot \wedge} \text{Ur}^2 \int_{L \ll c} \text{J C}_n \text{Pn} (0 \text{ Pn} 0 \gg) + \int_{\ll-i} ? \text{D}_m \text{Pm}^{(1)} (0 \text{ Pm}^{(1)} \text{fr}) \int_{\text{J}} \end{cases} \quad (4.4)$$

By a procedure similar to that used in the preceding section, we find the solution to be

$$\psi_e = \frac{1}{2} \text{Uc}^{\text{al}} (\text{T}^* + 1) (1 - \text{i}^*) [1 - \text{iAQO} (\text{IT}) - \text{iB} (3\text{t}^2 - 1) \text{Q}_2 (\text{ft}) - \text{iCQx}''' (\text{IT}) - \text{iD} (5/2 - 1) \text{Q}_8^{(1)} (\text{ft})] \quad (4.5 \text{ a})$$

and

$$\psi_i = \text{JUc}^{\text{a}} (\text{T}^* + 1) (1 - \text{i}^2) [\text{E} - \text{F} (\text{T}^2 - \text{t}^*) - \text{G}\tau^2 \text{t}^{\text{a}}] \quad (4.5 \text{ b})$$

where

$$\text{A} = \frac{[6 - 4\text{G}(\text{V} + 1)]}{\Delta} \quad (4.6 \text{ a})$$

$$\text{B} = \frac{[10\text{G}(\text{T}_0^2 \text{r} \text{DQ} \cdot 0 \gg)]}{\Delta} \quad (4.6 \text{ b})$$

$$\text{C} = \frac{[3 - 3\text{AiQ} (\text{IT}) - 2\text{DiQ} \gg (\text{iV}_0) - 2\text{G} (3\text{T} \ll + 2) (\text{T}_0^2 + 1)]}{\Delta} \quad (4.6 \text{ c})$$

$$\text{D} = \frac{\text{G} (\text{V} + 1) [2\text{V}_n \text{Q} (\text{ITQ}) - \text{Q}_1 (\text{i}\tau_0)]}{\Delta'} \quad (4.6 \text{ d})$$

$$\text{E} = \text{G} (2\tau_0^{\text{a}} + 1)^{\text{a}} \quad (4.6 \text{ e})$$

$$\text{F} = \text{G} (2\text{T}_0 \gg + 1) \quad (4.6 \text{ f})$$

$$\text{A} = 3 [\text{T}_0 - (\text{r} \ll - 1) \text{iQ}_0 (\text{V}_0)] \quad (4.6 \text{ g})$$

and

$$\text{A}' = 6\text{KU} \gg (\text{IT}) \text{Q} (\text{V}_0) - \langle \text{Qi} (\text{iV}_0) 0, 0 \rangle (\text{V}_0). \quad (4.6 \text{ h})$$

The velocity components can be determined by

$$\text{ft} = \frac{\text{U}}{\sqrt{(\tau^{\text{a}} + \tau^{\text{a}}) (\tau^{\text{a}} + 1)}} \frac{\text{U}}{\partial \text{t}} \quad (4.7 \text{ a})$$

$$q_2 = \frac{-\dot{r}}{c^2 \sqrt{(\tau^2 + t^2)} (1 - t^2)} \quad (4.76)$$

and so the normal velocity at the surface is given by

$$(\dot{r})_{r=T} = 2GU (T_0^* + 1)^{3/2} (T_0^2 + t_0^2)^{-1/2} \quad (4.7 c)$$

The pressure is then determined by the equations

$$\frac{1}{c} \frac{dp}{d\tau} = \frac{-p}{c(\tau^2 + 1)} \frac{\partial L_{-1} \psi}{\partial t}, \quad \frac{\partial p}{\partial t} = \frac{\mu}{c(1 - t^2)} \frac{\partial L_{-1} \psi}{\partial \tau}, \quad (4.8 a)$$

where

$$L_{-1} \psi = \int \left[\frac{1}{\tau^2 + 1} + (1 - t^2) \right] dt \quad (4.86)$$

Thus we have the following formula for the pressure

$$Pe = \int \left[-6BQ_X (fr) - \frac{1}{T} \frac{A}{F} \right] + \text{const}, \quad (4.9 a)$$

$$Pi = -4G(5r_0^2 + 3) \frac{1}{c} \frac{A}{F} + \text{const}. \quad (4.9 b)$$

The jump ΔP in the pressure at the surface is then

$$\Delta P = \frac{1}{c} \left[-6BQ_X (fr) - \frac{1}{T} \frac{A}{F} \right] \quad (4.10 a)$$

where

$$a = -6BQ_X (iV_0) + 4G (5r_0^* + 3) T_0 \quad (4.10 b)$$

and

$$fi = ar_0^2 - 2B - A. \quad (4.10 c)$$

For physically possible flows we must have $G > 0$ and $j\delta + a^{*2} < 0$ for all t ($-1 < t < 1$). It is easy to prove that $a > 0$ when $G \geq 0$. Hence, we must have $a + J\delta < 0$ when $G \geq 0$. Thus we have

$$0 < G < G_0 \quad (4.11 a)$$

where

$$G_0 = \frac{3A'}{2(T_0^* + 1) [-5Q_X (iV_0) \{3(r_0^* + 1) Q_X (t_0^*) + 1\} \Delta + A' \{(r_0^* + 1) + A^0 (5T_0^* + 3)\}]} \quad (4.11 b)$$

which (on) expansion in terms of $1/s_0$ is representable as

$$G = \frac{\frac{1}{s_0^4} \left(\frac{2}{7} + \frac{1}{3} \frac{1}{s_0^2} + \dots \right)}{7\pi - 15\pi + \dots} \quad (4.11 c)$$

The drag D on the spheroid is given by

$$D = 2^*c^* (r_0^2 + 1)^* \cdot \{ (T^e_{\xi\xi} - T^i_{\xi\xi})_{r_0} \cdot \sqrt{\tau_0^2 + 1} - (T^\wedge - T^i_{\xi\xi})_{r_0} V_{R=\wedge^2} \} * \quad (4.12 a)$$

and we see that

$$D = 4\pi U c A. \quad (4.12 \quad A)$$

As in the preceding section, from these results again we can recover the results corresponding to a sphere by a limiting process.

S. CIRCULAR DISC

As $T_0 \rightarrow 0$, the oblate spheroid degenerates to a circular disc of radius c facing the flow normally. In this case, the following results can readily be obtained from those of oblate spheroid by letting $T_0 \rightarrow 0$. The stream function reduces to

$$\begin{aligned} \psi = & U c^2 (\tau^2 + 1) (1 - \tau^2) \left[1 - \frac{2}{\pi} \left(\cot^{-1} \tau + \frac{\tau}{\tau^2 + 1} \right) \right. \\ & + \frac{2G}{\pi} \left\{ ((1 - \tau^2) \cot^{-1} \tau + \tau) + \tau^2 \left((1 - 3\tau^2) \cot^{-1} \tau + 3\tau \right. \right. \\ & \left. \left. - \frac{2\tau}{1 + \tau^2} \right) \right\} \left. \right] \quad (5.1) \end{aligned}$$

for the whole space of flow. The limits of the porosity parameter are given by

$$0 < G < \frac{1}{2} \quad (5.2)$$

and the drag is given by

$$D = \frac{16}{j} \wedge U c (3 - 2G). \quad (5.3)$$

REFERENCES

1. Berman, A. S. .. *J. Appl. Phys.*, 1953, 24, 1232-35.
2. Sellers, J. R. .. *Ibid.*, 1955, 26, 48*-90.
3. Yuan, S. W. .. *Ibid.*, 1956, 27, 267-69.
4. Berman, A. S. .. *Ibid.*, 1958, 29, 71-75.
5. Leonov, A. I. .. *(P.M.M.) J. Applied Mathematics and Mechanics*, 1962, 26, 564-66; *Ibid.*, 1962, 26, 842-47.
6. Payne, L.E. and Pell, W.H. .. *J. FL Mech.*, 1960, 7, 52[^]-49.
7. Hobson, E.W. .. *The Theory of Spherical and Ellipsoidal Harmonics*, Cambridge University Press, 1931.

RELATIVISTIC ESTIMATES OF X-RAY K-LINE INTENSITY RATIOS: CALCULATIONS INCLUDING RETARDATION AND SCREENINGS

BY T. V. KRISHNAN

{Spectroscopy Division, Bhabha Atomic Research Centre, Trombay, Bombay}

AND

AMAR NATH NIGAM

(Physics Department, H.B. Technological Institute, Kanpur)

Received April 16, 1969

(Communicated by Dr. R. K. Asundi, F.A.S.C.)

ABSTRACT

X-ray K-line intensity ratios a_2/a_1 , p_{jfa} and j_{3l}^B/V have been calculated following the method due to Payne which accounts for the retardations. In addition screening has been included. It is found that a-line intensity ratios are given best by Sommerfeld screening but that Slater screening is better for the M-lines. Field theoretically corrected energies have also been used and it is found that the agreement is less favourable. The necessity of including the potentials corresponding to these effects as perturbations to the wavefunctions has been pointed out.

INTRODUCTION

It is well known in X-ray spectra that the intensity ratios K_{a_2}/K_{a_1} and K_{β_3}/K_{β_1} are both equal to 0.5. This is a characteristic associated with all the spin relativity doublets since the value 0.5 is found to be independent of Z the atomic number except in case of low Z elements where the L and the M levels are influenced by the chemical effects and by solid state properties. Since this value agrees well with the non-relativistic estimates of the intensity ratios, its validity remained unquestioned till the experiments done with the heavy elements ($Z = 75$ and above) revealed distinct departures. These accurate measurements were made by Beckman.¹ Since the inner levels of the heavy elements hardly show any response to the chemical bond effects one presumes that these levels retain their atomic character even in the metallic state of these elements; the K and the L levels in uranium,

$$\begin{aligned} & \times \left(\frac{2Zr}{Na_0}\right)^{\gamma-1} \times \left[n'F\left(-n'+1, 2\gamma+1, \frac{2Zr}{Na_0}\right) + (N-x) \right. \\ & \left. \times F\left(-n', 2\gamma+1, \frac{2Zr}{Na_0}\right) \right] \\ g = & \frac{Vr(2\gamma+M-+1)}{T(2\gamma+1) V^{*!}} \cdot \frac{1+\epsilon}{V4N(N-*)} \cdot \frac{jZ}{iW} \cdot e^{-Zr'Na_0} \cdot \left(\frac{2Zr}{Na_0}\right)^{\gamma-1} \\ & \times \left[-n'F\left(-n'+1, 2\gamma+1, \frac{2Zr}{Na_0}\right) + (N-x) \right. \\ & \left. \times F\left(-n', 2\gamma+1, \frac{2Zr}{Na_0}\right) \right] \end{aligned}$$

(Signs of / and g as used by Payne)

(Eqn. 14.37 of Bethe and Salpeter⁶)

$$\frac{1}{V^{*+}(n'+r)^*}$$

(Eqn. 14.29 of reference 6)

where / and g are the two component Dirac wavefunctions as given by Bethe and Salpeter,⁶ f_{ab} is the oscillator strength and ε is the energy of the emitted photon. The photon wavenumber k in units of af^l is 137.0 times the energy differences of the quantum states in me² units. The intensity is given by

$$I_{lab} = \frac{2e^2h}{k^3 S} \langle \rangle^* abfab \tag{2}$$

where ω_{ab} is the angular frequency of the emitted line.

All the calculations were done with a CDC 3600 computer. Our results for zero screening agree with those of Payne.

Tables I, II and III contain the results for K_{atil} (K — L_{n,ni}), K_{jstl} (K — M_{n,ni}) and K_{p,^{11*1}} (K — N_{n,in}) lines respectively. Calculations were done for the three cases, viz., a = 0, a = a_x of Sommerfeld and o—s of Slater.

TABLE I

Oscillator strengths and intensity ratios for K-Hines (with Dirac energies)

Z	Oscillator strengths						$I_{J\&S}/I_{\text{K}\alpha 1}$		
	$K_{\alpha 1}$			$K_{\alpha 2}$...	$\sigma = \sigma_1$ (Somm.)	a-S (Slater)
	a=0	$\sigma = \sigma_1$ (Somm.)	$\sigma = S$ (Slater)	a=0	$\sigma = \sigma_1$ (Somm.)	$\sigma = S$ (Slater)			
70	•2121	•1011	•1837	•1149	•0540	•0999	•5030	•5321	•5136
71	•2102	•1007	•1824	•1145	•0549	•0997	•5056	•5339	•5154
72	•2082	•1003	•1810	•1141	•0540	•0995	•5075	•5358	•5173
73	•2062	•0998	•1705	•1137	•0548	•0993	•5004	•5378	•5104
74	•2042	•0993	•1780	•1133	•0548	•0991	•5115	•5398	•5216
75	•2021	•0987	•1765	•1130	•0548	•0990	•5137	•5421	•5239
76	•2001	•0981	•1750	•1126	•0547	•0988	•5161	•5444	•5263
77	•1080	•0975	•1734	•1123	•0547	•0986	•5185	•5468	•5289
78	•1957	•0974	•1718	•1119	•0540	•0984	•5211	•5492	•5317
70	•1937	•0961	•1701	•1116	•0546	•0082	•5239	•5521	•5346
80	•1916	•0955	•1684	•1113	•0545	•0980	•5267	•5550	•5376
81	•1894	•0047	•1667	•1110	•0544	-0979	•5298	•5580	•5408
82	•1872	•0945	•1650	•1107	•0546	•0977	•5329	•5609	•5441
83	•1850	•0963	•1633	•1104	•0560	•0975	•5362	•5631	•5476
84	•1828	•0923	•1615	•1101	•0541	•0973	•5396	•5678	•5512
85	•1806	•0915	•1597	•1098	•0540	•0972	•5432	•5714	•5550
80	•1783	•0906	•1578	•1095	•0530	•0970	•5469	•5752	•5589
87	•1760	•0897	•1560	•1092	•0538	•0068	•5507	•5791	•5630
88	•1737	•0888	•1541	•1089	•0537	•0967	•5547	•5832	•5672
89	•1714	•0879	•1522	•1086	•0536	•0965	•5588	•5875	•5716
00	•1691	•OSGO	•1503	•1083	•0535	•0063	•5630	•5920	•5761
01	*1668	•0860	•148*5	•1081	•0533	•0961	•5674	•5966	•5808
02	•1644	0850	•1463	•1078	•0533	•0959	•5718	•6014	•5856

TABLE II

Oscillator strengths and intensity ratios for K β -lines (with Dirac energies)

Z	Oscillator strengths						I K ^α /I K _{βi}		
	K _{β₁}			K _{β₂}			...	σ=σ ₁ (Somm.)	σ=S (Slater)
	o=0	σ=σ ₁ (Somm.)	σ=S (Slater)	a>>0	σ=σ ₁ (Somm.)	σ=S (Slater)			
70	•0431	•0085	•0301	•0198	•0046	•0151	•4500	•5458	•4978
71	•0428	•0084	•0300	•0197	•0046	•0151	•4504	•5477	•4987
72	•0425	•0084	•0299	•0195	•0046	•0151	•4508	•5498	•4997
73	•0422	•0083	•0298	•0194	•0046	•0151	•4513	•5519	•5009
74	•0419	•0083	•0296	•0193	•0046	•0150	•4520	•5542	•5021
75	•0416	•0083	•0295	•0192	•0046	•0150	•4527	•5563	•5035
76	•0412	•0084	•0294	•0191	•0047	•0150	•4535	•5585	•5050
77	•0409	•0084	•0292	•0100	•0047	•0150	•4544	•5608	•5066
78	•0406	•0084	•0291	•0189	•0047	•0150	•4555	•5632	•5084
79	•0402	•0084	•0289	•0188	•0048	•0149	•4566	•5657	•5102
60	•0399	•0085	•0287	•0187	•0048	•0149	•4578	•5684	•5122
81	•0395	•0085	•0286	•0186	•0048	•0149	•4591	•5712	•5144
82	•0392	•0085	•0284	•0185	•0049	•0149	•4605	•5741	•516f>
83	•0388	•0085	•0282	•0184	-0049	•0148	•46L9	•5772	•5190
84	•0385	•0084	•0280	•0183	•0049	•0146	•4635	•5804	•5216
85	•0381	•0084	•0278	•0182	•0049	•0148	•4651	•5837	•5242
86	•0377	•0084	•0276	•0181	•0050 ^N	•0148	•4668	•5872	•5270
87	•0374	•0084	•0273	•0180	•0050	•0147	•4685	•5909	•5299
88	•0370	•0084	•0271	•0180	•0050	•0147	•4703	•5947	•5330
89	•0366	•0083	•0269	•0179	•0050	•0147	•4722	•5987	•5362
90	•0363	•0083	•0266	•0178	•0050	•0146	•4741	•6023	•5395
91	•0359	•0082	•0264	•0177	•0050	•0146	•4760	•6072	•5429
92	•035*	•0082	•0261	•0176	•0050	•0146	•4779	•6117	•5464

TABLE III

Oscillator strengths and intensity ratios for $K\beta_{2,1}^{II}$ -Hnes (with Dirctc energies)

2	Oscillator strengths						$I K\beta_{2,1}^{II} / I K\beta_{2,1}^I$		
	$K\beta_{2,1}^I$			$K\beta_{2,1}^{II}$			$\langle r=0$	$_{OSSQ_1}$ (Somm.)	$\langle r=S$ (Slater)
	a=0	$a=O_i$ (Somm.)	$\sigma=S$ (Slater)	$\langle r=0$	$\sigma=\sigma_x$ (Somm.)	$\langle T=S$ (Slater)			
70	•0160	•000436	•004887	•0070	•000247	•00265	•4307	•5655	•5418
71	•0159	•000464	•004954	•0069	•000263	•00269	•4305	•5675	•5432
72	•0158	•000431	•005017	•0069	•000246	•00274	•4305	•5704	•5447
73	•0167	•000424	•005075	•0063	•000243	•00278	•4305	•5730	•5463
74	-0156	•000425	•005128	•0068	-000245	•00281	•4307	•5756	•5481
75	•0155	•000445	•005177	•0067	•000257	•00285	•4309	•6780	•5490
76	•0154	•000464	•005220	•0067	•000269	•00289	•4312	-5805	•6519
77	•0152	•000483	•005259	•0066	•000281	•00292	•4316	-5831	•5540
78	•0151	•000601	•005294	•0066	•000293	•00295	4321	•5858	•5562
79	•0150	•000518	•005324	•0066	•000306	•00298	•4327	•5886	•5585
80	•0149	•000535	•005350	•0065	•000317	•00301	•4333	•6916	•5611
81	•0148	•000551	•005372	•0065	•000328	•00303	•4341	•6946	•6637
82	•0146	•000567	•005389	•0064	•000339	•00306	•4349	•5977	•5665
83	•0145	•000581	•005403	•0064	•000349	•00308	•4368	•6010	•5695
84	•0144	•000595	•005413	•0064	•000360	•00311	•4367	•6044	•6726
85	-0143	•000608	•005418	•0063	•000370	•00313	•4377	•6080	•5758
86	•0141	•000620	•005420	•0063	•000380	•00315	•4387	•6117	•5793
87	•0140	•000632	•005419	•0062	•000389	•00317	•4398	•6155	•5829
88	•0139	•000642	•005414	-0062	•000398	-00318	•4409	•6195	•5867
89	•0138	•000652	•005405	•0062	•000407	•00320	•4420	•6337	•5906
90	•0136	•000661	•005393	•0061	•000415	•00322	•4431	•6280	•5947
91	•0135	•000669	•005375	•0061	•000423	•00323	-4442	•6325	•5991
92	•0134	•000676	•005360	•0060	•000431	00324	•4453	•6371	•6035

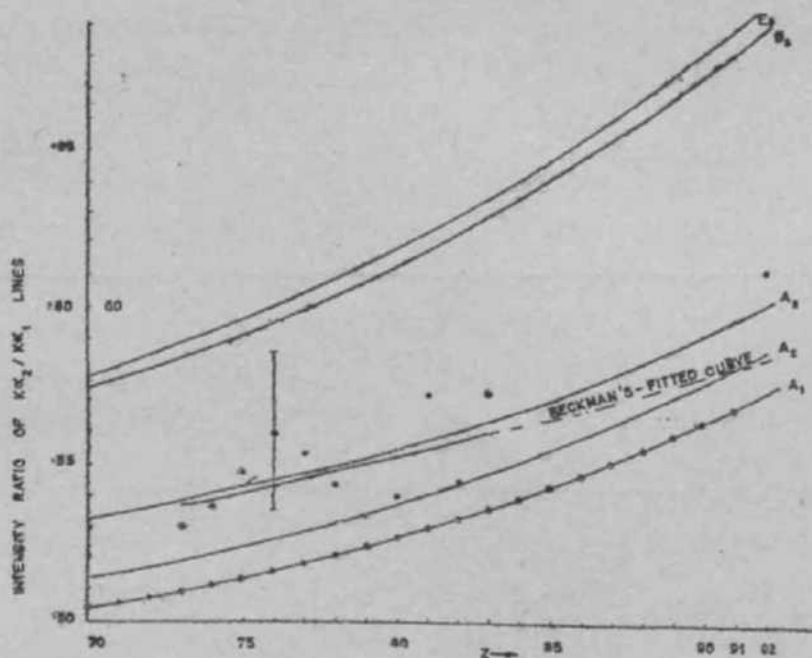
TABLE IV

No.	Energy used in	Energy-used in	Screening in Z in wavefunction	Remarks		
				Kat,2	$K_{\beta 1,s}$	$K_{\beta 2}^I, K_{\beta 2}^{II}$
A ₁ A ₂ A ₈	Dirac, $\langle r=0$ Slat. Somm	Dirac, $\langle r=0$ „ $\langle r=S$ Slat. „ $c=ff_i$ Somm.	$\langle r=0$ $\langle r=S$ Slat. $\langle r=\langle T_i$ Somm.	Curve A ₁ (Fig. 1a »i A _j , „ » A ₃ , „	Curve A _n Fig. 2 „ A ₂₁ „ » A ₃ , „	Curve A _x , Fig. 3 „ A ₂ , „ f _l / f ₀ range •566-637
B ₁ B ₂ B ₈	Dirac Using $\langle T_x$ and $\langle S_x$ of Sommerfeld	Dirac with 0% of Sommerfeld	$\langle r=\langle S$ Slat. $cr = C \setminus$ Somm.	* a _s / a _i ranges between 0*24-0*31 from 0-29-0*36 Curve B ₃ in Fig. 1a	• I ^{^s} /I ^{^i} -046-08 * „ -117-167 * „ -645-807	* -0015-0014 * -037 -070 Curve B _j in Fig 3
C ₁ C ₂ C _a	Dirac with 0% and $\langle r_3$ Field theo. corrections	Dirac with * _{li} c _x of Sommerfeld	o= $\langle S$ Slat. 0= $\langle T_x$ Somm.	* c _u / a _i fangs 0*24-0*31 * „ 0*29-0*36 Results coincide with B ₃ in Fig. 1 a	* I ^{^s} /I ^{^i} -04&-077 * „ -117-166 * „ -644-801	* -0015-0014 * -036 --069 Curve C ₃ in Fig. 3
J _h D ₂ D ₈	Field theo. corrections	Dirac, $\langle r\ll 0$ „ $\langle r=S$ Slat. „ $\int ff=ff_i$ Somm*	$\langle r=0$ $cr=S$ Slat. $\langle r=\langle T_2$ Somm.	Curves D _j . D _c , D ₃ shown in Fig. 1 b	Curve D _i „ D ₂ in Fig 2 „ D ₃	* -421 -*429 D _i in Fig. 3 * *57 -65
E ₁ E* E ₈	Field theo. correctors	Dirac with $\langle n$ and a 2 +fieU theo. corrections*	(T=0 $\langle r=S$ Slat. $\langle r=\langle T_i$ Somm.	* W a _i range 0*24-0*30 * I _{a2} 0-2B-0-37 Curve E ₃ in Fig. 1a	* p _a / p _i -047-80 * „ -110—170 * „ -eco-sls	* -0015--0016 * -037 —072 * *46 -59

DISCUSSION

The results of Tables I, II and III are shown graphically in Figs. 1, 2 and 3. The curves for $a = 0$ correspond to Payne's results. The following observations can be made from the curves:

The $K\alpha$ lines.—The calculated ratio I_{a-j}/I_{aj} increases (Fig. 1 *a*) with Z though the individual oscillator strengths decrease. As screening increases the curves are raised up with *Sommerfeld screening giving the best fit with the experimental points (shown by the solid dots)*. As shown in the figure the experimental values contain rather large errors.* The experimental accuracy should be increased tenfold in order to ascertain deviations from the best theoretical curve mentioned above. Such deviations will not be surprising at all because we have not taken into account various field theoretical effects. We now discuss the effect of using various theoretical energies.!

FIG. 1 *a*

In equation (2) the energy term \ll^* occurs outside the integration sign. The wavefunctions contain the energy term in the parameter e . In the calculations mentioned above Dirac energies without screening have been

* Vertical error bar at $Z = 76$ in Fig. 1 *a* shows the error of measurement.

† Effect of using the experimental energies in w above has been discussed by Payne *et al.*

used, and only the Z in the wavefunctions has been modified by including screening. Thus the energies used do not correspond exactly to the wavefunctions. If one uses Dirac energies with screening, both in σ and ϵ , Curve B_3 (Fig. 1 *a*) is obtained which shows that the agreement is worsened. On including the field theoretical effects in the σ energies Curve E_3 is obtained. However, if only σ is modified by using Dirac energies with screening and field theoretical effects but ϵ contains as before Dirac energies without any field theoretical corrections, curves shown in Fig. 1 *b* are obtained. These have been calculated for various screenings in Z in the wavefunction, they lie below the experimental points but are certainly above the Curve A_x of Fig. 1 *a*. It may be noted that the differences between the Curve A_3 of Fig. 1 *a* and $D_{1f,2}$ of Fig. 1 *b* are greater than 1%, which according to reference (4) is the limit of accuracy if one works in the hydrogenic approximation.

We thus conclude that although the energies corrected for various field theoretical effects give a better agreement with the *observed energies* of the lines^{7,9} their use in intensity estimates [*i.e.*, in Eqn. (2)] worsens the agreement with the experimental intensity ratios. That the field theoretical effects markedly influence the intensity estimates goes against the conventional belief that their effect might be too small to be noticeable. The reason for the worsening of the agreement mentioned above is obvious; the Lamb shift and vacuum polarisation, etc., correspond to certain potential (e.g., Welton potential) which in principle should perturb the usual wavefunctions. A possibility therefore exists that the perturbed wavefunctions might well give a better result, but the use of field theoretically corrected energies and unperturbed wavefunctions is certainly erroneous, though it gives a better result than the calculations done without screening. This qualitatively explains the observation of Payne *et al* that if one used experimental energies in Eqn. (2), one gets closer to the experimental points (*i.e.*, there is an improvement on the Curve K_x of Fig. 1 *a*).

The K β lines.—Here again the ratio $I_{h\beta}/I_{K\alpha}$ increases with Z and the individual oscillator strengths decrease. The same holds for W_{VI}/V . However, for all the Mines Slater screening (instead of Sommerfeld screening) gives a closer fit with the experimental results. This is clear from Fig. 2 for $p_{u,3}$ and from Fig. 3 for $p_{2,1}$ $j_{8,2}^n$ lines where the Curve A_2 represents the case $a = 0$, A_2 corresponds to $\sigma = S$ (Slater) while A_3 refers, the results

{Calculations in this direction are in progress.

obtained by using $a = a_x$ (Sommerfeld). The experimental data for β_2^1 , p_2^n lines are not available. For $\&, _3$, A_2 curve gives the best fit. The D curves again correspond to the case when field theoretical corrected energies are used only in w in Eqn. (2).

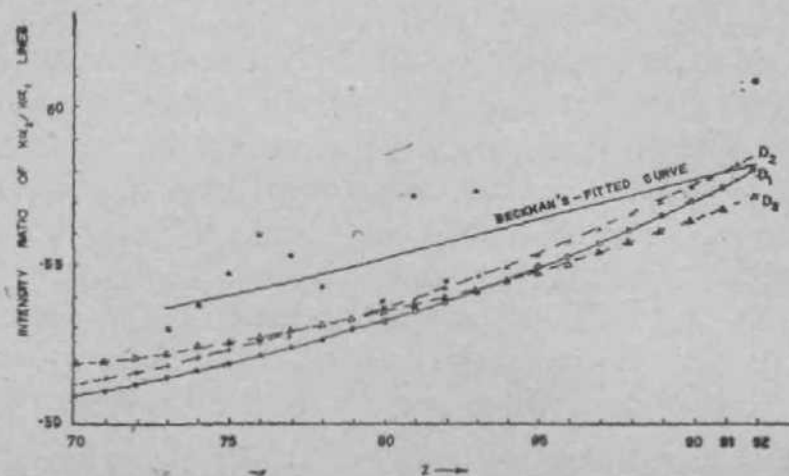


FIG. 1 b

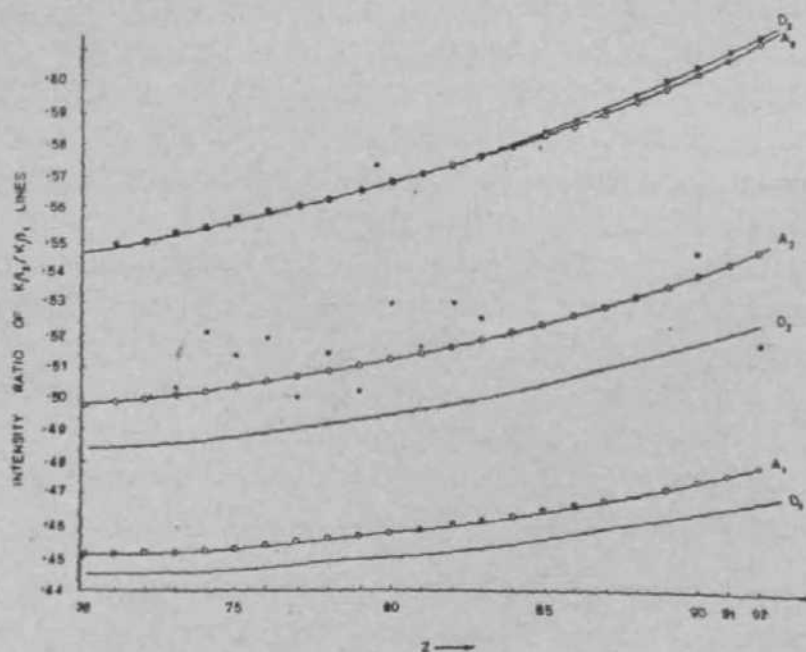


FIG. .

The suffixes I, 2, 3 refer to $cr = 0$, $u = S$ (Slater) and $a = a_i$ (Sommerfeld) respectively applied to 2 in the wavefunction. D_2 is nearest to the observed values; again Slater screening gives the best fit. We note here again that these curves correspond to ϵ containing Dirac energies without

field theoretical corrections. As soon as these corrections are applied to the agreement worsens (we have not shown the curves). The range of the intensity ratios is given in the tabular description that follows. We show B and C curves for $j_{3/2}$ lines whose detailed specifications are described below. Cases marked * have not been shown in the figures since these values are absurd. Tables 1, II, III refer to A_1 , A_2 , A_3 curves in each case.

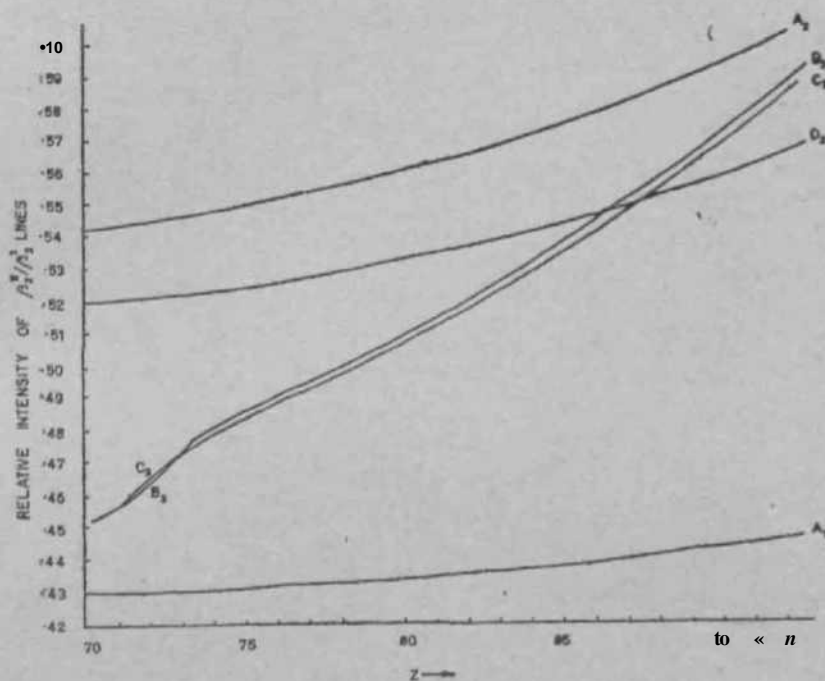


Fig. 3

ACKNOWLEDGEMENTS

The authors thank Dr. W. B. Payne for a copy of his thesis which was quite helpful in carrying out the calculations. Thanks are also due to Prof. R. L. Shacklett for his comments on the preprint of this paper. The authors are thankful to Prof. R. K. Asundi and Dr. N. A. Narasimham for their kind encouragement and keen interest in our work.

REFERENCES

1. Beckman, O. *Arkiv för Fysik*, 1955, 9, 495.
2. Massay, H. S. W. and Burhop, E. H. S. *Proc. Camb. Phil. Soc.*, 1936, 32, 461.
3. Payne, W. B. and Levinger, J. S. *Phy. Rev.*, 1956, 101, 1020.

4. Taylor, G. R. and Payne, W. B. *Ibid.*, 1960, 118, 1549.
5. Payne, W. B. .. Dissertation, Louisiana State University, 1955 (unpublished).
6. Bethe, H. A. and Salpeter, E. E. *Handbuch der Physik*, Springer Verlag, Berlin, 1957, 35.
7. Shacklett, R. L. and DuMond, J. W. M. *Phy. Rev.*, 1957, 166, 501, for $L_{IP\ m}$ -levels.
8. Krishnan, T. V. and Nigam, A.N. *Proc. Ind. Acad. Sci.*, 1964, 60, 75, for $L_{, n}$ -levels.
9. Brenner, S. and Brown, G. E. *Proc. Roy. Soc. (Lond.)* 1953, 218 A, 422, for K-level.

COSMIC RAY NUCLEI OF CHARGE $Z > 3$ DURING THE PERIOD OF LOW SOLAR ACTIVITY

BY K. C. ANAND, S. BISWAS, P. J. LAVAKARE, S. RAMADURAI AND
N. SREENIVASAN *

{Tata Institute of Fundamental Research, Bombay}

AND

V. S. BHATIA, V. S. CHOCHAN AND S. D. PABBI

[Department of Physics, University of Panjab, Chandigarh]

Received April 28, 1969

(Communicated by Prof. R. R. Daniel, F.A.S.C.)

ABSTRACT

A detailed study of the composition and energy spectra of heavy nuclei of charge $Z \geq 3$ in the primary cosmic rays has been made during the period of low solar activity, using two stacks of nuclear emulsions exposed in balloon flights from Fort Churchill, Canada, in June 1963. Each of the stacks was composed of 120 nuclear emulsions of three different sensitivities and was exposed at about 3-5 g. cm² of residual air for about 11.1 hr. Reliable resolution of charges of nuclei from lithium to oxygen was obtained; for heavier nuclei, charge groups were determined. From the analysis of 793 tracks of nuclei with $Z \geq 3$, results on the following aspects were obtained:

(1) The differential energy spectra of L ($Z = 3-5$), M ($Z = 6-9$) and H ($Z = 10-28$) nuclei were measured in the energy interval 150-600 MeV/nucleon; integral fluxes were obtained for energy > 600 MeV/nucleon;

(2) The energy dependence of the L/M ratio at the top of the atmosphere was determined; the ratios were obtained as 0.45 ± 0.06 and 0.29 ± 0.03 in the energy intervals of 200-575, and > 575 MeV/nucleon respectively;

(3) Relative abundances of individual nuclei of Li, Be, B, C, N and O at the top of the atmosphere were determined as 36, 29, 55, 100, 60 and 106 respectively in the energy interval 150-600 MeV/nucleon; corresponding values were also obtained for energy > 600 MeV/nucleon.

•Present Address: Department of Physics, Hansraj College, New Delhi-7.

(4) The differential fluxes of multiply charged nuclei measured by us and by other investigators were used to determine the solar modulation between solar maximum to solar minimum. It was found that solar modulation of the fluxes of M and He nuclei were consistent with R/J dependence and that the modulation parameter A^* between 1965 and 1957 was about 1.1.

The implications of these results are discussed.

1. INTRODUCTION

It is well known that a detailed study of the primary cosmic ray nuclei in the vicinity of the earth can provide important information in the understanding of the propagation, acceleration and origin of cosmic rays. A number of experiments have been made so far with the object of understanding these aspects of cosmic rays (for summary and references, *see, e.g.*, Webber, 1967; Biswas, 1968). The present investigation was undertaken to study in detail the charge composition, fluxes and energy spectra of the heavy nuclei of charge $Z \geq 3$ and of energy > 200 MeV/nucleon during the period of low solar activity. For this purpose two large stacks of nuclear emulsions were exposed to cosmic rays in two high altitude balloon flights from Fort Churchill, Canada, in June 1963.

The two emulsion stacks were flown to altitudes of 3 to 4 g. cm² of residual atmosphere, so that the correction for the loss by fragmentation of nuclei in the overlying atmosphere was rather small. Nuclear emulsions of varying sensitivities such as Ilford G-5, G-2 and G-0 were used for resolving individual charges of $Z = 3$ to 8 and for charge groups of higher charges. In addition, the present analysis is based on a fairly large sample of 793 nuclei of charge $Z > 3$ so that statistically meaningful results were obtained.

In the present paper we discuss first the experimental procedure for determining the charge and energy of heavy nuclei and then obtain the relative abundances, fluxes and the energy spectra of these nuclei (or groups of nuclei) incident at the top of the atmosphere. The energy spectra measured in this experiment were used together with those of other investigators to study the solar modulation of the fluxes of multiply charged nuclei from solar maximum (1957) to solar minimum (1965). The implications of some of these results are discussed.

A brief report of the experimental results of this investigation was published earlier in the form of a letter (Anand *et al.*, 1966).

2. EXPERIMENTAL PROCEDURE

Emulsion stack and flight details.—Two identical nuclear emulsion stacks were exposed on two balloon flights from Fort Churchill, Canada (geomagnetic latitude 73.5° N). The first stack (Stack A) was exposed on 15th June 1963 for 11.2 hr. at a ceiling altitude of 3.1 g. cm.^{-2} while the second (Stack B) was exposed on 18th June 1963 for 11.1 hr. at an altitude of 4.3 g. cm.^{-2} . The flight curves for the two exposures are shown in Fig. 1. The amount of packing material above the Stacks A and B was negligibly small and consisted of styrofoam and black tape. During the balloon flights, the plane of the emulsions in each case was kept horizontal until the balloon reached ceiling altitude and was then flipped through 90° so that it became vertical.

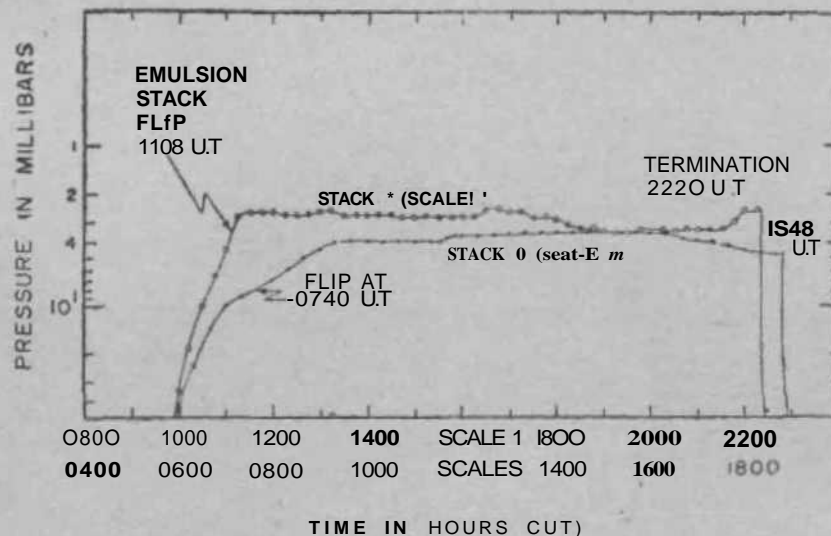


FIG. 1. Time-altitude curves of Stack A and Stack B in balloon flights on June 15, 1963 and June 18, 1963 respectively.

Each stack consisted of 120 ilford nuclear emulsion pellicles each of size $10 \times 20 \times 0.06 \text{ cm}$. At ceiling altitude the 10 cm . side was vertical. The central 90 emulsions consisted of most sensitive (G-5) and less sensitive **emulsions** (G-2 and G-0) arranged in a sequence G-5, G-2, G-5, G-2, G-5, G-0 which was repeated 15 times. These were flanked by **fifteen** G-5 emulsions on either side. After the exposure, the stacks were processed in the conventional manner. Stack A was analysed by the Bombay group while Stack B was analysed by the Chandigarh group in an identical manner.

Scanning and acceptance criteria.— Only the G-5 emulsions from the middle portion of the stack were **scanned** systematically. Using a total

magnification of 15×10 , a line scan was made along the 20 cm. side at a distance of 5 mm. below the top edge of the emulsion. Tracks satisfying the following criteria were accepted:

(1) Projected zenith angle $< 45^\circ$; (2) dip angle $< 11-2^\circ$; (3) ionisation > 8 times that of a singly charged minimum ionising particle; and (4) enter the stack from the top edge.

All particle tracks satisfying the above criteria were then followed into the stack until the particles either came to rest, interacted, or left the stack. In order to make suitable measurements on the interacting particles, it was necessary to impose additional condition for their acceptance, namely, the interacting particle tracks should have a length of at least 5 cm. available in the stack before they produced nuclear interactions.

In order to carefully determine the scanning efficiency of various observers, about 40% of the total scanning was rescanned by different observers. The scanning efficiency was almost 100% for particles of ionisation greater than 16 times minimum and about 90-95% in the case of particles having about 9-16 times minimum ionisation. Appropriate corrections for scanning loss have been very carefully made wherever necessary.

Heavy nuclei of the primary cosmic rays have been classified into the following groups: L-Nuclei, $Z = 3$ to 5 ; M-nuclei, $Z = 6$ to 9 ; H⁺-nuclei, $Z = 10$ to 15 ; H₂-nuclei, $Z = 16$ to 19 ; H₃-nuclei, $Z = 20$ to 28 ; S-nuclei, $Z > 6$; H-nuclei, $Z > 10$.

Charge and Energy Determinations of the Heavy Primaries

The identification of charge and the subsequent energy determination was done by using a combination of the following methods:

- (i) Grain-density *versus* residual range,
- (ii) Change of grain-density with range,
- (iii) Grain-density *versus* multiple coulomb scattering,
- (iv) Delta-ray density *versus* residual range,
- (v) Change of delta-ray density with range, and
- (vi) Delta-ray density *versus* multiple coulomb scattering.

Since these methods are standard ones and are already discussed in literature {e.g., Powell *et al.*, 1959; AizuetaL, 1960), only some details rele-

vant to the present analysis are included here. (For further details, see Sreenivasan, 1967; Bhatia, 1967.)

Grain-density measurements were done mainly in G-2 and G-0 emulsions whereas delta-ray measurements were done only in G-5 emulsions. The delta-ray density method was used only when the tracks did not pass through a G-2 or a G-0 plate or when the grain-density was too high to permit a reliable measurement.

Grain-density calibration.—All measurements of grain-density were restricted to emulsion depths $0.15 Z_0$ — $0.65 Z_0$ from glass (Z_0 is the total thickness of emulsions) where there was no measurable change of sensitivity with depth. The calibration of measured grain-densities in terms of primary ionisation of the particle was made by using particles which were known to be relativistic either from the nature of interactions they produced or from measurements of multiple coulomb scattering. The comparison of these grain-density measurements with those of relativistic nuclei showing charge indicating interactions, e.g., $C^{12} \rightarrow 3a$, $O^{16} \rightarrow 4a$, etc., was used to determine the calibration. In most cases plate calibration could be made by using, on an average, 5 to 6 tracks of relativistic particles in the G-2 and G-0 plates. Typical calibration curves of G-5, G-2 and G-0 emulsions are shown in Fig. 2. It is seen from the figure that ionisations up to about 6 times minimum ionisation could be measured reliably in a normal G-5 emulsion, up to about 150 times in a G-2 and up to about 250 times in a G-0 emulsion. Each observer set up his own calibration curves for each emulsion plate used for ionisation measurement. Thus, we have avoided any uncertainty which might arise due to plate-to-plate variation of grain-density.

Delta-ray density calibration.—The delta-ray density calibration as a function of the ionisation produced by heavy primaries in G-5 emulsions was done by making measurements on relativistic heavy nuclei selected in the same manner as for grain-density calibrations. For relativistic particles of charge Z the delta-ray density w_3 was thus obtained by using the relation, $n\delta = aZ^2 + b$, where a and b are constants over a certain charge interval.

In order to determine the variation of delta-ray density with kinetic energy for a given charge it is necessary to construct calibration curves, using particles of known energy. This is so, because for a given charge, observed variation may differ from the theoretically predicted relation, $n\delta \propto v^2$ where v is the velocity of the particle. Such calibration was done by

measuring $\langle n \rangle$ on the tracks of stopping α -particles at different residual ranges as well as on alpha-particles whose energies were determined from multiple scattering measurements. Thus from the measured variation of $\langle n \rangle$ with kinetic energy for alpha-particles, $w_0 \propto \sqrt{E}$. kinetic energy per nucleon (or residual range) curves for other charges were obtained.

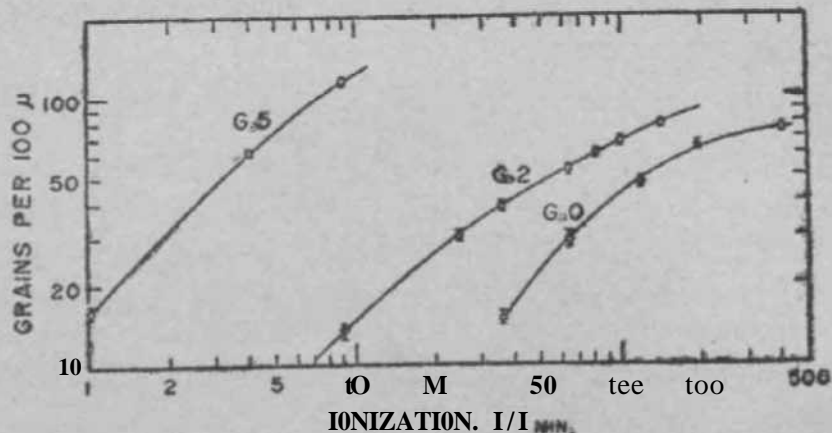


FIG. 2. Calibration curves of grain-density vs. ionisation for some typical G-5, G-2 and G-0 emulsions.

The delta-ray density measurements were made using two conventions, namely, the usual 4-grain delta-ray counting and the long delta-ray" criterion in which only those delta-rays having projected range greater than 5μ were accepted. The latter criterion was used when the delta-ray density was too high for reliable measurements with the 4-grain delta-ray method.

Identification of particles.— From the sample of particles which satisfied the scanning and acceptance criteria, we separated out singly and doubly charged particles by following the tracks into the stack and by using one of the methods of identification as noted above. Particular care was taken to separate out alpha-particles of ionisation 8 to 10 \times I_{min}. from relativistic Li-nuclei. Thus a total of 793 nuclei of charge $Z > 3$ were obtained for further analysis (335 nuclei in Stack A and 458 in Stack B). In order to analyse these multiply charged nuclei we have grouped them into three different categories:

- (a) Stopping particles (S-particles).
- (b) Particles producing interaction after a range of 5 cm. in the stack ('interacting' particles), and
- (c) Particles traversing the entire stack ('through' particles).

The identification of the stopping multiply charged particles was established by using either method (i) or (iv) mentioned earlier. For method (i), we first used the calibration curve of grain-density *vs.* ionisation of the particular emulsion plate (for example, as shown in Fig. 2) and determined the ionisation of the particle. Then the ionisation *vs.* residual range curves for charges $Z = 1$ to 28 were used. These curves were derived from the restricted energy loss *vs.* kinetic energy and the range-energy relation for protons as given by Barkas (1965). For method (iv), w_a *vs.* residual range curves, for different charges, were constructed according to the procedure mentioned above. The charge identification of 'interacting' and 'through' particles was made using one or more of the methods (ii), (iii), (v) and (vi) mentioned above. Among these groups, we had a class of particle tracks which showed large change of ionisation ($\sim 20\%$) in traversing 5 to 10 cm. of emulsions; identification of these nuclei could be easily made using method (ii) or (v). The other class of nuclei were those which showed very little change of ionization in traversing 5 to 10 cm. of emulsion. In these cases it was sometimes found that method (ii) or (v) was unable to identify whether it was a relativistic particle of charge Z or a non-relativistic particle of charge $Z-1$. In all such cases unambiguous identification was made by multiple coulomb scattering measurements [method (iii) or (vi)]. Multiple scattering measurements were made on a Koristka microscope and energies as high as ~ 3 BeV/nucleon could be measured by this method. Fractional charges were assigned, using the methods of ionisation *vs.* residual range, change of ionisation with range or ionisation *vs.* multiple scattering. The charge spectrum for nuclei of $Z = 3$ to 9 and of energy < 575 MeV/nucleon is shown in Fig. 3. In the same figure we have also fitted the expected Gaussian distribution for an experimentally determined standard deviation of 0.25 unit of charge for the Medium nuclei assuming the relative abundances of C, N and O nuclei to be 100, 60 and 106 respectively. Similar fit was made in the case of L-nuclei, with a standard deviation of 0.2 unit of charge and a relative abundance of Li, Be and B as 36, 29 and 50 respectively. Appropriate corrections for extrapolation of the two change groups to the top of the atmosphere have been made. For resolving the component like F which has rather small relative abundance higher degree of charge resolution is necessary.

For nuclei of energy > 575 MeV/nucleon, a large number of particle tracks traverse the stack without significant change of ionisation. In order to obtain reliable identification of these individual nuclei of $Z \geq 10$, two independent measurements of charge were made when necessary. This was

so for roughly 10% in the case of M group and 15% in the case of L group nuclei. Thus the charge of these relativistic or near relativistic nuclei were determined unambiguously and their energy was known to be greater than 575 MeV/nucleon. For these nuclei fractional charge was not assigned as only the lower limit of energy is known.

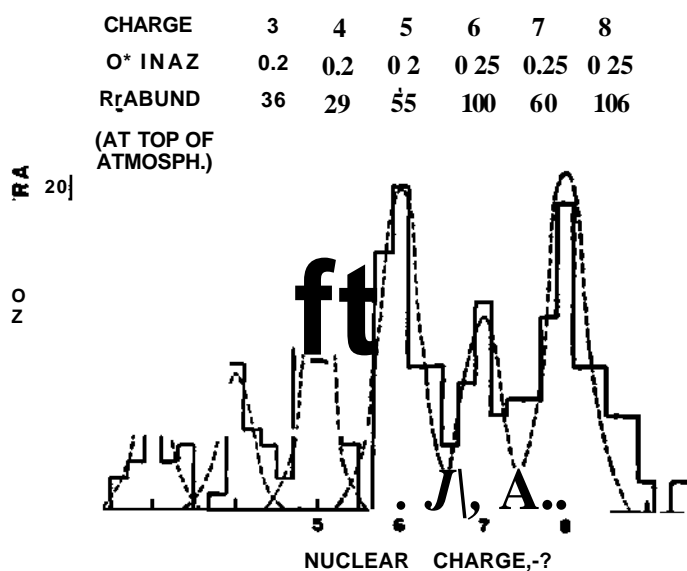


FIG. 3. The measured charge distribution for nuclei of $Z=3$ to 8 of energy 150-600 MeV/nucleon. The measured standard deviations in the charge determination are shown. The dotted lines indicate the normalised gaussian distributions for the measured standard deviations. The relative abundances of these nuclei at the top of the atmosphere are shown (*see text*).

The nuclei with charge $Z > 10$ were assigned charges so that they could be classified into H_{10} , H_2 and H_3 groups of nuclei.

The energies of all the multiply charged stopping particles at the point of entry in the emulsion stack were determined using the range energy relation curves in emulsion (Barkas, 1965). The energies of the interacting particles and the 'through' particles were determined either by the scattering measurement or by using the method of change of ionisation with range. In order to determine the flux values of different groups of nuclei at the top of the stack, each accepted particle of $Z \geq 3$ crossing the scan line was given weight factors to correct for the loss due to interaction in the stack and that due to scanning efficiency. Thus a stopping particle with a residual range $R < 5$ cm. in the stack was given a weight factor $e^{-R/A}$ and those particles having total ranges in the stack greater than 5 cm. were each given a weight factor $e^{-R/A}$ where A is the interaction mean free path in cm. for a particular group of nuclei in the nuclear emulsions. The corrections for

scanning loss were made by using the scanning efficiencies determined for different ionisation groups.

Extrapolation to the top of the atmosphere.—For extrapolating the observed fluxes and energy spectra to the top of the atmosphere it is necessary to take into account certain corrections due to the overlying atmosphere. Firstly, the ionisation loss in the air is taken into account by using range energy relation in air. For our stacks this air-cut-off energy is about 125 MeV/nucleon for L-group nuclei, 150 MeV/nucleon for M-group nuclei and ~ 250 MeV/nucleon for the H-group nuclei. Hence, flux values could be determined only above these air-cut-off energy values. Secondly, as a result of interaction and fragmentation of the cosmic ray nuclei in collision with the air nuclei, there will be a certain amount of diffusion of one group of nuclei into another. This can be corrected either by using the growth curves in air or by solving the one-dimensional diffusion equations (see Daniel and Durgaprasad, 1962). In this work, we adopted the following procedure. We extrapolated the measured flux of M-nuclei at the top of the stack $J_M(x)$ to the top of atmosphere $J_M(0)$, by means of diffusion extrapolation using interaction length of M-nuclei in air as 23.9 g./cm.² (Durgaprasad, 1964), and fragmentation parameter, P_{MM} as 0.14, which is the weighed mean of values for air-like media, graphite, teflon, celluloid and polythene (see Durgaprasad, 1964; Friedlander *et al*, 1963 and references therein). Then the H/M and L/S ratios observed at the flight altitude were extrapolated to the top of the atmosphere using the slopes of the best fitting experimental growth curves of these ratios in air as summarised by Webber (1967). Thus knowing the flux of M-nuclei, L/S and H/M ratios at the top of atmosphere, the fluxes of L, M and H-nuclei at the top of the atmosphere were obtained. The flux of H-nuclei, $J_H(0)$ was further subdivided into those of H_1 , H_2 and H_3 groups according to the following procedure. The fluxes of H_1 , H_2 and H_3 nuclei at the top of the stack were extrapolated to the top of the atmosphere using the diffusion equations and fragmentation parameters (Durgaprasad, 1964). It was found that the fluxes of H_1 , H_2 and H_3 nuclei at the top of atmosphere were in the ratios of 1 : 0.21 : 0.36. The sum of the fluxes of these three groups was normalized to the flux $J_H(0)$. We believe that the above procedure of extrapolation to the top of the atmosphere yields satisfactory results, since this is based on the measured growth curves of the ratios in the atmosphere as well as the best estimates of the fragmentation parameters in air. So far there is no evidence of any significant energy dependence of the interaction and fragmentation parameters in the energy region of relevance here; hence the effect

has been ignored. We wish to emphasise here that since the fluxes were measured under small atmospheric depths, the uncertainties in the parameters used do not significantly affect the extrapolated values. The procedure of extrapolation was carried out separately for groups of nuclei in each stack, there was good agreement between the results obtained from the two stacks. The final results at the top of the atmosphere were then obtained by combining the data from the two stacks according to their statistical weights.

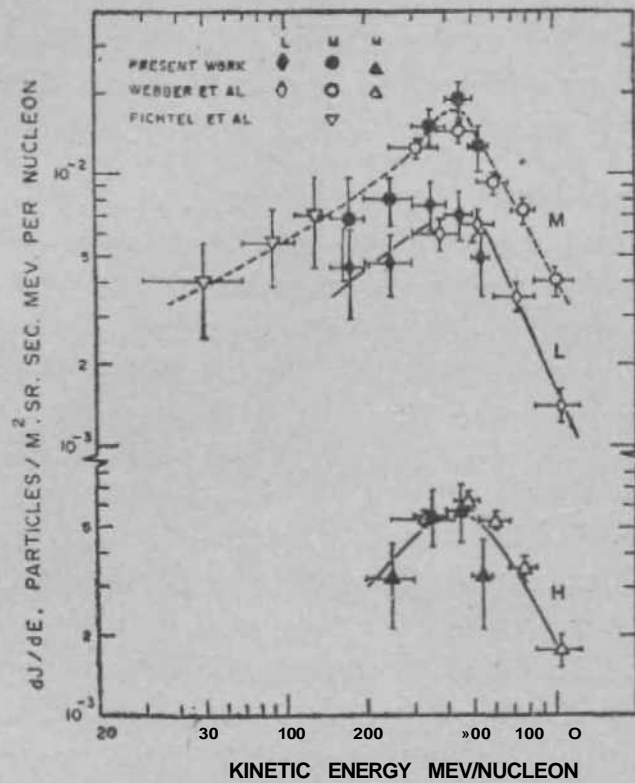
In order to determine the relative abundances of individual elements in a particular charge group we have assumed that while extrapolating to the top of the atmosphere these relative abundances remain the same, since the residual atmosphere is only about 4g./cm.^2 and the differences in the mean free paths are negligibly small. For example, the carbon to oxygen ratio at the top of the atmosphere will be only about 1-5% higher than that measured by us at the flight altitude.

3. RESULTS AND DISCUSSION

Using the above-mentioned methods of charge identification, energy determination and extrapolation to the top of the atmosphere we have obtained the results concerning the differential and integral spectra of L, M and H-nuclei for the period of mid-1963, the energy dependence of the L/M ratio and the relative abundances of individual elements.

Some features of these observations have already been discussed earlier (Anand *et al.*, 1966; Biswas *et al.*, 1966) and in the present analysis we will confine our detailed discussion only to the interpretation of these results in terms of solar modulation.

(i) *Differential energy spectra of light, medium and heavy nuclei.*— The differential and integral energy spectra of L, M and H-nuclei are shown in Fig. 4 and Table I. For comparison we have also included the results of other investigators obtained during the same period of solar activity as indicated by the Mt. Washington Neutron Monitor Rate (2320) (Webber *et al.*, 1966; Fichtel *et al.*, 1966). It is clear from these data that the results obtained by these groups are in good agreement with each other and the mean curve drawn here represents the best shape of the spectra in mid-1963. The maxima in the spectra of L, M and H-nuclei occur at 400 ± 50 MeV/nucleon, 450 ± 50 MeV/nucleon, 450 ± 50 MeV/nucleon respectively. The position of the maximum in the case of helium nuclei occurs at 250 ± 50



RG. 4. Differential energy spectra of L, M and H-nuclei measured in the present work together with other measurements during the middle of 1963. The Mt. Washington neutron monitor rate corresponding to these data are: Present work; 2320 (Stack A, 2330, Stack B, 23JO); Webber *et al.* (1966) 2310; Fichtel *et al.* (1966) 2320.

TABLE T

Differential and Integral fluxes of L, M and H-nuclei at the top of atmosphere

Kinetic energy, MeV/nucleon	Differential flux, dJ/dE , in nuclei (M^2 Sr. Sec. MeV per nucleon) ¹		
	L ($8 < Z < 5$)	M ($6 < Z < 4$)	H ($Z > 10$)
150-200	0.0046 ± 0.0017	0.0089 ± 0.0021	..
200-300	0.0047 ± 0.0012	0.0081 ± 0.0018	0.0032 ± 0.0011
300-400	0.0077 ± 0.0015	0.0162 ± 0.0024	0.0051 ± 0.0013
400-500	0.0071 ± 0.0015	0.0140 ± 0.0029	0.0058 ± 0.0014
500-675	0.0050 ± 0.0015	0.0126 ± 0.0025	0.0033 ± 0.0012
	Integral flux, in nuclei (M^2 Sr. Sec.) ¹		
>160	6.67 ± 0.42	16.39 ± 0.79	..
>200	6.44 ± 0.11	11.04 ± 0.78	8.01 ± 0.48
>300	4.97 ± 0.40	15.21 ± 0.75	$6.6J \pm 0.8$
>400	4.20 ± 0.36	13.71 ± 0.72	5.14 ± 0.44
>575	3.5 ± 0.31	10.88 ± 0.64	4.30 ± 0.41

MeV/nucleon, lower than in the case of L, M and H-nuclei. The implications of these in terms of propagation and solar modulation effects have been discussed by Biswas *et al* (1967, 1968).

Recent experiment by Von Rosenvinge *et al* (1969), performed at a time when the neutron monitor rate (2350) was more or less at the same level shows a large discrepancy as compared to the mean spectra of L and M-nuclei determined in the present experiment. This discrepancy has been discussed by Biswas (1969). The results of Lim and Fukui (1965) which seem to give anomalous flux values have not also been included in the present analysis {see Anand *et al*, 1966}.

(ii) *The energy dependence of L/M ratio.*—The ratios of L/M, L/S and H/M at the top of the atmosphere obtained in our experiment are shown in Table II. It is seen from this table that in the energy interval 200-575 MeV/nucleon the ratio L/M is increasing with decreasing energy. Using the recently determined L/M ratios and energy-dependent spallation cross-sections (Bernas *et al*, 1967; Yiou *et al*, 1967, 1968) the amount of matter traversed in space by cosmic ray nuclei as a function of energy was determined by several investigators {see for summary Biswas, 1968}. These results indicate that at energy greater than 1.5 BeV/nucleon, the mean path length of cosmic ray nuclei is about 4 ± 1 g./cm.² of hydrogen and at 200-400 MeV/nucleon it is higher by a factor of about two.

TABLE II

L/M, L/S and H/M ratios at the top of the atmosphere

K. Energy MeV/n.	200-300	300-400	400-500	500-575	200-575	>575
Ratios						
L/M	0.58±0.19	0.51±0.13	0.37±0.10	0.40±0.14	0.45±0.06	0.20±0.03
L/S	0.42±0.13	0.37±0.09	0.29±0.07	0.31±0.11	0.34±0.05	0.21±0.02
H/M	0.53±0.04	0.40±0.04

(iii) *Relative abundances of individual elements.*—In this work we obtained good charge resolution for nuclei of $Z = 3$ to 8 as described earlier and intensities of Li, Be, B, C, N and O nuclei were determined. These are shown in Table III in two energy intervals, $E = 150-575$ MeV/nucleon

and $E > 575$ MeV/nucleon. The fluorine abundance is an upper limit since it includes the tail of the distribution of the oxygen nuclei and also of Ne.

TABLE III

Fluxes and relative abundances of nuclei as percentage of the total

Nuclei	Kinetic Energy 150-575 MeV/nucleon		Kinetic Energy >575 MeV/nucleon		Kinetic Energy >1.5 BeV/nucleon (O'Dell <i>et al.</i> , 1962)
	P/M ² . Sr. Stc.	Relative abundance	P/M ² . Sr. Sec.	Relative abundance	Relative abundance
Li	0.74±0.15	7.2	1.05±0.19	5.8	5.3
Be	0.60±0*14	5.9	0.41±0.11	2.2	2.3
B	1.14±0.18	11.1	1.65±0.22	9.0	7.4
L	2.48*0.28	24.2	3.11±0.31	17.0	15.0
C	2.07±0.30	20.1	4.39±0.41	24.0	30.1
N	1.24±0.22	12.1	2.39±0.30	13.1	9.7
O	2.20±0*32	21.4	3.21±0.36	17.5	19*4
F	0.48±0.12	4*6	0.87±0.28	4.8	2.4
M	5.97±0.42	58.2	10.86±0.6*4	59.4	61.6
Hi	1.11±0.20	10.8	2.72±0.32	14*9	..
H ₂	0.37±0.12	3.6	0.68±0.16	3.7	..
Ha	0.30±0.11	2.9	0.91±0.21	5.0	..
H	1.79±0.27	17.5	4.30±0.41	23.5	23.4
Z>3	10*24±0.62	100.0	18*27±0.81	100.0	100*0

Next we examine the relative abundance of carbon, nitrogen and oxygen nuclei in the primary cosmic rays. The ratio of carbon to oxygen nuclei measured at different energy intervals by various investigators with fairly satisfactory charge resolution are shown in Fig. 5. The C/O ratio is independent of solar modulation. Although the experimental errors on the ratio are fairly large, it is seen in Fig. 5, that the general trend of results indicate that C/O ratio is about 0.90 at energy about 100 MeV/nucleon and it increases to a value of about 1.5 at energy > 1.5 BeV/nucleon. The value of the C/O ratio at $E > 1.5$ BeV/nucleon obtained by various investigators, *e.g.*, von

Rosenvinge *et al.* (1969) and O'Dell *et al.* (1962) are in disagreement with each other. This discrepancy needs further examination.*

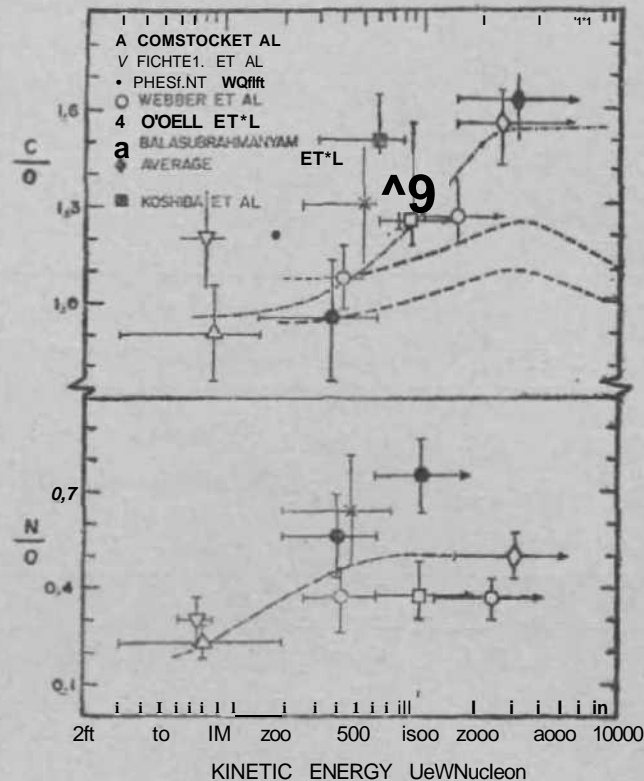


Fig. 5. Carbon to oxygen and nitrogen to oxygen ratios as a function of energy obtained from the present work and other investigations "Average" denotes the average calculated by Webber (1967J). The dashed lines indicate range of C/O ratios determined by von Rosenvinge* *et al.* (1968). The dot dashed lines indicate the approximate variations of the ratios from other data. (The reference Fichte! *et al.* should read as Hagge *et al.*, *Can. J. Phys.*, 1968, 46, S539.)

The N/O ratios measured in this investigation and by others are also shown in Fig. 5. In this case also there is considerable scatter of data points. In the lowest energy interval, 90 MeV/nucleon, N/O is about 0.25 whereas at relativistic energies, > 1.5 BeV/nucleon its value is ~ 0.50 , indicating N/O ratio changes by a factor of about two in this energy interval.

Detailed calculation of the energy dependence of the C/O and N/O ratios taking into account ionisation loss and the most recent spallation cross-section measurements have been made by Bhatia *et al.* (1969). These results indicate that the measured C/O and N/O ratios in cosmic rays at low and high energies are incompatible with the conventional one component

* Note added in proof: In recent experiments, Dayton *et al.* [*Proc. Int. Conf. Cosmic Rays*, Budapest, 1969, to be published) and O'Dell *et al.* (1969, *ibid.*) reported the C/O ratio at $E > 1.5$ BeV/nuc] as ~ 1.1 .

model of cosmic rays and supports the hypothesis of two component models of cosmic rays proposed in recent years (Comstock *et al.*, 1967; Biswas *et al.*, 1966, 1968; Comstock, 1968; Burbidge *et al.*, 1967).

(iv) *Solar modulation energy spectra of medium and helium nuclei between solar maximum and minimum.*— In this work we have studied the changes in the intensity and the spectral shape of medium nuclei and helium nuclei during the solar maximum (mid-1957) to near solar minimum (1963-65) to investigate the solar modulation during the last solar cycle. Many studies have been made on the changes of P and He fluxes during last solar cycle (For summary, see, e.g., Webber, 1968). But this represents an attempt to use the M-nuclei and He spectra for this purpose.

The best estimate of the differential energy spectrum of medium nuclei during mid-1963, obtained from the present data as well as that of Webber *et al.* (1966) and Fichtel *et al.* (1966) is shown in Fig. 4 as discussed earlier. The differential spectrum of M-nuclei during solar maximum was measured by Aizu *et al.* (1960) in September 1957. Since helium and medium nuclei have same mass to charge ratio they are expected to be modulated in the same manner and hence it is useful to compare the changes of helium and medium nuclei fluxes over the same period. The differential spectrum of helium nuclei during the middle of 1963 is obtained from the data of several investigators and is summarised in Fig. 3 of Biswas *et al.* (1967 a). The He spectrum measured during mid-1957 is obtained from the results of Aizu *et al.* (1960), Engler *et al.* (1958) and Freier *et al.* (1959), measured during May-September 1957.

Recent studies of the changes of fluxes of protons and alpha-particles during 1963-66 showed that solar modulation during this period could be represented by the Parker's theory of modulation by solar wind (Parker, 1963) in the following form

$$\frac{J_i^e(E, t)}{J_i^{00}(E)} = e^{-\eta(t) R^n \beta}$$

where $J_i^e(E, t)$ is the differential flux of i^{th} type of nuclei at kinetic energy, E MeV/nucleon, $J_i^{00}(E)$ the corresponding flux outside the solar system, $-\eta(t)$ a constant depending only on time, R and β , rigidity and velocity of the nuclei and $n \ll 1$ for rigidity $R > 0.8 \text{ BV}$, and $n \approx 0$ for $R < 0.8 \text{ BV}$ (Gloeckler and Jokipii, 1967; Jokipii, 1968; O'Gallagher, 1968; Webber, 1968).

To study the solar modulation of medium and helium nuclei from mid-1957 to mid-1963 we plotted $\log_e [J(E, 1963)/J(E, 1957)]$ vs. R_0 for medium and helium nuclei in Fig. 6. It is seen that changes in M and He nuclei are consistent with one another and hence both the components are used to obtain the best fitting line given by $R^{-1.15}$. This was obtained by replotting the data in the form $f_i \log_e J(E, 1963)/J(E, 1957)$ vs. R (not shown), and the best fitting line is found to be $R^{1.15}$. Thus the present analysis indicates in the rigidity interval 1-2 to 2-7 BV rigidity dependence as close to $R_j S$. In Fig. 6 we have shown the lines corresponding to f_i , $R_j S$ and $R_j^2 S$ dependence; it is seen that although $R_j^2 S$ dependence cannot be ruled out, $R_j S$ dependence gives a better fit.

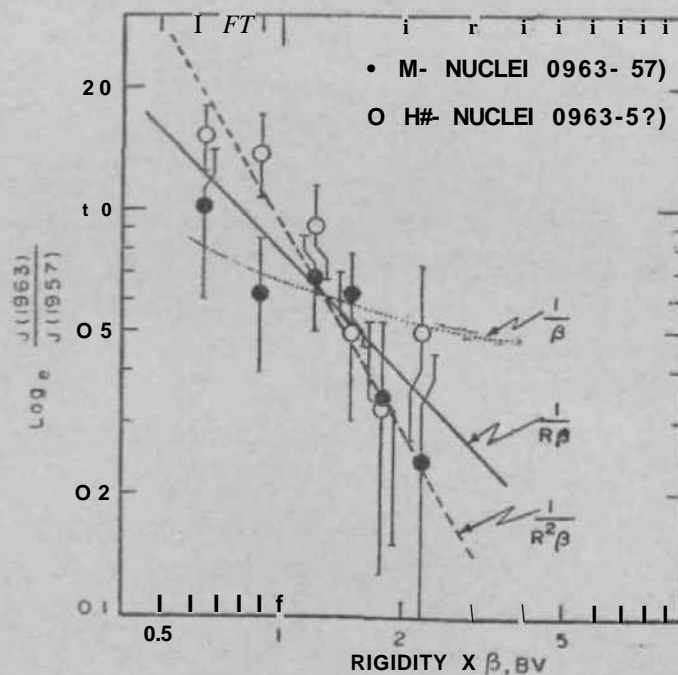


FIG. 6. $\log_e [J(1963)/J(1957)]$ vs. Rigidity X_0 plotted for M-nuclei and He-nuclei. The lines corresponding to $1/R$, $1/R\beta$ and $1/R^2\beta$ dependence of solar modulation are shown. The best fit line is given by $R_j^2 S$ dependence.

On the basis of $R_j S$ dependence it is found from Fig. 6 that the change in T , from 1963 to 1957 (ΔT) is 0.8 BV. The value of ΔT for 1963-65 was found to be about 0.25 (Biswas *et al.*, 1967, Gloeckler and Jokipii, 1967). Hence, ΔV for 1965-57 is obtained as 1.05 BV. The residual modulation at solar minimum 1965 was determined as 0.65 BV by Biswas *et al.* (1967-6). Therefore the value of modulation parameter $-q$ at solar

maximum in 1967 is obtained as 1.70 BV. In Table IV we have summarised the data of this work and those of other investigators on the change of solar modulation during 1957-65.

on the basis of R/J dependence of solar modulation, as well as the residual modulation in 1965, estimated by different methods. It seems that these observations would be consistent with the value of solar modulation parameter 13 (1965) at solar minimum as 0.65 ± 0.10 , A*7 (1957-65) as about 1.4 ± 0.4 and $t|$ (1957) at solar maximum as 2.0 ± 0.4 , indicating a change in 77 by a factor of about three between solar maximum and minimum during the last solar cycle.

TABLE IV
(a) Solar modulation during 1957-65

Authors	Method	Period	A_{7J} (BV)
Present work and Biswas <i>etal.</i> (1967 a, b)	M and He-nuclei	1957-65	1-05
Lockwood and Webber (1968)	Neutron Monitor and P and He-nuclei	1959-65	1-40
O'Gallagher(1968)	P and He nuclei	1958-65	1-80

(b) Residual solar modulation in 1965

Authors	Method	$\bullet n$ (1965) (BV.)
Biswas <i>etal.</i> (1967 A)	He ⁵ /He ratios and He- energy spectrum	0.65 ± 0.05
Gloeckler and Jokipii (1967)	Cosmic ray energy density	<1
Ramaty and Lingenfelter (1968)	He ³ /He ⁴ and H ² /He ⁴ ratios	0.4 ± 0.1
Anand, Daniel and Stephens (1968)	Non-thermal radio emission and cosmic ray electron spectrum	$\wedge 0.65$
Webber (1968)	do.	0-75

ACKNOWLEDGEMENT

The authors are grateful to Indian National Committee on Space Research (INCOSPAR) and National Aeronautics and Space Administration (NASA) of U.S.A. for providing us the emulsion stacks and to Drs. F. B. McDonald and C. E. Fichtel of NASA Goddard Space Flight Center for the exposure of the stacks in balloon flights from Fort Churchill, Canada. We are thankful to Professor R. R. Daniel for helpful discussions. The

authors, VSB, VSC and SDP, are thankful to the Cosmic Ray Committee of the Department of Atomic Energy, Government of India, for the financial support for the work done at Panjab University.

REFERENCES

- Aizu, H., Fujimoto, Y.,
Hasegawa, S., Koshiha, M.,
Mito, I., Nishimura, J.
and Yokoi, K. *Progr. of Theor. Phys. (Kyoto) Supl.*, 1960, 16, 54.
- Anand, K. C., Biswas, S.,
Lavakare, P. J., Ramadurai, S.,
Sreenivasan, N., Bhatia, V. S.,
Chohan, V. S. and Pabbi, S. D. *J. Geophys. Res.*, 1966, 71, 4687.
- , Dañiel, R. R. and
Stephens, S. A. *Nature*, 1968, 217, 25.
- Balasubrahmanyam, V. K.,
Hagge, D. E., Ludwig, G. H.
and McDonald, F. M. *J. Geophys. Res.*, 1966, 71, 1771.
- Barkas, W. H. .. *UCRL Rept. No. 2426 (rev)*, 1965.
- Bernas, R., Epherre, M.,
Gradsztajn, E., Klapisch, R.
and Yiou, F. *Phys. Utters*, 1965, 15, 147.
- Bhatia, V. S. .. *Ph.D. Thesis*, Panjab University, 1967.
- , Biswas, S. and
Ramadurai, S. 1969 (Space Research) (to be published).
- Biswas, S. .. *Colloquium on Cosmic Ray Studies in Relation to Recent Advances in Astronomy and Astrophysics, Bombay, Nov. 1968*, Published by Tata Institute of Fundamental Research, p. 45.
- .. *Astrophys. Space Sci.*, 1969, 5, 59.
- , Ramadurai, S. and
Sreenivasan, N. *Phys. Rev.*, 1966, 149, 1037.
- , Lavakare, P. J.,
Ramadurai, S. and Sreenivasan,
N. *Proc. Ind. Acad. Sci.*, 1967 a, 65, 104.
- , Ramadurai, S. and
Sreenivasan, N. .. *Phys. Rev.*, 1967 6, 159, 1063.
- .. *Can. J. Phys.*, 1968, 46, S 593.
- Burbidge, G. R., Fowler, W. A.
and Hoyle, F. *Nature*, 1967, 216, 22.
- Comstock, G. M., Fan, C. Y.
and Simpson, J. A. *Astrophys. J.*, 1966, 146, 51; 1969, 155, 609.
- Comstock, G. M. .. *Can. J. Phys.*, 1968, 46, S 553; *Astrophys. J.*, 1969, 155, 619.

- Daniel, R. R. and Durgaprasad, N. *Nuovo Cim. Suppl.*, 1962, 23, 82.
- Durgaprasad, N. .. *Ph.D. Thesis*, University of Bombay, 1964.
- Engler, A., Kaplon, M. F. and Klarmann, J. *Phys. Rev.*, 1958, **112**, 597.
- Fichtel, C. E., Guss, D. E., Neelakantan, K. A. and Reames, D. V. *Phys. Rev.*, 1966, 138, 732.
- and Reames, D. V. .. *Ibid.*, 1968, **175**, 1564.
- Foster, F. and DeBenedetti, A. .. *Nuovo Cim.*, 1963, 28, 1190.
- Freier, P. S., Ney, E. P. and Waddington, C. J. *Phys. Rev.*, 1959, **113**, 921.
- and Waddington, C. J. *Can. J. Phys.*, 1968, 46, S 578.
- , Rno, J. S. and Waddington, C. J. *Proc. Int. Conf. Cosmic Rays, London, 1966*, **1**, 38.
- Friedlander, N. W., Neelakantan, K. A., Tokunaga, S., Stevenson, G. R. and Waddington, C. J. *Phil Mag.*, 1963, 8, 1691.
- Glockler, G. and Jokipii, J. R. .. *Astrophys. J.*, 1967, **148**, L 41.
- .. *Phys. Rev. Letters*, 1966, **17**, 203.
- Jokipii, J. R. .. *Can. J. Phys.*, 1968, 46, S950.
- Koshiba, M., Lohrman, E., Aizu, H. and Tamai, E. .. *Phys. Rev.*, 1963, 131, 2692.
- Lim, Y. K. and Fukui, K. .. *Nuovo Cim.*, 1965, 40, 102.
- Lockwood, J. A. and Webber, W. R. *Can. J. Phys.*, 1968, 46, S903.
- Malmquist, L. .. *Arkiv. Fur. Phys.*, 1967, **34**, 33.
- McDonald, F. B. and Webber, W. R. .. *J. Geophys. Res.*, 1962, **67**, 2119.
- O'Dell, F. W., Shapiro, M. M. and Stiller, B. *J. Phys. Soc. Japan*, 1962, 17, Sup. A III, 23.
- O'Gallagher, J. .. *Can. J. Phys.*, 1968, 46, S946.
- Parker, E. N. .. *Interplanetary Dynamical Processes*, Interscience, New York, 1963.
- Powell, C. F., Fowler, P. H. and Perkins, D. H. *Study of Elementary Particles by the Photographic Method*, Pergamon Press, London, 1959, p. 74.
- Ramaty, R. and Lingenfelter, R. E. *Can. J. Phys.*, 1968, 46, S627.
- Reames, D. V. and Fichtel, C. E. .. *Ibid.*, 1968, 46, S544.

- Sreenivasan, N. .. *Ph.D. Thesis'*, Bombay University, 1967.
- von Rosenvinge, T. F., Ormes, J. F. and Webber, W. R. .. *Astrophys. Space Set'*, 1969,3, 4; 3, 80.
- Webber, W. R., Ormes, J. F. and von Rosenvinge, T. F. .. *Proc. Int. Conf. Cosmic Rays* London*, 1966, 1, 407.
- and ————— .. *J. Geophys. Res.*, 1967, 72, 5957.
- Webber, W. R. .. *Aust. J. Phys.*, 1968, 21, 845.
- .. *Handbuch der Physik*, 1967, 46/2, p. 173.
- Yiou, F, and Beck, F. .. *Astrophys. Letters*, 1968, 1, 75.
- , Drefaure de Citres, J., Frehel, F., Gradsztajn, E. and Beraas, R. .. *Can. J. Phys.*, 1968, 46, S557.

SPECTRAL STUDIES ON SOME ORGANIC COMPLEXES OF URANYL ION

Part I. Absorption Spectra of Pyridine Complexes.

BY D. N. SANWAL AND D. D. PANT

(Physics Department, Th.D.S.B. Govt. College, Nainital)

Received June 17, 1968

(Communicated by Dr. R. K. Asundi, F»A.S.C.)

ABSTRACT

The absorption spectra of new crystalline uranyl complexes with pyridine, at 80° K are described. Pyridine uranyl chloride crystallises in two forms, both forms give sharp line like bands at low temperatures. In Form I the bands are analysed in terms of five electronic transitions F, M, D, U and SU of which the former four were suggested for uranyl ion by Dieke *et al.* Results on analogous compounds with deuteropyridine are also reported. Chloride complex seems to have pyridine in the first co-ordination sphere while the acetate complex is of the type of double salt.

INTRODUCTION

INVESTIGATIONS on the spectroscopic properties of uranyl ion under the action of various ligands already exist in literature.¹⁻⁴ A simple organic complexing agent is, however, the pyridine molecule. The effect of this molecule in the sphere of solvation or co-ordination of uranyl ion was found rather interesting and was pursued in some detail. New crystalline uranyl compounds were obtained by the complexing of pyridine with various uranyl salts. Some analogous compounds with deuteropyridine* were also studied. We describe in this paper the absorption spectra of some uranyl complexes with pyridine.

EXPERIMENTAL

Absorption spectra of solutions were obtained on the Hilger Uvispec Spectrophotometer. The spectra of crystalline compounds were photographed on a Bausch and Lomb 1-5 meter grating spectrograph, having

* Kindly sent by Prof. M. Kasha, Department of Chemistry, Florida State University.

a dispersion of 16 Å per mm. The chemicals used were A.R. grade. Purification of pyridine was done by conventional methods.

Pyridine complex with uranyl chloride was found to crystallise in two forms. We call the microcrystalline precipitate obtained on adding pyridine to the solution of uranyl chloride in concentrated HCl as form I which re-dissolves in excess of pyridine and also crystallises as hexagonal plates. Also if the Form I crystals are left in the mother liquor itself for a couple of days at temperatures below 5° C. crystals of Form II having a different morphology begin to grow, those of Form I dissolving as Form II crystals appear. On heating to about 25° C. or above crystals of Form II are converted to Form I. Both Form I and Form II are highly fluorescent and give very sharp bands at low temperatures. With uranyl nitrate and acetate also new crystalline compounds were obtained. The details in the absorption of nitrate complex, however, could not be studied.

(a) Absorption Spectra in Pyridine Solutions

Unlike aqueous solutions, the absorption curves of solutions in pyridine for various uranyl salts consist of broad unresolved bands except for uranyl chloride. In this case eight bands were observed at 4950 Å, 4800 Å, 4640 Å, 4465 Å, 4322 Å, 4195 Å, 4075 Å and 3955 Å respectively. The first band is red shifted with respect to the corresponding band in aqueous solutions.

(b) Absorption Spectra of Crystalline Pyridine Complexes

(i) *Chloride*.—The spectra, at 80° K, for Form I and Form II are shown in Figs. 1 and 2. The spectra have been photographed both by taking a single crystal of microcrystalline powder pressed between two quartz plates. Various series, starting from the longer wavelength side, are termed as fluorescence (F), magnetic (M), diffuse (D), ultraviolet (U) and second ultraviolet (SU). The first four electronic transitions in uranyl salts were suggested by Dieke and Duncan.² Starting of a new transition after the U series was first observed by Pande⁹ in this laboratory. Evidence for these vibronic transitions has also been obtained from spectra of uranyl solutions.^{7*8,10}

Form I.—On the basis of intensity considerations and vibrational analysis the five electronic transitions are clearly observed in Form I. The positions of observed bands are given in Table I which also contains the positions of prominent bands for the analogous compound with deuterio-pyridine and the vibrational analysis. The spectra for the two compounds are similar, there is no appreciable shift within 2 cmr¹ in the positions of

TABLE I

Absorption bands of pyridine uranyl chloride and deuterio-pyridine uranyl chloride Form I at 80° K.

Nature	Pyridin*, uranyl chloride ^e		Deutefo-pyridine uranyl chloride		Designa- tion	Interpretation
	Position in cmr ¹	A''	Position in cmr ¹	A''		
w, 3	2006 $\bar{4}$..	20063	..	a_0	Resonance band
w, 3	20081	\bar{n}	20080	17	..	a_0+17
m,s	20154	90	20155	92	L_x	Ligand
w, s	20260	196	20260	197	L_2	Ligand
m,s	20311	247	20312	249	..	a_0+v_2'
m, b	20395	331	20394	331	} w M_0	Magnetic Series
S, b	20422	358	20416	353		
vw, b	20452	388	..	mm	..	$a_0+2v_2'-17$
vw, b	20477	413	..	m.	..	$M_0'+L_1$
vw, b	20500	436	mm	am
w, b	20536	472	20538	475
vw, b	20548	484	#.	mm	..	a_1+2v_2'
S, b	20660	596	20656	593	M_x	Magnetic series.
w, 3	20770	706	20767	704	..	$a_x- v_x'$
m, 3	20787	723	20782	718	a_x	$a_x+ l$
m, s	20798	734	20794	731	..	a_0+v_0'
m, s	20860	796	20859	796	..	$f_{1j}t+L_2$
m, s	20962	898	20960	897	..	a_1+L_2
m, s	21014	950	21015	952	..	a_1+v_1'
m, b	21098	1034	21096	1033) AM * ivf_{1j}^A / v_a	
S, b	21120	1056	21117	1054		
m, b	21238	1134
S, b	21346	1288	21338	1275	} M_x	M_0+v_x'
S, b	21358	1294	21353	..		
m, b	21369	1305	..	1290	j	
m, s	21472	1408	21467	1407) $\bar{a}vz$	$j_0- _2v_1'$ $f_{10}+2v_1'+17$
m, s	21488	1424	21484	1421		
m, b	21568	1504	21570	1507	..	a_2+L_1
m, b	21578	1514
vw, b	21662	1598
vw, s	21716	1652	..	mm	..	a_2+v_2'
w, b	21793	1729
S, b	21814	1750	21808	1745	} \bar{A} ' $\sqrt{t} \cdot i_{0\ll}$	M_0+2v_x'
m, b	21839	1775	21832	1769		
w, s	21961	1897	21963	1900	..	a_2+2v_x'
m, b	22030	1966	22024	1961	} $\bar{A}t$ \bar{M} $\bar{A}X \cdot i_{0\ll}$	M_0-fiv_j
m, b	22048	1984	22045	1962		

TABLE I—Contd.

Notation	Pyridine uranyl Chloride		Deutero-pyridine uranyl chloride		Designation	Interpretation
	Position in cm. ⁻¹	$\Delta\nu$	Position in cm. ⁻¹	$\Delta\nu$		
<i>w₉ s</i>	22154	2090	} °3	<i _A 4-3i// a _u +3v ₁ -4-14
<i>s₉ s</i>	22168	2104		
<i>m, d</i>	22210	2146		
<i>m₉ d</i>	22232	2168
<i>m₉ b & d</i>	22253	2189
<i>m₉b&d</i>	22266	2202
<i>w₉ b</i>	22404	2340	22409	2346
<i>m₉ b</i> *	22496	2432	22480	2416) M ₁ '	M ₀ ' + 3v ₁ '
<i>m, b</i>	22524	2460	22519	2456		
<i>m₉ d</i>	22644	2580	22648	2582
<i>w₉ d</i>	22713	2649
<i>S, d</i>	22738	2674	22747	2684	D ₀	Diffuse series
<i>S, d</i>	22759	2694
<i>w, d</i>	22784	2720
<i>w, d</i>	22872	2808
<i>w, d</i>	22904	2840
<i>m, d</i>	22939	2875
<i>m, d</i>	22952	2888
<i>m, d</i>	22992	2928
<i>S, d</i>	23015	2951
<i>S, d</i>	23037	2973	23023	2960
<i>m, d</i>	23098	3034
<i>m, d</i>	23119	3055	23144	3061	D ₀ '	Diffuse series
<i>m, d</i>	23157	3093
<i>ms, s</i>	23208	3144	23209	3146	M ₄ '	M ₀ ' + 4v ₃ '
<i>W, 5</i>	23233	3179
<i>w, d</i>	23306	3242	23299	3236
<i>m, d</i>	23349	3275	23346	3283
<i>m, d</i>	23389	3325
<i>m, d</i>	23416	3352
<i>S, d</i>	23443	3379
<i>vS, d</i>	23464	3399	23460	3397	D ₁	D ₀ ' + v ₁ '
<i>m, d</i>	23491	3427
<i>m, d</i>	23571	3507*
<i>m, d</i>	23615	3551«
<i>m, d</i>	23663	3599
<i>m, d</i>	23687	3623
<i>S, d</i>	23712	3648
<i>vS, d</i>	23737	3673	23725	3662	D ₁ '	D ₀ ' + v ₁ '
<i>S, b</i>	23819	3155	23824	3761

TABLE I—Contd.

Nature	Pyridine uranyl chloride		Deutero-pyridine uranyl chloride		Designation	Interpretation
	Position in cm. ⁻¹	A''	Position in cm. ⁻¹	A''		
w, b	23912	3858	M ₅ '	M ₀ ' + 5v ₁ '
m, d	23987	3923
m, d	24046	3982	24048	3985
m, d	24094	4030
m, d	24123	4059
S, d	24144	4080
vS, d	24172	4106	24161	4098	D ₂	D ₀ + 2 [^] ₁ '
w, d	24271	4207
w, d	24318	4254
w, d	24333	4269
m, d	24378	4314	24376	4353
S, d	24412	4348
vS, b	24435	4371	24423	4360	D ₂ '	D ₀ ' + 2iY
m, d	24512	4458	24509	4446
w, d	24539	4475
w, d	24743	4679	24750	4687
S, d	24850	4786	24862	4799	D ₈	D ₀ - 3i » x ₁ '
S, d	24874	4810
w, d	24959	4895
w, d	24991	4827	24982	4919
m, s	25036	4972	25039	4976	U ₀ '	Ultraviolet series
w, s	25058	4994
S, ft	25106	5042	25103	5040
S, ft	25129	5063	25128	5065	D ₈ '	D ₀ ' 4 - 3 [^] ₁ '
w, b	25221	5157	U ₀ '	Ultraviolet series
m, b	25434	5370
S, d	25550	5486	25556	5493	^{mm} D ₄	^{mm} D ₀ + 4 [^] ₁ '
w, b	25567	5503
vw, d	25659	5595
vw, d	25684	5620
m, s	25730	5666	25732	5669	U _a ^f	U ₁ ' + » i ₁ '
m, s	25751	5685
m, b	25798	5734	25795	5732
w, b	25819	5755	25820	5757	D ₀ '	D ₀ ' + 4v ₁ '
m, s	25964	5898	U _x	U ₀ 4 - v _x '
w, d	26224	6160
w, d	26246	6182
w, s	26363	6299
w, s	26400	6336	U ₀ '	U ₀ ' + 2v ₁ '
m, d	26487	6423	26480	6417	U ₀ '	D ₀ ' + 5v ₁ '
m, d	26508	6444	U ₀ '	D ₀ ' + 3v ₁ '

TABLE I—Contd.

Nature	Pyridine uranyl chloride		Deutero-pyridine uranyl chloride		Designation	Interpretation
	Position in cm. ⁻¹	A''	Position in cm. ⁻¹	A''		
<i>w,s</i>	26681	6617	U ₂	U ₂ + 2i>/
<i>m,b</i>	29937	6873	26940	6877	D ₄	
<i>w,s</i>	27012	6948	U ₃ '	U ₀ ' + 3ν ₁ '
<i>w,s</i>	27059	6995		
<i>w,d</i>	27080	7016	D ₆ '	..
<i>vw,d</i>	27114	7050		
<i>w,s</i>	27168	7104
<i>w,b</i>	27398	7334	U _n	U _n + 3ν ₁ '
<i>S,s</i>	27771	7707	SU ₀	Second ultraviolet series
<i>S,s</i>	27816	7752		
<i>m,s</i>	27993	7929	SU ₀ + γ
<i>m,s</i>	28039	7975
<i>S,s</i>	28464	8398	SU	STJ _A 4-ν/
<i>S,s</i>	28509	8443

sharp bands and the uranyl frequencies are not changed. There is a doublet in the first group of fluorescence series, *i.e.*, a_0 at $ca 2CC63 \text{ cm.}^{-1}$ ($A'' = 17 \text{ cm.}^{-1}$). The three uranyl vibrations associated with this series ν_1' , ν_2' and ν_3' are 704 cm.^{-1} , 245 cm.^{-1} and 732 cm.^{-1} respectively and the series can be traced to its third member. The ν_3' which alone can be identified with certainty in other series has an approximate value of 700 cm.^{-1} . The M, D and U series have two components each with *ca* 265 cm.^{-1} and 180 cm.^{-1} respectively. Finally, there is observed a series of strong and sharp bands, with a doublet structure ($A'' = 45 \text{ cm.}^{-1}$) starting at about 7707 cm.^{-1} above a_0 . Only two members are observed with a frequency interval of *ca* 696 cm.^{-1} and after this the absorption reaches a high value resulting in a continuous absorption. This series is designated as SU (second ultraviolet series). A complete microphotometer tracing of the absorption spectrum is given in Fig. 1 to demonstrate the presence of this series.

Form II.—The observed bands for Form II are given in Table II both for pyridine and deutero-pyridine compounds. Both spectra are similar however, the crystal for the case of deutero-pyridine happened to be of

TABLE II

Absorption bands of pyridine uranyl chloride and deuterio-pyridine uranyl chloride Form II at 60°K.

Nature of band	Pyridine uranyl chloride		Deuterio-pyridine uranyl Chloride		Designation	Interpretation
	Position in cm. ⁻¹	ν	Position in cm. ⁻¹	ν		
IV, S	20027	..	20026	..	b_0	Resonance band
VIV, S	20041	17	20043	17
viv, d	..	a	20156	130	la	..
w ₉ d	20270	243	20269	243	..	$b_1 + \nu_1'$
w ₉ d	20284	256	20284	258	..	$b_1 + \nu_1' + 15$
iv, b	20338	310	20332	306	L _a	..
w, d	20389	362	20391	365	L ₃	Ligands
iv, d	20456	429	20453	427	L ₄	..
iv, b	..	##	20479	453	L _s	..
w ₉ S	..	mm	20564	538	L ₀	..
S, b	20598	571	20603	577	M ₀	Magnetic series
IV, S	20615	589		
IV, S	20734	707	20733	707	..	$b_0 + \nu_1'$
IV, S	20748	721	20748	722	b_1	$b_0 + \nu_1' + 15$
w ₉ S	20763	736	20764	737	..	$b_0 + \nu_2'$
viv, d	20863	837	..	$6_1 + L_3$
w ₉ d	20977	950	20978	952	..	$b_x + \nu_1'$
IV, d	20989	963	20992	966	..	$6_x + \nu_1' + 14$
IV, d	21039	1012	21041	1015	..	$b_x - \nu_1'^2$
w ₉ d	21096	1069	21096	1070	..	$A_x + L_8$
IV, d	21163	1136	21140	1114
IV, rf	21180	1154	..	$b_1 + L_5$
iv, d	21242	1216
VW, S	21268	1242	..	$b_1 + L_8$
S, 6	21301	1274	21309	1273	Mi'	M ₀ + V
IV, S	m%	..	21321	1295
iv, d	mm	mm	21330	1304
IV, J	21429	1404	21428	1403	..	$b_0 + 2\nu_1'$
S, J	21445	1418	21445	1419	h	$i_0 + 2\nu_1' + 17$
S, S	21460	1433	21661	1435	..	$b_1 + \nu_2'$
IV, 6	21499	1472	21488	1462	M ₀ '	Magnetic series
IV, 6	..	mm	21503	1477
iv, d	..	mm	21526	1500
viv, d	21564	1538	..	$b_3 + L_2$
vw, d	21607	1581
iv, d	21601	1655	..	$h_2 - \nu_2'$
w, d	21687	1660	21695	1669	..	$b_3 + \nu_2' + 14$
vw, d	21744	1717	21741	1715	..	AJ + LJ
vw, d	21791	1764	21795	1769	..	$b_3 + L_3$
w, d	21859	..	21873	1747	..	$b_3 + \nu_2'$

TABLE II—Contd.

Nature	Pyridine uranyl chloride		Deutero-pyridine uranyl chloride		Designation	Interpretation
	Position in cm. ⁻¹	A''	Position in cm. ⁻¹	A''		
<i>vw₉ s</i>	21960	1960	..	b_2+L_6
<i>S, b</i>	21997	1997	22010	1984	M ₂	M ₀ +2ν ₁ '
<i>vw, s</i>	22019	1993
<i>w₉ b</i>	22049	2023
<i>vw₉ s</i>	22ii7	2090	22106	2080	J	b*
<i>w₉ d</i>	22136	2110	J	A ₀ +3''/
<i>iv, d</i>	22J44	2i17	22149	2123
<i>w₉ d</i>	22185	2159	M ₁ '	M ₀ '+ν ₁ '
<i>w₉ d</i>	22i92	2165	22196	2170
<i>w₉ d</i>	22244	2218	22247	2221
<i>w₉'b</i>	22265	2238
<i>vw₉d</i>	22339	2312	..	b_2+L_1
<i>w₉ d</i>	22425	2398	..	$b_2+ν_3$
<i>w₉ d</i>	22483	2456	..	b_2+L_2
<i>S₉b&d</i>	22581	2554	22583	2556	D ₀	b_2+
<i>m, d</i>	22699	2672	22696	2669	..	Diffuse series
<i>m₉ b</i>	22715	2688	22723	2696
<i>m₉ b</i>	22734	2707
<i>m₉d</i>	22787	2760	22788	2761
<i>m, d</i>	22816	2789	22821	2794
<i>m₉ d</i>	22841	2814	22846	2819
<i>S₉b</i>	22879	2852	22876	2849	M ₂ '	M ₀ '+2ν ₁ '
Red edge	22888	2861
<i>S, vb&d</i>	22925	2898	22911	2884
Violet edge	22977	2950	D ₀ '	Diffuse series
<i>m₉ b</i>	23076	3049	23081	3050
<i>m₉ b</i>	23150	3123	23142	3115
<i>m₉ b</i>	23192	3165	23197	3170
<i>νS₉b&d</i>	23291	3264	23285	3258	D ₁	D ₀ +ν ₁ '
<i>m₉ b</i>	23304	3277
<i>m₉b</i>	23338	3311
<i>w₉ d</i>	23392	3365	23392	3366
<i>*t\ d</i>	23403	3375i	23411	3384
<i>w₉d</i>	23455	3428
<i>w₉ d</i>	23487	3460	23472	3445
<i>w₉b</i>	23557	3530	M ₂ '	..
Red edge)
<i>νS</i>]	23493	3466
Violet edge)
<i>νS₉d</i> }	23638	3611	23569	3542
Red edge
<i>νS</i> }	23611	3584

TABLE II—Contd.

Nature	Pyridine urenyl chloride		Dev tero-pyridiue uranyl chloride		Desig- nation	Interpretation
	Position in cm. ¹	AP	Position in cm. ¹	AP		
Violet edge	23691	3664
<i>w₉b</i>	23786	3769	23786	3759
<i>w₉b</i>	23820	3793	23849	3822
<i>w₉b</i>	23858	3831	23865	3838
<i>w₉b</i>	23893	3866	23908	3881
<i>w₉b</i>	23926	3899
<i>S₉b&d</i>	24013	3986	24001	3974	D₈	D₀+2v₁'
	24051	4024
<i>w₉d</i>	24190	4163	24194	4167
<i>w₉b</i>	24220	4193	24228	4201	M ₄ '	M ₀ [#] -4v ₁ '
red edge	24309	4282
vS, <i>b</i> & <i>d</i>	24337	43'io	D7'	IV+2V
violet edge	24391	4364
<i>w, d</i>	24600	4573	24612	4585
<i>s₉b</i>	24698	4671	24704	4677	D₉	D₀+3v₁'
<i>s₉b</i>	24966	4939	24984	4957
<i>w, d</i>	25016	4989	25005	4978
<i>s₉b</i>	25037	5010	25052	5025	D₈'	D₀+3V
<i>S₉b</i>	25061	5034	25075	5048
<i>m₉b</i>	25392	5365	25404	5377	D₄	..
<i>vw₉b</i>	25596	5569	25596	5569
<i>vw₉b</i>	25639	5612	25625	5598	U ₀	Ultraviolet series
<i>vw₉d</i>	25670	5643	25688	5661	M _c '	M ₀ ' + 6iV
<i>w₉b</i>	25720	5693	25730	5703
<i>S₉b</i>	25733	5706	25750	5723	D₄'	D₀' + 4v₁'
<i>m₉b</i>	25751	5724	25770	5743
<i>vw₉s</i>	26163	6136	26167	6140	U ₀	Ultraviolet senes
<i>vw₉s</i>	26189	6162	26178	6151	U ₀	Ultraviolet senes
<i>m₉b</i>	26285	6258	26255	6228	U ₀	U ₀ + 3v ₁ '
<i>w₉s</i>	26298	6271	26305	6278	U _x	U ₀ + 3v ₁ '
<i>S, b</i>	26425	6398	26448	6421	D₁'	..
<i>w, s</i>	26880	6853	26885	6858	U ₁	..
<i>w₉s</i>	26903	6876	26901	6874	U ₁	..
<i>S, b</i>	27010	6983	27025	6998	U ₁ '	..
<i>w₉b</i>	27136	7109	27126	7099	D₈	..
<i>u₉b</i>	27712	7685	27695	7668
<i>m₉d</i>	27806	7779	27833	7806	D₇'	..
<i>S, d</i>	27900	7873
S, d	27936	7909	279651	7938
Heavy absorp- tion	28281	..	28300

a suitable thickness for greater details of absorption to be investigated. A number of vibrations, other than uranyl frequencies, were thus found associated with the fluorescence series. The spectrum is classified in four series. The absorption beyond U series could not be studied because thin single crystal could not be obtained of an adequate size. On making a thin film with powder the crystalline modification was found to get converted partly to Form I, thus making the spectrum very complicated.

(ii) *Acetate*.—The spectrum is shown in Fig. 3 and the observed bands are given in Table III with assignments. The fluorescence series starts with b_0 at *ca* 20974 cm^{-1} . A series of strong bands, M series, starts at *ca* $ITS \text{ cm}^{-1}$ above b_0 and can be followed upto its fourth member with repetition frequency of *ca* 690 cm^{-1} and consists of doublets with $A^v = 3C0 \text{ cmr}^{-1}$. The doublet nature of D series, which starts at about 1660 cmr^{-1} above b_0 , is evident after its second member ($A^* = 355 \text{ cmr}^{-1}$). The frequency interval between successive members of this series is about 715 cmr^{-1} . A series of comparatively sharper bands starts at about 6040 cmr^{-1} above fluorescence series and is designated as U series in conformity with the general usage. From *ca* 7990 cm^{-1} above b_0 the absorption seems to become continuous.

DISCUSSION

The identification of various electronic transitions in the pyridine complexes has been made through vibrational analysis, structure of bands and intensity considerations. In the case of diffuse bands with multiplet structure the vibrational analysis becomes unreliable, however, the second criterion is helpful that the intensity in the second group is higher than the first group and falls again after the second or the third group. It is an experimental generalisation that in almost all cases M, D and U series are doublets with separations varying from 150 cm^{-1} to 400 cm^{-1} , the violet member being in general weaker. In uranyl sulphate a doublet separation of this order has also been observed in fluorescence series.^{6*6*11} It is again a general observation that in going from a single salt to a double salt M series becomes more intense than D or F series. The solutions also accord with this conclusion where anionic complexing enhances M series and with hydrolysis D series becomes intense. In solid hydrolysed samples also M series is known to get weaker than in normal salt. The spectrum of pyridine uranyl acetate resembles that of double acetates, the M series bands are rather broad and have highest intensity. Pyridine complexes with uranyl

TABLE III

Absorption bands of pyridine uranyl acetate at liquid air temperature

Nature	Position in cm. ⁻¹	A*	Designation	Interpretation
<i>w,s</i>	20974	#.	b_0	Resonance band
<i>vw,d</i>	21104	130
<i>w,b</i>	21149	175
<i>w,b</i>	21209	235	..	$b_0 + \nu_2'$
<i>w,b</i>	21237	263	L	Ligand
<i>w,b</i>	21665	691
<i>S,b</i>	21704	730	b_1	$b_0 + \nu_2'$
VS, vb	21747	773	} M_0	Magnetic series
<i>S, vb</i>	21831	857		
<i>vw,b</i>	21922	948
<i>vw,b</i>	21983	1009
<i>S,b&d</i>	22049	1075	M_0'	Magnetic series
<i>vw,b</i>	22341	1367
<i>vw,b</i>	22384	1310	K	$b_0 + \nu_1'$
<i>S, vb</i>	22423	1459	} M_x	$M_0 + \nu_1'$
VS, vb	22551	1577		
<i>S, vd</i>	22635	1661	D_0	Diffuse series
<i>S,b&d</i>	22749	1775	M_1'	$M_0' + \nu_1'$
<i>Vw,b</i>	22821	1847
<i>vS, vb</i>	23108	2134	} M_2	$M_0 + 2V$
<i>vS, vb</i>	23246	2272		
<i>S,d</i>	23305	2331	} D_i	$D_0 + \nu_1'$
<i>S,d</i>	23350	2376		
<i>S,b&d</i>	23457	2501	M_2'	$M_0' + 2\nu_1'$
<i>S,b&d</i>	23704	2730	} D_1'	Diffuse series
<i>S,d</i>	23793	2819		
<i>S, vb</i>	23840	2866	} M_3	$M_0 + 3\nu_1'$
<i>S, vb</i>	23959	2985		
<i>S,d</i>	24018	3044	} D_2	$D_1' + \nu_1'$
<i>S, vb&d</i>	24160	3186		
<i>S, vb&d</i>	24404	3430	} D_2'	$D_2' + \nu/$
<i>S, vb&d</i>	24586	3612		
<i>S,b&d</i>	25085	4111	D_1'	$D_1' + 2\nu_1'$
<i>w,b</i>	25564	4590
<i>vw,b</i>	25817	4843	D_4'	$D_1' + 3\nu_1'$
<i>S,s</i>	27016	6042	U₀	Ultraviolet series
<i>S,d</i>	27666	6692
<i>w,b</i>	27746	6742	U_1	$U_0 + \nu_1'$
<i>w,b</i>	27840	6865
<i>S, vb&d</i>	28478	7504	SU_0	New series starts
Heavy absorption	28969	7995

tJ—very, w—weak, S—strong, m—moderate, 5—sharp, 6—broad and rf—diffuse.

chloride partly resemble the double chlorides and partly the unhydrolysed single chlorides. The spectra are red shifted with respect to the single salt and violet shifted compared to double salt (caesium uranyl chloride).⁹ The red shift seems to originate due to basic nature of pyridine in the first co-ordination sphere. Red shift is also observed in spectra of pyridine solutions with respect to the corresponding aqueous solutions. The resemblance of spectra, with single salts in that D and M series are almost equally intense and also with the double salts so far as red shift is concerned, indicates both anionic and nitrogen complexing in the equatorial plane of uranyl ion. The intimate structure and positions of various bands are not altered in the analogous compound with deuterio-pyridine. An interesting feature of the spectra of pyridine uranyl chloride complexes is the extra sharpness of bands. The multiplet structure of D series could thus be observed. Each member of D series (red component) is found to consist of four bands, the interval of stronger central components is *ca* 20 cm.⁻¹ and that of wings on either side *ca* 25 cm.⁻¹. The members of D' series consist of three bands each, the separation being 23 cm.⁻¹. There have been indications regarding a new transition to start after U series in a number of solids as well as solutions.⁹ In pyridine uranyl chloride Form I this transition is brought forth very clearly. It is not to be confused with U series which is weak. The bands of U series are clearly recognised by their sharp character among the broad bands of diffuse series.

ACKNOWLEDGEMENT

We are thankful to the Ministry of Education, Govt. of India, and C.S.I.R. for financial assistance and to Dr. S. D. Sinhal for permission to work on the microphotometer at U.P. State Observatory, Nainital. We are also grateful to Dr. R. K. Asundi for valuable comments and suggestions.

REFERENCES

1. Nichols, E. L. and Howes, H. L. *Fluorescence of the Uranyl Salts*, Carnegie Inst. Wash. Pub., 1919.
2. Dieke, G. H. and Duncan, A. B. F. *Spectroscopic Properties of Uranium Compounds*, National Nuclear Energy Series, Div. III, Vol. 2, McGraw-Hill, N.Y., 1949.
3. Rabinowitch, E. and Belford, R. L. *Spectroscopy and Photo-Chemistry of Uranyl Compounds*, International Series of Monographs on Nuclear Energy, Div. XII, Vol. I, Pergamon Press, Inc., N.Y., 1964.
4. Jozowaska-Trzebiatowska, B. *Theory and Structure of Complex Compounds*, Pergamon Press, Inc., N.Y., 1964.

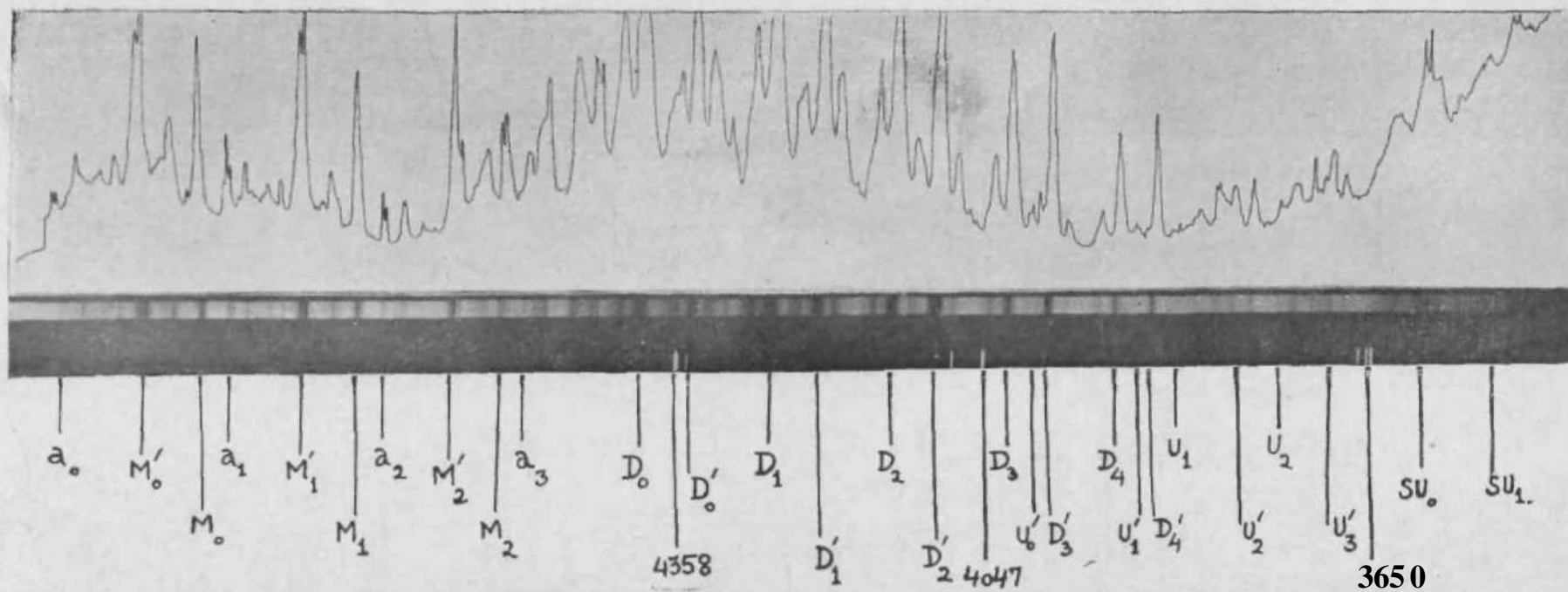


Fig. I. Absorption spectrum of pyridine uranyl chloride form I at liquid air temperatures along with complete micro-photometer tracing.

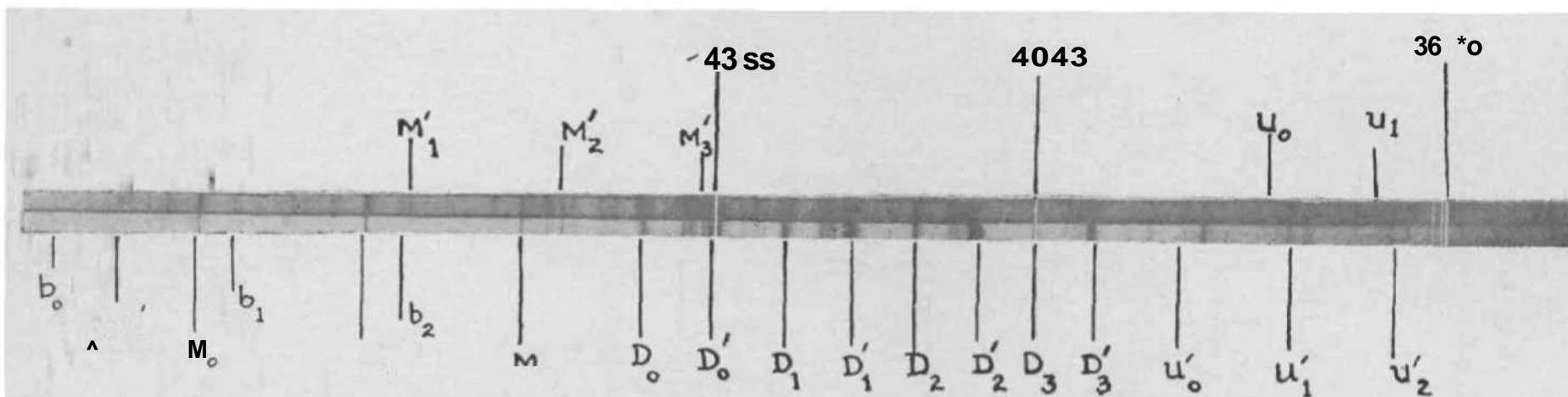


FIG. 2, Absorption spectrum of pyridine uranyl chloride form II at liquid air temperature.

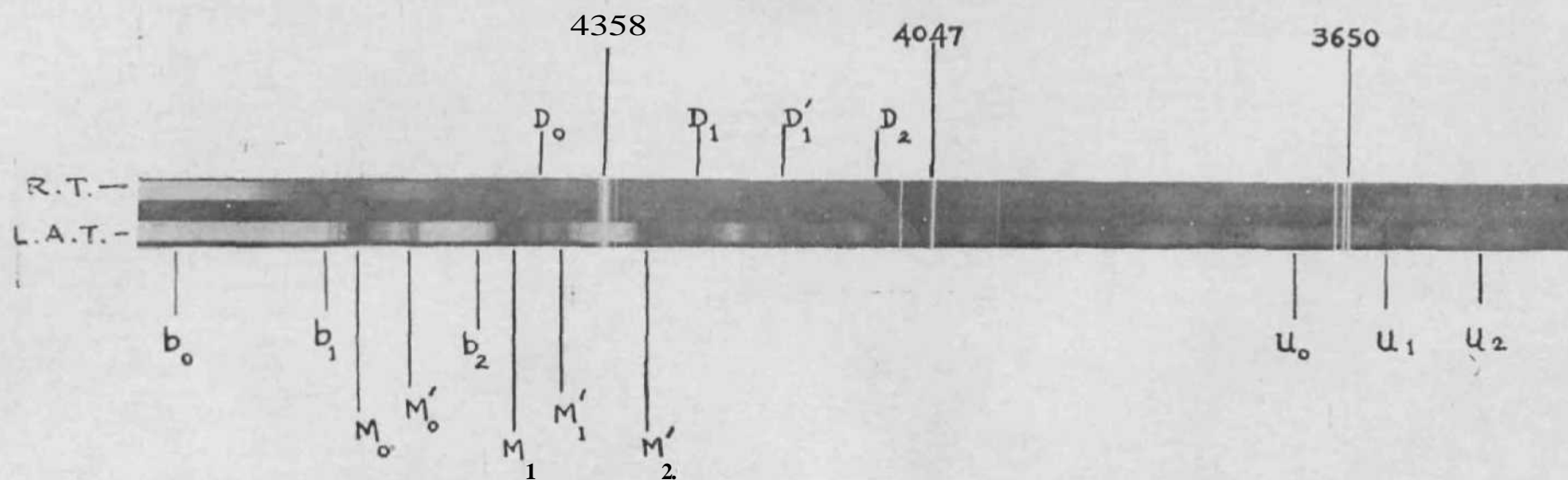


FIG. 3. Absorption spectrum of pyridine uranyl acetate at liquid air temperature and room temperature.

5. Pant, D.D. .. *J. ScL Res. B.H.U.*, 1952, 3, 27.
6. ———— and Pande, B. C .. *I. ScL & Ind. Res.*, 1957₃ It B, 280.
7. Khandelwal, D. P. .. *Ph.D. Thesis*, Agra University, 1958.
8. Bist, H. D. .. *Ibid.*, 1962.
9. Pande, D.N. .. *Ibid.*, 1962.
10. Sanwal, D. N. .. *Ibid.*, 1967.
11. Pant, D. D. and Pande, D. N. *Ind. J. Pure and Applied Physics*, 1966, 4, 470.

SLOWLY OSCILLATING FUNCTIONS AND A GENERALIZATION OF QUASI-MONOTONE COEFFICIENTS

BY CHARLES S. REES

{Department of Mathematics, University of Tennessee, Knoxville, Tennessee, U.S.A.}

Received April 19, 1969

(Communicated by Prof. S. M. Shah, F.A.S.C.)

ABSTRACT

We first state a conjecture due to Yong concerning equality of two classes of functions, and then give examples to disprove the conjecture. Later we extend some theorems concerning integrability of Fourier series.

SECTION 1

In this paper we extend several theorems of Yong³ and also prove a conjecture of his. One of the main tools is the class of slowly oscillating functions. A continuous, positive-valued function s , defined for all large values, is called slowly oscillating if it satisfies the condition $\lim_{x \rightarrow \infty} s(kx)/s(x) = 1$ for every fixed $k > 0$. Some of the properties possessed by slowly oscillating functions are set forth below,

(i) s is slowly oscillating if and only if

$$s(x) = F(x) \exp. \left[\int_a^x \frac{\delta(t)}{t} dt \right],$$

where F is a positive-valued continuous function which tends to a positive, finite limit, a is some positive constant, and S is a continuous function which tends to zero.

(ii) $xr*s(x) \rightarrow 0$ and $x^a s(x) \rightarrow \infty$ for every fixed $a > 0$.

(iii) if $a > 0$, then there are positive, finite numbers A_x and A_a such that for every natural number n

$$A_1 n^a s(n) \leq k^a s(k) \leq A_2 n^a s(n).$$

(iv) if $a > 0$, then as $0 \rightarrow \infty$

$$\min_{0 < s < \infty} [x^* s (*)] \sim q^{\%} s (q).$$

(v) the sum and the product (but not necessarily the difference) of any two slowly oscillating functions is itself slowly oscillating.

SECTION 2

The first theorem in Yong's paper is concerned with two classes of functions, and at the end of the proof of his Theorem 1 he states that he has been unable to decide which inclusion relations hold between the two classes. He conjectures, however, that the classes are not comparable. We prove this conjecture by exhibiting two functions, each of which is in one class but not the other. For both classes the functions must be defined for all large values, be positive, and satisfy

$$\sum_{K} 1 \tag{1}$$

(Here and throughout this paper K denotes some unspecified positive constant whose value may change from one occurrence to the next.) The two classes are then defined respectively as those functions / which satisfy the above conditions and are

(A) slowly oscillating,

(B) non-decreasing for all large values and satisfy

$$f(x^*) \leq c f(x) \tag{2}$$

for some fixed $k > 1$, $c = c(k)$ some positive constant. We show first that (A) is not contained in (B). Letting

$$f(x) = \exp. \left[\int_{10}^x \frac{dt}{\{tL(t)\}} \right]$$

[in this section $L(x) = \log \log x$] we know that / is slowly oscillating by (i). Now for all large x we have

$$\begin{aligned} f(x) &\geq \exp. \left[\left(\frac{1}{L(x)} \right) \int_{10}^x \frac{dt}{t} \right] \\ &= \left(\frac{x}{10} \right)^{1/L(x)} \geq \log^3 x, \end{aligned}$$

so (1) holds and f is in A. Now let $k > 1$. Then

$$\frac{f(x^k)}{f(x)} = \exp. \left[\int_1^{x^k} \frac{dt}{\{tL(t)\}} \right] \\ \geq \exp. \left[\int_{\lfloor L(x^k) \rfloor}^{\lfloor L(x) \rfloor} \frac{dt}{t} \right] = \exp. \left[\frac{(k-1) \log x}{\log k + L(x)} \right],$$

which tends to infinity with x . Thus (2) does not hold and f is not in (B).

We turn now to an example of a function which is in (B) but not (A). Let $E(x) = e^{e^x}$ and define I_n to be the closed interval $[E(n/2), 1 + E(n/2)]$. Define the function h for $t \geq 10$ by $h(t) = E(n/2)$ if $t \in I_n$ and $h(t) = 0$ otherwise. Finally, define g by

$$g(x) = \exp. \int_1^x h(t) dt$$

We proceed to show that g is the desired function. We note first that for every positive integer n we have

$$\frac{2}{3} \int_1^{E(n/2)} \frac{h(t)}{t} dt < 1. \quad (3)$$

If g were in (A) it would have to satisfy $g(kx)/g(x) \rightarrow 1$ for every fixed $k > 0$, that is $\int_1^{kx} h(t)/t dt \rightarrow \int_1^x h(t)/t dt$. But choosing $k > 1$ and letting $x \rightarrow \infty$ through the values $E(n/2)$ yields by (3)

$$\limsup_{x \rightarrow \infty} \int_1^{kx} \frac{h(t)}{t} dt \geq \frac{2}{3}.$$

Thus g is not slowly oscillating, hence not in (A). To show that g is in (B) we observe that $h(t) \geq 0$, so g is non-decreasing and positive. Now $h(t) > 0$ in $[x, x^k]$ if and only if $x - 1 \leq E(n/2) \leq x^k$, that is $L(x - 1) \leq n/2 \leq \log k + L(x^k)$. But $\log k + L(x^k) - L(x - 1)$ is bounded, so

$h(t) > 0$ in $[x, x^k]$ at most, say T times (T being independent of x). We thus may say, by (3), that

$$\frac{g(x^k)}{g(x)} = \exp. \left[\int_x^{x^k} \frac{h(t)}{t} dt \right] \leq \exp. [T],$$

and so (2) holds. It remains only to show that (1) holds also. Now $9 \leq E\{njl\} \leq x$ if and only if $2L(9) \leq n \leq 2L\{x\}$, so $h(t) > 0$ in $[10, x]$ at least $[2L(JC) - 2L(9) - 3]$ times (here the brackets denote the greatest integer function). But for all large x this last expression is larger than $(7/4)L(x)$, so for such values of x we have by (3)

$$g(x) \geq \exp. \left[\left(\frac{7}{4}\right) (J) L(x) \right] = (\log xy) \gg.$$

Thus (1) holds, g is in (B) and Yong's conjecture is proved.

SECTION 3

We now turn to extension of Yong's results by extending the concept of quasi-monotone sequences. A sequence $\{a_k\}$ of positive terms is called quasi-monotone if $a_{k+1} \leq a^k (1 + a_j k)$ for some $a \geq 0$. We consider sequences which satisfy

$$a_{k+1} \leq a_k \left(1 + \frac{S(k)}{k} \right), \tag{4}$$

where S is a slowly oscillating function which increases to infinity. By (ii) we have $S(k)/k \rightarrow 0$.

Theorem 1.—Let $p > 0$, L be a slowly oscillating function, $\{a^k\}$ and S as above. Then

(a) if

$$\sum_1^{\infty} k^{p-1} L(k) S^*(k) a_k < \infty$$

then

$$\sum_1^{\infty} k^p L(k) S(k) |a_k - a_{k+1}| < \infty,$$

(b) if

$$\sum_1^{\infty} k^p L(k) S(k) |a_k - a_{k+1}| < \infty$$

then

$$\sum_1^{\infty} k^{p-1} L(k) S(k) a_k < \infty.$$

Proof.—(a) By partial summation

$$\sum_1^n nP^{-1} L(\ll) S(n) a_n = \sum_1^n F s_n (a_n - a_{n+i}) + s_n a_n, \quad (5)$$

where

$$s_n = \sum_1^n k^{p-1} L(k) S(k).$$

We define

$$u_n = n + \left[\frac{n}{S(n)} \right],$$

where $[x]$ is the greatest integer not exceeding x . Now consider

$$t_n = \sum_n^{u_n} k^{p-1} L(k) S^2(k) a_k.$$

we have, for each k satisfying $n \leq k \leq u_n$, that $k/u_n \geq n/u_n \geq l_0$, so

$$\left(k^{p-1} \right) \quad (6)$$

Using the representation in (i) we may write *

$$\frac{L(k)}{L(u_n)} = \frac{F(k)}{F(u_n)} \exp. \left[\int_k^{u_n} -\frac{\delta(t)}{t} dt \right].$$

But for all large n , $F(k)/F(u_n) \geq 1$ and $-\delta(t) > -1$, so

$$t_n \geq \exp. [-\log \frac{1}{K}] = K \cdot K.$$

Thus by (v)

$$\frac{L(k) S^2(k)}{L(u_n) S^2(u_n)} \geq K > 0. \quad (7)$$

For the last part of t_n , we have

$$a_k \geq \frac{a_{k+1}}{1 + \frac{S(k)}{k}} \geq \dots \geq \frac{a(u_n)}{\left(1 + \frac{S(k)}{k}\right) \dots \left(1 + \frac{S(u_n)}{u_n}\right)}.$$

By $(*)$ for all large n each factor of the last denominator is dominated by

$$1 + \left\{ \max_{\ln k < \infty} f \mid < 1 + \frac{2}{n} \right\}$$

and

$$\log \left\{ 1 + \frac{2S(n)}{n} \right\}^{1 + [f/S(n)]} \approx \frac{2S(n)}{n} \left(1 + \frac{f}{S(n)} \right)^{[f/S(n)]}$$

so

$$t_n \geq K a_n \ll n. \tag{8}$$

Thus from (6), (7), and (8), we have

$$t_n \geq \frac{K u_n^{p-1} L(u_n) S^2(u_n) a(u_n) n}{S(n)} \geq K \ll n P L(i/n) S(M_n) a(\ll n).$$

However, by hypothesis $t_n \rightarrow 0$, so the sequence $\{n P L(n) S(n) a_n\}$ tends to zero as n tends to infinity through the sequence $\{u_n\}$. But since S increases we have

$$\begin{aligned} u_{n+1} - u_n &\leq 1 + \left[\frac{n+1}{S(n+1)} - \frac{n}{S(n)} \right] \\ &\leq 1 + \frac{1}{S(n+1)} + \frac{[S(n) - S(n+1)]}{S(n) S(n+1)} \\ &\leq 1 + \frac{1}{S(n+1)} \rightarrow 1, \end{aligned} \tag{9}$$

so the gaps in $\{\ll, \}$ are bounded and $n L(n) S(\ll) f_{n \rightarrow 0}$. Now by (iii)

$$S q O q \leq A^p L(q) S(?) a, \rightarrow 0,$$

and so from (5)

$$\sum_{n=1}^{\infty} n^{p-1} L(n) S(n) a_n = \sum_{n=1}^{\infty} Z_{s_n} (a_n - a^{\wedge}), \tag{10}$$

With Young⁸ and Shah² for the sequence $\{a_k\}$ we define two new sequences $\{i_j\}$ and $\{p_j\}$ by saying that $a_{k+1} \geq a_k$ if $i_j \leq k \leq n_j + p_j - 1$ and $0 \leq i_j < n_j$ if $n_j + p_j \leq k < n_{j+1} - 1$. Writing the right side of (10) as two sums and transposing one of them gives

$$\begin{aligned} & \sum_1^{\infty} s_n (a_n - a_{n+1}) + \sum_{i=1}^{\infty} \sum_{k=i}^{i+p_j-1} s_k (a_{k+1} - a_k) \\ &= \sum_{i=1}^{\infty} \sum_{k=i}^{i+p_j-1} s_k (a_{k+1} - a_k) \end{aligned} \tag{11}$$

This is permissible since by (4) and (iii) the second sum in (11) is dominated by

$$\sum_1^{\infty} \sum_{n_j}^{n_j+p_j-1} A_2 k^p L(k) S(k) \frac{a_k S(k)}{k} \leq A_2 \sum_1^{\infty} k^{p-1} L(k) S^2(k) a_1$$

which is finite by hypothesis. The first sum in (11) is finite by (10), hence so is the third sum. However, from (iii),

$$s_k |a_k - a_{k+1}| > A^L L(k) S(k) |a_k - a_{k+1}|,$$

so

$$\sum_1^{\infty} k^p L(k) S(k) |a_k - a_{k+1}| < \infty$$

which is the conclusion of (a).

To prove (b) we again appeal to partial summation and (iii) and obtain

$$\begin{aligned} & \sum_1^{\infty} n^{p-1} S(n) L(n) a_n \\ &= \sum_1^{r-1} s_n (a_n - a_{n+1}) + s_q a_q + \sum_1^{q-1} w^{*L} (j) S(j) L(j) a_{n+1} \\ & \quad + s_q a_q. \end{aligned} \tag{12}$$

But from (iv)

$$\begin{aligned} & \sum_1^{\infty} n^p L(n) S(n) |a_n - a_{n+1}| \\ & \geq \sum_1^{\infty} \min_{n \geq i} \{r^{*L}(i) S(i) L(i)\} |a_n - a_{n+1}| \end{aligned}$$

$$\begin{aligned} &\geq KqPL(q)S(q)Z \quad I \ll \infty - \ll n_i I \\ &\geq Kq^*L(q)S(q)a_q \end{aligned}$$

so from the hypothesis $rfl L(n) S(n) a_n \rightarrow 0$. Thus $s_q a_q$ is bounded and the conclusion of (b) follows.

It is natural to ask if $S^2(k)$ may be replaced by $S(fc)$ in the hypothesis of part (a) of the theorem. We give here an example to show that it may not. Let $L(k) = \log k$, $S(k) = (\log k)^{2t}$ for some fixed $e > 0, p = 1$, and define $\{ah\}$ by $a_x = a_2 = 1$ and $ft: \geq 3$

$$a_k = \frac{1}{k (\log k)^{2+3e}}$$

if k is odd

$$a_k = \frac{1}{k (\log fc)^{2+3e}} \left[1 + \frac{(\log k)^{2e}}{k} \right],$$

if Ar is even. Then $\{ajc\}$ satisfies (4), L and S are slowly oscillating, and $2 A: ?^{-1} L(k) S(k) \text{ ofc} < \infty$. However for k even

$$|a_k - a_{k+1}| \geq \frac{1}{k (\log k)^{2+3e}} \frac{(\log k)^{2e}}{k} = \frac{1}{k^2 (\log k)^{2+e}}$$

and so

$$\sum_1^N k^p L(k) S(k) |a_k - a_{k+1}| \geq \sum_{fc \text{ even}}^N \frac{1}{k (\log k)^{1+e}}$$

which tends to infinity with N .

We note that, by the theorem, for such an example as this we must have $Z'fcP-i L(k) S^2(k) a^* = \infty$. That this last relation holds follows from

$$\sum_1^{\infty} \frac{(\log k) (\log k)^{4e}}{k (\log k)^{2+3e}} = \infty.$$

The only place where the hypothesis that S increases is used is in showing that

$$\frac{n+l}{S(n+1)} - \frac{n}{S(n)}$$

A4

is bounded [see (9)]. That we may not obtain this result by assuming only that $S(x) = o(1)$ instead of $S(JC) = o(1)$ follows from the example given here. Let $S(JC) = \log JC - \frac{1}{2} \cos nx$, which is slowly oscillating. Then for n even we have

$$\frac{n+l}{S(n+l)} - \frac{n}{S(n)} \sim \frac{In + \log n + 1 + n [\log n - \log(n+1)]}{[\log(n+1) - 1] [\log n + l]} = o(1).$$

We may use Theorem 1 to obtain integrability theorems similar to those of Yong and Boas [see (3) and (1)]. These results are stated here but not proved.

Theorem 2.—Let $\{a_k\}$ satisfy (4) and suppose $0 < p < 1$.

(a) if $\sum_{k=1}^{\infty} L(k) S^*(k) a_k < \infty$, then $\sum_{k=1}^{\infty} a_k \sin kx$ converges, say to $g(x)$, and

$$x^{-p} L\left(\frac{1}{x}\right) S\left(\frac{1}{x}\right) g(x) \in L[0, \pi].$$

(b) if $\sum_{k=1}^{\infty} a_k \sin kx$ converges to $g(x)$ and

$$x^{-p} L\left(\frac{1}{x}\right) S\left(\frac{1}{x}\right) g'(x) \in L(0, \pi),$$

then $\sum_{k=1}^{\infty} L(k) S(k) a_k < \infty$.

Similar results hold for cosine series.

REFERENCES

1. Boas, R. P. (Jr.) .. "Quasi-positive sequences and trigonometric series," *Proc. London Math. Soc.*, 1965, 14 A, 38-46.
2. Shah, S. M. .. "Trigonometric series with quasi-monotone coefficients," *Proc. Amer. Math. Soc.*, 1962, 13, 266-73.
3. Chi-Hsing Yong .. "Integrability theorems of certain trigonometric series with quasi-monotone coefficients," *Monatsh. Math.*, 1965, 69, 441-50.

THREE-DIMENSIONAL PERIODIC BOUNDARY LAYERS

BY C. L. NARAYANA AND N. R. SUBRAMANIAN

(National Aeronautical Laboratory; Bangalore-II)

Received August 22, 1968

(Communicated by Dr. K. S. Viswanathan, F.A.S.C.)

ABSTRACT

The method of successive approximations used by Eichelbrenner and Agkovič¹ for the study of unsteady three-dimensional boundary layer flow has been extended to analyse the periodic boundary layers in three dimensions. The analysis, which is valid for oscillations of small amplitude, shows some special features such as "steady streaming" flow in the first-order cross-flow similar to the one that has been predicted and observed by Schlichting for two-dimensional periodic boundary layers.

INTRODUCTION

THE analysis of Eichelbrenner and Aškovič¹ in which the principle of '*prevalence*' has been adapted to study the unsteady three-dimensional boundary layers has been used here to study the periodic boundary layers in three dimensions. This analysis is also an extension of Schlichting's² work in two-dimensional periodic boundary layers. The usual method of solving the three-dimensional boundary layer equations of a steady flow past a finite obstacle is based on the following three hypotheses:

Hypothesis 1.—Every stream line inside the boundary layer has a well-determined limiting position on the surface of the obstacle as well as at the edge of the boundary layer. Conversely, at every point of the boundary layer there exists only one streamline. This is true at the wall as well as at the edge.

Hypothesis 2.—In a system of curvilinear co-ordinates based on the direction of the external streamlines (*viz.*,⁴ Streamline co-ordinates') around an obstacle, we can, in the first approximation, neglect to the order of Rr^* (where R is the Reynolds number) the transverse component of the velocity vector with respect to the longitudinal component. Then the

three-dimensional boundary layer equations degenerate into a system of two-dimensional boundary layer equations *plus* an additional equation for the transverse flow. This is the principle of prevalence.

Hypothesis 3.—In a stream tube, the quasi-two-dimensional system for the longitudinal flow can be interpreted as the system corresponding to a local axisymmetric flow.

On this basis the equations have been generalised to the case of the unsteady flow. The above three hypotheses have been adopted to the case of the unsteady three-dimensional boundary layer flow in reference (1). Following the same reasoning in the present problem also it is assumed that

$$\frac{V_e(p; t) - V_e(p; t_0)}{|V_e(p; t)|} \dots$$

for $t_x < l < h$ where t_0 represents a characteristic time, say, the period $T = 2\pi/\omega$, ω being the frequency. Further in the streamline co-ordinates, as the cross-flow velocity w has to become zero at the edge of the boundary layer and it is also zero at the wall, it is assumed to be small everywhere compared to the streamwise velocity u . That is $w/u \ll 1$ throughout the boundary layer. The equations are further simplified by assuming the curvature variations also as small.

THE EQUATIONS

We use the curvilinear co-ordinate system (ξ, η, ξ) where $\eta = 0$ represents the general three-dimensional body surface on which ξ and η are assumed to be orthogonal and the η -axis is taken to be perpendicular to the surface so that the above system of co-ordinates are 'locally' orthogonal at the surface. The error in such an assumption is negligible as our region of interest is quite close to the body surface according to the Prandtl's boundary layer assumptions. Hence, the boundary layer equations can now be written as

$$\begin{aligned} \frac{1}{\rho} \frac{\partial}{\partial \xi} \left(\rho u \frac{\partial u}{\partial \xi} \right) + \frac{1}{\rho} \frac{\partial}{\partial \eta} \left(\rho v \frac{\partial u}{\partial \eta} \right) + \frac{1}{\rho} \frac{\partial}{\partial \xi} \left(\rho w \frac{\partial u}{\partial \xi} \right) &= -\frac{1}{\rho} \frac{\partial p}{\partial \xi} + \nu \frac{\partial^2 u}{\partial \xi^2} \\ \frac{1}{\rho} \frac{\partial}{\partial \xi} \left(\rho u \frac{\partial v}{\partial \xi} \right) + \frac{1}{\rho} \frac{\partial}{\partial \eta} \left(\rho v \frac{\partial v}{\partial \eta} \right) + \frac{1}{\rho} \frac{\partial}{\partial \xi} \left(\rho w \frac{\partial v}{\partial \xi} \right) &= \nu \frac{\partial^2 v}{\partial \xi^2} \\ \frac{1}{\rho} \frac{\partial}{\partial \xi} \left(\rho u \frac{\partial w}{\partial \xi} \right) + \frac{1}{\rho} \frac{\partial}{\partial \eta} \left(\rho v \frac{\partial w}{\partial \eta} \right) + \frac{1}{\rho} \frac{\partial}{\partial \xi} \left(\rho w \frac{\partial w}{\partial \xi} \right) &= \nu \frac{\partial^2 w}{\partial \xi^2} \end{aligned}$$

$$\frac{\partial p}{\partial \eta} = 0,$$

$$\begin{aligned} \frac{\partial w}{\partial \xi} + u \frac{\partial w}{h_x \partial n} + v \frac{\partial w}{K \partial n} + \frac{uw}{h_1 h_2} \frac{\partial h_2}{\partial \xi} - \frac{u^2}{h_1 h_2} \frac{\partial h_1}{\partial \xi} \\ = -\frac{1}{\rho M} \frac{\partial p}{\partial \xi} + \nu \frac{\partial^2 w}{\partial \eta^2}, \\ \frac{\partial (\rho h_x u)}{\partial \xi} + \frac{\partial (\rho h_x v)}{\partial \eta} + \frac{\partial (\rho h_2 v)}{\partial \eta} = 0 \end{aligned} \quad (1)$$

where w, H, z ; are the velocities in the directions ξ, η, ζ and h_x, h_2 (ξ, η) are, respectively, the scale factors in these directions. These scale factors are related to the line element dl by

$$dl^2 = h_x^2 d\xi^2 + h_2^2 d\eta^2 + h_3^2 d\zeta^2 \quad (2)$$

Let the differential line elements in the three directions be ds, dz , and dn so that

$$ds = h_x d\xi, \quad dz = h_2 d\eta, \quad dn = d\zeta \quad (3)$$

Further, as has been done in reference (1), we assume that the transverse velocity component or the cross-flow w is much smaller compared to u . The equations (1) then become

$$\frac{\partial u}{\partial \xi} + u \frac{\partial u}{h_x \partial n} = -\frac{1}{\rho} \frac{\partial p}{\partial \xi} + \nu \frac{\partial^2 u}{\partial n^2} \quad (4)$$

$$\frac{\partial (h_x u)}{\partial \xi} + \frac{\partial (h_x v)}{\partial n} = 0 \quad (5)$$

$$\frac{\partial w}{\partial \xi} + u \frac{\partial w}{\partial s} + v \frac{\partial w}{\partial n} - \frac{u^2 \partial h_1}{h_1 \partial z} = -\frac{1}{\rho} \frac{\partial p}{\partial z} + \nu \frac{\partial^2 w}{\partial n^2} \quad (6)$$

The equations (4) and (5) are independent of (6) and are the same as the equations for the two-dimensional boundary layers. Hence, they can be solved to obtain u and v which on substitution in (6) give w .

The boundary conditions are

$$u = v = w = 0, \quad n = 0; \quad u = u_\infty, \quad n = \infty \quad (7)$$

where $u_e = u_e(s, z, t)$ is the velocity of the unsteady potential flow at the edge of the boundary layer. The pressure gradients in equations (4) and (6) are then given by (since $dp/dt = 0$)

$$-\frac{1}{\rho} \frac{\partial p}{\partial s} = \frac{\partial u_e}{\partial t} + u_e \frac{\partial u_e}{\partial s}, \quad (8)$$

$$-\frac{1}{\rho} \frac{\partial p}{\partial z} = -\frac{u_e^2}{h_1} \frac{\partial h_1}{\partial z}. \quad (9)$$

Now we are interested in obtaining the solutions of (4), (5) and (6) for a periodic potential flow with zero steady part, *i.e.*, the problem is to solve for u, v, w in the boundary layer when the velocity at the edge of the boundary layer u_e is of the form

$$u_e = U_0(s, z) \cos \omega t$$

$$\text{or} \quad = U_0(s, z) e^{i\omega t} \quad (10)$$

with the convention that only the real parts of the complex quantities in question have physical meaning attached to them. With the known outer velocity distribution as given by (10) the calculation of the boundary layer flow will be carried out by successive approximations. That is, we decompose the velocity components u, w and v into sums

$$u = u_0 + u_1 + u_2 + \dots$$

$$w = w_0 + w_1 + w_2 + \dots$$

$$v = v_0 + v_1 + v_2 + \dots$$

iii

where w_0, v_0, V_0 are the solutions of first-order approximation, u_1, w_1, v_1 are the solutions of second-order approximation and so on, and that

$$u_0 \gg u_1 \gg u_2 \gg \dots$$

$$w_0 \gg w_1 \gg w_2 \gg \dots$$

$$v_0 \gg v_1 \gg v_2 \gg \dots$$

(12)

Following Schlichting we state that it is possible to solve equations (4) to (6) using the method of successive approximation of reference (1) for the case of periodic boundary layers also if

$$\left| u_e \frac{\partial u_e}{\partial s} \right| \ll \left| \frac{\partial u_e}{\partial t} \right|$$

which leads to the condition that $S \ll d$ where S is the amplitude of oscillations and d is the linear dimension of the body. That is, the proposed method of solution may be used in cases where the amplitude of oscillations is small compared to the dimensions of the body. Hence using (11) in (4)-(6) we obtain the equations for the first-order approximation as [reference (1)]

$$\frac{\partial u_0}{\partial t} - \nu \frac{\partial^2 u_0}{\partial n^2} = \frac{\partial u_e}{\partial t}, \tag{13}$$

$$\frac{\partial (h_2 u_0)}{\partial s} + \frac{\partial (h_2 v_0)}{\partial n} = 0, \tag{14}$$

$$\frac{\partial w_0}{\partial t} - \nu \frac{\partial^2 w_0}{\partial n^2} = \frac{u_0^2 - u_e^2}{h_1} \frac{\partial h_1}{\partial z}, \tag{15}$$

with the boundary conditions

$$\begin{aligned} u_0 = v_0 = w_0 = 0 \quad \text{at } n = 0 \\ u_0 \rightarrow u_e \quad \text{as } n \rightarrow \infty. \end{aligned} \tag{16}$$

The equations for the second-order approximation are

$$\frac{\partial u_1}{\partial t} - \nu \frac{\partial^2 u_1}{\partial n^2} = u_e \frac{\partial u_e}{\partial s} - u_0 \frac{\partial u_0}{\partial s} - v_0 \frac{\partial u_0}{\partial n}, \tag{17}$$

$$\frac{\partial (h_2 u_1)}{\partial s} + \frac{\partial (h_2 v_1)}{\partial n} = 0. \tag{18}$$

$$\begin{aligned} \frac{\partial w_1}{\partial t} - \nu \frac{\partial^2 w_1}{\partial n^2} = \frac{(2U_p U_1 + u_1^2)}{K} \frac{\partial h_1}{\partial z} - (u_0 + u_1) \frac{\partial w_0}{\partial s} \\ - (v_0 + v_1) l Q, \end{aligned} \tag{19}$$

and the corresponding boundary conditions are

$$u_1 = v_1 = w_1 = 0 \quad \text{at } n = 0 \quad \text{and } \infty. \tag{20}$$

SOLUTIONS

First approximation.—Introducing a dimensionless co-ordinate η defined by

$$y = n \int \frac{\omega}{\nu} \tag{21}$$

and assuming that the first-order velocity u_0 is of the form

$$w_0 = U_0 K(y) e^{i\omega t} \quad (22)$$

we get from (14)

$$v_0 = -ji \wedge g^{(0)} \phi_0(y) e^{i\omega t} \quad (23)$$

where

$$6 > ' (0) = 0, fa(0) = 0, fa'(\infty) = 1. \quad (24)$$

Substituting (10), (21) and (22) in (13) we obtain the following differential equation for $\langle f \rangle_0'$,

$$fa''' - ifa' = \sim i \quad (25)$$

with the boundary conditions (24) equation (25) has the solution

$$fa' = 1 - \langle r \rangle^* \quad (26)$$

where

$$x = ay \quad \text{and} \quad a = \frac{1+i}{\sqrt{2}j^*} \quad (27)$$

Hence we obtain (in real notation)

$$u_0(s, z, y, t) = U_0 \left[\cos \langle at - e^{-y/y/i} \cos \left(\omega t - \frac{JL}{\sqrt{2}} J J_y \right) \right] \quad (28)$$

and integrating (26) once again and using (24) we get

$$, \quad x - 1 + e^{-x} \quad (29)$$

which, on substitution in (23), gives

$$v_0(s, z, y, t) = - \sqrt{\frac{\nu}{\omega h_2}} \frac{1}{\partial s} \frac{\partial (h_2 U_0)}{\partial s} \left[y \cos \omega t - \cos \left(\omega t - \frac{\pi}{4} \right) + e^{-y/\sqrt{2}} \cos \left(\omega t - \frac{\pi}{4} - \frac{y}{\sqrt{2}} \right) \right]. \quad (30)$$

First-order cross-flow.—The differential equation governing the first-order cross-flow w_0 is the equation (15), viz.,

$$\frac{\partial w_0}{\partial t} + v \frac{\partial w_0}{\partial x} + h_x \frac{\partial w_0}{\partial z} = \dots \quad (14)$$

with the boundary conditions

$$w_0 = 0 \quad \text{at} \quad n = 0, \infty. \quad (15)$$

Before assuming some form for w_0 it must be observed that the right-hand side of (14) contributes terms like $\cos W, \sin^2 \omega t$ which in turn can be reduced to terms with $\cos 2 \omega t, \sin 2 \omega t$ and steady state, i.e., time-independent terms. Hence, under these circumstances we can express the first-order cross-flow as

$$w_0(x, z, y, t) = \sum_{\alpha} \hat{\psi}_{\alpha}^*(y) e^{i \alpha z} + \hat{\psi}_0(y) \quad (31)$$

where $\hat{\psi}_{\alpha}^*(y)$ and $\hat{\psi}_0(y)$ denote respectively the periodic and the steady state contributions. Substituting (31) in (15) we get

$$\psi_{\alpha\alpha}'' - 2i\psi_{\alpha\alpha}' = 1 - \phi_0'^2 \quad (32)$$

$$\psi_{00}'' = 1 - \phi_0' \bar{\phi}_0 \quad (33)$$

where the bar indicates the complex conjugate. The actual boundary conditions are that the cross-flow should vanish both at the wall and at large distances from it. But as will be seen that though the fluctuating part can be made equal to zero at both the points ($y = 0, \infty$) the steady part can be made zero only at the wall and not at infinity. At the most we can see that it is finite at infinity.* Hence, with this point in view we obtain the solutions for (32) and (33) as

$$\psi_{\alpha\alpha} = P e^{-\alpha y} + 0.5 e^{-2\alpha y} - 2.5 \frac{e^{-\alpha y}}{\alpha} \quad (34)$$

$$\psi_{00} = 0.5(1 - e^{-\alpha y}) - 2e^{-M^*} \sin \frac{y}{\alpha} \quad (35)$$

so that

$$\psi_{00}(\infty) = 0.5,$$

Hence, the cross-flow is seen to contain a steady state term which does not vanish outside the boundary layer. Now the actual expression for this first-order cross-flow is given by

$$\begin{aligned}
 w_0(s, z, y, t) &= \frac{U_0^2}{2\omega h_1} \frac{\partial h_1}{\partial z} \left[2e^{-y/\sqrt{2}} \sin\left(\frac{y}{\sqrt{2}} - 2\omega t\right) \right. \\
 &\quad + 0.5 \langle n^{**}v \sin W2y \sim 2a \rangle t - 2.5 e^{-v} \sin(y - 2 \langle ot \rangle) \\
 &\quad \left. + 0.5 (1 - en/**v) - 2 \langle \langle r y / \sqrt{2} \rangle \sin \sqrt{2} J \right] \tag{36}
 \end{aligned}$$

The streamwise and the crosswise velocity profiles

$$2a > A_x h z$$

given by equations (28) and (36) respectively are plotted in Figs. 1, 2a and 2b. In Fig. 2a the fluctuating velocity component $*v_M*$ of the

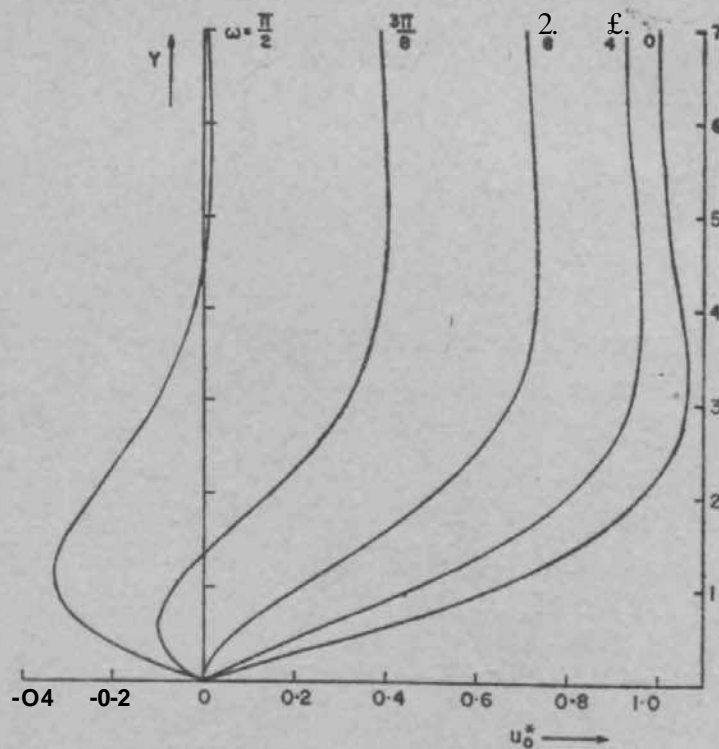
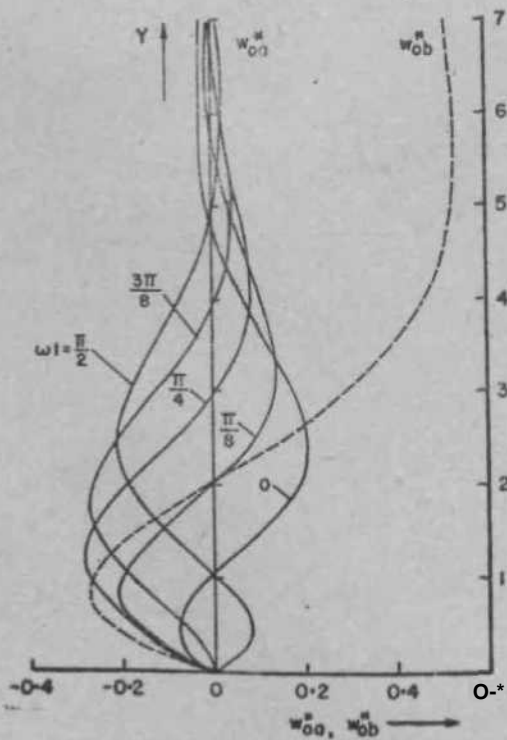


FIG. 1. First order streamwise velocity profiles
 In curves 3 and 4 for $\omega = \pi/8$, $w/4$ read respectively $w t - \pi/2$, $\pi/4$ and $\pi/8$.

As has been done by Stuart,* it may be necessary to do a separate analysis assuming an outer boundary layer in between the potential flow and the inner boundary layer, in which the flow is irrotational and satisfies the boundary conditions of zero velocity at infinity.

cross-flow for different mt and its steady velocity component w_0^{*} are plotted separately whereas in Fig. 2b the resultant cross-flow for the same values of wt are plotted. In both these figures the dotted line indicates the steady component. It may be recalled that in reference (2) (and also here) this interesting feature of the oscillatory potential flow, namely, the existence of a steady stream outside the boundary layer is observed only in the second approximation for the velocity and there an experimental evidence is also provided. The existence of the steady stream can be explained as due to the fact that the negligence of inertial terms in the first-order equations is valid only very near to the wall and the Reynolds stresses in this oscillatory boundary layer cause the formation of steady streaming flow: and there is an outer boundary layer within which this steady streaming velocity decays to zero. The thickness of this outer layer is large compared with that of the inner oscillatory layer, but small compared with a typical dimension of the body. These observations are also confirmed by Riley.⁴ But an evidence for steady 'streaming motion*' in the cross-flow direction is yet to forthcome.



Fia. 2 (a)

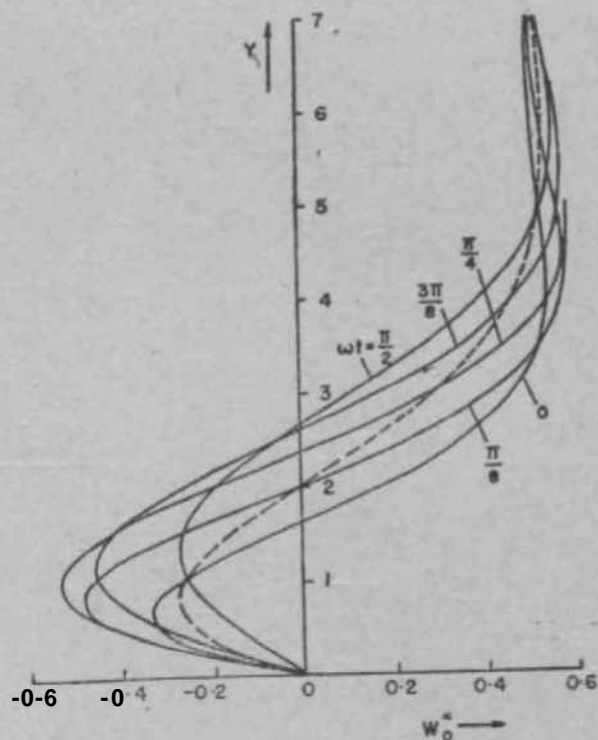


FIG. 2 (b)

Fio. 2 (a). First order crosswise velocity profiles.

(H_M^* - fluctuating part, $w_{,b}^*$ - steady part)

Fro. 2 (6). First order crosswise velocity profiles (Resultant).

Second approximation.—The differential equations governing the second approximation are (17), (18) and (19). Using real parts of (10), (22) and (23) to calculate the right-hand side of (17) we obtain the differential equation for u_x as

$$\begin{aligned} \frac{\partial u_1}{\partial t} - \nu \frac{\partial^2 u_1}{\partial x^2} &= \frac{1}{2} \left[U_0 \frac{\partial U_0}{\partial S} \left\{ (1 - \phi_0'^2 + \phi_0 \phi_0'') e^{2i\omega t} \right. \right. \\ &\quad \left. \left. + \left(1 - \phi_0' \bar{\phi}_0' + \frac{\phi_0 \bar{\phi}_0'' + \bar{\phi}_0 \phi_0''}{2} \right) \right\} + \frac{U_0^2}{h_2} \frac{\partial h_2}{\partial S} \right. \\ &\quad \left. \times [MS^{**} + \frac{1}{2} M''] \right]. \end{aligned} \quad (37)$$

Hence, it would be appropriate to write the solution of u_{\pm} in the form

$$\begin{aligned} u_1 &= \frac{1}{2\omega} \left[e^{2i\omega t} \left\{ U_0 \frac{\partial U_0}{\partial S} \phi_{11}'(y) + \frac{U_0^2}{h_2} \frac{\partial h_2}{\partial S} \phi_{12}'(y) \right\} \right. \\ &\quad \left. + \left\{ U_0 \frac{\partial U_0}{\partial S} \phi_{13}'(y) + \frac{1}{2} M'' \right\} \right]. \end{aligned} \quad (38)$$

with this we get the following four differential equations:

$$\phi_{11}''' - 2i\phi_{11}' = - (1 - \phi_0'^2 + \phi_0 \phi_0''), \quad (39)$$

$$\phi_{12}''' - 2i\phi_{12}' = - \phi_0 \phi_0'', \quad (40)$$

$$\phi_{13}''' = - \left(1 - \phi_0' \bar{\phi}_0' + \frac{\phi_0 \bar{\phi}_0'' + \bar{\phi}_0 \phi_0''}{2} \right), \quad (41)$$

$$\phi_{14}''' = - \frac{\phi_0 \bar{\phi}_0'' + \bar{\phi}_0 \phi_0''}{2}. \quad (42)$$

The boundary conditions are:

$$\begin{aligned} 011(0) &= *u'(0) = *u'(00) = 0 \\ \wedge \ll (0) &= 4 > i \dot{2}'(0) = \wedge 12'(00) = 0 \\ 0i \gg (0) &= V(0) = 0i4(0) = 0i4'(0) = 0 \\ 018(0^\circ) &\gg 014(0^\circ) < 00, \end{aligned} \quad (43)$$

Equations (39H43) have solutions:

$$\phi_{11}' = i [(1 - x) e^{-x} - e^{-\sqrt{2}x}] \tag{44}$$

$$\phi_{12}' = i \left[(3 - x) e^{-x} + \frac{e^{-2x}}{2} - \frac{7}{2} e^{-\sqrt{2}x} \right] \tag{45}$$

$$\begin{aligned} \phi_{13}' = & -\frac{3}{2} + \frac{e^{-\sqrt{2}y}}{2} + e^{-y/\sqrt{2}} \left[4 \sin \frac{y}{\sqrt{2}} + \cos \frac{y}{\sqrt{2}} - \frac{y}{\sqrt{2}} \right. \\ & \left. \times \left(\cos \frac{y}{\sqrt{2}} - \sin \frac{y}{\sqrt{2}} \right) \right] \end{aligned} \tag{46}$$

$$\begin{aligned} \phi_{14}' = & -1 + e^{-y/\sqrt{2}} \left[\cos \frac{y}{\sqrt{2}} + 2 \sin \frac{y}{\sqrt{2}} - \frac{y}{\sqrt{2}} \right. \\ & \left. \times \left(\cos \frac{y}{\sqrt{2}} - \sin \frac{y}{\sqrt{2}} \right) \right]. \end{aligned} \tag{47}$$

" From the above four solutions the functions $\langle f \rangle_w$, $\langle f \rangle_{12}$, $\langle f \rangle_{13}$ and $\langle f \rangle_{14}$ can be obtained by integrating once. Then equation (18) gives the solution for v_x in the form

$$\begin{aligned} v_x = & -\frac{1}{\sqrt{f}} \frac{1}{\cos 2cu/t_2} \left[\frac{\partial (h_2 U_0 \frac{\partial U_0}{\partial s})}{\partial s} (\phi_{11} e^{2i\omega t} + \phi_{12}) + \frac{\partial (U_0^2 \frac{\partial h_2}{\partial s})}{\partial s} \right. \\ & \left. \times (\phi_{13} e^{2i\omega t} + \phi_{14}) \right]. \end{aligned} \tag{48}$$

It may be observed in the right-hand side of the equation (37) that the curvature lh^s brings in additional functions $\langle f \rangle_{12}$ and $\langle f \rangle_{14}$ into existence. These are absent in a two-dimensional rectangular or cylindrical system of co-ordinates. This is an additional feature of the second-order stream-wise velocity component in general three-dimensional flow.

Second-order cross-flow.—The differential equation for the second-order cross-flow is given by the equation (19). From the already known solutions of v_0 , v_Q and v_t the right-hand side of this equation can be easily written down in terms of $\langle f \rangle_s$ and $\langle f \rangle_{12}$ as:

$$= \sum_{j=1}^7 F_j [X_j + X_{(j+1)} e^{i\omega t} + X_{(j+2)} e^{2i\omega t}]$$

$$+ \dots$$

where

$$F_1 = \frac{U_0^2}{4\omega^2 h_1} \left(\frac{\partial h_1}{\partial z} \right)^2, \quad F_2 = \frac{U_0^4}{4h_1^2 \omega^2} \frac{\partial h_1}{\partial z} \left(\frac{\partial h_2}{\partial s} \right)^2,$$

$$F_3 = \frac{U_0^3}{4\omega^2 h_1 h_2} \frac{\partial h_1}{\partial z} \frac{\partial}{\partial s} \left(\frac{U_0^2}{h_1} \frac{\partial h_1}{\partial z} \right),$$

$$F_4 = \frac{U_0^2}{4\omega^2 h_1 h_2} \frac{\partial h_1}{\partial z} \frac{\partial}{\partial s} \left(U_0 h_2 \frac{\partial U_0}{\partial s} \right),$$

$$F_5 = \frac{U_0^2}{4\omega^2 h_1 h_2} \frac{\partial h_1}{\partial z} \frac{\partial}{\partial s} \left(U_0^2 \frac{\partial h_2}{\partial s} \right), \quad F_6 = \frac{U_0^2}{\omega h_1} \frac{\partial h_1}{\partial z} \frac{\partial U_0}{\partial s},$$

$$F_7 = \frac{U_0^2}{4\omega^2 h_1 h_2} \frac{\partial h_1}{\partial z} \frac{\partial}{\partial s} \left(U_0^2 \frac{\partial h_2}{\partial s} \right), \quad F_8 = \frac{U_0^2}{\omega h_1} \frac{\partial h_1}{\partial z} \frac{\partial U_0}{\partial s},$$

$$F_9 = \frac{U_0^2}{2\omega A} \frac{D^a a^a Up}{\partial s},$$

and

$$X_1 = \dots$$

$$X_2 = \dots$$

$$X_3 = \phi_{13}' \phi_{14}' + \frac{\phi_{11}' \bar{\phi}_{12}' + \bar{\phi}_{11}' \phi_{12}'}{4},$$

$$X_4 = \psi_{0b} \phi_{13}' + \frac{\psi_{0a} \bar{\phi}_{11}' + \bar{\psi}_{0a} \phi_{11}'}{4},$$

$$X_5 = \psi_{0b} \phi_{14}' + \frac{\psi_{0a} \bar{\phi}_{12}' + \bar{\psi}_{0a} \phi_{12}'}{4},$$

$$\begin{aligned}
 \chi_1 &= \psi_{0b}'\phi_{13} + \frac{\phi_{11}\bar{\psi}_{0a}' + \bar{\phi}_{11}\psi_{0a}'}{4}, \\
 \chi_2 &= f_c r t u + \frac{\phi_{12}\bar{\psi}_{0a}' + \bar{\phi}_{12}\psi_{0a}'}{4}, \quad \chi_3 = \phi_{13}W + \frac{\bar{\phi}_0 \bar{\psi}_{11}}{2} \\
 \chi_4 &= \phi_{14}'\phi_0' + \frac{\bar{\phi}_0'\phi_{12}'}{2}, \quad \chi_{10} = \psi_{0b}\phi_0' + \frac{\bar{\phi}_0'\psi_{0a}}{2} \\
 \chi_{11} &= \psi_{0b}'\phi_0 + \frac{\bar{\phi}_0\psi_{0a}'}{2}, \quad \chi_{12} = 2\phi_{13}'\phi_{11}', \quad \chi_{13} = 2\phi_{14}'\phi_{12}', \\
 \chi_{14} &= \phi_{13}'\phi_{12}' + \phi_{14}'\phi_{11}', \quad \chi_{15} = \psi_{0b}\phi_{11}' + \phi_{13}'\psi_{0a}, \\
 \chi_{16} &= \psi_{0b}\phi_{12}' + \phi_{14}'\psi_{0a}, \quad \chi_{17} = \phi_{13}\psi_{0a}' + \phi_{11}\psi_{0b}', \\
 \chi_{18} &= \phi_{14}\psi_{0a}' + \phi_{13}\psi_{0b}', \quad \chi_{19} = \frac{\phi_0'\phi_{11}'}{2}, \quad \chi_{20} = \frac{\phi_0'\phi_{13}'}{2}, \\
 \chi_{21} &= \frac{\phi_0'\psi_{0a}}{2}, \quad \chi_{22} = \frac{\phi_0\psi_{0a}'}{2}, \quad \chi_{23} = \frac{\phi_{11}'^2}{2}, \quad \chi_{24} = \frac{\phi_{12}'^2}{2} \\
 \chi_{25} &= \frac{\phi_{11}'\phi_{12}'}{2}, \quad \chi_{26} = \frac{\psi_{0a}\phi_{11}'}{2}, \quad \chi_{27} = \frac{\psi_{0a}\phi_{12}'}{2}, \quad \chi_{28} = \frac{\phi_{11}\psi_{0a}'}{2} \\
 \chi_{29} &= \frac{\phi_{12}\psi_{0a}'}{2}.
 \end{aligned} \tag{50}$$

Hence, it is seen that the solution of the second-order cross-flow has to be written in the form

$$\begin{aligned}
 w_1 &= \sum_{j=1}^7 F_j \psi_j + e^{i\omega t} \sum_{j=8}^{11} F_j \psi_j + e^{2i\omega t} \sum_{j=1}^7 F_j \psi_{(j+11)} \\
 &\quad + e^{3i\omega t} \sum_{j=8}^{11} F_j \psi_{(j+11)} + e^{4i\omega t} \sum_{j=1}^7 F_j \psi_{(j+22)}.
 \end{aligned} \tag{51}$$

The second-order cross-flow is thus found to consist of fluctuating flow with frequencies ω , 2ω , 3ω and 4ω in addition to a steady streaming component which does not vanish outside the boundary layer. On substitution of (51) in the equation (19) we obtain twenty-nine ordinary linear second-order differential equations with constant coefficients which are easily solvable analytically. They can be formally written as:

$$*i^m = - \chi_i$$

$$\begin{aligned}
 \psi_k'' - i^*l^*k &= - Xk \\
 \psi''_{(j+11)} - 2i\psi_{(j+11)} &= - X(j+11) \\
 \psi''_{(k+11)} - 3i\psi_{(k+11)} &= - X(fc+u) \\
 \psi''_{(j+22)} - 4i\psi_{(j+22)} &= - X(j+22)
 \end{aligned} \tag{52}$$

where $j = 1, 2, 3, \dots, 7$; $fc = 8, 9, 10$ and 11 , and the x s are as given in equation (50).

REFERENCES

1. Eichelbrenner, E. A. and Askovic, R. .. "Sur une methode approchee de traiter les couches limites laminaires en regime instationnaire dun ecoulement dans un fluide incompressible a trois dimensions," *J. de Mecanique*, 1967, 6, 353.
2. Schlichting, H. .. *Boundary Layer Theory. Chapter XL* McGraw-Hill, 1960.
3. Stuart, J. T. .. "Double boundary layers in oscillatory viscous flow," *N.P.L. Aero. Report*, 1965, p. 1153.
4. Riley, N. .. "Oscillating viscous flows," *Mathematika*, 1965, 12, 161.

ENERGY SPECTRUM AND THE ABSOLUTE FLUX OF VARIOUS CELESTIAL X-RAY SOURCES

BY U. R. RAO, F.A.S.C, E. . CHITNIS, A. S. PRAKASA RAO

AND

U. B. JAYANTHI

(*Physical Research Laboratory, Ahmedabad, India*)

Received July 12, 1969

ABSTRACT

The results on the flux of low energy X-rays in the range 2-18 Kev from Sco-X1, Tau-X1 and Cen-X2 celestial sources observed during two rocket flights, flown from the Thumba Equatorial Rocket Launching Station (TERLS), Trivandrum, India, are presented. The absolute flux and the energy spectrum obtained for these sources are compared with other similar observations. The results indicate a long-term exponential decrease in the energy flux of X-rays from Sco-X1 over the period 1965-1968. The X-ray source Cen-X2, which showed a remarkable outburst of X-rays in April 1967, had ceased to be active after May 1967. We present here the first evidence of the rediscovery of the low energy, X-ray flux from Cen-X2 since May 1967. These short-lived X-ray outbursts may be attributed to a shock wave from the nova outburst expanding into the circumstellar medium.

INTRODUCTION

SINCE the discovery of stellar X-ray source Sco-X1 by Giacconi *et al*¹ in 1962, a number of experiments have been performed by different groups for determining the absolute flux and the energy spectrum of various galactic as well as extra-galactic X-ray sources. After the optical identification of Sco-X1 by Sandage *et al.*² a large number of photometric observations have been conducted by Hiltner and Mook³ and others. Such studies have clearly revealed that the optical intensity of Sco-X1 undergoes very rapid variations between 12-2 and 13-2 magnitudes, large flare type enhancements occurring during nearly 50% of the time when Sco-X1 is brighter than 12-6 magnitude. A search by Rao *et al.** for hidden periodicities has shown that besides rapid fluctuations, Sco-X1 optical intensity varies by about a factor of two with a periodicity of about 3 hours. Recent radio observa-

tions by Andrew and Purton⁵ and Abies⁶ have also shown the existence of similar variations in the radio emission from Sco-X1. The possibility of finding correlated changes in X-ray, optical and radio emissions from the same object is truly exciting and will reveal a common origin for the widely different radiations. The observation of X-ray flare from Sco-X1 at balloon altitudes by Lewin *et al.*⁷ and the discovery of the highly variable source Cen-X2 by Harries *et al.*⁸ have focussed a great attention on the systematic measurements of the absolute flux and the time variation of X-ray luminosity from different celestial sources.

In this paper, we describe the results of the two rocket flights carried out from the Thumba Equatorial Rocket Launching Station (TERLS), Trivandrum (Geogr. Latitude $8^{\circ} 32' N$; Geogr. Longitude $76^{\circ} 51' E$), India. Two identical X-ray payloads were launched, one on a Centaure rocket at 0319 UT on November 3, 1968 and the second on a Nike-Alpache rocket at 0305 UT on November 7, 1968 almost vertically (85° elevation) such that the X-ray detector mounted with its axis perpendicular to the spin axis of the rocket scanned the rocket horizon. The launch time was chosen when the Sco-X1, Cen-X2 and Tau-X1 were all in the rocket horizon. The present experiments were conducted with the following objectives:

(a) To measure the absolute flux and the energy spectrum of Sco-X1, Tau-X1 and Cen-X2 in the energy range 2-20 Kev.

(b) To measure the time variability of the X-ray flux from these sources in the above energy range.

(c) To conduct a survey of the southern sky with a view to detect hitherto undiscovered X-ray sources.

INSTRUMENTATION

The X-ray detector consisted of a proportional counter filled with Xenon (90%) and Methane (10%) at one atmospheric pressure and having a 2 mil. thick Beryllium entrance window. The counter had an effective path length of 2 inches. The counter resolutions were typically 15% full width half-maximum at 6.0 Kev (Fe^{5*}) and 22% full width half maximum at 22 Kev (Cd^{109}). A slat type collimator mounted in front of the proportional counter defined a $8.7^{\circ} \times 17.2^{\circ}$ full width half-maximum field of view, with the long axis parallel to the spin axis of the rocket. The effective area of the counter, after taking into account the collimator occultation, was 60-8 cm.². Figure 1 shows the detector. In Fig. 2 is shown the calculated efficiency of the

counter as a function of X-ray quantum energy. The efficiency of the counter $S(X)$ is calculated using the well-known equation

$$S(\lambda) = e^{-\mu_w \chi_w} (1 - e^{-\mu_g \chi_g})$$

where μ_w and μ_g are the absorption coefficients of the window and the gas and χ_w and χ_g are the respective path lengths.

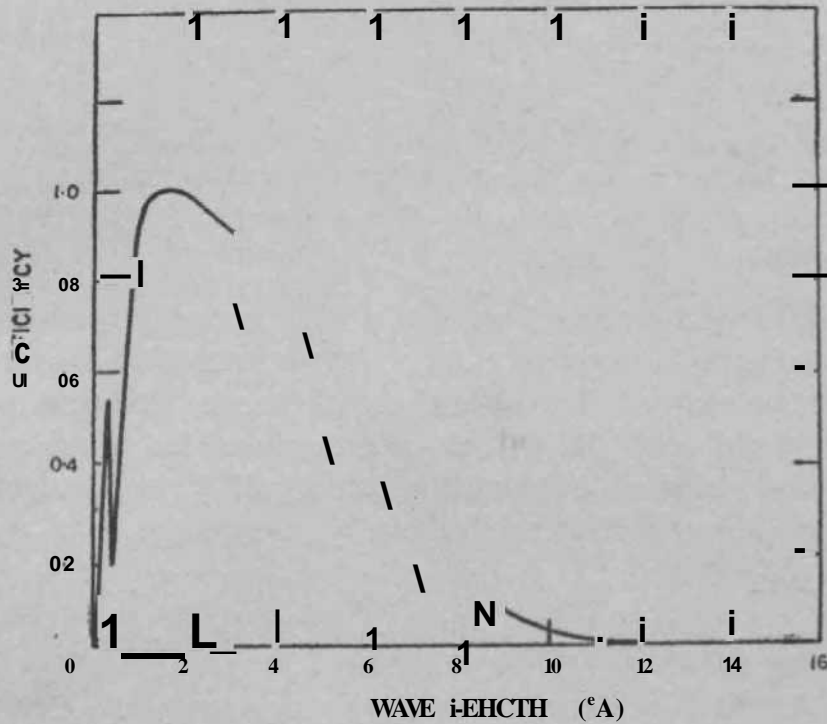


FIG. 2. Efficiency of the proportional counter filled with Xenon (90%) and Methane (10%) at 1 atmospheric pressure and having a 2 mil. thick Beryllium window.

The pulses from the proportional counter were amplified, shaped and pulse height analysed in the energy range 2-18 Kev into four consecutive energy windows. A redundant analogue signal giving the actual pulse height of each pulse was also telemetered separately. The entire information was telemetered by FM/FM telemetry system. Monitoring of the 6.0 Kev line from the Fe^{55} radioactive source mounted on the split nosecone provided the inflight calibration upto 70 Km., at which altitude, the source and the nosecone were explosively ejected.

The attitude of the rocket was determined by two suitably mounted geomagnetic aspect sensors, one along the spin axis and another perpendicular to it. The alignment of the detector and the geomagnetic aspect sensors were made to an angular accuracy better than 0.1° . Both the Centaure and Nike-Apache rockets reached an apogee of about 160 Km. Out of

the total flight time of about 420 seconds, useful X-ray data above 90 Km. altitude were obtained for about 200 seconds.

ASPECT ANALYSIS

Assuming the rocket to behave like a rigid body, one can estimate the half apex-angle of the precession cone a , using the well-known formula

$$\cos a = \frac{H^* - A}{\omega_p I_2 - H}$$

where ω_s and ω_p are the angular velocities of spin and precession respectively and I_x and I_2 are the moments of inertia relative to the spin axis and a direction perpendicular to it. The above serves as a crude estimate of the precession cone angle.

After deriving the approximate spin and precession periods from the horizontal and vertical magnetic sensors, a spin precession diagram is drawn showing the time dependence of the phase of the magnetic field in each spin during each precession. Adjustment of the spin period to achieve synchronization of the phase of the magnetic record will yield the right spin and precession periods which can be normally represented as a power series in time t as

$$\omega_s + \omega_p = W_0 + At + Bt^2 + \dots$$

where W_0 , A and B are constants. In practice, only the first two terms are of importance.

The peak-to-peak amplitude of the horizontal magnetic sensor ($2M$) is equal to $2M_{Bas} \sin \theta$ where θ is the angle between the spin axis and the magnetic vector. The equation $\sin^{-1} \theta = 2M/2M_{nrt}$ is used to determine θ at each maximum of the magnetometer, taking into account the variation of M_{nrt} with altitude using the Finch and Leaton expansion of the geomagnetic field. Knowing θ for each spin, one can construct the precession circle which is correct to probably within a few degrees. It must be noted that θ will vary between the two limits of $a + \delta$ and $a - \delta$ where a is the halfcone precession angle and δ is the inclination of the precession axis to the vertical. The celestial co-ordinates calculated using the well-known formulas of spherical astronomy at the time of two launches are given in Table I.

A further refinement of the attitude was accomplished by using the successive Sco-XI sighting. From the spin phase diagram for the passage

of X-ray source Sco-X1, the average spin phase difference between Sco-X1 and the magnetic direction which was about 118° and the variation of X-ray intensity in each precession cycle has been employed to refine the precession axis of the rocket to better than 1° using the method described by Wada *et al.*⁹

TABLE I
Celestial Co-ordinates at the Time of Launching

	Flight I		Flight II	
	R.A.	Declination	R.A.	Declination
Sun	.. 14 ^h 33'	-15° 1'	14 ^h 49'	-16° 14'
Zenith	.. 11 ^h 18'	8° 33'	11 ^h 16'	8° 33'
Magnetic field	.. 0 ^h 42'	81° 54'	0 ^h 40'	81° 54'

The spin stabilized Centaure rocket flown on November 3, 1968, with a spin rate of about 8 RPS, had its axis centered at 10^h 18' Right Ascension and 15-0°N. declination on the celestial sphere. Consequently, the X-ray detector was able to look at Sco-X1 and Cen-X2 sources during the entire duration of the flight (about 200 seconds from 90 Km. altitude to the time of entry into the atmosphere). The Nike-Apache rocket launched on November 7, 1968, however, got into precession after the ejection of the nosecone at 70 Km. and its spin rate which was initially about 9 RPS, changed to about 2-8 RPS. after the nosecone ejection. The precession axis of the rocket, as derived from the attitude sensor analysis described above and Sco-X1 sighting, is 10^h 8' R.A. and 36° N. declination with the half-cone precession angle being 54°. In the 7 precessions containing 93 spins each, Sco-X1, Tau-X1 and Cen-X2 sources were all scanned for about 8-9 consecutive spins. Figure 3 shows the relevant trajectories of the detector axis in the celestial sphere for both the flights.

The data from all the spins from the Centaure rocket launched on November 3, 1968 have been summed up. Figure 4 shows the observed X-ray counting rates in the energy range 2-6 Kev, as a function of the rocket azimuth. For the flight of November 7, 1968 (Nike-Apache), the data for all consecutive scans during which each source could be observed are summed up and presented in Fig. 5. The relevant scan numbers are also indicated in the figure. In both the figures, the position of Sco-X1, Tau-X1 and

Cen-X 2 sources are marked. The observed data in each scan (spin) was fitted to a theoretical response function of the type $A.g. (t - t_0)$ where A is the absolute strength of the source, t_0 is time of maximum response and $g(0) = 1$. The response is obviously a triangular one with a base equal to $17/360 \times T_s$ where r_s is the spin period. A and t_0 are chosen for least square fitting, *i.e.*, when

$$E = \sum_t [X(t_i) - A.g.(t_i - t_0)]^2$$

is a minimum. Having obtained the source strength as observed in each scan, the least square method is applied again for consecutive scans, in an identical manner as explained above to obtain the absolute flux of the source.

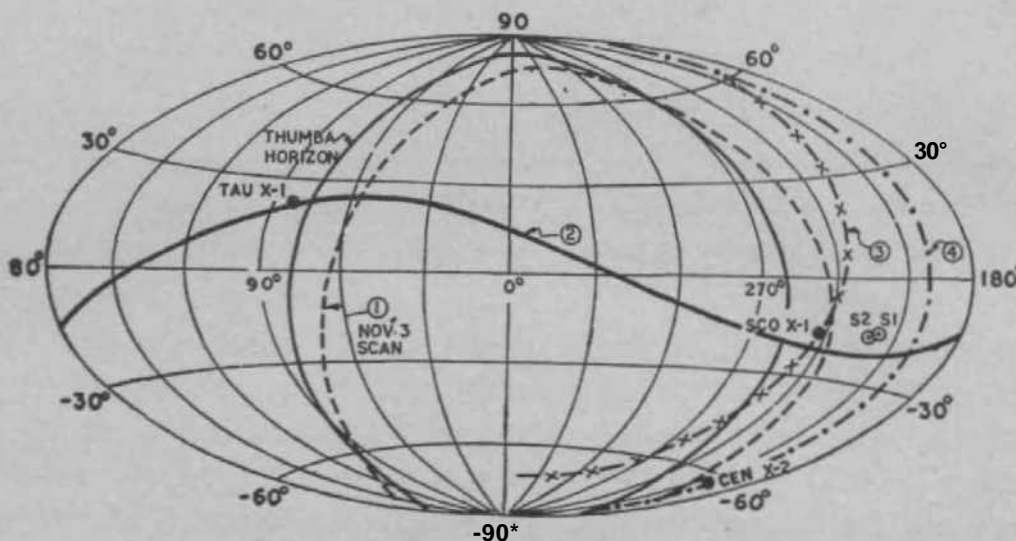


FIG. 3. Trajectories of sky scans for the two flights of November 3, 1968 (Number 1) and November 7, 1968 (Numbers 2, 3 and 4). The Thumba horizon at the time of launching is also indicated. S1, S2 indicate positions of sun on November 3 and November 7 respectively.

ABSOLUTE FLUX OF TAU-X1 SOURCE

Figure 6 shows the energy spectrum of Tau-X1 in the range 2-18 Kev. The observations by Chodil *et al.*¹⁰ and Boldt *et al.*ⁿ are also plotted in the same figure. Our results show an excellent agreement with the observations made by other workers and are consistent with a power law energy spectrum of the type

$$f(E) = 8.0 E^{-0.9 \pm 0.2} dE$$

The flux in the energy range 2-5 Kev is found to be $(1.6 \pm 0.3) \times 10^{-8}$ ergs/cm.² sec.

The recent discovery of an X-ray pulsa by Fritz *et al.*¹² in the general direction of the crab nebula and its tentative identification with the optical

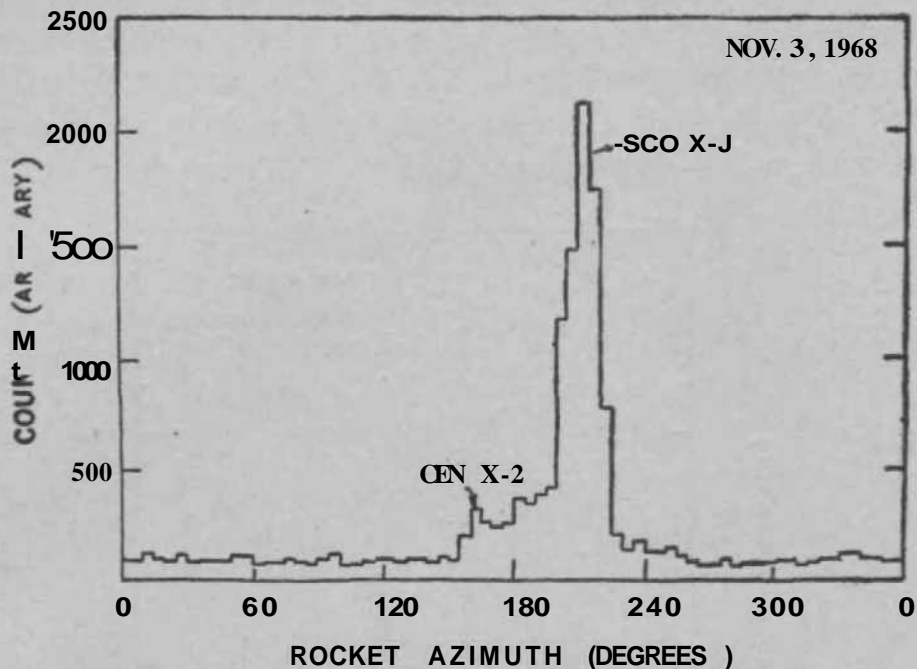


FIG. 4. Observed X-ray counting rates in the energy range 2-6 Kev as a function of rocket azimuth for the flight of November 3, 1968.

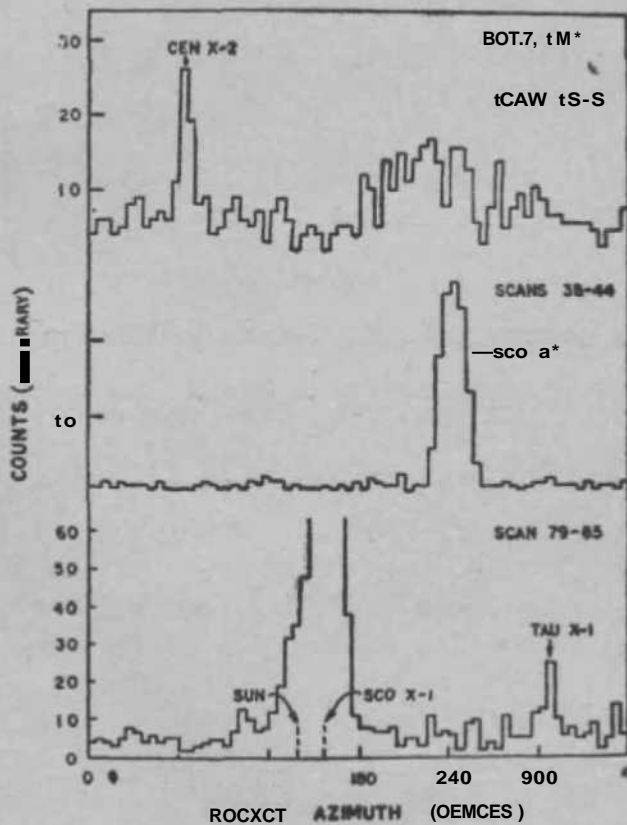


FIG. 5. Observed X-ray counting rates in the energy range 2-6 Kev as a function of rocket azimuth for the flight of November 7, 1968,

pulsar NP 0532 has increased the importance of the study of this X-ray source. The frequency of the X-ray pulsations in the crab nebula is in close agreement with the frequency of radio and optical pulsations. However, since only 5 per cent of the total X-ray power of the nebula appears in the pulsed component, the absolute flux of X-ray from Tau-XI is practically constant which is also borne out from our observations which are in close agreement with other observations made at different times.

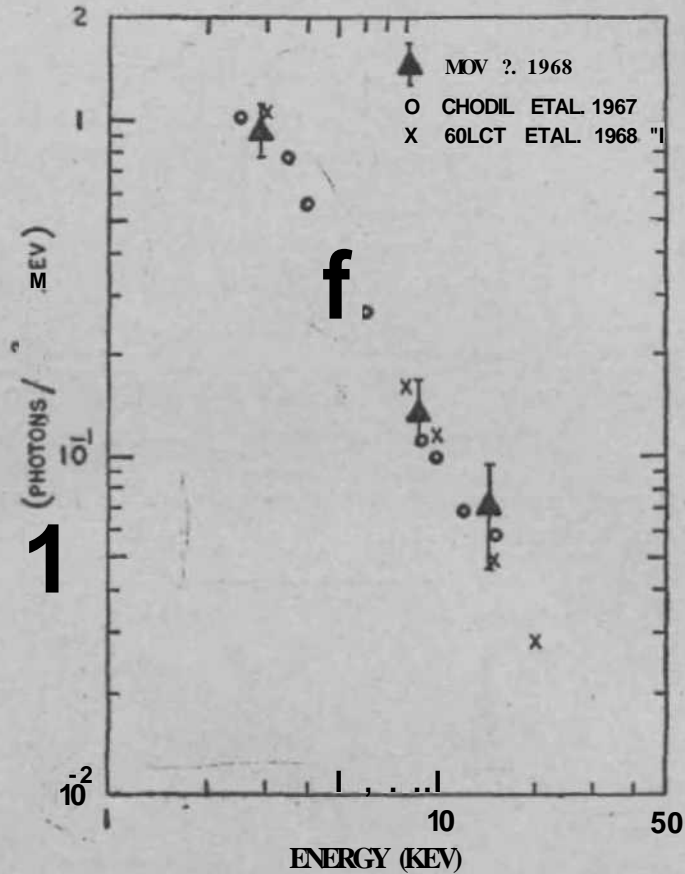


Fig. 6. Energy spectrum of Tau-XI X-ray source in the range 2-18 KeV.

ABSOLUTE FLUX AND TIME VARIATION OF Sco-X1

Figure 7 shows the observed counting rate as a function of the rocket azimuth for different energy windows of nominal value 2-4 KeV 4-6 KeV 6-12 KeV and 12-18 KeV for both flights of November 3, 1968 and November 7, 1968 respectively. The data have been fitted to an energy spectrum of the type

$$I(E) = K \exp^{-E/E_0} dE$$

The value of E_0 for both the flights has been found to be 4.4 ± 0.2 KeV corresponding to a temperature of a hot thin plasma of 5.1×10^7 K. The

energy spectrum beyond 12 FceV, however, is consistent with only $E_0 \ll 18$ Kev in agreement with the observations of Busseli *et al.*¹² The flattening of the spectrum at higher energies has been explained in terms of the multi-layer complex model for Sco-X1 proposed by Shklovsky,¹⁴ the higher energies being emitted from the higher temperature plasma in the core of the object.

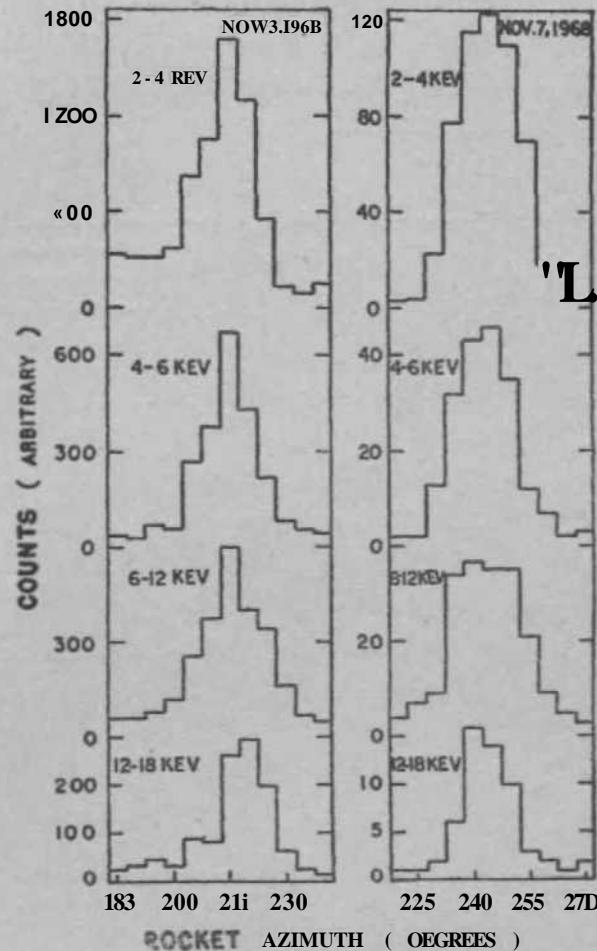


Fig. 7. X-ray count rate of Sco-X1 source for different differential energy windows.

In Fig. 8 are plotted the observational data on the intensity of low energy X-ray flux in different windows observed during the two flights. The observations of Chodil *et al.*,¹⁵ Hill *et al.*¹⁶ and Overbeck *et al.*¹⁷ are also plotted in the same figure. Our observations are in quite a good agreement with the observations by other workers.

Investigation of the time variation of the absolute flux of Sco-X1 is of great importance in understanding the nature of the source. The large number of observations in the visible, in the near ultraviolet by Hiltner and Mook and by Stepien,¹⁸ in the near infrared by Neugebauer *et al.*,¹⁹ and in

the radio region by Andrew and Purton have all pointed out to the large variability of Sco-XI. Simultaneous optical and X-ray measurements by Chodil *et al.*¹¹ has shown that the brighter optical intensity is accompanied by a lower temperature and a bluer emission spectrum. The measurements seem to be consistent with the model of both the X-ray and optical continuum being produced by thermal bremsstrahlung from the same hot thin plasma. Observations of X-ray flares from Sco-XI at balloon altitudes by Lewin *et al.*¹⁰ and Agarwal *et al.*¹⁰ seem to add strength to the above hypothesis, even though a large number of simultaneous optical and X-ray observations of Sco-XI are needed to make any positive conclusion regarding the nature of the source.

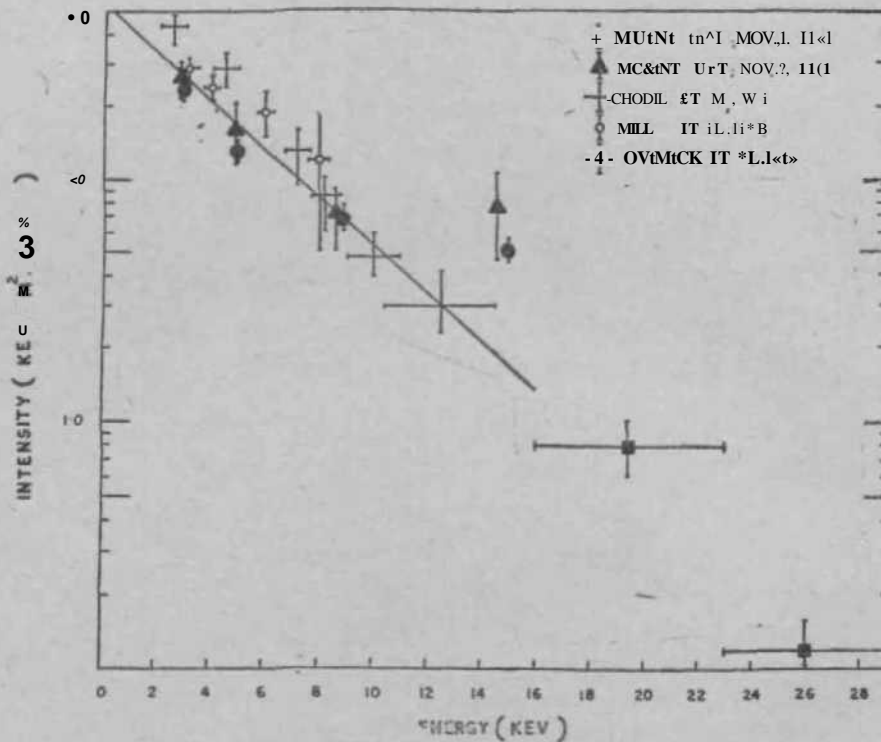


FIG. 8. Energy spectrum of Sco-XI X-ray source in the energy window 2-18 KeV.

Taking reasonable numbers for the distance of Sco-XI and the total energy flux as 1000 light-years and 6×10^{30} ergs/sec, respectively, the radius of Sco-XI has been estimated to be between 3×10^{10} and 10^{13} cm. In order to keep the X-ray source going, the cooling time of the cloud, which is variously estimated between 10 and 10^6 seconds, should be of the same order as the heating time. This would indicate the possible existence of time variations in the X-ray flux from Sco-XI, having a time scale of 10 to 10^6 seconds. We do not observe any statistically significant variation between the absolute flux of Sco-XI measured on November 3, 1968 and November 7, 1968. Addition over shorter periods of time have also been intercompared to make

sure that statistically significant variations of Sco-X1 flux over periods of about 4 minutes do not exist. We may, however, point out that Overbeck *et al.* have reported significant time variations over time scales of about a month for X-rays in the energy range 16-30 Kev at balloon altitudes. Even though such large variations in the high energy flux can result from very small changes in temperature, nevertheless, the evidence together with the flare-like increases of X-ray flux strongly indicate the time variability of Sco-X1 X-ray source.

In Fig. 9 is shown the measurements of absolute flux of X-rays from Sco-X1 since 1965. Since many of the observations in the past did not have their sensor and attitude well calibrated, only those measurements from which reasonably accurate measurements can be derived are plotted in the figure. Table II gives the flux at 4-0 Kev, 6-0 Kev and the energy in the range 2-5 Kev as well as the temperature. It is evident from the figure as well as the table that the absolute flux of Sco-X1 has undergone significant time variations. The most conspicuous result from Fig. 9 is that the flux and the energy of Sco-X1 has steadily decreased over the period 1965-1968. Sporadic short time variations are superimposed upon

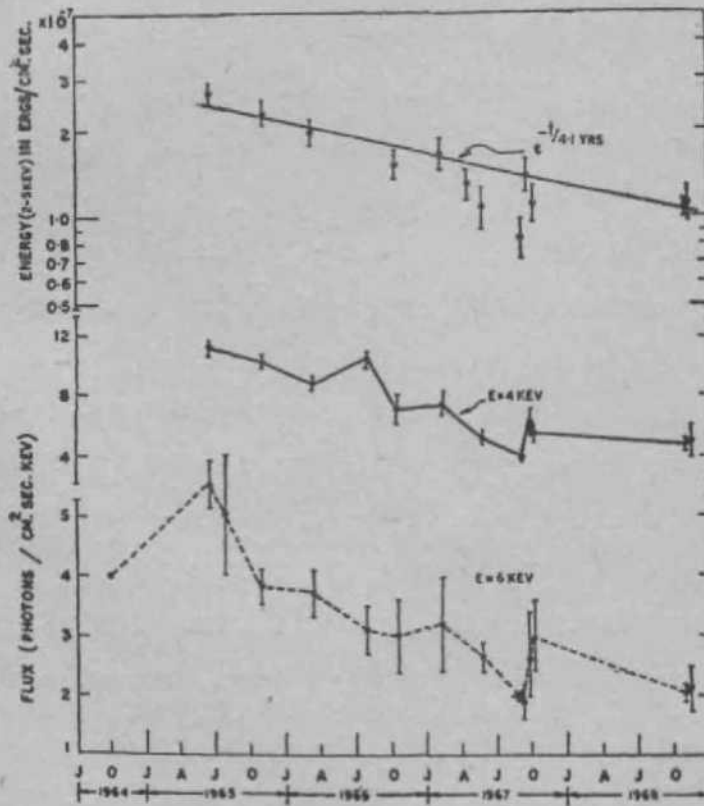


FIG. 9. Time variation of the flux and energy spectrum of Sco-X1 X-ray source during 1964-1968.

this general decrease in flux. The observations indicate that the general pattern of the time variation of Sco-X1 is consistent with an exponential decay of X-ray luminosity with a time constant of about 4-1 years which would mean that the flux of Sco-X1 would decrease by two orders of magnitude in a period of about 20 years.

TABLE II
Time variation of SCQ-X1

Experimenter	Flight date	Flux of 4 Kev photons/cm. ² sec. Kev	Flux of 6 Kev photons/cm. ² sec Kev	Energy (2-6 Ksv range) X 10 ⁻⁷ ergs/cm. ² sec.	Temperature X10 ⁷⁰ K
Fisher <i>et al.</i> ²¹ ..	1 October 1964	..	4*0	..	1-6
Chodilrftf/. ⁸² ..	12 June 1966	11-26 ±0-6	5-5±0-4	2-65±0-23	4*8
Hayakawa*/ <i>ai.</i> ^{2c} ..	26 July 1965	..	5*0dbl*0	..	3-8
Grader <i>et al.</i> ⁸⁴ ..	28 October 1965	10-3 ±0-4	3<<8±0-3	2-28±0-22	4-6
Guiskyrrffl/. ²⁵ ..	8 March 1966	8-8 ±0-5	3-7±0-4	1-93±0-21	5*0
ChodiU/<iA ²⁶ ..	28 July 1966	10*5 ±0-5	3-1±0-4	..	5-8
Gunkyrffl/. ²⁷ ..	11 October 1966	7-1 ±0-9	3-0±0-6	1-49x0.17	4-8
Matsuoka <i>et al</i> ?* ..	6 February 1967	7-6 ±0<<8	3.2±0-8	1-64 ±0-20	6-0
Cooked <i>a/.</i> ²⁹ ..	10 April 1967	1-30 ±0-10	..
Chodil <i>et al</i> ^h ..	18 May 1967	5-2 ±0-4	2-6±0-2	1*08±0*1»	8-1
<i>Fritzetat.</i> ³⁰ ..	8 September 1967	4-0 ±0-4	1*9±0>3	0*85±0-U	10*4
ChodUrffl/. ¹⁶ ..	29 September 1967	6-3 ±0-8	2-6±0-6	1*41 ±0*17	4*6
<i>Hill etai.</i> ^{1*} ..	2 October 1967	5*4 ±0<<6	2*9±0-6	1.12±0<<16	10-4
Rao <i>et al.</i> (present experiment)	3 November 1968	4-9 ±0*3	2-1±0-2	1*07±0<<15	5-1
ii	7 November 1968	5-2 ±0-7	2-2±0-3	1-12±0-16	5*1

Different theoretical models give different estimates ranging from 10-50 years for the lifetime of Sco-X1. For example, if we consider Manley's³¹ model of a protostar shedding its magnetic field, where the high energy electrons are produced through the utilisation of magnetic energy, which upon interaction with the same field, can produce X-rays an estimated lifetime of about 30 years is obtained for an extar like Sco-X1. Such an estimate is obtained from considerations of energy for the magnetic field

required to supply energy to electrons. The experimental observation of about 20 years for the lifetime of Sco-X1 obtained from the long-term variation of the absolute X-ray flux of Sco-X1 is consistent with the theoretical models.

ABSOLUTE FLUX AND TIME VARIATION OF CEN-X2

The rediscovery of low energy X-ray flux in the range 2-18 Kev from Cen-X2 source is the most important result of these flights. The presence of low energy flux from Cen-X2 is unambiguously proved in both the flights as may be seen from Figs. 4 and 5. The level of detection of Cen-X2 on November 3, 1968 flight is more than 10 standard deviation level and on November 7, 1968 flight at about 6 standard deviation level. The best estimate of the position of Cen-X2 as determined from our experiment is $201 \pm 2^\circ$ R.A. and $-62.5 \pm 2^\circ$ declination, which is consistent with the position of Cen-X2 observed by Harries *et al.* and Chodil *etal.*

In Fig. 10 is plotted the energy spectrum of the X-ray intensity from Cen-X2 observed during both the flights. Even though the data from both the flights can be adequately represented by an exponential spectrum with a characteristic temperature of about 5.4 Kev ($T = 6.3 \times 10^7$ K), a power law spectrum fits the data better. The X-ray flux on November 3, 1968 can be represented by the spectrum

$$f(E) = 5.8 E^{-1.2 \pm 0.2} dE$$

and that on November 7, 1968 by the spectrum

$$f(E) = 5.1 E^{-0.9 \pm 0.2} dE.$$

We conclude that the energy spectrum of the X-ray flux measured on November 3, 1968 and November 7, 1968 are same within the statistical error. In the same figure, the observations of high energy flux observed at balloon altitudes by Lewin *et al.*² on October 15, 1967 are also plotted. The low and high energy observations taken one year apart seem to fit a single power law spectrum with an exponent of 1-2.

Figure 11 summarizes the remarkable time variation of the X-ray flux from Cen-X2, the numerical data being given in Table III. It was not detected in October 1965, was observed as a time-varying object in April-May 1967 and again could not be detected in September 1967. The decreases in the X-ray flux during the period April-May 1967 was found

to be exponential, with a time constant of 23-4 days. This decrease was also accompanied by a softening of the spectrum. Even though Cen-X2 was again sighted in the high energy range in October 1967, no low energy flux from the same source was detected in June 1968, by Pounds *et al*. They provide an upper limit of 0-15 photons/cm.² sec. for the flux in the energy range 2-5 Kev, which is more than an order of magnitude below the low energy flux that has been detected in our experiments in November 1968. Our observations are the first evidence for the existence of the low energy X-ray flux from Cen-X2 in the range 2-20 Kev since May 1967.

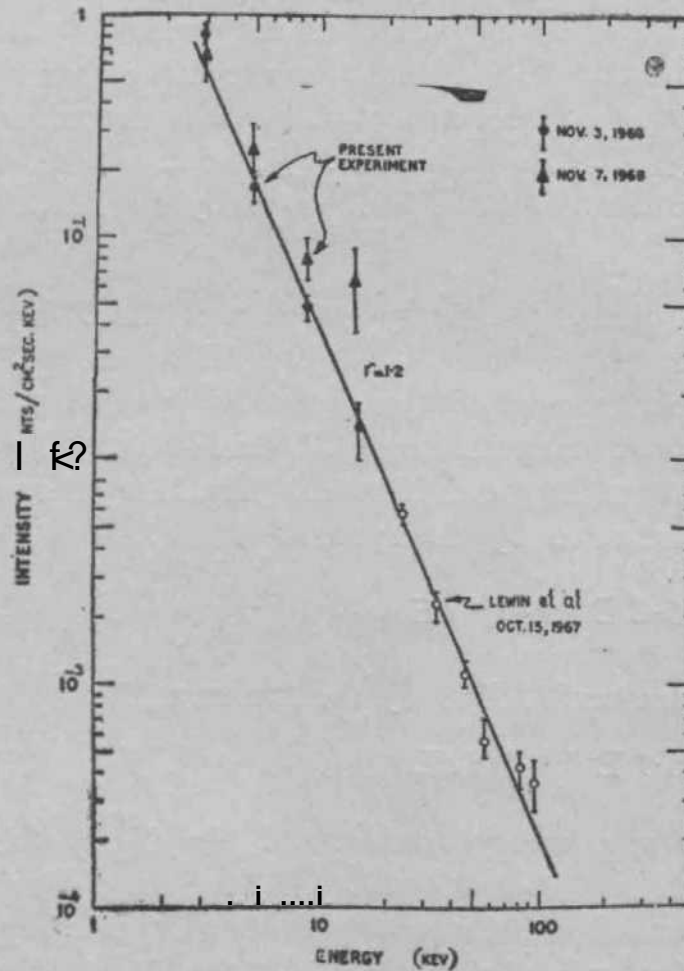


FIG. 10. Energy spectrum of Gen-X2 X-ray source in the range 2-18 Kev.

The remarkable time variability of Cen-X2 makes this extra a unique object of interest. The spectacular outburst in April-May 1967 was followed by the outbursts in October 1967 as observed by Lewin *et al.*, and in November 1968 as observed in the two rocket flights conducted by us from India. The totality of observations made so far clearly indicate that Cen-X2 is a nova-like source giving rise to recurring X-ray outbursts, each

TABLE III
Time variation of X-ray Intensity from Cen-X2

Experimenter	Flight	Energy flux in 2-5 Kev range 10^{18} trgd/cm. ³ sec
Grader <i>et al</i> ¹	28 October 1965	< 0-25
Hanies <i>et al.</i> ^a	4 April 1987	11*0 ±1-0
Cooke <i>et al</i> * [*]	10 April 1967	16*0 ±1*0
Francey <i>et al.</i> ³³	20 April 1967	7*5 ±1-0
Chodil rt a. ⁸¹	15 May 1967	2*6 ±0*4
Chodiltffl. ¹⁶	28 September 1997	< 0-3
Lewin <i>et al.</i> ["]	15 October 1967	0'62 (extrapolated)
Pounds <i>et at.</i> ®	12 June 1868	< 0*1
Rao <i>et at.</i> (present experiment)	3 November 1968	0-68±0-08
"	7 November 1968	0-83±0-H

outburst lasting probably a short period of time. In order to explain this behaviour, Manley proposed an expanding constant mass plasma model for the source, according to which a dense plasma cloud of radius $\ll 10^w$ cm. was heated at constant volume to nearly 2×10^7 °K which then proceeded to expand isothermally and cool off. The recurring short-lived outbursts like the one observed by Lewin *et ah* and more recently our low energy observations can be attributed to a shock wave from the nova

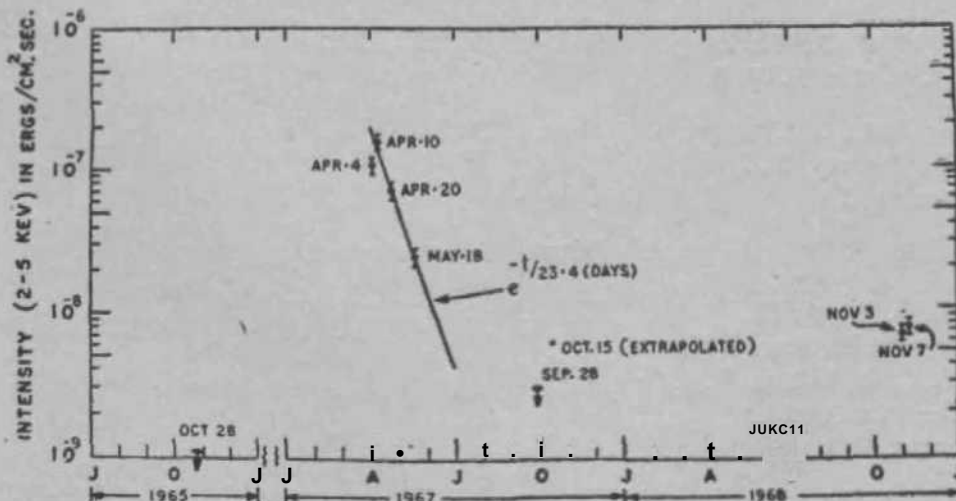


FIG. II. Time variation of the X-ray flux from Ceo-X2 source.

outburst expanding into the circumstellar medium. Such a shock could accelerate and heat the gas to a high temperature as it propagates into a medium of decreasing density.

ACKNOWLEDGEMENTS

The Nike-Apache rockets for the experiments were made available under the Nasa-Incospar agreement. Thanks are due to Mr. H. G. S. Murthy and his colleagues for their able assistance in launching the rockets. The authors are thankful to Professors V. A. Sarabhai, K. R. Ramanathan and M. Oda for many helpful discussions.

REFERENCES

1. Giacconi, R., Gursky, H., Paolini, F. R. and Rossi, B. *Phys. Rev.*, 1962, 9, 439.
2. Sandage, A., Osmer, P., Giacconi, R., Gorenstein, P., Gursky, H., Waters, J., Bradt, H., Garmire, G., Sreekantan, B. V., Oda, M., Osawa, K. and Jugaku, J. *Ap. J.*, 1966, **146**, 316.
3. Hiltner, W. A. and Mook, D. E. *Ibid.*, 1967, **150**, 851.
4. Rao, U. R., Prakasarao, A. S. and Jayanthi, U. B. *Nature*, 1969, **222**, 864.
5. Andrew, B. H. and Purton, C. R. *Ibid.*, 1968, **218**, 855.
6. Abies, J. G. *Ap. J. (Letters)*, 1969, **155**, L27.
7. Lewin, W. H. G., Clark, G. W. and Smith, W. B. *Ibid.*, 1968, **152**, L55.
8. Harries, J. R., McCracken, K. G., Francey, R. J. and Fenton, A. J. *Nature*, 1967, **215**, 38.
9. Wada, M. *Private Communication*.
10. Chodil, G., Mark, H., Rodrigues, R., Seward, F., Swift, C. D., Hiltner, W.A., WaUerstein, G. and Manney, E. J. *Phys. Rev.*, 1967, 19, 681.
11. Boldt, E.A., Desai, U.D. and Holt, S.S. Preprint—NASA Document No. X-611-68-353.

Energy Spectrum & Absolute Flux of Various Celestial X-Ray Sources 273

12. Fritz, G., Henry, R. C. *Science*, 1969, **155**, 709.
Meekins, J. F., Chubb,
T. A. and Friedman, H.
13. Busseli, G., Clancey, M. C., *Nature*, 1968, **219**, 1124.
Davison, P. J. N., Edwards,
P. J., McCracken, K. G.
and Thomas, R. M.
14. Shklovsky, I. S. .. *Ap. J. (Utters)*, 1967, **148**, LI.
15. Chodil, G., Mark, H., *Ap. J.*, 1968, **154**, 645.
Rodrigues, R., Seward,
F. D., Swift, C. D.,
Turiel, I., Hiltner, W. A.,
Wallerstein, G. and
Mannery, E. J.
16. Hill, R. W., Grader, R. J. *Ibid.*, **1968**, **154**, 655.
and Seward, F. D.
17. Overbeck, J. W. and *Ibid.*, 1968, **153**, 899.
Tananbaum, H. D.
18. Stepien, K. .. *Ap. J. (Letters)*, 1968, **151**, L15.
19. Neugebauer, G., Oke, J. B., *Ap. J.*, 1969, **155**, 1.
Becklin, E. and Garmire, G.
20. Agarwal, P. C, Biswas, S., *Presented at Symposium No. 37 of the I.A.U. on Non-*
Gokhale, G. S., Iyengar, *Solar Gamma and X-ray Astronomy at Rome, 1969.*
V. S., Kunte, P. K.,
Manchanda, R. K. and
Sreekantan, B. V.
21. Fisher, P. C, Johnson, *Ap. /.*, 1966, **143**, 203.
H. M., Jordan, W. C,
Meyerott, A. J. and
Acton, L. W.
22. Chodil, G., Jopson, R. C. *Phys. Rev.*, 1965, 15, 605.
Mark, H., Seward, F. D.
and Swift, C. D.
23. Hayakawa, S., Matsuoka, *Report of Ionosphere and Space Research in Japan.*
M. and Yamashita, K.
24. Grader, R. J., Hill, R. W., *Science*, 1966, **152**, **1499**.
Seward, F. D. and Toor, A.
25. Gursky, H., Gorenstein, P. *Ap. J. (Utters)*, 1967, **150**_f L50.
and Giacconi, R.
26. Chodil, G., Mark, H., *Ap. /.*, 1967, **150**, 57.
Rodrigues, R., Seward,
F. D. and Swift, C. D.
A2

27. Gursky, H., Gorenstein, P. and Giacconi, R. *Ap. J. (Letters)*, **150**, L85.
28. Matsuoka, M., Oda, M., Ogawara, Y., Hayakawa, S. and Kato, T. *Can. J. Phys.*, 1966, p. 8466.
29. Cooke, B. A., Pounds, K. A., Stewardson, E. A. and Adams, D. J. *Ap. J. (Letters)*, **1967**, **150**, L18>.
30. Fritz, G., Meekin, J. F., Harry, R. C, Byram, E. T. and Friedman, H. *Ibid.*, 1968, **153**, L199.
31. Manley, O. P. .. *Ap. J.*, 1966, **144**, 1253.
32. Lewin, W. H. G., Clark, G. W. and Smith, W. B. *Ap. J. (Utters)*, **1968**, **152**, L49.
33. Francey, R. J., Fenton, A. G., Harries, J. R. and McCracken, K. G. *Nature*, 1967, **216**.
34. Chodil, G., Mark, H., Rodrigues, R. and Swift, C. D. *Ap. J. (Letters)*, **1968**, **152**, L45.
35. Pounds, K. A. .. Presented at Symposium No. 37 of the I.A.U. on Non-Solar Gamma and X-ray Astronomy at Rome, 1969.

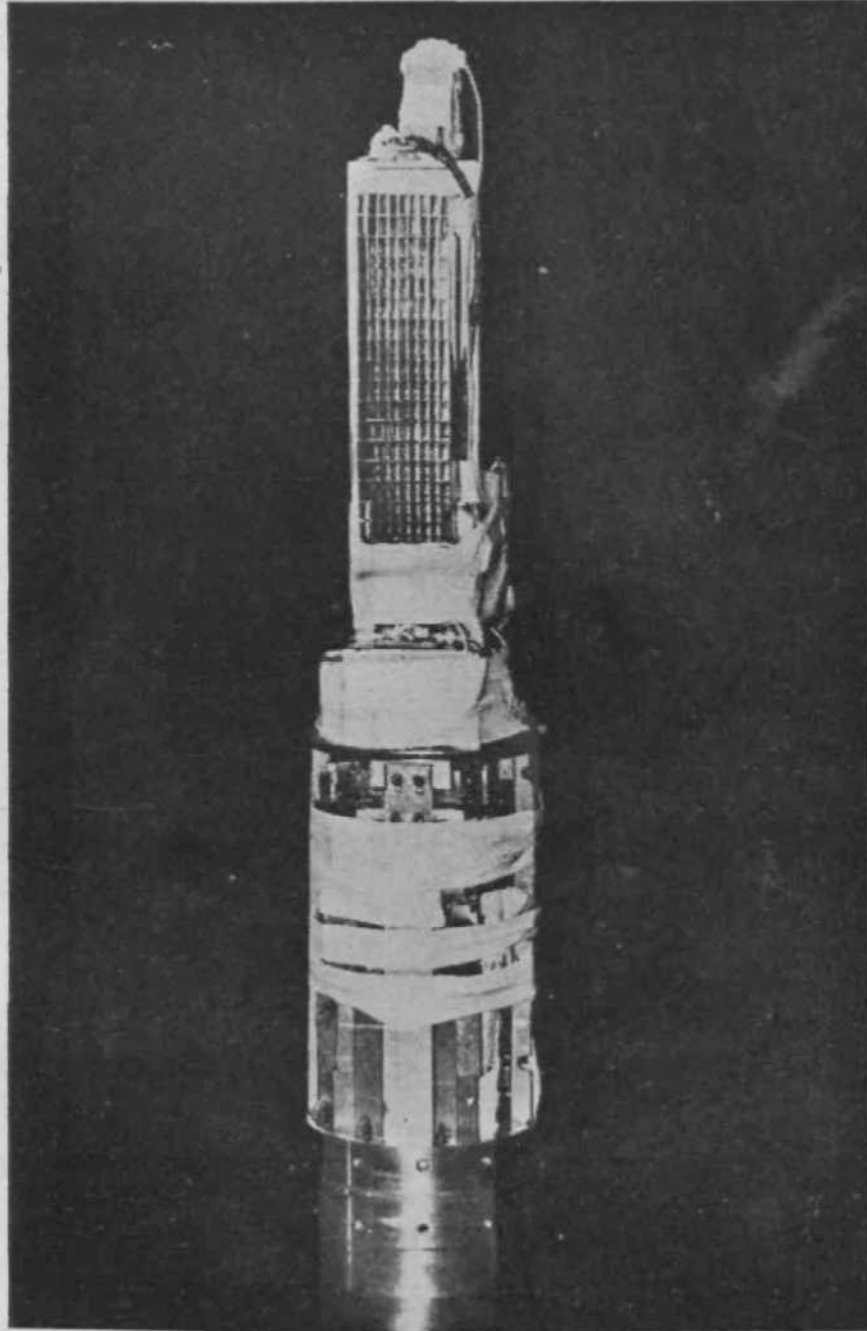


FIG. I. Rocket-borne X-ray payload to measure extra-terrestrial X-rays.

PIEZO-ROTATORY COEFFICIENTS AND STRESS-INDUCED OPTICAL ACTIVITY

BY G. S. RANGANATH AND S. RAMASESHAN, F.A.S.C.

(Materials Science Division, National Aeronautical Laboratory, Bangalore-M, India)

Received April 15 1969

ABSTRACT

This paper reports the methods of obtaining the components of the fourth rank axial piezo-rotatory tensor in different crystal classes. The methods of recovering the two piezo-rotatory coefficients R_n and R_{12} of isotropic optically active glasses, the three coefficients R_n , R_{12} and R_{44} of cubic crystals belonging to the point group 432 and the four coefficients R_n , R_{12} , R_{13} and R_{44} of crystals like NaClO_3 (point group 23) have been described in detail. The non-centrosymmetric class 33 m. which is not optically active has one non-vanishing piezo-rotatory coefficient, showing that stress induces optical activity in it. A method of retrieving this coefficient has also been described. In most of the other point groups, the difficulty of measuring optical activity in directions other than those of the optic axes severely limits the number of coefficients that can be extracted. The paper also touches upon some interesting methods of obtaining the components of the gyration tensor in non-enantiomorphic optically active crystals.

1. INTRODUCTION

THE present authors have, of late, been investigating the effect of stress on the optical rotatory power of crystals (Ramaseshan and Ranganath, 1969). Optical activity can be represented by the second rank symmetric axial gyration tensor (g) while stress (X) and strain (x) by second rank symmetric polar tensors. The effect of stress or strain on the optical rotatory power would therefore be represented, in a first-order theory, by fourth rank axial tensors; (R) being the stress-rotatory tensor and (S) the strain-rotatory tensor. The number of independent non-vanishing coefficients and the nature of the piezo-rotatory matrix for the various point groups have also been worked out by the present authors (Ranganath and Ramaseshan, 1969 *a*).

This paper mainly concerns itself with the methods of recovering the piezo-rotatory coefficients for some of the point groups. The problem in this case is different from that in other stress-optic phenomena where the

directions of stress and light propagation may be chosen arbitrarily. In the case of piezo-rotatory effects it is very difficult to measure the rotatory power or its change along directions other than that of the optic axis. This constraint limits the number of coefficients that may be recovered and also demands special strategy for making the measurements.

2. THE GYRATION, PIEZO-ROTATORY AND PIEZO-OPTIC TENSORS

In a crystal if ρ is the optical rotatory power along any direction (s_1, s_2, s_3)

$$\rho = g_{ij} s_i s_j$$

i.e.,

$$P = g_{11}s_1^2 + g_{22}s_2^2 + g_{33}s_3^2 + 2g_{12}s_1s_2 + 2g_{23}s_2s_3 + 2g_{31}s_3s_1$$

and when referred to the principal axes the optical rotation and the tensor surface are given by

$$\frac{x^2}{a^2} + \frac{y^2}{b^2} + \frac{z^2}{c^2} = 1$$

and

$$g_{11}x^2 + g_{22}y^2 + g_{33}z^2 = 1$$

where there is no *a priori* restriction on the signs of g_{ij} . The matrices representing the gyration tensor for the various non-centrosymmetric point groups are given in Table I. It may be noted that of the 21 non-centrosymmetric point groups only 15 are optically active (Tables I and II) and 6 are optically inactive (Table III). Further just as a liquid may show optical activity an isotropic solid may also exhibit optical activity. These are usually glasses or stereo-specific plastics.

In the first-order phenomenological theory of piezo-rotation, changes in g_{ij} i.e., Δg_{ij} are assumed to be linear functions of stress X_{kl} or strain x_{kl}

i.e.,

$$\Delta g_{ij} = - R_{ijkl} X_{kl}$$

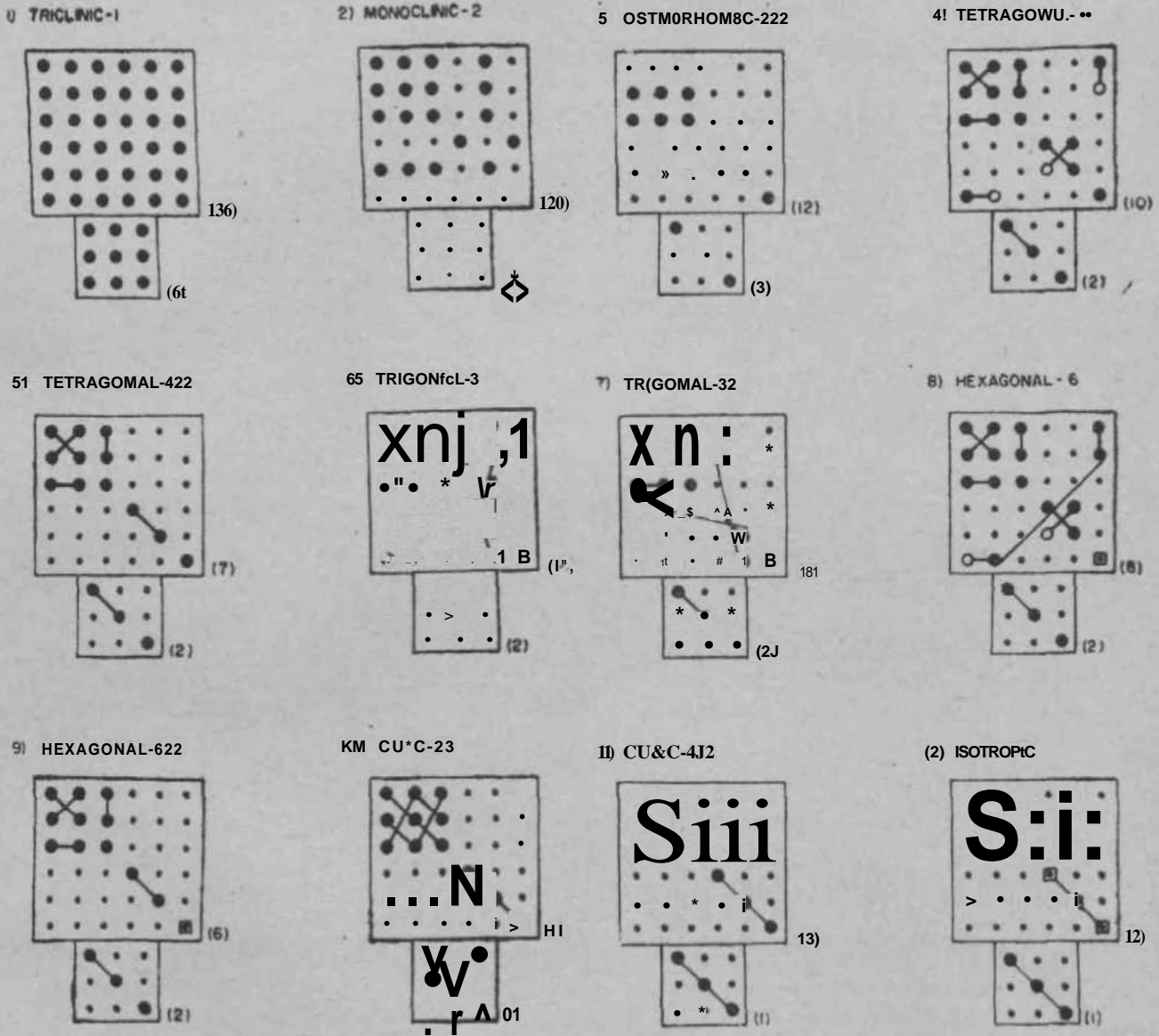
or

$$\Delta g_{ij} = S_{ijkl} x_{kl}$$

When the non-vanishing coefficients are evaluated (Ramaseshan and Ranganath, 1969) one finds that

TABLE I

The form of the piezo-rotatory $\{R\}$ and piezo-optic $\{q\}$ matrices, and the gyration matrix $\{g\}$ in the enantiomorphic optically active point groups. $\{R\}$ and $\{q\}$ have the same form



KEY TO TABLES I, II AND HI

0—Zero component.

#—Non-zero component.

•—# Equal components of same sign

○—• Equal components of opposite sign

In $\{R\}$ or $\{q\}$ matrices

In $\{S\}$ or $\{p\}$ matrices

0 —A component equal to + 2 times that to which it is joined is joined.

0 —A component equal to -2 times that to which it is joined, to which it is joined, the minus of that

H $\ll (R_{ij} - R_{ji})$

tg $= 1/2(S_{ij} - S_{ji})$

or $(q_{11} - q_{33})$.

or $\sqrt{2} (p_{11} - p_{33})$.

(a) piezo-rotatory coefficients exist only for the 21 non-centrosymmetric point groups;

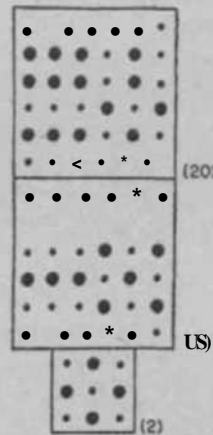
(b) in the 11 enantiomorphically optically active point groups the piezo-rotatory and piezo-optic matrices have the same form (Table I);

(c) in the 4 non-enantiomorphically optically active point groups the photo-elastic and piezo-rotatory matrices are of different forms (Table II);

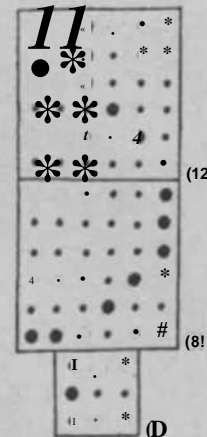
TABLE II

The piezo-optic (q), piezo-rotatory (R) and the gyration matrix (g) of the non-enantiomorphically optically active point groups

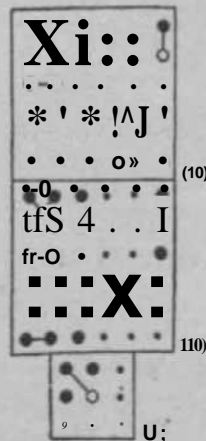
1) MONOCLINIC-m



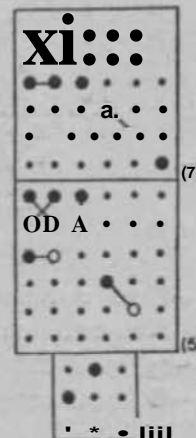
2) ORTHORHOMBIC-mir.2



3) TRIGONAL-?



4) TETRAGONAL-42m

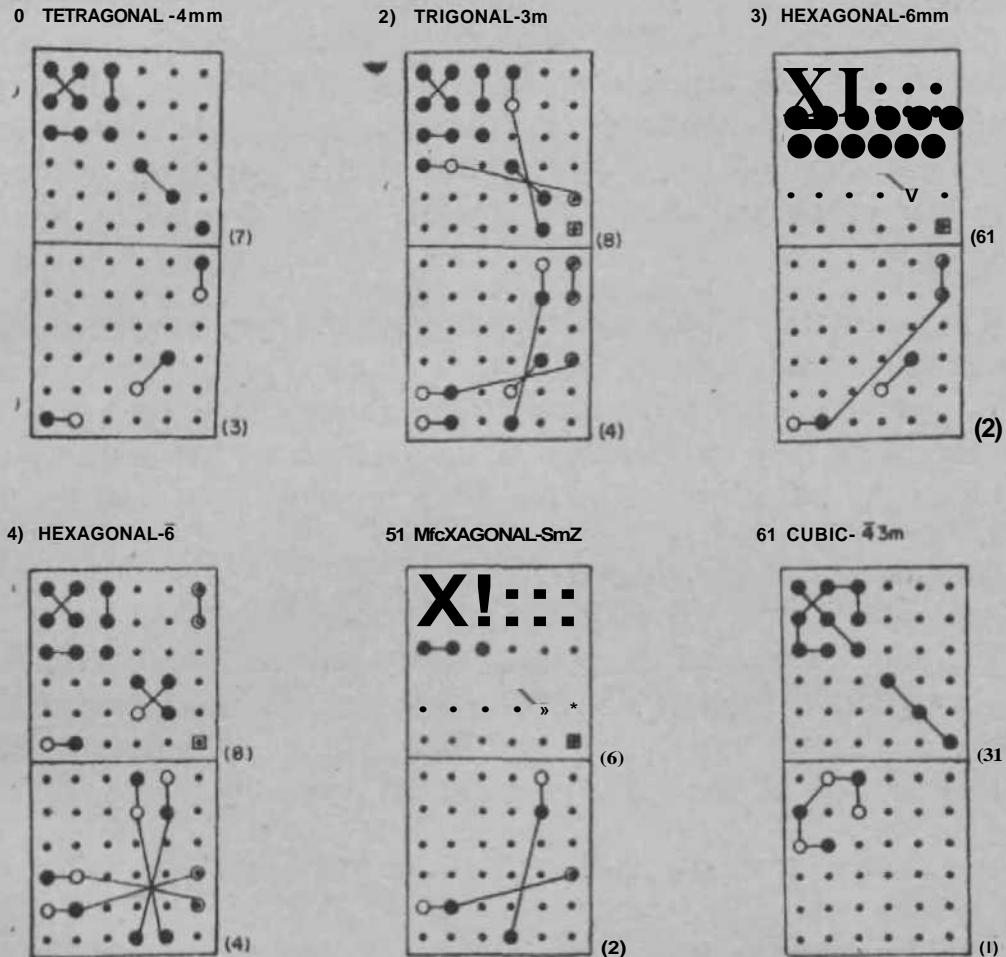


(d) in the remaining 6 non-enantiomorphically, optically inactive classes the piezo-rotatory coefficients do not vanish, *i.e.*, stress actually induces

optical activity in these crystals. The piezo-rotatory and piezo-optic matrices are given in Table HI.

TABLE III

The piezo-optic (q) and the piezo-rotatory (R) matrices of the non-enantiomorphic non-optically active point groups (i.e., $g\% = 0$)



It has been mentioned that optical activity may be most conveniently measured along the optic axes. In the uniaxial crystals of trigonal, tetragonal and hexagonal classes the optic axis coincides with the 3-fold, 4-fold and 6-fold axes respectively. In biaxial crystals the optic axial angle is given by

$$\sin^2 \alpha_v = \frac{a_2 - a_1}{a_3 - a_1} \quad a_1 > a_2 > a_3$$

where

$$a_1 = \frac{1}{n_1^2}, \quad a_2 = \frac{1}{n_2^2}, \quad a_3 = \frac{1}{n_3^2};$$

where n_1, n_2, n_3 being the principal refractive indices. The optic axes lie in the plane containing n_1 and n_3 .

We shall now summarise the effect of stress on the optical ellipsoid (Ramaseshan and Vedam, 1958; Ramachandran and Ramaseshan, 1961).

When a crystal is uniaxially stressed along a 3-fold, 4-fold or 6-fold axis of symmetry, the crystal becomes or remains uniaxial with the optic axis along the stress direction. But if the same uniaxial stress acts along a 2-fold, or a 1-fold axis, the crystal becomes biaxial even if it be a cubic crystal. However, in the latter case the optic axial angle is dependent only on the stress direction and is independent of the magnitude of the stress. In the case of uniaxial and biaxial crystals it also depends on the magnitude of stress.

When a crystal is hydrostatically stressed the symmetry does not alter. An isotropic crystal remains isotropic, a uniaxial crystal remains uniaxial. In the case of biaxial crystals, however, although the symmetry remains the same, there may be a change in the position of the optic axes as the changes in the refractive indices for the 3 principal axes may be different.

3. ISOTROPIC SUBSTANCES

The photoelastic and the piezo-rotatory matrices (which have the same form) are given in Table I (No. 12). There are only two independent piezo-rotatory coefficients namely R_{11} and R_{12} . For a unidirectional stress X , the deformations of the index ellipsoid are given by

$$\Delta g_{11} = -R_{11}X, \quad \Delta g_{22} = \Delta g_{33} = -R_{12}X, \quad \Delta g_{ij} = 0 \quad (i \neq j)$$

The solid therefore becomes uniaxial with its optic axis coinciding with the stress direction. Rotatory power along this direction could be measured if suitable holes are provided in the stress apparatus for sending the light along the direction of stress. The deformations in the gyration surface are given by

$$\Delta g_{11} = -R_{11}X, \quad \Delta g_{22} = \Delta g_{33} = -R_{12}X, \quad \Delta g_{ij} = 0 \quad (i \neq j)$$

Hence, if ΔP is the change in the optical rotation along the stress direction

$$\Delta P \approx -R_U X \quad \text{or} \quad R_U = -4 \rho \frac{P}{\lambda^2} \quad (9)$$

For an hydrostatic stress X_h

$$\Delta g_{11} = \Delta g_{22} = \Delta g_{33} = - (O_n + 2g_{r12}) X_h, \quad \Delta g_{ij} = 0$$

and therefore the substance remains optically isotropic. The changes in the gyration tensor may be described by

$$\Delta g_n = \Delta g_2 = \Delta g_3 = - (R_n + 2R_{i2}) X_h, \quad \Delta g_{ij} = 0.$$

Therefore, if we measure the change Δp_k in rotatory power along any direction

$$\Delta p_k = - (R_n + 2R_{12}) X_h. \tag{2}$$

From (1) and (2)

$$R_{12} = \frac{1}{2} \left(\frac{\Delta p}{X_h} \right).$$

Thus all the components of the piezo-rotation tensor may be determined by measuring changes in the rotatory power for a uniaxial stress along the stress direction and for an hydrostatic stress in any direction.

4. OPTICALLY ACTIVE CUBIC CRYSTALS

(0) *432 Class:*

This is the simplest of the cubic classes wherein all the piezo-rotatory coefficients can be recovered. Unfortunately no crystal belonging to this class has been reported in the literature. The piezo-rotatory and the photoelastic tensors have the same form (Table I, No. 11). There are 3 independent piezo-rotatory coefficients R_u , R_{i2} and R_{44} .

Application of a stress X_{100} along the cube axis (100) deforms the index ellipsoid and the gyration surface in the following manner:

$$\Delta g_{ii} = - O_u X_{100}, \quad \Delta g_{22} = \Delta g_{33} = - \frac{1}{2} X_{100}^* \quad \Delta g_{ij} = 0$$

and

$$\Delta g_{11} = - R_{11} X_{100}, \quad \Delta g_{22} = \Delta g_{33} = - R_{12} X_{100}, \quad \Delta g_{ij} = 0,$$

The crystal becomes uniaxial with the optic axis along the stress direction (100). If $\Delta \rho_{100}$ is the change in rotation along the (100) direction, then

$$\Delta \rho_{100} = -R_{11} X_{100} \quad \text{or} \quad R_u = \frac{\Delta \rho_{100}}{X_{100}}. \quad (3)$$

For an hydrostatic stress X_h , deformations in the index ellipsoid are given by

$$\Delta n_{11} = \Delta n_{22} = \Delta n_{33} = -(\alpha_{11} + 2g_{12}) X_h, \quad \Delta n_{12} = 0.$$

Hence, the crystal remains isotropic, but the radius of the gyration sphere changes and it is given by

$$\Delta g_{11} = \Delta g_{22} = \Delta g_{33} = -(\alpha_{11} + 2R_{12}) X_h, \quad \Delta g_{12} = 0.$$

If Δp_h is the change in the optical rotatory power in any direction under the hydrostatic stress X_h

$$\Delta p_h = -(\alpha_{11} + 2R_{12}) X_h. \quad (4)$$

From (3) and (4)

$$R_{12} = \frac{1}{2} \left(\frac{\Delta \rho_{100}}{X_{100}} - \frac{\Delta p_h}{X_h} \right).$$

Changes in the index and gyration tensors under a uniaxial stress X_{u1} along the cube diagonal (111) are given by

$$\Delta n_{11} = \Delta n_{22} = \Delta n_{33} = -\alpha_{11} X_{u1},$$

$$\Delta n_{12} = \Delta n_{23} = \Delta n_{31} = -\alpha_{12} X_{u1}$$

and

$$\Delta g_{11} = \Delta g_{22} = \Delta g_{33} = -\frac{\alpha_{11} + 2R_{12}}{3} X_{u1},$$

$$\Delta g_{12} = \Delta g_{23} = \Delta g_{31} = -\frac{R_{12}}{3} X_{u1}.$$

The first set of equations establish that the crystal becomes uniaxial with the optic axis along the cube diagonal (*i.e.*, stress direction). If p_m^* and p_m

(iii) For a stress X_{100} along the cube axis (100) the deformations in the index and the gyration surfaces are given by

$$\Delta n_{11} = -n_{100} X_{100} \quad \Delta n_{22} = -n_{100} X_{100} \quad \Delta n_{33} = -q_{12} X_{100},$$

$$\Delta n_{ij} = 0$$

and

$$\Delta S_{11} = -R_n X_{100} \quad \Delta S_{22} = -R_i X_{100} \quad \Delta S_{33} = -R_{12} X_{100},$$

$$\Delta g_{ij} = 0.$$

The first set of equations shows that the crystal becomes biaxal. Generally, $n_{11} < n_{13} < n_{12}$ hence the plane containing the two optic axes is the ZX plane. The angle V that one of the optic axes makes with the stress direction, i.e., X-axis is given by

$$\sin^2 V = \frac{n_{22} - n_{11}}{n_{33} - n_{11}} = \frac{n_{13} - n_{11}}{n_{12} - n_{11}}$$

If $\Delta \rho$ is the change in rotation along this optic axis, then

$$\Delta \rho = - (R_n \cos^2 V + R_{12} \sin^2 V) X_{100} \quad (7)$$

determination of $\Delta \rho$ should not be difficult because the optic axial angle and the optical axial plane can be completely worked out from a knowledge of photoelastic constants. The optic axial angle is independent of the stress magnitude. Hence, the crystal can be so cut that the optic axes in the stressed crystal are in proper positions to make the measurements.

(iv) When the crystal is subjected to a uniaxial stress X_{110} acting along the (110) direction, the index and the gyration surfaces deform according to the following set of equations:

$$\Delta a_{11} = - (q_{11} + q_{12}) \frac{X_{110}}{2}, \quad \Delta a_{22} = - (q_{11} + q_{12}) \frac{X_{110}}{2},$$

$$\Delta a_{33} = - (q_{12} + q_{13}) \frac{X_{110}}{2}, \quad \Delta a_{13} = - q_{44} \frac{X_{110}}{2}$$

$$\Delta a_{83} = \Delta a_{31} = 0$$

and

$$\Delta g_{11} = - (R_{11} + R_{12}) \frac{X_{110}}{2}, \quad \Delta g_{22} = - (R_{11} + R_{12}) \frac{X_{110}}{2},$$

$$\Delta g_{33} = - (R_{12} + R_{13}) \frac{X_{110}}{2}, \quad \Delta g_{12} = - R_{44} \frac{X_{110}}{2},$$

$$A g_{23} = A g_{3l} = 0.$$

The first set of equations shows that (1) the index ellipsoid undergoes a rotation about the XY plane; (2) the crystal becomes biaxial with YZ as the optic axial plane. If one of the optic axes of the stressed crystal makes an angle V with the Z-axis, then

$$\sin \alpha Y = \frac{f_0 - a'_{33}}{n_{11} - n_{33}} = \frac{A}{B}$$

where

$$A = (q_{X2} + q_{vd} - \frac{q_{12} + q_{13} + 2q_{11} - \sqrt{(q_{12} - q_{13})^2 + 4q_{44}^2}}{2})$$

$$B = (q_{12} + q_{13}) - \left\{ \frac{q_{12} + q_{13} + 2q_{11} + \sqrt{(q_{12} - q_{13})^2 + 4q_{44}^2}}{2} \right\}$$

and the angular displacement θ from the stress direction is given by

$$\tan 2\theta = \frac{q_{12} - q_{13}}{q_{44}}.$$

From a knowledge of V and θ one can work out direction cosines l, m, n of the optic axis with reference to the unstressed state. Then the change ΔP_2 in that direction for a stress X_{110} is given by

$$\Delta P_2 = - [(R_{11} + R_{12}) l^2 + (R_{11} + R_{13}) m^2 + (R_{12} + R_{13}) n^2 + R_{44} / m]^2. \tag{8}$$

From the 4 equations (5), (6), (7) and (8) all the piezo-rotatory constants can be worked out. R_{44} is the easiest of all the coefficients to find.

$$R_{44} = \frac{1}{2} \left(\frac{\Delta \rho_h}{X_h} - \frac{\Delta \rho_{111}}{X_{111}} \right).$$

5. STRESS-INDUCED OPTICAL ACTIVITY IN CUBIC CRYSTALS

(a) $\bar{4}3m$ Class:

In this interesting point group, to which ZnS belongs, stress actually should induce optical activity. The photoelastic and the piezo-rotatory tensors are of different forms (Table III, No. 6). From the nature of the two matrices it can be easily concluded that although a uniaxial stress along the 4-fold or 3-fold axis makes the crystal uniaxial with the optic axis along the stress direction, yet the rotation along the optic axis is zero. Even for stress along the 2-fold axis the rotation along the optic axes is zero. For hydrostatic stress also induced optical activity is zero. Hence, to detect this induced rotation and to extract the piezo-rotatory coefficient R_{12} , one should stress the crystal in a general direction (l, m, r) which is only a 1-fold symmetry axis. Let X be the uniaxial stress acting along (l, m, r) . The deformations in the index and gyration surfaces are given by

$$A_{11} = - [0l^2 + q_{12} (m^2 + r^2)] X$$

$$A_{22} = - [q_{12} m^2 + q_{12} (P + r^2)] X$$

$$A_{33} = - [q_{12} r^2 + q_{12} (l^2 + m^2)] X$$

$$A_{023} = - 044 \text{ "MX}$$

$$A_{031} = - 044 \text{ fa X}$$

$$A_{012} = - 044 \text{ fat X}$$

and

$$A_{fti} = - R_{12} (l^2 - r^2) X$$

$$\Delta g_{ij} = - R_{12} (n^2 - l^2) X \quad \Delta g_{ij} = 0$$

$$A_{g33} = - R_{12} (l^2 - W^2) X.$$

Hence, in general the crystal becomes biaxial. Index and the gyration surfaces in the stressed crystal are

$$- \text{flu}^2 + 2SLV^2 + R_{33}Z^2 + 2a_{12}xy + 2a^{\wedge}yz + 2a_{B1Z}x = 1$$

and

$$g_{11}x^2 + g_{22}y^2 + g_{33}z^2 = 1.$$

If X, Y, Z be the principal axes of the index ellipsoid, then the index ellipsoid and the Gyration surface are given by

$$A_{11}X^2 + A_{22}Y^2 + A_{33}Z^2 = 1$$

$$G_{11}X^2 + G_{22}Y^2 + G_{33}Z^2 + 2G_{12}XY + 2G^{12}YZ + 2G_{31}ZX = 1$$

A_{ij} 's and G_{ij} 's can be obtained from a knowledge of the refractive index of the unstressed crystal and its photoelastic constants. In the most general case A_{11}, A_{22} and A_{33} will be different.

If $A_{11} < A_{22} < A_{33}$, then the biaxial plane is XZ and if V is the angle that one of the optic axes makes with X -axis. Then rotation along that axis is

$$\rho = G_u \cos^2 V + 2G_{18} \cos V \sin V + G_{83} \sin^2 V$$

along the other optic axis also we get the same rotation. If this rotation is measured, we can easily find the only existing piezo-rotatory coefficient R_x

$$\rho = -R_{12} (\cos^2 V + f_1 \cos V \sin V + f_3 \sin^2 V) X$$

i.e.,

$$R_x = \frac{\rho/X}{\cos^2 V + f_1 \cos V \sin V + f_3 \sin^2 V}$$

where

$$f_1 = \left\{ (l^2 - m^2) + \left(\frac{q_{44}}{q_{11} - q_{12}} \right)^2 \left[\frac{n^2 - l^2}{(l^2 - m^2)^2} l^2 m^2 + \frac{l^2 - m^2}{(n^2 - l^2)^2} n^2 l^2 \right] \right\}$$

$$f_3 = \left\{ (l^2 - m^2) + \left(\frac{q_{44}}{q_{11} - q_{12}} \right)^2 \left[\frac{m^2 - n^2}{(n^2 - l^2)^2} l^2 n^2 + \frac{n^2 - l^2}{(m^2 - n^2)^2} m^2 n^2 \right] \right\}$$

and

$$\sin^2 V = \frac{11}{A_{33} - A_n}$$

6. ENANTIOMORPHIC OPTICALLY ACTIVE UNIAXIAL CRYSTALS

The photoelastic and the piezo-rotatory matrices are of the same form in all these crystals and they are shown in Table I (Nos. 4, 5, 6, 7, 8 and 9). The crystal remains uniaxial under an hydrostatic stress X^h as well as a stress X_o along the optic axis. In both the cases the optic axis in the stressed crystal is in the same direction as that of the unstressed crystal. If Δp^* and Δp_o are Δp^e changes in the optical rotatory power along the optic axis for these two stresses, then

$$R_{33} = - \frac{\Delta p_o}{X_o}$$

and

$$Z_{31} - K_{33} = - \frac{\Delta p_h}{X_h}$$

i.e.,

$$R_{31} = \frac{1}{2} \left(\frac{\Delta p_o}{X_o} - \frac{\Delta p_h}{X_h} \right)$$

Hence, the two constants R_{31} and R_{33} can be easily found out. Determination of other constants involve many experimental complications. The actual values of these constants for a-quartz have been computed by the authors (Ranganath and Ramaseshan 1969 6).

7. NON-ENANTIOMORPHIC OPTICALLY ACTIVE UNIAXIAL CRYSTALS

Crystals belong to $\bar{4}$ and $\bar{4}2m$ point groups come under this heading. In these the photoelastic and the piezo-rotatory tensors are of different forms as Table II shows. It is clear from the nature of the gyration tensor (Table II, Nos*. 3 and 4) that the unstressed crystal has no optical rotation along the optic axis. Again no rotation can be induced by an hydrostatic stress or a uniaxial stress along the optic axis. If we subject the crystal to a stress X acting perpendicular to optic axis, then the changes in the index and gyration tensors are given by

$$A_{11} = -0uX, \quad A_{22} = -012X, \quad A_{33} = -031X, \quad A_{44} = 0$$

and

$$A_{fti} = -R_{iX}, \quad A_{\xi 22} = -R_{12X}, \quad A_{\xi 33} = -R_{31X}, \quad A_{gii} = 0.$$

Hence, the crystal becomes biaxial. Normally $q_{zi} > q_{it} > q_{129}$ and hence the optic axial plane is YZ plane. The angle V that one of the optic axes makes with Z axis is given by

$$\begin{aligned} \sin^2 V &= \frac{a_{11} - a_{33}}{\#22 - \#33} = \frac{a_{33} - a_{11}}{\#33 - \#22} \\ &= \frac{-(q_{31} - q_{11})X + (a^{\circ}_e - a^{\circ}_o)}{-(q_{31} - q_{11})X + (a^{\circ}_e - a^{\circ}_o)}. \end{aligned}$$

For most of the crystals this tilt will be very small for normal stresses. In ADP this is 1° per K bar. The optical rotation along the optic axis is given by

$$\begin{aligned} P &= \xi_{33} \cos^2 V + g_{22} \sin^2 V \\ &= - (R_{31} \cos^2 V - R_{12} \sin^2 V) X \end{aligned}$$

As V is very small,

$$P \approx -R_{31}X$$

$$R_{31} \ll -j^r \rho.$$

Hence, one of the constants can be evaluated.

8. NON-ENANTIOMORPHIC OPTICALLY INACTIVE UNIAXIAL CRYSTALS

Crystals belonging to this class are not optically active in the unstressed state, but they become optically active under stress. The photoelastic and the piezo-rotatory matrices have different forms and they are shown in Table III (Nos. 1, 2, 3, 4 and 5). In none of the classes a stress along the optic axis induces any rotation along the stress direction. Stresses acting perpendicular to the optic axis even though they induce rotation, their maximum effect is felt along directions along which birefringence is also present. Thus experimentally it is difficult to extract any of the piezo-rotation coefficients.

9. OPTICAL ACTIVITY IN NON-ENANTIOMORPHIC CRYSTALS

As has been mentioned earlier it is difficult to make measurements of the optical activity in directions other than that of the optic axis. The only crystal in which accurate measurements of the optical activity have been made perpendicular to the optic axis is a-quartz (Bruhat and Grivet, 1935; Munster and Szivessy, 1935). A method of measuring optical activity perpendicular to the optic axis in the case of the uniaxial crystal benzil was suggested (*see* Ramachandran and Ramaseshan, 1961, p. 166) some years ago. In this positive uniaxial crystal the birefringence progressively decreases as one goes from red to blue so that at $\lambda = 4900 \text{ \AA}$ the crystal shows no birefringence. It was suggested that the rotation could be measured at this wavelength in any direction with ease. It is interesting that this method of measuring the rotation when a birefringent crystal becomes isotropic has been used with success by Hobden (1969) in AgGeS_2 . By this experiment the long-standing problem of the measurement of optical activity in non-enantiomorphic crystals which do not exhibit optical activity along the optic axis has been solved.

At these wavelengths crystals like AgGeS_2 and benzil become isotropic and so it must also be possible to obtain the different piezo-rotatory coefficients.

The method of obtaining the piezo-rotatory coefficient given in Section 5 for the point group $\bar{4}3m$ suggests a method by which optical activity could be measured in different directions in these non-enantiomorphic classes. In theory by stressing the crystal in a particular direction it is possible to get the optic axis in a direction that is different from that in the unstressed crystal. It would then be possible to measure the optical activity along the new optic axis. Again, in theory, it should be possible, by choosing different directions and magnitudes of stress, to map out the gyration surface. Here one assumes that the change in the optical activity due to stress is so small that the measured value may be taken to correspond to the optical activity of the unstressed crystal in that direction.

Unfortunately, these speculations prove to be of no use in the cases of ADP and KDP which belong to the non-enantiomorphic group $42m$. The maximum tilt of the optic axis that one could obtain experimentally is much lower than a degree. However, in the case of less birefringent crystals this possibility must be kept in mind.

REFERENCES

1. Bruhat, G. and Grivet, R. .. *J. Phys. Radium*, 1935, 6, 12.
2. Hobden, M. V. .. *Ada Cryst.*, 1968, 24 A, 676.
3. Munster, C. L. and Szivessy, G. *Z. Physik.*, 1935, 36, 101.
4. Ramachandran, G. N. and Ramaseshan, S. *Crystal Optics—Handbuch der Physik*, Springer Verlag, Berlin, 1961.
5. Ramaseshan, S. and Ranganath, G. S. *Piezo-optic Phenomena—Physics of the Solid State*, Bhagavantam, Festschrift, Academic Press, London, New York, 1969.
6. ——— and Vedam, K. *Photoelastic Effect—Progress in Crystal Physics*, Edited by R. S. Krishnan-Viswanathan, Madras, 1958.
7. Ranganath, G. S. and Ramaseshan, S. *J. Opt. Soc. Amer.*, 1969 a, 59, 1229.
8. ——— .. *Curr.Sci.* 1969 b, 38, 303.

ALKYLATION AND ARAALKYLATION OF N-HETEROCYCLES

Part m. Methylation and Benzylation of 5 (or 6)-Chloro Benzimidazoles

BY K. KONDAL REDDY AND N. V. SUBBA RAO, F.A.S.C.

(Department of Chemistry, Osmania University, Hyderabad-!)

Received September 18, 1968

ABSTRACT

Methylation and benzylation of 5 (or 6)-chloro benzimidazoles have been carried out under uniform conditions and the structures of the products obtained have been established by comparison with authentic samples prepared by unambiguous methods. The results are explained on the basis of inductive ($-I$) and resonance ($+M$) effects of chlorogroup and the tautomer stabilisation.

INTRODUCTION

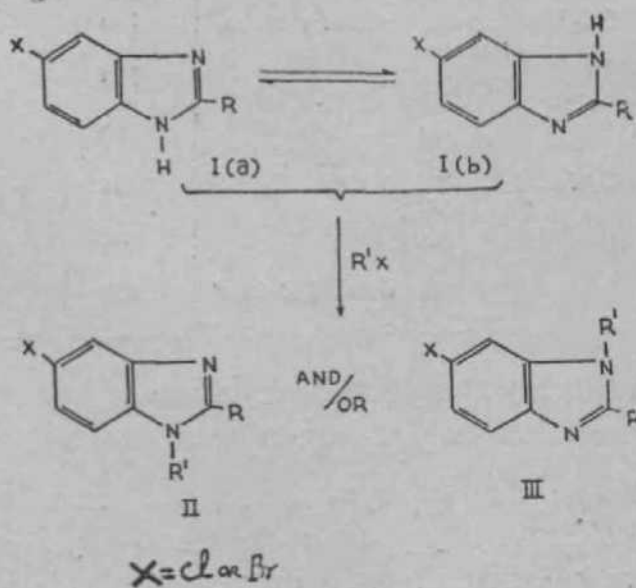
THE methylation of tautomeric halo benzimidazoles under different conditions, was first studied by Fischer and co-workers,^{1* 2} later by Phillips³ and more recently by Ridd and co-workers.⁴ Their results are summarised in Table I.

Phillips concluded that the formation of 1,6-isomer (III) is favoured when methyl sulphate is the methylating agent. In the presence of alkali, however, the proportion of 1, 6-isomer was observed to be reduced. Results obtained by the repetition of Phillips experiments by Smith and Ridd⁴ suggested that the almost exclusive formation of 1, 6-isomer must be incorrect. Quite recently, Aliprandi *et al*.⁵ obtained exclusively 1, 5-isomer (II) by the alkylation of 5 (or 6)-chlorobenzimidazole (I; X = Cl; R = H) with potassium alkyl sulphates under alkaline conditions. Rao and Ratnam⁶ reported the formation of 1,5-isomer (II; X = Cl, R = C₆H₅ and R' = C₆H₅CH₂) by refluxing 5 (or 6)-chloro-2-phenyl benzimidazole (I; X = Cl; R = QH₅) with 2 moles of benzyl chloride in the presence of fused sodium acetate and a speck of iodine.

TABLE I

Results of *N*-substitution in 5 (or 6)-Halo benzimidazoles (T)

St. No.	X	R	Reagent	Product	Reference
				Ratio of 1, 5 to 1, 6-isomer	
1	Cl	H	CK,I in CH ₃ OH	Methiodide of 1, 6-Uomer	1
2	Cl	H	KOSO ₃ CH ₃ + OH ⁻	1, 5-Isomer only	
3	Cl	H	(C ₆ H ₅) ₂ SO ₄ + OH ⁻	h	:
4	Cl	CH ₃	CH ₃ I	Methiodide of 1, 5-isomer	
5	Br	H	CH ₃ I	ii	:
6	Br	CH ₃	CH ₃ I	ii	2
7	Br	CH ₃	(CHO ₂) ₂ SO ₄	1:60	3
8	Br	CH ₃	(CH ₃) ₂ SO ₄ + OH ⁻	1:12	.
9	Br	CH ₃	(CH ₃) ₂ SO ₄	1:1	4
10	Br	CH ₃	(CH ₃) ₂ SO ₄ + OH ⁻	6:6	4
11	Br	CH ₃	CH ₃ I in CH ₃ OH	1, 6-isomer only	3
12	Cl	C ₆ H ₅	C ₆ H ₅ CH ₂ Cl CH ₃ COONa + Ia	1, 6-isomer only	6



The results obtained by earlier workers are so varying that no positive conclusions regarding the influence of substituents can be drawn. Hence it was considered desirable, in continuation of our studies of methylation and benzylation of 5 (or 6)-methyl benzimidazoles,⁷ to carry out a systematic study of methylation and benzylation of 5 (or 6)-chloro benzimidazoles (I; X = Cl, R = H, CH₃ and C₆H₅).

5 (or 6)-Chloro- and 5 (or 6)-chloro-2-methyl benzimidazoles have been prepared from 4-chloro-o-phenylenediamine by Phillips method.⁸ 5 (or 6)-Chloro-2-phenyl benzimidazole was obtained by heating 4-chloro-o-phenylenediamine with benzoic acid under pressure.⁹ To characterise the products of methylation and benzylation of these tautomeric benzimidazoles, the required N-substituted-5-chloro and 6-chloro benzimidazoles (II and III) have been obtained by unambiguous methods. Methylation and benzylation has been carried out as described earlier.⁷ The mixtures obtained on benzylation of 5 (or 6)-chloro and 5 (or 6)-chloro-2-methyl benzimidazoles could not completely be separated into the components. However, they could be separated as methiodides by fractional precipitation. The results of methylation and benzylation are summarised in Table II.

TABLE II

Results of methylation and benzylation of 5 (or 6) Chloro Benzimidazoles (I)

Sl. No.	X	R	Conditions	Relative percentage yields of		
				1,5-isomer	1, 6-isomer	Quaternary salt
1	Cl	H	CH ₃ I in acetone, potassium carbonate, 40 hours	100
2	Cl	CH ₃	do.	100
3	Cl	C ₆ H ₅	do.	50	..	60
4	Cl	H	C ₆ H ₅ CH ₂ Cl, CH ₃ COONa, I _a , IS hrs., 170-180°C.	34	66	..
5	Cl	CH ₃	do.	63	97	..
6	Cl	C ₆ H ₅	do. 0 hr., 160-180°	100

In general, on methylation and benzylation of tautomeric halo benzimidazoles, the formation of 1,5-isomer seems to be favoured.

It is well known that halogen atoms can exert inductive (−I) and mesomeric (+M) effects that oppose each other. By a study of pK_a values it has been shown^{1*,12} that all halo benzimidazoles are less basic than

benzimidazole regardless of position of substituent. The halogen atom must, therefore, exhibit a predominantly base-weakening effect (—1). The order of basicity for the halo benzimidazoles has been shown to be $F > I > Cl > Br$. Thus chlorine and bromine show a smaller mesomeric effect (+M) and their inductive effect (—1) is more noticeable. While pK_a values show that halogen atoms exert predominantly an inductive effect, the ultraviolet data¹¹ support the existence of resonance effects similar to those observed for the halogenated benzenes.

In 5 (or 6)-chloro benzimidazoles (I; X = Cl; R = alkyl and aryl) if the electron attracting character of the chloro group predominates the tautomer (I *b*) is stabilised which reacts with the alkylating agent by $S_E 2'$ -mechanism, resulting in the formation of 1, 5-isomer (II). But due to electro-meric effects tautomer (I *a*) is likely to be stabilised leading to the formation of 1,6-isomer (III). Normally, one would expect mixtures of 1,5- and 1,6-isomers to be obtained in the chloro compounds unless one of the effects is predominant. Since 1, 5-isomer is obtained exclusively on methylation, the inductive effect seems to be dominating. On benzylation of 5 (or 6)-chloro and 5 (or 6)-chloro-2-methyl benzimidazoles, mixtures of 1, 5- and 1, 6-isomers have been obtained in 1 :2 and 2 :1 proportions respectively. These results indicate that both inductive and electro-meric effects are operating. In the case of 5 (or 6)-chloro-2-phenyl benzimidazole, 1,5-isomer alone has been obtained as reported by Rao and Ratnam.⁸

EXPERIMENTAL

1, 2-Dimethyl-5-chloro benzimidazole

N[^]Methyl-5-chloro-o-phenylenediamine¹³ (1.2 g.) was condensed with acetic acid by refluxing in 4 N hydrochloric acid (25 ml.) for two hours. The reaction mixture was diluted, filtered free from solid impurities and basified with dilute ammonia when an almost colourless solid (1 g.) melting at 69-70° was obtained. This was dried at 110° for one hour and crystallised from benzene-petroleum ether to get pure 1,2-dimethyl-5-chloro benzimidazole as colourless rectangular plates, m.p. 132-33° C. (Found: C: 59.5; H : 5.2; N : 15.6; C₉H₉ClN₂ requires C : 59.8; H : 5.0; N: 15.5%).

1-Methyl-2-phenyl-5-chloro benzimidazole

A mixture of N[^]methyl-5-chloro-o-phenylenediamine (1.5 g.) and benzaldehyde (1 g.) in alcohol (15 ml.) and nitrobenzene (10 ml.) was heated on a steam bath for two hours. After evaporation of the alcohol, the

reaction mixture was steam distilled to remove nitrobenzene and aldehyde. The dark brown residue (1 g.) was dried and recrystallised from alcohol and then repeatedly from benzene-petroleum ether to give pure 1-methyl-2-phenyl-5-chloro benzimidazole, m.p. 139-40°C. colourless] plates (Found: C:69.6; H:4.9; N:11.2; $C_{14}H_{10}ClN_2$ requires C:69.3; H:4.5; N:11.5%).

1-Methyl-2-phenyl-6-chloro benzimidazole

Condensation of N^2 -methyl-4-chloro-0-phenylenediamine¹⁸ (1.5 g.) with benzaldehyde (0.9 g.) in alcoholic nitrobenzene and working out the reaction mixture gave a brown solid (1.1 g.). On recrystallisation from benzene-petroleum ether pure 1-methyl-2-phenyl-6-chloro benzimidazole was obtained as bushy needles, m.p. 124° (Found: C:69.4; H:4.8; N:11.6; $C_{14}H_{10}ClN_2$ requires C:69.3; H:4.5; N:11.5%).

The following methiodides were obtained by leaving over-night the appropriate 1-benzyl benzimidazole with methyl iodide in benzene solution. The solid separated was filtered, washed with dry ether.

(a) 1-Benzyl-5-chloro benzimidazole methiodide; m.p. 215° (Found: C:46.4; H:3.9; N:7.0; $C_{15}H_{14}ClIN_2$ requires C:46.8; H:3.6; N:7.3%).

(b) 1-Benzyl-2-methyl-5-chloro benzimidazole methiodide, m.p. 225° (Found: C:48.6; H:3.9; N:7.2; $C_{16}H_{16}ClIN_2$ requires C:48.2; H:4.0; N:7.0%).

(c) 1-Benzyl-6-chloro benzimidazole methiodide; m.p. 182-83° (Found: C:46.3; H:3.3; N:7.5; $C_{16}H_{14}ClIN_2$ requires C:46.8; H:3.6; N:7.3%).

(d) 1-Benzyl-2-methyl-6-chloro benzimidazole methiodide; m.p. 219-220° (Found: C:47.9; H:4.2; N:7.4; $C_{16}H_{16}ClIN_2$ requires C:48.2; H:4.0; N:7.0%).

Methylation of 5 (or 6)-chloro benzimidazole

A solution of 5 (or 6)-chloro benzimidazole¹ (0.92 g.) and methyl iodide (0.9 g.) in dry acetone (50 ml.) was gently refluxed over anhydrous potassium carbonate for forty hours. Acetone was evaporated, the residue was treated with cold water (100 ml.) and extracted with chloroform. The chloroform extracts were evaporated when a low melting solid (0.8 g.) was obtained. This was dissolved in dry acetone saturated with hydrogen fluoride gas. The precipitated hydrochloride was filtered, washed with

benzene and recrystallised from ethanol-ether mixture giving colourless needles, m.p. 238° C. This was found to be identical in all respects with an authentic sample of 1-methyl-5-chloro benzimidazole hydrochloride¹³ (m.p. 240-41°) and their mixed melting point was found to be undepressed.

Methylation of 2-methyl-5 (or 6)-chloro benzimidazole.

Methylation of 2-methyl-5 (or 6)-chloro benzimidazole² (0.68g.) gave a low melting solid. This was dissolved in dry chloroform and saturated with hydrogen chloride gas and the precipitated hydrochloride (m.p. 273°) was filtered and decomposed by the addition of ammonia when a compound (0.55 g.), m.p. 65° was obtained. This was dried at 110° for one hour and recrystallised from benzene-petroleum ether giving colourless rectangular rods, m.p. 132°. By comparison with synthesised 1,2-dimethyl-5-chloro and 6-chloro¹³ benzimidazoles this compound was found to be identical with the former. Its mixed melting point with 1, 2-dimethyl-5-chloro benzimidazole was undepressed (131°) whereas that with 1, 2-dimethyl-6-chloro benzimidazole was depressed (90-102°).

Methylation of 5 (or 6)-chloro-2-phenyl benzimidazole

Methylation of 2-phenyl-5 (or 6)-chloro benzimidazole⁹ (0.8 g.) with methyl iodide (0.7 g.) gave a solid (0.8 g.). This was triturated with dry benzene (100 ml.) and the insoluble compound (0.4 g.) was filtered. It recrystallised from benzene-alcohol mixture as colourless needles, m.p. 236-38° and analysed for 1, 3-dimethyl-2-phenyl-5-chloro benzimidazolium iodide (Found: C :46.5; H :3.9; N :7.0; C₁₆H₁₄ClIN₂ requires C: 46.8; H :3.7; N :7.3%). The residue (0.4g.) obtained on evaporation of the benzene solution, crystallised from benzene petroleum ether mixture as colourless plates, m.p. 140°. This was found to be identical with a synthetic sample of 1-methyl-2-phenyl-5-chloro benzimidazole in crystalline shape and their mixed melting point was undepressed. However, it differed from 1-methyl-2-phenyl-6-chloro benzimidazole in crystalline shape and their mixed melting point was depressed (88-102°).

Benzylation of 5 (or 6)-chloro benzimidazole

5 (or 6)-Chloro benzimidazole (1.5g.), freshly distilled benzyl chloride (1.2 g.) fused sodium acetate and a speck of iodine were thoroughly mixed and heated for fifteen hours on an oil-bath maintained at 170-80°. The reaction mixture while still hot was poured into crushed ice with vigorous stirring. The solid obtained was filtered and washed repeatedly with CQ14

petroleum ether. On crystallisation from dilute alcohol a colourless solid (1.7 g.) melting at 80-100° was obtained. Its mixed melting point with authentic samples of 1-benzyl-5-chloro¹⁴ and 1-benzyl-6-chloro¹³ benzimidazoles was undepressed. This could not be separated into the components directly. 0.5 g. of the benzylation product was converted into methiodide (m.p. 160-170°) by leaving overnight its benzene solution with methyl iodide. The mixture of methiodides thus obtained was dissolved in chloroform and fractional precipitation by the addition of small quantities of petroleum ether (60-80°) gave compound A (0.23 g.) m.p. 214° in the first fractions, whereas last fractions gave compound B (0.45 g.) m.p. 180°. The compounds (A) and (B) were found to be methiodides of 1-benzyl-5-chloro and 1-benzyl-6-chloro benzimidazole respectively by comparison with authentic samples.

Benzylation of 2-methyl-5 {or 6}-chloro benzimidazole

Benzylation of 2-methyl-5 (or 6)-chloro benzimidazole (1.2 g.) by general method gave a colourless compound (1.3 g.), m.p. 85-102°, indicating it to be a mixture. This could be resolved into its components by converting 0.5 g. of the material into methiodides (m.p. 200-10°) and by fractional precipitation from the acetone solution by the addition of small quantities of petroleum ether. Compound A (0.42 g.) m.p. 224° obtained in the first fractions and compound B (0.25 g.), m.p. 220° from the last fractions were found to be identical in all respects with authentic samples of 1-benzyl-2-methyl-5-chloro and 6-chloro benzimidazole methiodides respectively.

Benzylation of 2-phenyl-5 (or 6)-chloro benzimidazole

Benzylation of 2-phenyl-5 (or 6)-chloro benzimidazole (1.0 g.) at 160-80° for nine hours by the general method, gave a resinous solid which on treatment with a little alcohol gave a granular solid (0.88 g.). This was recrystallised from alcohol yielding prismatic rods, m.p. 170°, found to be identical with synthesised 1-benzyl-2-phenyl-5-chloro benzimidazole¹⁶ in crystalline shape and melting point. Their mixed melting point was found to be undepressed; whereas its mixed melting point with 1-benzyl-2-phenyl-6-chloro -benzimidazole¹⁶ was depressed (45-50°).

REFERENCES

1. Fischer .. *Ber.* 1904, 37, 552.
2. ———— and Mouson .. *Ibid.*, 1905, 38, 32Q

3. Phillips .. *J. Chem. Soc.*, 1931, p. 1143.
4. Ridd and Smith .. *Ibid.*, 1960, p. 1363.
5. Aliprandi *et al.* .. *Chem. Abstr.*, 1962, 56, 15500.
6. Rao and Ratnam .. *J. Chem. Soc.*, 1959, p. 3087.
7. Reddy and Rao .. *Proc. Ind. Acad. Sci.*, 1969, 70, 81.
8. Phillips .. *J. Chem. Soc.*, 1928, p. 2393.
9. Poiai-Koshitse/a/. .. *J. Gen. Chem.*, 1947, 17, 1768; 1949, 19, 1545.
10. Davies *et al.* .. *J. Pharm. Pharmacol.*, 1951,3, 420.
11. Rabiger and Joullie .. *J. Chem. Soc.*, 1964, p. 915.
12. Reddy, Rao and Kost .. (Under Publication).
13. Feitelson *et al.* .. *J. Chem. Soc.*, 1952, p. 2389.
14. Reddy, Rao and Ratnam .. *Ind. J. Chem.*, 1963, 1, 96.
15. Rao and Ratnam .. *Proc. Ind. Acad. Sci.*, 1958, 47, 77.

RAMAN AND INFRARED SPECTRA AND NORMAL VIBRATIONS OF N-METHYLPROPIONAMIDE AND N-DEUTERATED N-METHYL PROPIONAMIDE

BY P. USHA BAI AND K. VENKATA RAMIAH

{Department of Physics, College of Science, Osmania University, Hyderabad-!}

Received April 22, 1968

(Communicated by Dr. N. A. Narasimham, F.A.S.C.)

ABSTRACT

Raman and infrared spectra of N-methyl-propionamide and N-deuterated N-methyl-propionamide were recorded in various states of aggregation—pure amide, in solution and vapour state—and the frequency changes of the functional groups were studied. The inplane skeletal vibrations of N-methyl-propionamide and its deuterated compound were calculated treating these molecules as six-body problems. The distribution of potential energy of each normal mode among various symmetry co-ordinates was calculated and the nature of the amide I, II and III bands and the mixing up of the inplane vibrational frequencies of N-methyl-propionamide and the deuterated amide are discussed on a **quantitative** basis.

INTRODUCTION

THE infrared spectroscopic studies of amides received considerable attention in recent times, since the spectroscopic study of -CONH- group plays an important role in the elucidation of the structure of peptide linkages and investigations of proteins. Miyazawa *et al.*,^{1*} DeGraaf and Sutherland,⁸ Suzuki,^{4,6} Beer *et al.*¹ and Venkata Ramiah *et al.*⁵ studied the infrared spectra of a number of primary, secondary and tertiary amides and of their deuterated species and carried out the normal co-ordinate treatment of some of these molecules. However, a full analysis of the normal vibrations of N-methyl-propionamide molecule has never been attempted. The authors* have recorded the infrared and Raman spectra of N-methyl propionamide and its N-deuterated amide in various states of aggregation and subjected them to normal co-ordinate treatment with a view to clarify the nature of the inplane normal vibrations of these molecules.

EXPERIMENTAL

The infrared spectra of N-methyl-propionamide, and of the amide in vapour state were recorded in the region 3500 cmr^{-1} to 250 cmr^{-1} with Perkin-Elmer Model-521 grating spectrophotometer. The spectrum of the liquid amide was recorded by using a microfilm of unknown thickness between two plates of cesium bromide. The spectrum of the amide in the vapour state was recorded by introducing a few drops of the amide in evacuated 10 cm. cells with NaCl and CsBr windows and maintaining their temperatures from 40° C. to 80° C. Lower temperatures were used for recording strong absorption bands and higher temperatures were maintained for weak bands. The spectra of the amide and its deuterated amide were recorded in the region of 3500 cmr^{-1} to 1300 cmr^{-1} with Perkin-Elmer Model-221 infrared spectrophotometer and in the region of 1300 cmr^{-1} to 400 cmr^{-1} by Perkin-Elmer Model-337 grating spectrophotometer. The Raman spectrum of N-methyl-propionamide was recorded with Hilger-Raman source unit and Fuess glass spectrograph and A 4358 A was used as exciting radiation.

Replacement of the H-atom of the N-H group by Deuterium was accomplished by adding threefold excess of D_2O to the amide, pumping off the heavy water and repeating the process three times. About 80% of the amide could be converted into the deuterated amide.

RESULTS AND DISCUSSION

The Raman and infrared frequencies of N-methyl-propionamide, and in the vapour state are given in Table I and the frequencies of the functional groups of the amide and the N-deuterated amide are given in Table II.

The corresponding infrared and Raman spectra are shown in Figs. 1, 2, 3 and 4.

In Figs. 2 and 3, the absorption bands arising out of the stretching and bending modes of vibrations of N-H and N-D groups are indicated by arrows.

The results in Table II indicate that the frequencies of $\nu(\text{N-H})$ and amide I band of N-methyl-propionamide in vapour state are much higher and those of amide II, amide III and $\delta(\text{N-H})$ bands are much lower than the frequencies of the corresponding bands in the pure amide: The N-D stretching frequencies appear in the region of 2475 cmr^{-1} and 2417 cmr^{-1} and

TABLE I

Raman and infrared frequencies of N-Methyl-propionamide(Frequencies in cm.^{-1})

Raman	Infrared		Assignment
	Pure amide	Vapour	
..	..	3430	$\nu(\text{N-H})$ free
3337 (2)	3300	..	$\nu(\text{N-H})$ bonded
...	3150 (m)	3135 (w)	..
..	3095 (m)	..	2 x 1550
..	2970 (m)	2980 (ms)	$\nu_0(\text{CH}_2)\text{N}$
2940 (4)	2935 (ms)	2940 (ms)	$\nu_m(\text{CH}_2)\text{C}$
2860 (4)	2875 (m)	2875 (m)	$\nu(\text{CH}_2)\text{N}$
..	2800 (w)	2800 (vw)	$p(\text{CH}_2)\text{C}$
1662 (7)	1640 (vs)	1715 (vs)	$\nu(\text{C=O})$ amide I
..	1550 (s)	1495 (s)	5 (N-H) Amide-II
1458 (3)	1460 (m)	..	$S_{\ll}(\text{CH}_2)\text{N}$
1406 (1)	1410 (m)	1418 (w)	$f(\text{CH}_2)\text{C}$
1356 (6)	1372 (m)	1385 (ms)	$\ll(\text{CH}_2)\text{N, C}$
1266 (2)	1273 (m)	1258 (m)	$\nu(\text{C-N})$ Amide III
1234 (4)	1238 (m)	1210 (ms) J	
1146 (6)	1160 (ms)	1140 (ms)	$\diamond(\text{CH}_2)\text{N}$
..	..	1080 (ms)	$\gamma(\text{CH}_2)\text{N}$
..	1040 (ms)	1030 (sh)	$\gamma(\text{CH}^{\wedge}\text{C}$
1000 (5)	970 (w)	970 (w)	$\nu(\text{N-CH}_2)$
864 (9)	865 (m)	860 (m)	$\nu(\text{C-CH}^{\wedge})$
..	800 (m)	800 (m)	$\nu(\text{C-CH}_2)$
..	695 (s, br)	680 (s, br)	$S(\text{N-H})\text{X}$
590 (4)	575 (s)	575 (m)	$\delta(\text{O=C-N})$
423 (6)	430 (m)	430 (m)	$\gamma(\text{C-CH}^{\wedge})$
283 (1)	315 (m)	315 (m)	$a(\text{C-N-CH}_2)$

TABLE II
Infrared frequencies of the functional groups
 (Frequencies in cm.⁻¹)

N-methyl-propionamide				N-de (iterated N- methyl- piopionamide		
Mode of vibration	Amide	In solution of CCl ₄ *	Vapour	Mode of vibration	Amide	In solution of eCu
	..	3430	3430	..	S475	2476
ν (N-H)	..	3300	..	ν (N-D)	2417	2417
Amide I	..	1640	1650	Amide I	1627	1627
.. II	..	ISM	1045	.. II	1475	1475
.. III	..	1272! 1238/	1270 I 1236 I	.. III	1100	1100
& (N-H) J_	..	695	690	8 (N-D) Ji	000	500

with increasing dilution of the deuterated amide in CCl₄ the band at 2475 cm⁻¹ becomes more prominent. The amide II, III and 8 (N-H)J_ bands at 1550 cm⁻¹, 1273 cm⁻¹ and 1238 cm.⁻¹ and 695 cm.⁻¹ in the pure amide appear at 1475 cm.⁻¹, 1100 cm⁻¹ and 500 cm.⁻¹ in the deuterated amide, as indicated by arrows in Figs. 2 and 3. The functional groups responsible for H-bond in amides are the NH and CO groups and the higher frequencies of ν (N-H) and amide I bands or the lower frequencies of the amide II, amide III and S (N-H)X bands of the amide in the vapour state compared to those of the corresponding bands of the pure amide are due to the breaking up of the intermolecular associations resulting in free N-H and C=O linkages. Beer *et al.*² assigned the two bands at 1273 cm⁻¹

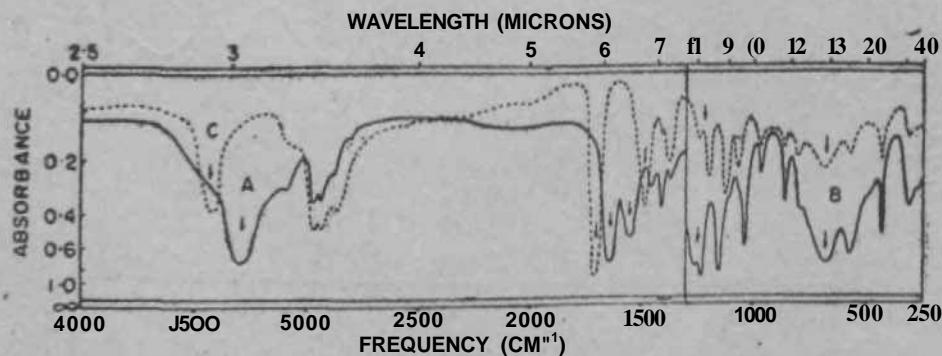


FIG. 1. Infrared spectra of *N*-methyl-propionamide (liquid). A, Film of smaller thickness (full line); B, film of higher thickness (full line); C, in vapour state (dotted line).

and 1238 cm.^{-1} together as the amide III band. The frequency of the band at 1238 cm.^{-1} in pure amide shifts by 18 cm.^{-1} towards lower frequency in the spectrum of the amide in vapour state; and the shift in case of the other band at 1273 cm.^{-1} is 15 cm.^{-1} . In the deuterated amide these two peaks almost disappear and a new band appears at 1100 cm.^{-1} .

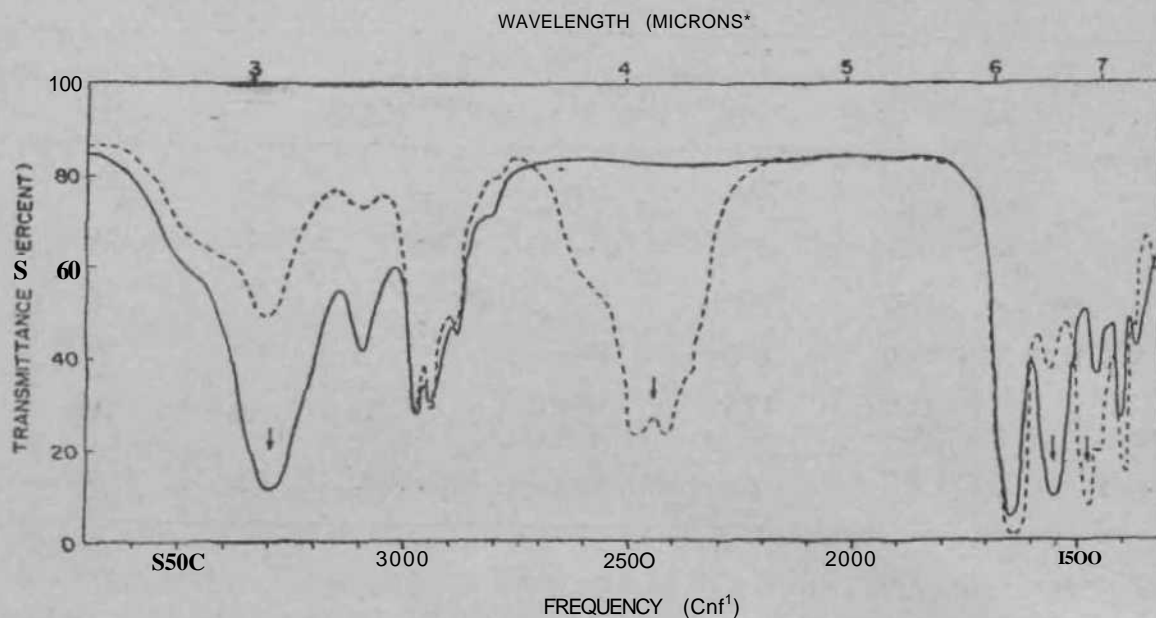


Fig. 2. Infrared spectra of N-methyl-propionamide (full line) and N-deuterated N-methyl-propionamide (dotted line).

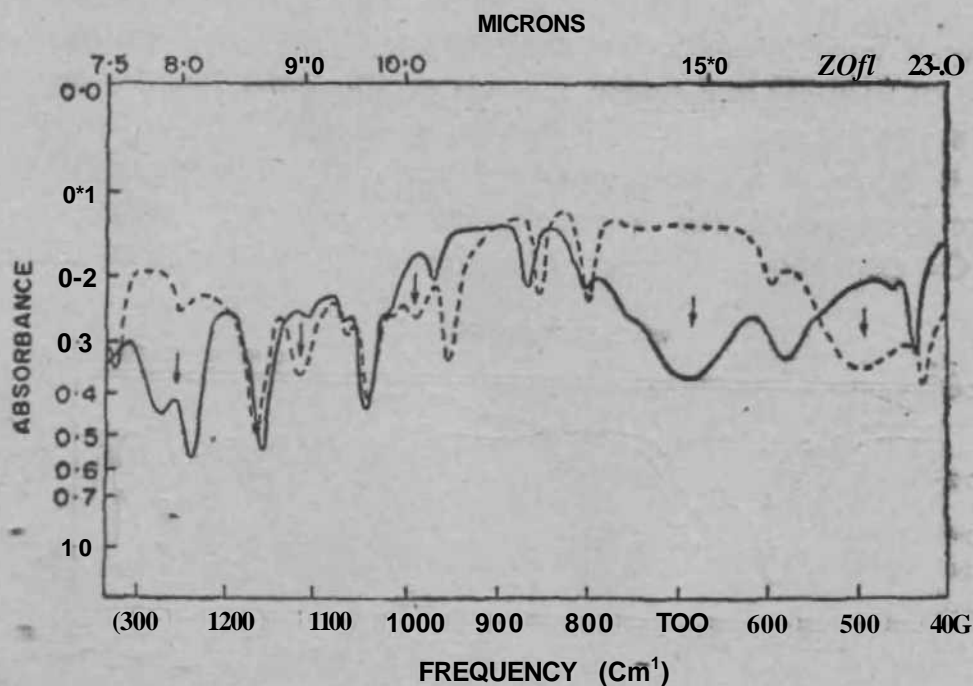
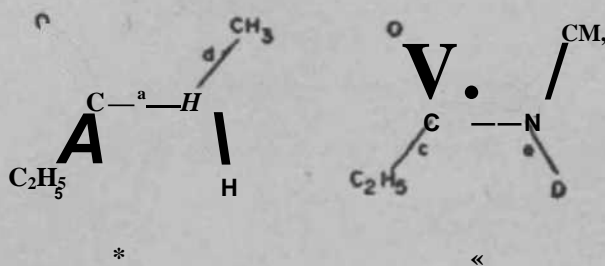


FIG. 3. Infrared spectra of N-methyl-propionamide (full line) and N-deuterated N-methyl-propionamide (dotted line).

NORMAL CO-ORDINATE TREATMENT

The structures of *N*-methyl-propionamide and *N*-deuterated *N*-methyl-propionamide are given in Fig. 5.



Bo. 5. A, *N*-methyl-propionamide; B, *N*-deuterated *N*-methyl-propionamide.

These molecules are treated as six-body problems taking CH₃ and C₃H₅ groups as point masses. They are planar with the point group C_s and the twelve fundamental frequencies are classified into nine inplane (A') and three out-of-plane (A'') vibrations. The orthonormalised set of symmetry co-ordinates for the inplane vibrations of the molecule are given in Table III.

TABLE III

The symmetry co-ordinates

Symmetry co-ordinates	Vibrational mode	Abbreviation
$S_1 = \Delta a$	C - N stretching	ν (C - N)
$S_2 = \Delta b$	C=O stretching	ν (C=O)
$S_{3 \sim} \Delta c$	C - C ₂ H ₅ stretching	ν (C - C ₂ H ₅)
$S_4 = \Delta d$	N - CH ₃ stretching	ν (N - CH ₃)
$S_5 = \Delta e$	N - H stretching	ν (N - H)
$S_6 = \frac{1}{\sqrt{6}} (2 \Delta ab - \Delta bc - \Delta ca)$	O=C - N bending	δ (O = C - N)
$S_7 \approx \frac{1}{\sqrt{2}} (Abe - Aca)$	C-C ₂ H ₅ bending	δ (C - C ₂ H ₅)
$S_8 = \frac{4i}{\sqrt{5}} (2 Aad - Ade - Aw)$	N - CH ₃ bending	S(N-CH ₃)
$S_9 = \frac{1}{\sqrt{2}} (\Delta ae - \Delta ad)$	N - H bending	S(N-H)

The elements of the F-matrix obtained by using the coefficients of the general quadratic potential energy function and the expression

*

$$F = ufn \quad (1)$$

are

$$F_u = / a$$

$$F_{12} = / \ll b$$

$$F_{13} = / a^c$$

$$F_{14} = / a^d$$

$$F_{15} = / a^e$$

$$F_{16} = \frac{1}{\sqrt{6}} (J_a^{ob} - J_a^{bc} - J_a^{ca})$$

$$F_{17} = \wedge J_a^{hc} \sim J_a^{ca}$$

$$F_{18} = \frac{1}{\sqrt{6}} (2f_a^{ad} - f_a^{ed} - f_a^{ae})$$

$$F_{19} = \frac{1}{\sqrt{2}} (-f_a^{ed} + f_a^{ae})$$

$$F_{20} = / b$$

$$F_{21} = / b^c$$

$$F_{22} = / b^d$$

$$F_{23} = f_b^e$$

$$F_{24} = \wedge g (2/b^{ob} - / b^{be} - / b^{ca})$$

$$F_{25} = \wedge (A^{bc} \sim / b^{cf})$$

$$F_{26} = \frac{1}{\sqrt{6}} (2f_b^{ad} - f_b^{ed} - f_b^{ae})$$

$$F_{27} = \frac{1}{\sqrt{2}} (-f_b^{ed} + f_b^{ae})$$

$$F_{33} = f_c$$

$$F_{34} = /c^*$$

$$F_{35} = /e^*$$

$$F_{36} = \frac{1}{\sqrt{6}} (2f_c^{ab} - f_c^{bc} - f_c^{ca})$$

$$F_{37} = \frac{1}{\sqrt{2}} (f_c^{be} - f_c^{ca})$$

$$F_{38} = \frac{1}{\sqrt{6}} (2f_c^{ad} - f_c^{ed} - f_c^{ae})$$

$$F_{39} = \frac{1}{\sqrt{2}} (-f_c^{ed} + f_c^{ae})$$

$$F_{44} = f_d$$

$$F_{45} = f_d^e$$

$$F_{46} = \frac{1}{\sqrt{6}} (2f_d^{ab} - f_d^{bc} - f_d^{ca})$$

$$F_{47} = \frac{1}{\sqrt{2}} (f_d^{bc} - f_d^{ca})$$

$$F_{48} = \frac{1}{\sqrt{6}} (2f_d^{ad} - f_d^{ed} - f_d^{ae})$$

$$F_{49} = \frac{1}{\sqrt{2}} (-f_d^{ed} + f_d^{ae})$$

$$F_{55} = f_e$$

$$F_{56} = \frac{1}{\sqrt{6}} (2f_e^{ab} - f_e^{bc} - f_e^{ca})$$

$$F_{57} = \frac{1}{\sqrt{2}} (f_e^{be} - f_e^{ca})$$

$$F_{58} = \frac{1}{\sqrt{6}} (2f_e^{ad} - f_e^{ed} - f_e^{ae})$$

$$F_{59} = \frac{1}{\sqrt{2}} (-f_e^{ed} + f_e^{ae})$$

$$F_{66} = i (4/ab - 4/ab^{bc} - 4f_{ab}^{ca} + 2f_{bc}^{ca} + f_{bc} + f_{ca})$$

$$F_{67} = \frac{1}{\sqrt{12}} (2f_{ab}^{bc} - 2f_{ab}^{ca} - f_{bc} + f_{ca})$$

$$F_{68} = \frac{1}{6} (4f_{ab}^{ad} - 2/f_{fb}^{ed} - 2f_{ab}^{ae} - 2f_{bc}^{ad} + f_{bc}^{ed} + f_{be}^{ae} - 2/ca^{ad} + /c^{cd} + /c^{oe})$$

$$F_{69} = \frac{1}{\sqrt{12}} (-2f_{ab}^{ed} + 2f_{ab}^{ae} + f_{bc}^{ed} - f_{bc}^{ae} + f_{ca}^{ed} - f_{ca}^{ae})$$

$$F_{77} = i (/bc - 2/bc^{ca} + /ca)$$

$$F_{78} = \frac{1}{\sqrt{12}} (2f_{bc}^{ad} - f_{bc}^{ed} - f_{bc}^{ae} - 2f_{ca}^{ad} + f_{ca}^{ed} + f_{ca}^{ae})$$

$$F_w = i (-/bc^{ed} + /bc^{oe} + /c^{ed} - /c^{ae})$$

$$F^{\wedge} = \pounds (4/ad - 4 / ^ - 4/ad^{e} + /,,^{e} + /_{ae} + 2f_{de}^{ae})$$

$$F_{89} = \frac{1}{\sqrt{12}} (-2f_{ad}^{ed} + 2f_{ad}^{ae} + /_{dc} - /_{oe})$$

$$F_{99} = \frac{1}{2} (f_{de} - 2f_{de}^{ae} - f_{ae}).$$

The elements of the G-matrix were derived from the Decius tables.⁹ They are :

$$G_{11} = \mu_N + \mu_C$$

$$G_{12} = /^*_C \cos ab$$

$$G_{13} = \mu_C \cos ac$$

$$G_{14} = /^*_N \cos ad$$

$$G_{15} = HN \cos ae$$

$$G_{16} = -\frac{\sqrt{3}}{\sqrt{2}} \mu_C \frac{\sin ab}{b}$$

$$G_{17} = \frac{1}{\sqrt{2}} \mu_C \left(\frac{\sin ab}{b} + 2 \frac{\sin ac}{c} \right)$$

$$G_{18} = -\frac{\sqrt{3}}{\sqrt{2}} \mu_N \frac{\sin ad}{d}$$

$$G_{19} = \frac{1}{\sqrt{3}} (\sin ad + \sin ae)$$

$$G_{22} = \mu_C + \mu_O$$

$$G_{23} = \mu_C \cos bc$$

$$G_{24} = 0$$

$$G_{25} = 0$$

$$G_{26} = -\frac{\sqrt{3}}{\sqrt{2}} \mu_C \frac{\sin ab}{a}$$

$$G_{27} = -\frac{1}{\sqrt{2}} \mu_C \left(2 \frac{\sin bc}{c} + \frac{\sin ac}{a} \right)$$

$$G_{28} = \frac{\sqrt{3}}{\sqrt{2}} \mu_C \frac{\sin ab}{a}$$

$$G_{29} = -\frac{1}{\sqrt{2}} \mu_C \frac{\sin ab}{a}$$

$$G_{33} = \mu_C + \mu_{C,H}$$

$$G_{34} = 0$$

$$G_{35} = 0$$

$$G_{36} = \frac{\sqrt{3}}{\sqrt{2}} \mu_C \left(\frac{\sin ac}{a} + \frac{\sin bc}{b} \right)$$

$$G_{37} = \frac{1}{\sqrt{2}} \mu_C \left(-\frac{\sin bc}{b} + \frac{\sin ac}{a} \right)$$

$$G_{38} = -\frac{\sqrt{3}}{\sqrt{2}} \mu_C \frac{\sin ac}{a}$$

$$G_{39} = \frac{1}{\sqrt{2}} \mu_C \frac{\sin ac}{a}$$

$$G_{44} = \mu_{CH_3} + \mu_N$$

$$G_{45} = \mu_{CH_3} \cos \theta$$

$$G_{46} = \frac{\sqrt{3}}{\sqrt{2}} \mu_N \frac{\sin ad}{a}$$

$$G_{47} = \frac{1}{\sqrt{2}} \mu_N \frac{\sin gd}{a}$$

$$G_{48} = -\frac{\sqrt{3}}{\sqrt{2}} \mu_N \frac{\sin ad}{a}$$

$$G_{49} = \frac{1}{\sqrt{2}} \mu_N \left(\frac{\sin af}{a}, -\frac{\sin de}{e} \right)$$

$$G_{55} = \mu_N + \mu_H$$

$$G_{56} = -\frac{\sqrt{3}}{2} \sin oc$$

$$G_{61} = -\frac{1}{\sqrt{2}} \mu_N \frac{\sin ae}{a}$$

$$G_{62} = \frac{\sqrt{3}}{\sqrt{2}} \mu_N \left(\frac{\sin de}{d} + \frac{\sin ae}{a} \right)$$

$$G_{63} = \frac{1}{\sqrt{2}} \mu_N \left(-\frac{\sin ae}{a} + \frac{\sin de}{d} \right)$$

$$G_{66} = \frac{3}{2} \left(\frac{\mu_N + \mu_C}{a^2} + \frac{\mu_C + \mu_O}{b^2} - 2\mu_C \frac{\cos ab}{ab} \right)$$

$$\wedge \quad \frac{\sqrt{3}}{2} \left(\mu_C + \frac{\mu_O}{a^2} + \frac{\mu_C + \mu_N}{a^2} - 2\mu_C \frac{\cos ac}{ac} + 2\mu_C \frac{\cos bc}{bc} \right)$$

$$\leftarrow \quad -\frac{3}{2} \left(\frac{\mu_C + \mu_N}{a^2} + \mu_C \frac{\cos ab}{aT} + \mu_N \frac{\cos ad}{ad} \right)$$

$$G_{68} = \frac{\sqrt{3}}{2} \left(\frac{\mu_C + \mu_N}{a^2} - \mu_C \frac{\cos ab}{ab} - 2\mu_N \frac{\cos ae}{ae} + \mu_N \frac{\cos ai}{S} \right)$$

$$+ \frac{\mu_C + \mu_N}{a^2}$$

$$- 4\mu_C \frac{\cos Ac}{bc} - \frac{\sqrt{3}}{2} \mu_C \frac{\cos ac}{ac} + 2\mu_C \frac{\cos ab}{ab}$$

$$G_{78} = \frac{\sqrt{3}}{2} \left(-\frac{\mu_C + \mu_N}{a^2} - \mu_C \frac{\cos ab}{ab} - \mu_C \frac{\cos ac}{ac} + \mu_N \frac{\cos ad}{ad} \right)$$

$$G_{79} = \frac{1}{2} \left(\frac{\mu_C + \mu_N}{a^2} + \mu_C \frac{\cos ab}{ab} - 2\mu_C \frac{\cos ac}{ac} - 2\mu_C \frac{\cos ae}{ae} + \mu_N \frac{\cos ad}{ad} \right)$$

$$G_{89} = \frac{\sqrt{3}}{2} \left(-\frac{\mu_N + \mu_C}{a^2} + \frac{\mu_N + \mu_{CH_3}}{d^2} - 2\mu_N \frac{\cos de}{de} + 2\mu_N \frac{\cos ae}{ae} \right)$$

$$G_{96} = \frac{1}{2} \left(\frac{\mu_H + \mu_N + \mu_{CH_3}}{e^2} - 4\mu_N \frac{\cos ae}{ae} - 4\mu_N \frac{\cos de}{de} + 2\mu_N \frac{\cos ad}{ad} \right)$$

The N-H and N-D stretching frequencies, although are in the region 3300-2400 cm^{-1} , are taken into consideration, in these calculations.

The structure parameters used are r (C-N) = 1.29 Å, r (C=O) = 1.23 Å, r (C-C₂H₆) = 1.55 Å, r (N-CH₃) = 1.47 Å and r (N-H) = 1 Å. All the bond angles are assumed to be 120°.

The calculations of normal vibrations of N-methyl-propionamide and N-deuterated N-methyl-propionamide were made by the method of Wilson. At first instance, the force constants of acetamide were transferred and slight alterations were made in some of the constants to obtain a close fit between the observed and calculated frequencies. The secular determinant which has the dimensionality of 9 X 9 was expanded by the Modified Selewsky's method using Model II, IBM 1620 Digital Computer and Serostto polynomial were extracted using IBM 1620 general programme.

The final set of force constants are given in Table IV.

TABLE IV
Force constants of N-methyl-propionamide

$f.$ = 7.0	$/^*$ = 0.75
$/,$ = 9.2	$/_M$ = 0.30
$/.$ = 4.6	$/_{rt}$ = 1.8
U = 3.5	$/_{\cdot\cdot} = !\cdot!$
$/.$ = 6.0	$/_{\cdot}' = 1.2$
$f_{\cdot\cdot} = 1.5$	$/_{\cdot\cdot} = 0.4$
$/^* = 1.2$	$/_{\cdot\cdot} = 0.9$
$f_{\cdot\cdot} = 0.8$	$/_{\cdot-} = 0.6$

The same force constants were transferred to N-deuterated N-methyl-propionamide and the frequencies were calculated. The calculated frequencies were found to be in good agreement with the observed one.

The elements of the L-matrices have been evaluated by the usual method and normalised to $\bar{L}\bar{L} = G$. Using the expression $FyLi_sLj_s/A_a \times 100$, the potential energy distribution of each normal mode among the various symmetry co-ordinates is calculated. These results, together with the observed and calculated frequencies are given in Table V.

DISCUSSION OF THE NATURE OF THE OBSERVED BANDS

The amide III band is a doublet with two frequencies at 1273 cm^{-1} and 1238 cm^{-1} and the average of these two frequencies, *i.e.*, 1256 cm^{-1} is taken as the frequency of amide III band for the following discussion.

The amide I, II and III bands in N-methyl-propionamide are thus at 1640 cm^{-1} , 1550 cm^{-1} and 1256 cm^{-1} , respectively, and the corresponding absorption frequencies in N-deuterated-N-methyl-propionamide are at 1627 cm^{-1} , 1475 cm^{-1} and 1100 cm^{-1} . The amide I band is essentially due to C=O stretching vibration although C-N stretch contributes considerably. The percentage contribution of C=O stretching vibration to the absorption at 1627 cm^{-1} in deuterated N-methyl-propionamide is higher than that of the corresponding mode to the amide I band at 1640 cm^{-1} in N-methyl-propionamide, but the contribution of C-N stretch to this frequency is relatively low,

TABLE V

Observed and calculated frequencies and potential energy distribution

Frequency		P.E.D.								
Observed	Calculated	s_1	s_2	s_3	s_4	s_5	s_6	s_7	s_8	s_9
(a) $C_2H_5.CC).NH.CH_2$										
1256	1275	25	0	12	1	1	16	1	6	42
1640	1636	32	47	0	1	0	0	7	4	8
865	869	5	2	31	46	0	5	2	3	5
970	980	12	19	0	27	0	9	2	20	0
3300	3301	2	0	0	1	99	0	0	0	0
575	589	0	0	46	7	0	23	16	4	1
430	405	14	0	10	13	0	5	34	23	0
315	307	0	0	0	0	0	38	33	28	0
1550	1565	8	37	11	5	0	13	2	2	45
• (b) $C_2H_5.CO .ND.CH_3$										
1100	1060	2	0	17	3	0	11	2	11	52
1627	1619	24	61	0	0	1	0	8	5	0
850	811	7	4	27	31	0	2	0	2	28
953	956	12	17	0	36	2	6	0	25	2
2417	2433	1	0	0	0	97	0	2	1	0
590	586	0	0	46	9	0	25	15	6	2
425	403	16	3	5	12	0	3	34	23	0
	302	0	2	0	0	0	32	35	28	2
1475	1486	37	16	7	8	0	15	0	1	16

To the amide II band at 1550 cm^{-1} , $\delta(N-H)$, $\nu(C=O)$ and $\nu(C-N)$ vibrations make contribution. But to the absorption at 1475 cm^{-1} which is the corresponding absorption in *N*-deuterated *N*-methyl-propionamide, the contribution of $S(N\sim D)$ and $\nu(C=O)$ vibrations becomes less and of *C-N* stretch increases substantially. In the deuterated amide, the band

at 1475 cm^{-1} is essentially due to C-N stretching vibration. To the amide III band at 1256 cm^{-1} in N-methyl-propionamide, the contributions of C-N stretching and N-H deformation vibrations are considerable. But the corresponding absorption at 1100 cm^{-1} in the deuterated amide is essentially due to δ (N-D) vibration and the contribution of C-N stretch to this frequency is negligible. These results may explain for relatively smaller differences in the frequencies of the amide I, II bands and larger difference in the frequency of the amide III band in N-methyl-propionamide and deuterated N-methyl-propionamide.

The frequencies at 865 cm^{-1} and 970 cm^{-1} are essentially due to ν (C-C₂H₅) and ν (N-CH₃) vibrations respectively. To the ν (C-CH₃) vibration, however, the contribution of ν (N-CH₃) is considerable and C-N and C=O stretches together contribute substantially to ν (N-CH₃) vibration.

The frequencies at 3300 cm^{-1} and 2417 cm^{-1} in N-methyl-propionamide and the deuterated amide are due to N-H and N-D stretching vibrations and the other modes of vibrations do not contribute to these absorptions. The band in the region of 575 cm^{-1} is assigned to S (O=C-N) vibration and ν (C-C₂H₅) vibration contributes to this mode. The frequencies at 430 cm^{-1} and 315 cm^{-1} are assigned to γ (C-C₂H₅) and δ (C-N-CH₃) vibrations respectively and the potential energy distribution results indicate considerable interaction between these two modes.

ACKNOWLEDGEMENTS

We express our sincere thanks to Dr. G. S. Sidhu, Director, Regional Research Laboratory, for giving us facilities of the Computer and to Mr. P. Jagan Mohan Reddy for his help in the use of the Computer for numerical computations. The authors express their thanks to Prof. P. Venkateswarlu and Dr. H. D. Bist for giving them facilities at I.I.T., Kanpur and Mr. Kama] Kumar and Mr. A. L. Verma for helping them in recording some of the infrared spectra. One of us (P. U. B.) is grateful to C.S.I.R. for financial assistance.

REFERENCES

1. tatsuo Miyazawa, Takehiko / *Chem. Phys.*, 1956, 24, 408.
Shimanouchi and
San-Ichiro Mizushima
2. _____.. *Ibid.*, 1958, 29, 611.

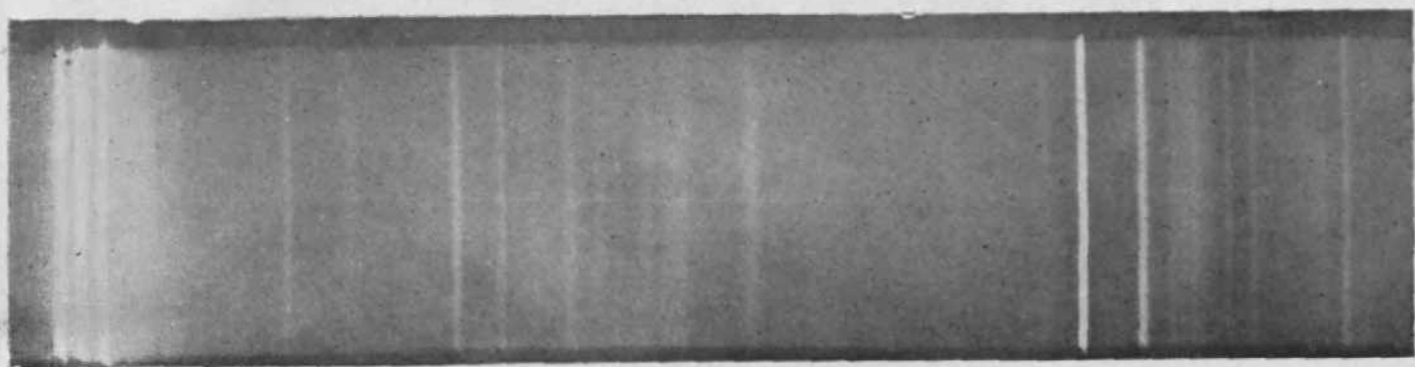


FIG. 4, Raman Spectrum of N-Methylpropionamide.

3. DeGraaf, D. E. and Sutherland, G. B. B. M. *J. Chem. Phys.*, 1957, 26, 716.
4. Isao Suzuki *Bull. Chem. Soc. Japan*, 1960, 33, 1360.
5. _____ *Ibid.*, 1962, 35, 540.
6. _____ *J. Chem. Phys.*, 1962, 35, 1280.
7. Beer, M., Kessler, H. B. and Sutherland, G. B. B. M. *J. Chem. Phys.*, 1958, 29, 1097.
8. Venkata Chalapathi, V. and Venkata Ramiah, K. *Proc. Ind. Acad. Sci.* 1968, 68, 109.
9. Decius, J. C. *J. Chem. Phys.*, 1948, 16, 1025.
10. Venkata Chalapathi, V. and Venkata Ramiah, K. *Proc. Ind. Acad. Sci.*, 1968, (77), 184.

INDEX TO VOL. LXIX (A)

AUTHORS' INDEX

- Banerjee, D. K., Sugavanam, B. and Nadamuni, G. Synthetic investigation on testosterone and its analogues, II, 229.
- Bhagavantam, S. and Radhakrishna, S. Piezoelectric relaxation in crystals containing point defects, 182.
- Bhat, P. K. .. Magneto-hydrodynamic flow between two non-conducting co-axial cylinders induced by deforming the walls of the container, 265.
- Chandra, G. • .. See Lagu and others.
- Chaudhari, K. N., Ganguli, S. N., Rao, N. K., Swami, M. S., Gurtu, A. and Singh, M. B. The ratio of non-mesic to γ -mesic decay of light hyperfragments, 78.
- Desai, B. N. .. Air-mass dynamics or subsidence processes in the Arabian Sea monsoon, 1.
- Ganguli, S. N. .. See Chaudhari and others.
- Gurtu, A. .. See Chaudhari and others.
- Indira Chary, C. A. and Venkata Ramiah, K. Infrared and Raman spectra and normal vibrations of N, N-dimethylthioformamide and N, N-dimethylthioacetamide, 18.
- Jagannadham, A. V. and Venkateswarlu, Putcha Electron paramagnetic resonance of Mn^{2+} in NaF single crystals, 67.
- Electron paramagnetic resonance studies of VO^{2+} in single crystals of NaCl, KCl and RbCl, 307.
- Jijee, K. and Santappa, M... Oxidation studies, VII, 117.
- Joshi, D. G. .. A solution of an integral equation, 36.
- Kamal, A. A., Rao, Y. V. and Rao, Rukmini Coherent production of pions in high energy π - π interactions, 218.
- Kapur, J. N. .. Some properties of entropy of order α and type B, 201.

- Krishnamurthy, K. S. .. *See* Krishnamurti and Krishnamurthy.
- Krishnamurti, D. and Krishnamurthy, K. S. Infrared absorption spectra of ethyl, α -propyl and ω -butyl stearates, 189.
- Kulkarni, V. G. .. *See* Lagu and others.
- Lagu, R. G., Kulkarni, V. G., Thosar, B. V. and Chandra, G. Formation and quenching of ortho-positronium in molecular materials, 48.
- Mande, Chintamani and Nigavekar, A. S. X-ray spectroscopic study of chemical bonding in NiSe and NiSe₂, 316.
- Merchant, J. R. and Patell, J. R. Reaction of nitriles, IV, 94.
- Nadamuni, G. .. *See* Banerjee and others.
- Nagana Goud, A. and Rajagopal, S. Furano compounds, XIII, 129.
- Nair, K. N. .. *See* Sarabhai and Nair.
- Natarajan, L. V. .. *See* Santappa and Natarajan.
- Nigavekar, A. S. .. *See* Mande and Nigavekar.
- Padma, S. and Santappa, M. Oxidation studies, VI, 7.
- Pant, D. D. .. *See* Sanwal and Pant.
- Pantulu, P. V. and Sudarshan, E. Magnetic symmetry and Onsager relations, 279.
- Patell, J. R. .. *See* Merchant and Patell.
- Radhakrishna, S. .. *See* Bhagavantam and Radhakrishna.
- Rajagopal, S. .. *See* Nagana Goud and Rajagopal.
- Raman, C. V. .. Floral colours and their origins, 169.
- Rao, K. S. R. Krishna Mohan *See* Subhadra Kumari and others.
- Rao, N. K. .. *See* Chaudhari and others.
- Rao, N. V. Subba .. *See* Subhadra Kumari and others.
- Rao, Rukmini .. *See* Kamal and others.
- Rao, Y. V. .. *See* Kamal and others.
- Rastogi, R. G. ... Lunar tidal variations in $^{19}F_2$ in the American Zone during periods of low solar activity, III, 250.
- Santappa, M. *See* Padma and Santappa.
See Jijee and Santappa.

- Santappa, M. and Natarajan, L. V. Vinyl polymerization, VIII, 284.
- Sanwal, D. N. and Pant, D. D. Electronic transitions of uranyl ion, 324.
- Sarabhai, V. and Nair, K. N. Geomagnetic plasma probe for solar wind, 291.
- Shah, G. M. .. Study of aerosols in the atmosphere by twilight scattering, 103.
- Shanmuganathan, Sp. and Vanajakshi, N. The ionization constants of some /7-alkylthio- and /J-alkylsulphonyl-anilines, 212.
- Singh, M. B. .. See Chaudhari and others.
- Somayajulu, B. L. K. .. Cosmic Ray produced silicon-32 in near-coastal waters, 338.
- Subhadra Kumari, S., Rao, K. S. R. Krishna Mohan and Rao, N. V. Subba Search for physiologically active compounds, XV, 88.
- Sudarshan, E. .. See Pantulu and Sudarshan.
- Sudarshan, E. C. G. .. A new formulation of relativistic quantum field theory, 133.
- Sugavanam, B. .. See Banerjee and others.
- Sundaram, S. and Venkatasubramanian, N. The chromic acid oxidation of hydroxy acids—Catalysis by manganous ions, 162.
- Swami, M. S. .. See Chaudhari and others.
- Thosar, B. V. .. See Lagu and others.
- Tuli, S. K. .. A note on *nn* scattering in the reaction $7r \rightarrow$
TTTTN, 42.
- Vanajakshi, N. .. See Shanmuganathan and Vanajakshi.
- Vcrikata Ramiah, K. .. See Indira Chary and Venkata Ramiah.
- Venkatasubramanian, N. .. See Sundaram and Venkatasubramanian.
- Venkaleswarlu, Putcha .. See Jagannadham and Venkateswarlu.

TITLE INDEX

- Aerosols in the atmosphere, study of, by twilight scattering (Shah), 103.
- Air-mass dynamics or subsidence processes in the Arabian Sea monsoon (Desai), 1.
- Chromic acid oxidation of hydroxy acids—catalysis by manganous ions (Sundaram and Venkatasubramanian), 162.
- Crystals containing point defects, piezoelectric relaxation in (Bhagavantam and Radhakrishna), 182.
- Entropy of order α and type/3, some properties of (Kapur), 201.
- Ethyl, *n*-propyl and *i*-butyl stearates, infrared absorption spectra of (Kxishnamurti and Krishnamurthy), 189.
- Floral colours and their origins (Raman), 169.
- Furano compounds, XIII (Nagana Goud and Rajagopal), 129.
- Geomagnetic plasma probe for solar wind (Sarabhai and Nair), 291.
- Integral equation, a solution of (Joshi), 36.
- Light hyperfragments, the ratio of non-mesic to γ -mesic decay of (Chaudhari and others), 78.
- Lunar tidal variations in $^{19}F_2$ in the American Zone during periods of low solar activity, III (Rastogi), 250.
- Magnetic symmetry and Onsager relations (Pantulu and Sudarshan), 279.
- Magnetohydrodynamic flow between two non-conducting co-axial cylinders induced by deforming the walls of the container (Bhat), 265.
- Mn^{2f} in NaF single crystals, electron paramagnetic resonance of (Jagannadham and Venkateswarlu), 67.
- NiSe and NiSe₂, chemical bonding in, X-ray spectroscopic study of (Mande and Nigavekar), 316.
- Nitriles, reaction of, IV (Merchant and Patell), 94.
- N, N-dimethylthioformamide and N, N-dimethylthioacetamide, infrared and Raman spectra and normal vibrations of (Indira Chary and Venkata Ramiah), 18.
- Ortho-positronium in molecular materials, formation and quenching of (Lagu* and others), 48.
- Oxidation studies, VI (Padma and Santappa), 7; VII (Jijee and Santappa), 117.
- i*-Alkylthio- and *p*-alkylsulphonyl-anilines, some, the ionization constants of (Shanmuganathan and Vanajakshi), 212.

- Physiologically active compounds, search for, XV (Subhadra Kumari and others), 88.
- Pions, coherent production of, in high energy γ -interactions (Kamal and others), 218.
- WII scattering in the reaction $ir-p-tmiN$, a note on (Tuli), 42.
- Relativistic quantum field theory, a new formulation of (Sudarshan), 133.
- Silicon-32 in near-coastal waters, cosmic ray produced (Somayajulu), 338.
- Testosterone and its analogues, synthetic investigation on (Banerjee and others), 229.
- Uranyl ion, electronic transitions of (Sanwal and Pant), 324.
- Vinyl polymerization, VIII (Santappa and Natarajan), 284.
- VO^{2+} in single crystals of NaCl, KCl and RbCl, electron paramagnetic resonance studies of (Jagannadham and Venkateswarlu), 307.

